Nanomedicine and Nanotoxicology

Misturu Akashi
Takami Akagi
Michiya Matsusaki *Editors*

Engineered Cell Manipulation for Biomedical Application

Springer

Nanomedicine and Nanotoxicology

Series Editor:

V. Zucolotto

For further volumes:
http://www.springer.com/series/10620

Misturu Akashi • Takami Akagi
Michiya Matsusaki
Editors

Engineered Cell Manipulation for Biomedical Application

Springer

Editors
Misturu Akashi
Osaka University
Osaka, Japan

Takami Akagi
Osaka University
Osaka, Japan

Michiya Matsusaki
Osaka University
Osaka, Japan

ISSN 2194-0452 ISSN 2194-0460 (electronic)
ISBN 978-4-431-55138-6 ISBN 978-4-431-55139-3 (eBook)
DOI 10.1007/978-4-431-55139-3
Springer Tokyo Heidelberg New York Dordrecht London

Library of Congress Control Number: 2014949887

Printed on acid-free paper

Springer is part of Springer Science+Business Media (www.springer.com)

Preface

In the 1940s, the invention of the electron microscope led to an understanding of inner cell structure that made it possible to clarify the inner working of organs. Because the results of studies of the functions of organs stimulated the development of biochemistry, life science now has reached new heights.

As well, the integration of molecular biology and biochemistry has created a new discipline, cell biology, which supports the field of life science. Cell biology has led to cell technology and already has begun making contributions to medical care and drug development. In such circumstances surrounding a new field, when we address the fundamental issues of cell culture, cell separation, cell fusion, research on ES and IPS cells, biotechnology-created bioreactors, and cell therapy using activated dendritic cells, we have come to understand what cell manipulation means in controlling cell functions. It is of great interest to know that confocal laser scanning microscopy supported by computer image processing had come on stage and become widely used in the 1980s to sustain advances in this field.

In this book we introduce cutting-edge information about cell manipulation**,** which has been extremely important in the biomedical field. Part I deals with controlling cell function and cell assembly formulation by tissue engineering. Three-dimensional (3D)-cell assembly is a minimum module, which has been defined as being between micrometer-size cells and centimeter-size tissues. However, as universal technology for construction of 3D-cell assembly is still a key challenge, unfortunately no academic systematization has been achieved yet. Accordingly, it will be one of the most important fields both in science and technology, especially in tissue engineering, regenerative medicine, and pharmaceutical assay. Part II describes controlling cell function in the field of drug delivery systems (DDS). In response to the recent progress of immunology and molecular cell biotechnology, the mechanism of the immune system can be understood at the molecular level. Therefore, the study of manipulating immune cells and controlling cell function for application to DDS is becoming more and more widespread.

As cell manipulation is widely used in the fusion region of biology, cell biology, biotechnology, immunology, pharmaceutical science, medicine, and engineering, many researchers have contributed to this book. On behalf of the editors, I would like to give our heartfelt thanks to all the authors.

Osaka, Japan Misturu Akashi

Contents

Part I
Cell Manipulation for Control of Cell Function and Assembly for Tissue Engineering

Chapter 1
Recent Advances in 3D Tissue Models

A. Kivelio and M. Ehrbar

Abstract Physiologically relevant tissue models that bridge the gap between 2D tissue culture and animal trials would be highly desirable to study the function of tissues in health and disease as well as for the validation of lead compounds during drug development. The field has made impressive advances in 3D culturing cells and organoids in naturally derived materials. Novel, rationally designed, biomimetic materials have been established, which allow the almost individual variation of matrix parameters, such as stiffness, cell adhesion, degradability, or growth factor binding and controlled release. The combination of innovative materials with novel technological platforms such as printing, microfluidics, and additive or preventive manufacturing provides a great potential to build unprecedented, complex tissue models. Here we review recent advances in the design of materials building blocks which allow the formation of 3D structured microenvironments. We will mainly focus on strategies to locally position cell-instructive molecular cues and discuss needs to generate models which would allow the investigator to controllably manipulate cells in their 3D context with the aim to generate complex but yet scalable tissue models.

Keywords 3D tissue models • Cell-instructive hydrogels • Growth factors • Patterning • Spatiotemporal control

A. Kivelio, M.Sc.
Department of Obstetrics, University Hospital Zurich, PATH,
G-48 Schmelzbergstr 12, Zurich, Switzerland

Institute of Bioengineering, Ecole Polytechnique Fédérale de Lausanne (EPFL),
Lausanne, Switzerland

M. Ehrbar, Ph.D. (✉)
Department of Obstetrics, University Hospital Zurich, PATH,
G-48 Schmelzbergstr 12, Zurich, Switzerland

Zurich Centre for Integrative Human Physiology, Zurich, Switzerland
e-mail: martin.ehrbar@usz.ch

M. Akashi et al. (eds.), *Engineered Cell Manipulation for Biomedical Application*, Nanomedicine and Nanotoxicology,
DOI 10.1007/978-4-431-55139-3_1

1.1 Introduction

For the understanding of fundamental biological phenomena and for development of novel drugs there is a large need for highly reproducible, reliable, and physiologically relevant test platforms. Over the past decades a wealth of detailed insight into cellular and molecular details has been acquired using 2D cell culture models. This knowledge has frequently been transferred to animal models, where among other techniques, genetic tools have helped to understand individual factors in the complex systemic context. However, though in vitro and in vivo experiments have been a very successful combination for many decades, both of them have clearly indefinable limitations. 2D tissue culture models provide limited information regarding physiologically relevant (1) tissue morphogenesis, (2) chemotaxis and haptotaxis, (3) cell morphology, (4) matrix remodeling, and (5) effects of matrix-mediated signaling.

In contrast, in vivo animal models are limited by (1) throughput, (2) systemic effects and compensation phenomenon, (3) differences in physiology between species, and (4) ethical concerns.

In order to study cells in a physiologically relevant environment, conditions nearly identical to the ones of the native tissue with respect to composition and 3D arrangement would have to be established in vitro. Cells in tissues are embedded in a microenvironment consisting of neighboring cells, extracellular matrix (ECM) components, and signaling molecules. Of course the cellular response is the result of an integration of these various signals. By dynamic changes of the microenvironmental composition, the cellular response can substantially adapt during both development and healing. To recapitulate developmental, physiological, or even pathological situations, ideally cells, matrix components, and signaling cues could be arranged in a rational and three-dimensionally controlled manner, such that single parameters can be individually varied.

In this chapter we will commence with a short discussion of 3D cell culture models which are based on matrix-free approaches. Since such assays are performed at high cellular density and rely on cell's own matrix production, the additional encapsulation of cells in a provisional matrix clearly offers the opportunity to provide and vary matrix signals. Thus, a summary of achievements using biologically derived materials to generate in vitro tissue models will be given next. Although with scaffold-based approaches impressive advances have been achieved, we will here focus our discussion mainly on hydrogel systems. For the establishment of fully defined, engineered tissue models the precise control over all components and their exact positioning in 3D would be desirable. Great advances in the engineering of naturally occurring and biomimetic extracellular hydrogel matrices towards the control of biological functions have been made. We will describe their fundamental design principles of currently available hydrogel platforms. Having done so, the achievements in design of functional building blocks and their spatial and temporal arrangement and release will be discussed. Finally, examples of sophisticated 3D tissue models which will be the basis for the development of in vitro tissue homologues will be given.

1.1.1 2D Cell Cultures

Many cell types are adhesion dependent and cannot be grown in suspension cultures without mechanical support. All freshly isolated, culture expanded, as well as immortalized cells have for many decades been cultured on tissue culture polystyrene plastic. In such cultures cells normally spread and form focal adhesions and stress fibers throughout the cytoplasm. Such cultures can relatively easily be used to determine gene and protein expression, biochemical pathways, and intracellular trafficking just to mention a few. However, 2D cultures do only to a certain degree represent the physiological environment with respect to cell shape, cell–matrix and cell–cell interactions, local chemotactic and haptotactic gradients, nutritional status, or interstitial flow [1, 2]. For example, tumor cells, when grown on 2D substrates, are flat, whereas in 3D they adapt a round morphology, much like seen in cancer biopsies. Also mesenchymal cells independent of substrate composition exhibit bipolar spindle-shaped morphology in 3D as compared to the observed artificial dorsal (upper side) ventral (lower side) polarity in 2D [3] as here illustrated for cells being cultured on top (Fig. 1.1a) or inside (Fig. 1.1b) poly(ethylene glycol) (PEG) hydrogels of identical composition.

Not surprisingly, recent findings suggest a strong correlation between cell shape and function. Impressively, the changes in morphology and cell–substrate interactions in 3D cultures translate to differential cell signaling [1] resulting among others functional differences in reduced sensitivity of tumor cells towards radiotherapy (cell adhesion-mediated radioresistance) and chemotherapy (cell adhesion-mediated drug resistance) [4]. The decreased sensitivity to doxorubicin or etoposide observed in small cell lung cancer cells cultured on fibronectin or laminin [5] and the increased radiosensitivity of lung carcinoma cells with altered cell shapes by destabilization of the actin filaments [6] point towards effects mediated by both matrix components as well as the 3D arrangement. Furthermore, in many organs and tissues, different

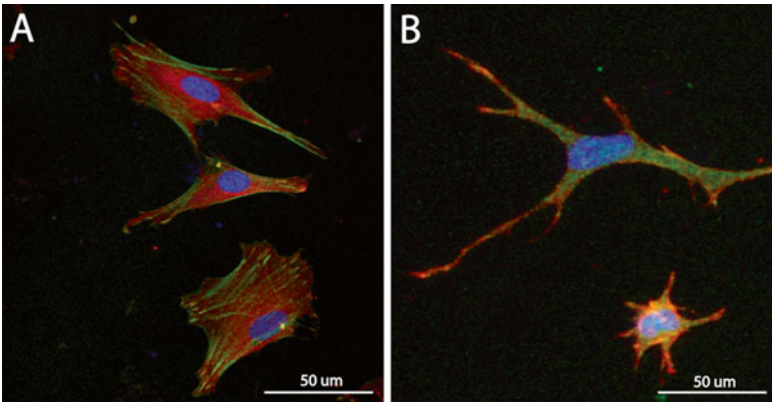

Fig. 1.1 Morphology of murine fibroblast cultured (**a**) on 2D substrates and (**b**) in 3D cultures

cell-types are arranged in spatially defined, repetitive manner and are structurally integrated with their neighbors. Together this might explain why some of the effects seen in 2D cultures are significantly different in the native tissue and thus findings from 2D cultures and even uniform 3D cultures likely have a limited predictive value [7]. Thus, the current workflow in pharmaceutical industry consists of screenings in 2D followed by validation in simple 3D models and animal models.

However, due to species-specific differences in physiology, metabolic activity, and cell function, also animal models have a restricted predictive value regarding drug therapeutic response. Thus, 3D tissue and organoid models partially representing functional properties of physiological or pathological human tissues are now seen as an interesting approach to bridge the gap between traditional 2D cultures and animal models [2, 8].

1.2 Top-Down Approaches (Matrix Free)

Typically tissue ECM undergoes tightly regulated remodeling through cells continuously secreting and subsequently remodeling their own ECM consisting of molecules such as collagens, fibronectin, elastin, and proteoglycans [9]. These secreted tissue-specific ECM components in turn will be sensed by cell integrin receptors and eventually influence the behavior of the cell itself as well as the one of neighboring or invading cell. When taken in culture, cells produce their own ECM [10] and are structurally and functionally integrated with their neighboring cells and the ECM [7]. During cell passaging, in order to permit the transfer of tightly adherent cells from one substrate to the next, cell–substrate interactions need to be disrupted by treatment with trypsin and EDTA by proteolytic cleavage and destabilizing of protein interactions. Due to cell surface-located proteins (e.g., growth factor receptors, syndecanes, integrins, proteases, and their regulators) engaged in receiving signals from the environment and providing modifying signals to the environment, passaging can have a significant impact on cell behavior.

1.2.1 Microtissues

Microtissues, also called spheroids, are 100–500 μm-sized multicellular clusters which can be formed on nonadhesive substrates by hanging drops or spinner flasks [11]. Microtissues can be assembled without the addition of matrix components and allow the formation of multicellular structures without the need of external signals. Additionally, within them cell–cell connections and connections of cells with their own ECM can be established. Due to 3D arrangement, cells adapt a more natural morphology and structure and function of deposited ECM takes the role of the natural environment. Microtissues present a straightforward approach to assemble a large variety of cell types as monotypic cultures or as cocultures in a mostly natural

environment; thus they have a great potential to be used in scalable drug screening platforms [12, 13]. They allow the determination of biochemical, morphological, functional, and morphogenesis-related parameters.

The major limitations of microtissues are the heterogeneity of the cellular environment and the limited ability to control the initial patterning of cells. The heterogeneity of cells within microtissues is largely due to the nonhomogeneous distribution of nutrients and oxygen, resulting in a hypoxic core with apoptotic cells and sufficiently nourished cells located on the outside. The difficulty to control the spatial arrangement of multiple cell types could potentially be overcome by varying the microtissue formation. The value of microtissues will rather be in understanding tissue self-organization processes and contact-mediated interactions between different cell types. For example in an attempt to create functional myocardial tissue rat cardiomyocyte-based microtissues were formed and exhibited coordinated beating after electrochemical coupling. When microtissues were coated with endothelial cells and assembled into macrotissues of mm^3 scale, they spontaneously formed microvessels with native vessel ultrastructural morphology. Transplantation of such prevascularized tissues into chick embryos or rat pericardium demonstrated both the functional integration of microvessels (60 h post transplantation) and the co-alignment of transplanted and host cardiomyocytes [14].

In order to take control over positioning of individual cell types DNA-programmed assembly of microtissues has been employed [7]. Using this approach the assembly of microsphere consisting of one MCF10A mammary epithelial cell with activated H-Ras and multiple control MCF10A cells could be achieved. The generated cell-to-cell variability in signaling was shown to lead cell mobility which is due to heterogeneity in pathway activation rather than in absolute pathway activity. Alternatively, polydimethylsiloxane (PDMS) molds have been generated in which by sequential seeding and sedimentation cells could be precisely positioned in 3D [15]. Such arrangement together with the stabilization of the structures within a hydrogel allowed the formation of liver-mimicking tissue structures in vitro. The arrangement of hepatic aggregates and liver endothelial cells demonstrated that the geometry of arrangement can have a large influence on cell function. If hepatocytes and endothelial cells were positioned in a compartmentally distinct localization allowing only paracrine signaling, albumin production could be sustainably enhanced compared to juxtaposed position. As such complex assays are clearly needed for the evaluation of tissue functions, such as that of liver, the combination of principles from bottom-up and top-down approaches as well as the use of patient's own cells will be necessary.

1.2.2 Cell Sheet Engineering

An interesting alternative to microtissues is cell-sheet engineering. This technology relies on a purely cell-based assembly of tissue structures. Again, cells are allowed to establish their own ECM and to form mature tissue structures. One of the first examples using this approach was the assembly of intermediate size blood vessels

(3 mm inner diameter) [16]. The construction of the vessel was initiated by first culturing fibroblast cell sheets, which were wrapped around a support and formed a tubular tissue. After decellularizing the remaining tissue matrix, forming an inner membrane, it was mounted on a perforated tubular mandrel before a sheet of smooth muscle cells was wrapped around to form the vascular media. This construct was maturated in a bioreactor before an additional sheet of fibroblasts, the adventitial layer, was wrapped around the vascular media. After another period of maturation in a perfusion bioreactor the tubular construct was removed from its support and seeded with endothelial cells which again were allowed to grow and maturate for 1 week. Histologically the constructs resembled a native vessel with intima, media, and adventitia and due to established ECM they were shown to resist physiologically relevant pressures (larger than 2,000 mmHg). Vessel constructs similarly produced using fibroblasts and endothelial cells were implanted as arteriovenous shunts in end-stage renal disease patients. In this study, the tissue-engineered constructs showed a patency rate of 78 % after 1 month and 60 % after 6 month of transplantation. Additionally, the constructs showed impressive resistance to intimal thickening and aneurysm formation [17].

Recent efforts towards the construction of engineered vessels concentrated on the development of production methods which give rise to constructs with better mechanical properties, are less time consuming, and are less dependent on cells' capacity to produce ECM. These aims were achieved by employing a single step assembly protocol [18] or the formation of fibroblast-derived, decellularized ECM which could be seeded with smooth muscle cells [19]. Together with the engineering of the vascular adventitia containing vasa vasorum, which was shown to improve graft integration and inosculation, engineered blood vessels hold great promise to become clinically applicable tissue-engineered products [20].

An alternative approach to harvesting of contiguous sheet of cells has been pursued by the development of surfaces where a simple shift of temperature (reviewed in [21]) or local charge [22] leads to a change of surface hydrophilicity or disintegration of the surface coating. The resulting sheading of the cell sheets without the use of proteolytic enzymes and EDTA allows cells to retain their structural and functional properties and to remain within the intact and functional ECM throughout the transfer [23]. The potential advantage of cell-sheet engineering lies in the ability to generate tissue constructs, which can be highly structurally ordered and allow the use of multiple different cell types. Initial attempts however have relied in single-cell-type sheets, which have even translated to clinical applications such as for the replacement of corneal tissue. Stratified epithelial cell sheets with normal cell profiles and functions were produced in human autologous serum and in the absence of feeder layers or bacterial or animal-derived products [24]. Later, using microcontact printing of fibronectin onto thermoresponsive surfaces, patterned cell sheets containing structurally arranged endothelial cells and hepatocytes could be produced [25]. In order to treat infarcted hearts, multiple myocardial cell sheets were stacked on top of a perfused vascular bed to generate functional 3D myocardial tissue constructs which contain a perfused vascular network [26]. With the advances in cell deployment using dispensing robots or microfluidics as well as the

layer-by-layer assembly of cell sheets could clearly help to generate more complex 3D tissue models. More likely, the integration of matrix-free and matrix-based approaches will be needed to generate models which recapitulate spatiotemporally regulated processes as they occur during tissue morphogenesis and healing.

1.3 Bottom-Up Approaches (Cells in Biomaterials)

In classical tissue engineering applications cells have been used in combination with biomaterials [27] which, with the aim to reconstruct or heal tissues, nowadays are often complemented with cell instructive factors provided with the biomaterial or with the cell culture medium. Biomaterials in this context are meant to substitute the native ECM and thus provide cells with an adequate provisional environment during tissue formation. ECMs in naturally occurring tissues consist mainly of fibrous proteins (collagens, fibrinogen, elastin, laminins) and proteoglycans. Both classes of molecules contribute to the mechanical (tensile and compressive) properties of tissues and are additionally involved locally in providing adhesion sites and molecular cues to embedded cells. Tissue engineering aims at replacing this naturally occurring matrix with (in most attempts) a provisional one to provide a template for the formation of novel tissue structures. A myriad of literature can be found on ceramic, polymeric, or biological materials which by different manufacturing processes give rise scaffolds with variable porosity, pore size distribution, and interconnectivity [28]. By providing structural support and a basis for the deposition of cell's own ECM, such porous scaffolds provide great platforms for both in vivo healing strategies and for the culture of cellular constructs in vitro. However, since the colonization with cells relies on their invasion from the outside or on dynamic seeding, porous scaffolds are not amenable for the exact positioning of cells as would be needed for advanced in vitro 3D tissue models. Therefore, within this chapter we will concentrate on hydrogel materials which are the generally used platform in advanced tissue models today.

1.4 Hydrogels

Hydrogels, comparable to glycosaminoglycans of the native ECM, are hydrophilic polymer networks which are highly swollen in aqueous solutions as they imbibe large quantities (often up to 99 %) of water [29]. Hydrogels, additionally to having similar mechanical properties to ECMs, permit the efficient diffusion of respiratory gasses, nutrients or waste products, and signaling molecules. Thus, they are often considered as good ECM models and broadly used for tissue engineering applications [29]. In all of these systems functional elements and means to control the materials function have been introduced over the years moving from simple hydrogels to hydrogels with more advanced properties. Functional elements can often be

employed in different materials and thus synthetic and biological elements become more and more integrated. However, in order to structure the following sections, we have made the distinction between biologically derived and synthetic materials.

1.5 Biologically Derived Hydrogel Materials

In early tissue engineering applications cells have been encapsulated and 3D cultured in a large variety naturally occurring, hydrogel-forming, protein-based materials such as collagens, fibrin, and matrigel or sugar-based materials such as alginate, agarose, hyaluronic acid, and chitosan [30]. Such 3D cultures have enabled the formation of relatively simple skin, bone, and cartilage tissue models, to name a few. Additionally they have allowed the study of morphogenetic events of, for example, intestine or mammary gland under tightly controlled culture conditions (reviewed in [31, 32]). They have also highlighted the influence of the dimensionality on the outcome of biochemical parameters. Due to the supportive biological properties of the naturally derived materials (e.g., their biodegradability and presentation of integrin ligands), such early approaches have led to impressive advances in the engineering of advanced tissue models.

1.5.1 Matrigel

Matrigel™ is a matrix that mainly consists of laminin, type IV collagen, entactin, and heparin sulfate proteoglycans [33]. Since Matrigel™ is isolated from Engelbreth–Holm–Swarm (EHS) mouse sarcoma, its composition is relatively ill defined, has large batch-to-batch variation, and can contain tumor-derived proteolytic enzymes and growth factors which can promote cellular function in an unpredictable manner. Despite the limitations of Matrigel™, this system has been successfully employed in a myriad of both tissue engineering applications and the formation of organoids in vitro. Impressive examples are the formation of small intestine organoids starting from intestine biopsies or even single intestine-derived leucine-rich-repeat-containing G-protein-coupled receptor 5 (Lgr5) positive intestinal crypt stem cells [34].

1.5.2 Collagen and Gelatin

(Review on collagen in Lanza et al., 2011 [35]). Collagens are the most abundant proteins in the ECM of most tissues. Besides providing tensile strength to the tissue, by presentation of integrin binding sites in their native and proteolytically degraded form, they largely contribute to cell function and signaling. Due to their limited solubility and the presence of covalent intermolecular (Schiff base, aldimine)

cross-links in native tissues, collagens are commonly isolated using pepsin or acidic extraction conditions. Thermal denaturation of insoluble collagen results in gelatin, which dependent on the source can have variable properties.

Physical hydrogels formed by collagen type I provide excellent cell substrates both in vitro and in vivo. For example, plastic compressed collagen type I hydrogels have been used to engineer dermo-epidermal skin substitutes that can be formed at clinically relevant size and be transplanted and in a rat model successfully reconstitute full-thickness skin defects [36]. However, as during the common isolation process of collagens, the Schiff base is reversed to amines and aldehydes which further are converted to alcohols, collagen cross-links cannot spontaneously form [37]. Thus, in order to improve collagen and gelatin stability, cross-linking using glutaraldehyde or carbodiimide is needed, which is clearly not applicable for the delivery of proteins or encapsulation of cells.

1.5.3 Fibrin

Fibrin gels are formed by the thrombin-mediated cleavage or fibrinogen resulting in the release of the fibrinopeptides and the lateral aggregation of fibrin monomers to fibrin fibrils. This physical matrix is subsequently enzymatically cross-linked by the transglutaminase factor XIIIa (FXIIIa). Fibrin hydrogels are commonly used as surgical tissue glue. Due to its high biocompatibility Fibrin in a large number of in vitro culture cell and in vivo tissue applications led to impressive results. For example, fibrin in combination with knitted fabric has been used to create myocardial patches. Upon in vitro culture under cyclical stretch the provisional matrix was remodeled as shown by the increasing amounts of collagen after 1 week of culture. After subcutaneous implantation in rats cardiomyocyte survival and vessel ingrowth into these constructs were shown [38].

1.5.4 Alginate

Alginate is an unbranched, sugar-based material which consists of 1-4′-linked b-D-mannuronic acid (M) and a-L-glucuronic acid (G) derived from brown algae. Alginate hydrogels readily form by the cooperative binding of Ca^{2+} ions to the G-block [39]. By the association of two G-blocks, junctions are being formed, leading to the formation of a network structure. Alginate hydrogels are highly biocompatible but are largely devoid of biological function in mammalian tissues. Thus for tissue engineering applications they need the chemical integration of adhesion sites such as RGD [40]. Additionally, the loss of divalent cations by diffusion results in an uncontrolled disintegration of the hydrogels, which can be controlled by oxidation and covalent cross-linking [30]. Modified alginate hydrogels have indeed been shown to be very suitable for the delivery growth factors as well as tissue engineering applications. For review please refer to [41].

1.5.5 Hyaluronic Acid

Hyaluronic acid (HA) is a negatively charged matrix component which is present in the ECM of most tissues [42] and contributes to the compressive properties of tissues [43]. It is a linear polysaccharide of 100–8,000 kDa, consisting of repeating disaccharides of -1,4-D-glucuronic acid-b-1,3-*N*-acteyl-D-glucosamine. HA is not immunogenic and can easily be chemically modified [44]. Due to binding to CD44 HA is involved in many cellular processes [45]. Therefore, HA is also often combined and cross-linked with synthetic polymers to form semisynthetic hydrogels for protein and cell delivery. For review please refer to [46].

1.5.6 Engineering of Naturally Derived Biomaterials

However, the major drawback in the use of naturally occurring materials in engineering applications is their inherent biological properties such as the presentation of integrin ligands, the proteolytic degradability, and available specific and unspecific protein binding sites. To achieve prolonged materials stability, collagen hydrogels have been cross-linked by *N*-(3-dimethylaminopropyl)-*N′*-ethylcarbodiimide (EDC) [47]. To decrease plasmin digestion of fibrin hydrogels, aprotinin was engineered to be covalently incorporated in fibrin [48]. Additionally, the chemical or enzymatic coupling of functional groups such as heparin or growth factor-binding peptides to naturally occurring hydrogels have allowed the mimicking of naturally occurring ECM growth factor binding (Fig. 1.2a) [48–53]. The covalent enzymatic or chemical immobilization of engineered growth factors or the use of affinity linkers have provided another possibility to generate growth factor repositories for the sustained long-term delivery of minute quantities of highly potent growth factors such as vascular endothelial growth factor (VEGF), bone morphogenetic proteins (BMPs), or insulin-like growth factor (IGF) (Fig. 1.2b) [54–56]. The various strategies employed to immobilize growth factors in biological biomaterials are summarized in Table 1.1.

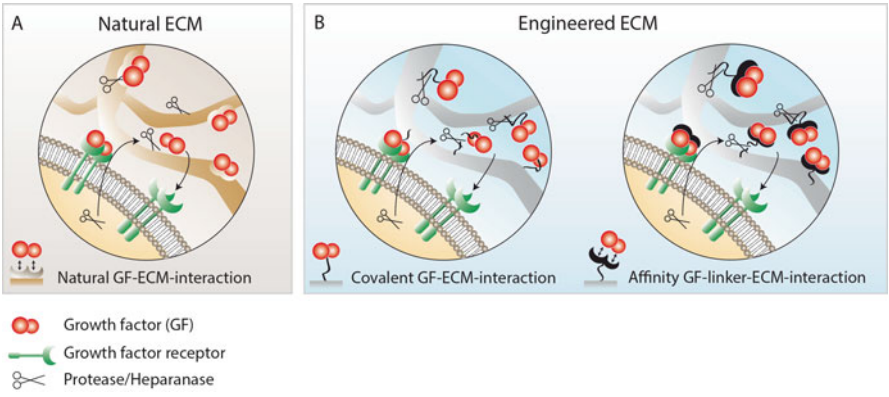

Fig. 1.2 Growth factor immobilization and release in (**a**) natural ECM, (**b**) engineered ECM with covalent interactions, and with affinity linkers

Table 1.1 Strategies for immobilization and release of growth factors in naturally occurring hydrogels (adapted from [57])

Matrix backbone	Linker	Ligand					References
		Native form	Modification	Immobilization	Release from		
					Matrix	Linker	
Fibrin	Heparin, Gln-HBP[a]	bFGF, β-NGF, PDGF-BB, NT-3	–	Affinity	Enz.	Dissoc.	[51, 58–65]
Collagen	Heparin, EDC/NHS[a]	VEGF, bFGF, SDF-1α	–	Affinity	Enz.	Dissoc.	[66–72]
Fibrin	FN-III9-10/12–14-Gln[a]	VEGF, PDGF-BB, BMP	–	Affinity	Enz.	Dissoc.	[53, 73]
Fibrin	–	bFGF	Ligand–Kringle fusion	Affinity	Enz./dissoc.	–	[74, 75]
Collagen	–	PDGF-BB, EGF, BDNF	Ligand–CBD fusion	Affinity	Enz./dissoc.	–	[76–78]
Collagen	SG-PEG-SG[a, b]	TGF-β2	Chemical	Covalent	Enz.	–	[79]
Collagen	SS-PEG-SS[a, b]	$VEGF_{165}$	Chemical	Covalent	Enz.	–	[80]
Collagen	EDC/sulfo-NHS[a, b]	$VEGF_{165}$	Chemical	Covalent	Enz.	–	[81]
Fibrin	SMCC-Gln[a, b]	KGF	Chemical	Covalent	Enz.	–	[82]
Fibrin	BTC-PEG-BTC[a, b]	SDF-1α	Chemical	Covalent	Enz.	–	[83]
Fibrin	–	β-NGF, BMP, $VEGF_{121}$, ΔAng-1, ephrin-B2, PTH, L1Ig6, IGF-1, Aprotinin	Ligand–Gln fusion[a]	Covalent	Enz.	–	[54–56, 84–93]
Fibrin	Gln-PIGF(123–144)	VEGF, BMP-2, PDGF-BB, multiple other ligands	–	Affinity	Enz.	Dissoc.	[94]

[a]Reacting with matrix
[b]Reacting with ligand
enz. enzymatic, *dissoc.* dissociation, *Gln* NQEQVSPL-peptide, *Gln-HBP* bifunctional NQEQVSPL-heparin binding peptide, *NHS N*-hydroxysuccinimide, *EDC N*-(3-dimethylaminopropyl)-*N′*-ethylcarbodiimide, *FN-III9-10/12–14* pieced together fibronectin III fragments from the 9th to 10th and 12th to 14th repeats, *SG-PEG-SG* disuccinimidyldiglutarate-polyethyleneglycol, *SS-PEG-SS* disuccinimidyldisuccinatepolyethyleneglycol, *SMCC* succinimidyl trans-4-(maleimidylmethyl) cyclohexane-1-carboxylate, *CBD* collagen binding domain, *ΔAng-1* truncated version of angiopoietin-1, *PIGF(123–144)* placental growth factor derived peptide sequence amino acids 123–144

All mentioned growth factor presenting materials can be engineered to instruct encapsulated or recruited cells to undergo differentiation or induce morphogenic processes in vitro and in vivo. For example the covalent immobilization of VEGF generated a growth factor repository for the sustained long-term delivery of minute quantities the highly potent growth factor [95]. Indeed this strategy has enabled the induction of large numbers of patent and morphological normal blood vessels in small animal models [85, 96]. Similarly, recently described linker peptides derived from fibronectin (FN) [53] have been shown to mediate the retention of growth factors and cytokines within fibrin hydrogels. Additionally to the efficient delivery of factors by the FN it also coordinated with growth factor receptors and integrin signaling. Delivery of platelet-derived growth factor-BB (PDGF-BB) was shown to improve in vitro mobilization of smooth muscle cells and in the presence of BMP-2 to improve bone healing in vivo.

The above examples illustrate those major achievements made by the engineering of biologically derived materials. However, though some of the inherent properties of biological materials can be overcome with engineering strategies, others such as proteolytic stability, presentation of integrin ligands, low affinity binding of proteins, or gelation kinetic cannot be so easily manipulated.

1.6 Synthetic Hydrogel Matrices

Ideally, for engineering applications the precise and independent control over following hydrogel parameters would be available: mechanical properties, gelation kinetics, micro- and/or nanoarchitecture, presentation of adhesion ligands, proteolytic degradability, specific protein binding and release. All of these parameters have to be considered when designing tissue engineering applications in vitro. Furthermore, mimicking dynamic changes throughout morphogenesis, materials should be available which allow trigger-inducible change in materials properties. Some of these materials have successfully been engineered to bind and locally present biological cues.

1.6.1 Backbone Design

Multiple (cationic, anionic, or neutral) polymeric molecules have been suggested for the use as biomaterials. For a more thorough review please refer to [29]. The architecture of the molecules giving rise to the hydrogel network can be varied regarding functionality and distance between the functionalities. Whereas the increase of functionality gives rise to higher cross-link density at constant polymer concentration, the increase in distance between functionalities will result in larger pore size. The polymer chemical composition largely influences the behavior of the material in aqueous environments. Whereas polymers containing ionizable pendant

groups such as copolymer networks of poly(methacrylic acid) grafted with poly(ethylene glycol) P(MAA-g-EG) respond with shrinkage or swelling, uncharged polymers are indifferent towards changes in buffer pH [97]. The use of block copolymers consisting of hydrophilic and hydrophobic domains, such as poly(ethylene glycol)-bl-poly(propylene glycol)-bl-poly(ethylene glycol) (PEG-PPG-PEG), results in a hydrogel system, which due to a shift in temperature is swelling or shrinking [98]. The copolymerization of materials building blocks which are temperature or pH sensitive results in hydrogels that responded to both stimuli [99].

1.6.2 Cross-Linking Mechanisms

For in vitro and in vivo applications, cross-linking of hydrogels must be performed under conditions which are not affecting cell viability. Hydrogels can be created by establishing affinity interactions or by chemical polymerization and depending on the affinity of physical interactions the stability of hydrogels can be modulated. Relatively weak interactions can be employed to form hydrogel systems which are responsive to stimuli such as glucose or antibiotics. Additionally they can result in hydrogels which are self-healing. The stability of chemically cross-linked hydrogels can be modulated by the introduction of linkages which are sensitive or insensitive towards hydrolytic degradation, proteolytic digestion, or reducing conditions. Chemical cross-linking today is mostly done by radical polymerization using photoinitiators, step-growth polymerization (Michael-type reaction), or enzymatic reactions presenting a spectrum of possibilities to choose for specific applications. Problems associated with cross-linking are lack of substrate specificity, cytotoxicity, and reaction time. Although some photoinitiators have been associated with cytotoxicity, for a number of them, the concentrations used are in a range where they are not compromising cell viability [100, 101]. Michael-type reactions have been shown to have high substrate specificity and fast reaction kinetics under physiological buffer conditions. Recently, the even more selective native chemical ligation which involves a thioesther and an *N*-terminal cysteine has been used for the formation of hydrogels [102]. Also copper free click-reactions are now being developed, which have a good substrate specificity and improved reaction kinetics [103]. Alternatively, enzymatic reactions which are known to have a very high substrate specificity have been used to form hydrogels [102] being highly compatible with the preservation of active growth factors.

1.6.2.1 Mechanics

The mechanical properties of hydrogels rely on hydrogel architecture, cross-linking efficiency, swelling behavior, initial concentration of monomers, and stoichiometry of reactants. Generally, higher polymer concentrations with high branching and short arm length can potentially lead to highly cross-linked hydrogels. Such hydrogels,

with increasing hydrophilicity of the backbone polymer, can take up large amounts of water and thus will be mechanically strong. Factors that can weaken the mechanical properties of the hydrogel are limited cross-linking efficiency for example due to unbalanced stoichiometry of reacting groups, competing reactions, or suboptimal reaction conditions (pH, salt concentration). For a more thorough review please refer to [30].

1.7 Synthetic Hydrogels with Engineered Biological Functions (Static/Controlled by Cells)

As mentioned above, synthetic hydrogels are devoid of biological functions and thus provide a blank canvas for the engineering of materials with tightly controlled properties. Early experiments provided evidence that cells 3D encapsulated in such small porous (pore size is typically in the nm range) hydrogels cannot spread migrate, proliferate, and survive long term [104]. It has been demonstrated that the modification of the hydrogel backbone with biological building blocks such as cell adhesion sites and the introduction of proteolysis-sensitive backbone elements are necessary for the 3D culture of cells. These minimal modifications allow the encapsulated cells to locally digest the hydrogels, form small pores, and move via complex processes via substrate adhesion and retraction of cell extensions. Of course, cells from different lineages have different requirements regarding the presented biological functional building blocks, which is where the challenges arise but also where novel hydrogel platforms with tunable properties prove their worth.

1.7.1 Modularly Designed Platforms as Artificial Extracellular Matrices

Although synthetic hydrogels make it possible to study cellular response to isolated biological parameters, up to date only few hydrogels developed for 3D cell culture allow the independent tuning of properties such as biochemical signals and mechanical stiffness. Such materials have been created for example based on click chemistry [105], peptide self-assembly [106], and interpenetrating polymer networks [107].

In order to create a modular artificial ECM platform where matrix properties can be modified almost independent of each other, the factor XIIIa-catalyzed cross-linking scheme of fibrin clot involving the formation of a covalent isopeptide bridge between Gln and Lys residues by the enzymatic action of the transglutaminase factor XIIIa was employed [108]. Star-shaped PEG-vinylsulfone molecules were functionalized with two peptides acting as substrates for FXIIIa via a Michael-type addition reaction, thus creating a homogeneous synthetic hydrogel with fibrin-like biomolecular characteristics upon cross-linking with the enzyme. Simultaneously with the hydrogel cross-linking, growth factors, adhesion peptides, or other biological entities functionalized with either of the FXIIIa substrates can be incorporated in a controlled

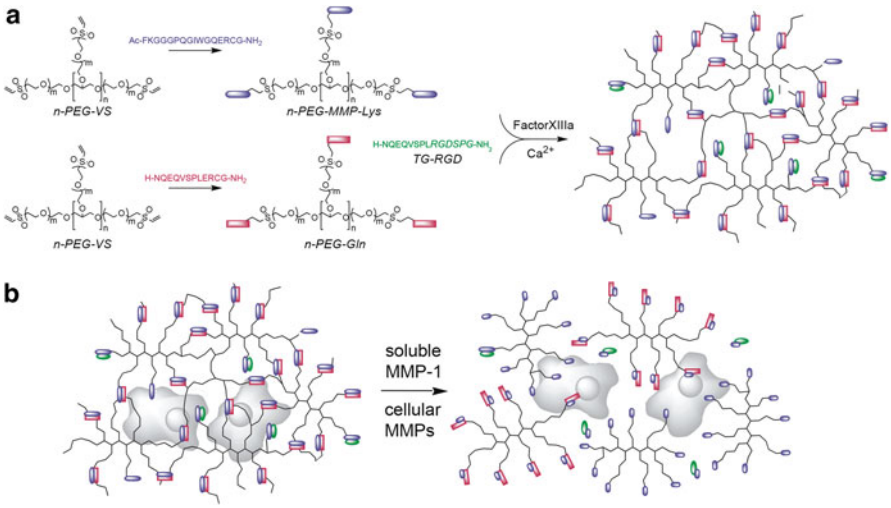

Fig. 1.3 Factor XIIIa-catalyzed PEG hydrogel formation and degradation. (**a**) The transglutaminase enzyme factor XIIIa was used to cross-link two multiarm *PEG* peptide conjugates, *n-PEG-MMP-Lys*, and *n-PEG-Gln* (here, $n = 8$), in combination with a cell adhesion peptide, *TG-Gln-RGD*, to form multifunctional synthetic hydrogels. (**b**) Gel degradation by cell-mediated proteolysis (reprinted with permission from [108])

manner (Fig. 1.3a). By engineering of the PEG backbone to contain matrix metalloproteinase (MMP) or plasmin-sensitive sites, the biomimicry of this system can be further extended (Fig. 1.3b). This platform (called TG-PEG from here on) has so far been used to elucidate the effect of physical and biochemical matrix properties on processes such as cell migration, proliferation, spreading, and angiogenesis and for creating structured microenvironments as discussed later.

Usefulness of modularity can be elucidated for example by the case of cell migration in 3D which has so far mostly been investigated in naturally occurring materials [109]. Findings from such experiments are limited in terms of studying the effect of biochemical and biophysical parameters since they cannot be decoupled from each other. For example, the effect of the ECM on the choice between proteolytic and nonproteolytic cell migration remains to be exhaustively answered [37]. Some light could be shed on the topic by using the TG-PEG hydrogels [110], which are devoid of microstructure therefore essentially nonporous for cells, as cross-linked polymers create pores in the range of tens of nanometer. By harnessing the modularity of this system in terms of protease sensitivity and stiffness, it was found that migration behavior was strongly dependent on matrix stiffness, with two regimes identified: a nonproteolytic migration mode dominating at relatively low matrix stiffness and proteolytic migration at higher stiffness. In nondegradable matrices with low stiffness, single cells could overcome the resistance of the matrix by engaging in a degradation-independent three-dimensional migration mode.

Similarly the TG-PEG system could be used for studying cell proliferation in 3D in response to selectively altered matrix characteristics [111]. To illustrate the

difference in cell behavior in naturally occurring materials and fully synthetic hydrogels, fibroblasts were studied in collagen and TG-PEG hydrogels. The main physical difference between the two systems was that the PEG gels are purely elastic, whereas collagen gels generally display viscoelastic behavior due to the physical entanglement of normally freely moving fibers. Cells are able to dislocate collagen fibers leading to predominantly physical modification of the matrix. The PEG gels on the other hand are mainly modified by biochemical processes, making it possible to systematically study such phenomena and their implications to other cellular processes, such as proliferation. By exploiting the modularity of the TG-PEG system, this study revealed that in spite of matrix sensitivity to proteases and the presence of cell integrin binding sites, proliferation in 3D was hindered by high stiffness (elastic modulus > 1,200 Pa).

1.7.2 Adhesion and Degradation Sites

Naturally occurring ECM contains numerous proteins and glycans which, dependent on the status of a tissue, are differently composed and thus provide different sets of adhesion domains. Ruoslahti et al. have found that a triple amino acid domain derived from fibronectin is sufficient for the integrin-mediated adhesion of cells [112]. Since then many cell-adhesive peptides, mostly derived from collagen, fibronectin, or laminin, to be linked into hydrogels have been described and used for the engineering of cell-instructive biomaterials (reviewed in [113]).

The polymeric backbone must provide space to cells in order to proliferate, deposit the cell's own matrix, and move. Degradability of the material can be achieved through spontaneous dissolution of the polymer as for example by the incorporation of poly(lactic acid) (PLA) within the polymer structure or the use of acryl–sulfhydryl bonds [114]. These modes of degradation are the material's autonomous properties. Materials stability is critical to appropriate tissue formation, as too fast degradation results in loss of structural and mechanical support and too slow degradation will inhibit cell, for example, cell ingrowth and function. To render materials with tunable, cell-responsive degradation properties, polypeptides derived from occurring naturally protease-sensitive sequences have been adapted and incorporated into linker molecules of the backbone [104]. Recently, a number of peptide sequences which are recognized and degraded with different efficiencies (kcat) have been described [115, 116]. The use of substrate with very well-defined degradation properties clearly will allow the fine tuning of materials properties towards specific applications.

1.7.3 Incorporation and Cell-Mediated Release of Growth Factors

Tissue development and regeneration depend on tightly coordinated spatial and temporal growth factor signals and recombinant growth factors have been widely proposed for therapeutic use in the regeneration and repair of diseased tissues.

Increased knowledge on growth factor signaling and advances in recombinant protein engineering and production have opened new possibilities is constructing artificial extracellular matrices. Strategies employed to immobilize growth factors in synthetic hydrogels are summarized in Table 1.1.

When growth factors are purely physically entrapped in the hydrogel matrix, availability for cells in space and time is determined by passive diffusion and coupled with hydrogel degradation. If not replenished in the culture medium, activity decreases over time. Diffusion can be controlled via modifications either on the hydrogel network properties or the growth factor by which the affinity to the matrix, bioactivity, stability, and bioavailability can be modified [117].

Effect of soluble factors on cells cultured in 3D can be studied in any hydrogel material, either by encapsulation to the material along with the cells or by addition to the growth medium, but for more sophisticated biomimicry, systems enabling the tethering and controlled release of growth factors are needed. Immobilization strategies allow the construction of gradients or localized areas where the factor is present, making it possible to more accurately recapitulate physiological situations. Natural ECM acts as a reservoir for growth factors from which they are released by cellular remodeling, which is often used as a release strategy in synthetic systems in addition to temporally controllable triggered release (Fig. 1.2a). In the following paragraphs, growth factor immobilization strategies for synthetic hydrogels are discussed first focusing on covalent tethering and then moving to affinity-based systems (Fig. 1.2b).

1.7.3.1 Covalent Immobilization

Covalent tethering of growth factors to synthetic or biologically derived hydrogels has been achieved by either chemical modification or genetic engineering of the factors to contain functional groups such as thiols, acrylates, azides, and Gln-tags (Table 1.2). Initial chemical conjugation approaches utilized, for example, homobifunctional PEG-based cross-linkers with terminal and primary amine selective succinimidyl groups [80, 148], which could serve both as hydrogel cross-linking entities and as means to incorporate growth factors. Another chemical conjugation strategy was based on hetero-bifunctional *N*-hydroxysuccinimide (NHS)-PEG-acrylate linker, which could be used by first modifying the factor of interest with the amine-specific NHS group reaction and subsequently coupling the acrylated biomolecules into PEG-diacrylate networks by photopolymerization [118, 119]. Also click chemistry has been successfully used for covalent immobilization of growth factors into synthetic hydrogels [123].

The downside of these broadly applicable strategies, such as the reaction of NHS with any accessible lysine or the *N*-terminus, is their lack of specificity. The exact site and number of modifications are difficult to control and may have drastic effects on the growth factor bioactivity [149]. More site-specific strategies have been realized by engineering recombinant proteins with additional cysteines as the abundance of reduced cysteines is inherently low in proteins and such modifications render them more susceptible to, for example, Michael-type reaction with vinylsulfone

Table 1.2 Strategies for immobilization and release of growth factors in synthetic hydrogels (adapted from [57])

Matrix backbone	Linker	Ligand			Release from		Reference
		Native form	Modification	Immobilization	Matrix	Linker	
PEG-DA	NHS-PEG-Acryloyl[a, b]	TGF-ß1, bFGF, EGF	Chemical	Covalent	Enz.	–	[118–121]
PEG-DA	SMC-PEG-Acryloyl[a, b]	PDGF-BB, FGF-2	Chemical	Covalent	Enz.	–	[122]
PLEOF	PEG-azide[a, b]	BMP peptide	Chemical	Covalent	Enz.	–	[123]
MAC	EDC/sulfo-NHS[a, b]	IFN-γ	Chemical	Covalent	Enz.	–	[124]
PEG-VS	–	$VEGF_{165}/VEGF_{121}$	Ligand-Cys fusion[a]	Covalent	Enz.	–	[125, 126]
PEG-TG	–	$VEGF_{121}$	Gln-Ligand fusion[a]	Covalent	Enz.	–	[127]
PEG-DA, (Hep/HA/Gtn)-SH	Heparin	VEGF, bFGF, Ang-1, HGF, KGF, PDGF-BB	–	Affinity	Enz./hydr.	Dissoc.	[50, 128–130]
PEG-DA, (Hep/CS)-SH	Heparin	bFGF	–	Affinity	Enz./hydr.	Dissoc.	[131, 132]
PEG-SBA, Hep-ADH	Heparin	VEGF		Affinity	Enz./hydr.	Dissoc.	[133]
PEG-NH2	Heparin, EDC/sulfo-NHS	FGF-2	–	Affinity	Enz.	Dissoc.	[134]
PEG-peptide, heparin	–	VEGF	–	Affinity	Enz.	Dissoc.	[135]
PEG-LMWH, $PEG\text{-}PF4_{ZIP}$	Heparin	bFGF	–	Affinity	Enz.	Dissoc.	[136]
PEG-LMWH, PEG-HIP	Heparin	bFGF	–	Affinity	Enz.	Dissoc.	[137]
PEG-SH, HMWH	Heparin	bFGF	–	Affinity	Enz.	Dissoc.	[138]

PEG-LMWH, VEGF	Heparin	VEGF	–	Affinity	Enz.	Dissoc.	[139]
PEG-DM, heparin-MA	Heparin	bFGF	–	Affinity	Enz.	Dissoc.	[140]
PEG-VS, Cys_3-peptide	Heparin	BMP-2	–	Affinity	Enz.	Dissoc.	[141]
PEG-DA	poly(AAC)-Cys-bFGF-bpa	bFGF	Cys-bFGF-bp	Affinity	Enz./hydr.	Dissoc.	[142]
PEG-TG	Gln-ZZ[a]	IL-4	Ligand–Fc fusion	Affinity	Enz.	–	[143]
PEG-TG	bead-Novo. GyrB-ZZ	PDGF-BB	Ligand–Fc fusion	Affinity	Enz.	Novo.	[144]
PEG-TG	Gln-GyrB[a]/Novo./GyrB-ZZ	FGF-7	Ligand–Fc fusion	Affinity	Enz.	Novo.	[145]
PEG-TG (Caged-Lys)		PDGF-BB, $VEGF_{121}$	Ligand–Fc fusion	Light/covalent	Enz.		[146]
PEG-TG		$VEGF_{121}$	Ligand–GyrB fusion	–	[c]		[146]
PEG-TG	$Fg\beta15–66_{(2)}$	FGF-2, PlGF-2	–	Affinity	Enz.	Dissoc.	[147]

[a]Reacting with matrix
[b]Reacting with ligand
[c]Coumermycin induced ligand dimerization
enz. enzymatic, *hydr.* hydrolyzed, *dissoc.* dissociation, *Novo.* novobiocin, *Gln* NQEQVSPL-peptide, *NHS N*-hydroxysuccinimide, *EDC N*-(3-dimethylaminopropyl)-*N′*-ethylcarbodiimide, *poly(AAC)-Cys-bFGF-bp* poly(acrylic acid) modified FGF-2 binding peptide, *PEG-NH_2* PEG-amine, *PEG-SH* PEG-thiol, *Hep* heparin, *HA* hyaluronan, *CS* chondroitinsulfate, *GEL* gelatine, *PEG-SBA N*-hydroxysuccinimidyl ester PEG-bis-butanoic acid, *$PF4_{ZIP}$* heparin binding, coiled-coil peptide, *HIP* peptide sequence from heparin interacting protein, *DM* dimethacrylate, *Cys* cysteine, *VS* vinyl sulfone, *PEG-TG* transglutaminase FXIII formed PEG hydrogel, $Fg\beta15-66_{(2)}$, *N*-terminus of the Fibrin(ogen) β-chain, *MAC* methacrylamide chitosane, *Coum.* coumermycin

groups of PEG macromers [125]. Another possibility for achieving high site specify while conserving bioactivity is employing enzymatic reactions as discussed next.

The TG-PEG system was developed having in mind the goal of a flexible and modularly designed artificial ECM allowing site-specific and stable immobilization of growth factor proteins into the gel network, without compromising the protein's bioactivity. The most straightforward way of doing this is by producing growth factors bearing a substrate for FXIIIa, as has been shown for VEGF [127]. $VEGF_{121}$ was engineered to contain the glutamine acceptor substrate NQEQVSPL, derived from the *N*-terminus of α_2-plasmin inhibitor (α_2PI_{1-8}) (termed Gln). This Gln-$VEGF_{121}$ could be covalently incorporated into the hydrogel and released in controlled manner by the cleavage of the MMP sites in the PEG backbone during cellular matrix remodeling. The ability of the matrix-bound Gln-$VEGF_{121}$ to stimulate angiogenesis was evaluated in the embryonic chick chorioallontoic membrane (CAM) assay and the response to it was found comparable to that of native, diffusible $VEGF_{121}$, indicating that this sequence-specific mode of morphogen affixation in aECM does not compromise a morphogen's activity, at least not in the case of VEGF. In contrast to conventional chemical bioconjugation schemes, the site-specificity of the enzymatic reaction gives precise control over the conformation of the immobilized molecules and results in no significant loss of its bioactivity. This may be crucial for applications involving sensitive transmembrane proteins (e.g., Notch ligands or cadherins) in order to recapitulate cell–cell interactions via aECMs.

1.7.3.2 Affinity Immobilization

In addition to covalent immobilization strategies, affinity interactions are another possibility for growth factor incorporation. These strategies take advantage of the interactions naturally occurring between growth factors and ECM components, such as heparin, chondroitin sulfate, hyaluronic acid, and fibronectin. Thus they do not require direct chemical or genetic modification of the protein offering high degree of flexibility. Synthetic hydrogels have been modified with heparin via for example EDC/sulfo-NHS chemistry [134] or with streptavidin to allow the immobilization of biotinylated factors [150]. Also recombinant affinity linkers, allowing simultaneous addition of growth factors and cells during cross-linking [143, 151], as well supramolecular peptide gels with affinity sites, have been engineered [152].

Recently a very interesting approach based on the functional domains of fibrinogen was presented [147]. Recombinantly produced heparin-binding domain of fibrin(ogen) located at the N terminus of the fibrin(ogen) β chain (Fg β) was covalently linked into TG-PEG hydrogels and then used for the immobilization of various growth factors, for example, FGF-2 and PIGF-2. Overall, interaction of the linker with 15 different growth factors were established which all displayed K_D values in the nM range. The fibrinogen fragment functionalized TG-PEG gels were successfully used to deliver growth factors into full-thickness skin wounds in mice which lead to faster wound closure and increased development of granulation tissue.

In order to develop a flexible affinity-based strategy for the conjugation of growth factors to the previously described synthetic TG-PEG platform, a linker peptide consisting of the TG-domain and two repeats of the synthetic protein A analog (Z) was designed [143]. The TG-domain of this TG-ZZ peptide can be covalently bound to the Lys-PEG component of the TG-PEG system by the factor XIII-mediated reaction. Due to the high affinity of the ZZ peptide (4.8×10^{-8} M^{-1}) to the fragment crystallizable (Fc) region of antibodies, Fc-tagged growth factors can be immobilized within the hydrogel network. Taking advantage of the high affinity of this interaction, the linker can be used to directly capture Fc-tagged proteins produced by mammalian cells encapsulated in the hydrogels. This creates a versatile platform to concentrate and purify large panels of recombinantly expressed growth factors for cell-based assays to identify novel regulators of cell behavior.

The fusion peptide Gln-ZZ was expressed in bacterial cultures and in its functionality demonstrated by capturing FITC-labeled IgG antibody from a solution into a linker containing hydrogel and retaining it throughout extensive washing. With the ultimate goal of growth factor immobilization in mind, the functionality of growth factor or cytokine-tethered hydrogels as cell-instructive matrices was demonstrated using the anti-inflammatory cytokine interleukin-4 (IL4). Protein-capture hydrogels and control hydrogels were patterned and placed in cultures of human embryonic kidney (HEK)-293 T cells expressing IL4-Fc and after washing, the activity of the captured IL-4 was demonstrated by a reporter cell line. ZZ-linker-modified hydrogels could be used for providing a reservoir of biomolecules, which can actively stimulate cellular responses, either in their matrix-immobilized form or after cell-mediated proteolytic degradation of the hydrogel in a soluble form.

1.7.4 Local 3D Structuring of Hydrogels

Homogeneous biomimetic hydrogels can only be used to address biological questions in a simplified manner, which for certain situations, such as high throughput screening platforms, can be sufficient or even desired. By creating spatially defined heterogeneous microenvironments, more sophisticated models recapitulating higher levels of biological complexity can be realized, helping to bridge the gap between current in vitro and vivo models. Bulk functionalization of synthetic hydrogels has been widely described in literature, but this alone is not sufficient for mimicking the natural ECM. Thus, efforts have been made for evolving hydrogels for cell encapsulation from physically and biochemically homogeneous materials into highly spatially defined environments structured in multiple size scales.

Heterogeneity can be introduced in 3D in terms of local biochemical composition (e.g., adhesion ligands and growth factors) or by introducing structural patterns (e.g., variation hydrogel composition, empty, or cell-filled spaces). Hydrogels with such features have been produced using techniques such as self-assembly of prefabricated building blocks (e.g., microscale hydrogels or fibers) [153–157],

casting [158], additive manufacturing (e.g., printing and layer-by-layer deposition) [159, 160], photo-patterning [161, 162], and microfluidics [163, 164]. Problems with spatial patterning of hydrogels in 3D arise from their thickness and extensive swelling.

Next, two approaches, namely the combination of printing with layer-by-layer deposition for modelling vascularized bone and electrochemical control of polymerization for creating channel structures and gradients of biomolecules, are discussed in the context of the TG-PEG system.

Generation of functional vascularized tissues remains the holy grail of tissue engineering, and in order to address related questions using in vitro models, structuring ECM-mimicking materials and cells comes into play. In the context of bone, combining the TG-PEG hydrogel system as an artificial ECM with matrix structuring technologies, namely robotic printing and layer-by-layer deposition, the role of biological constituents in the vascular bone microenvironment could be systematically evaluated [159].

Feasibility of layer-by-layer deposition of TG-PEG was demonstrated by combining 200 μm cell containing hydrogel blocks with confluent layers of cells (Fig. 1.4a). Since gel layers can be formed in the presence of cells or used as surfaces for the seeding of cells, even such a simple layering approach allows for a large variety of cell and matrix combinations. For introducing more heterogeneity with each gel layer, robotic printing platforms using a contact-spot arraying technology with a lateral precision of approximately 5 μm and robotic pipetting with a lateral precision of approximately 100 μm were used. With these systems spatially segregated hydrogel drops of ca. 100 μm of diameter and 20 μm height could be formed (Fig. 1.4a). The size of the droplets can be modified by adjusting different parameters such as the pin-head size and the amount of dispensed liquid or using repetitive printing steps.

Initially, conditions supporting the viability and spreading of osteoblasts (MC3T3-E1) and osteocytes (MLO) or blocking their migration were defined in terms of hydrogel stiffness and presentation of RGD ligand. The effect VEGF and mono-, co-, and tri-cultures on the formation of capillary like network in 3D was then assayed. Using a fully synthetic hydrogel platform, it was possible to provide evidence on the importance of single component on angiogenesis. It was demonstrated that besides the adhesion ligand RGD and the pro-angiogenic growth factor VEGF, the presence of both stromal cells appears to be critical for endothelial cells (ECs) to efficiently form tube-like structures in artificial environments.

Once the culture conditions were defined, the three cell types were assembled together to create spatially organized vascularized bone tissue-like constructs. A supportive layer of 4 % PEG hydrogel covered with a monolayer of MC3T3-E1 was used as a basis for the construct, and on top of this, human umbilical vein endothelial cells (HUVECs) were subsequently positioned in 1 μl-sized hydrolytically and proteolytically degradable PEG-acrylate gels. As PEG-acrylate degrades rapidly the drops were formed without RGD ligands to prevent high concentrations of soluble peptides which could potentially interfere with HUVEC viability. As a final step, a covering layer of PEG containing human osteocytes was added and the

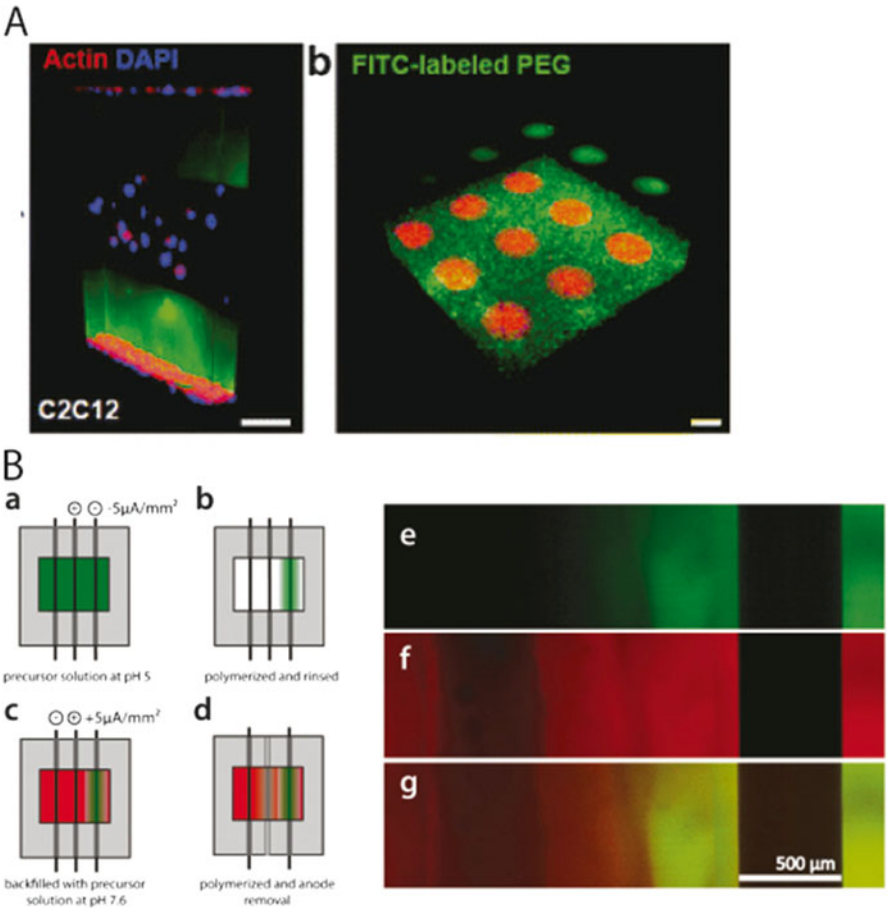

Fig. 1.4 Structured microenvironments in TG-PEG hydrogels. (**a**) Homogeneous layers of C2C12 cells and cell-containing or FITC-labeled gels (gel mass either in *green* or unstained) and different fluorescently labeled hydrogels arranged by robotic printing in defined positions on top of different layers of hydrogel (scale bar 100 µm). (**b**) Schemes depicting the production of an engineered microenvironment containing two different fluorophores using electrochemical structuring and confocal microscopic images of the resulting microenvironment. Reprinted with permission from [159, 160]

constructs were allowed to remodel for 10 days under the previously optimized conditions. Analysis of the constructs revealed a dense and interconnected network of HUVECs and preosteoblastic cells surrounding the endothelial structures.

These findings demonstrate that simultaneous patterning of matrix components, ligands, and cells to direct cellular spreading and to form artificial tissue-like constructs allows for the dissection of biological questions related to tissue remodeling and morphogenesis and their independent study in a fully controllable artificial environment.

In addition to the strategies described for biological functionalization of TG-PEG hydrogels, electrochemical polymerization has been employed for eliciting spatial control over the cross-linking in 3D [160]. This is based on the FXIII-catalyzed cross-linking reaction being pH-dependent and occurring with highest efficiency at pH 8 while being damped at more acidic or basic conditions [127]. The proteolysis of water induced by electric current was used to locally decrease (at the anode–electrolyte interface) or increase pH (at the cathode–electrolyte interface) and thereby prevent or promote hydrogel formation. This method was successfully used for creating microchannels within TG-PEG hydrogels in a PDMS mold using an anodically polarized tungsten wire as a template. By locally controlling the polymerization around the wire, it could subsequently be removed, while in absence of the current the TG-PEG hydrogel strongly adhered to the metal surface and was disrupted.

Electrochemical control of gel polymerization could also be used to form complex, locally functionalized 3D microenvironments in TG-PEG by a sequential approach (Fig. 1.4b). This was demonstrated by first polymerizing FITC functionalized gel around a cathode wire, followed by thorough washing to remove the unreacted components, and finally backfilling the mold with a TRITC functionalized gel while creating a second channel. The area between the two channels was thus functionalized with both molecules and the sides with one molecule alone. When injected into the preformed channels, various cell types such as bone-marrow-derived mesenchymal stem cells (MSCs), preosteoblasts, and fibroblasts were able to invade into the surrounding hydrogel mass, which will enable the study of cellular responses to different (graded) microenvironments. HEK cells expressing a yellow fluorescent protein (YFP) upon being exposed to IL-4 were used for demonstrating such spatial specificity of the channel surrounding microenvironments after functionalization with hydrogel bound IL-4. In conclusion, by electrochemically controlling the enzymatic cross-linking of TG-PEG hydrogels, it was possible to create spatially defined 3D microenvironments containing various tethered biomolecules and thereby control local cell functions.

Further understanding on how to best structure artificial microenvironments and automation of these procedures could lead to large-scale production of reproducible tissue-like constructs suitable for high-throughput screening approaching in vivo complexity, with yet a simple readout for evaluation.

1.8 Spatiotemporally Controllable Dynamic Microenvironments (External Control)

Native ECMs undergo tightly controlled, constant remodeling resulting in liberation of growth factors or other bioactive entities as well as changes in matrix mechanical properties. Although the above-presented synthetic hydrogel matrices have largely overcome the limitations of naturally occurring materials by handing over the control of the material's physical and biochemical properties to the scientists, they still do not

allow modulating the availability of extrinsic signaling molecules and material mechanics in time. Possible trigger mechanisms include changes in temperature [165–167], pH [22, 168], electromagnetic stimulation [169], or taking advantage of bioactive compounds [96, 170–172]. Most feasible in vitro approaches reported so far are based on light or using diffusible molecules interfering with interactions within the hydrogel, so the focus in this chapter is on such approaches. Light is an attractive candidate for spatiotemporal manipulation of hydrogels because its temporal patterning resolution can be controlled at single cell or even subcellular scale and in the visible and long-wave UV region has little effect on cell viability and behavior.

1.8.1 Dynamic Presentation of Biological Cues

Bioactive molecules such as growth factors can have cross-reactive effects on different cell types, making timing of their presentation in vivo as important as spatial control. This has promoted the development of experimenter-controlled culture matrices, in which adhesion sites and growth factors can be patterned and released on demand to change the biochemistry of the microenvironment to mimic processes such as differentiation.

Light-sensitive molecular building blocks can be attached to hydrogel networks to generate artificial ECMs in which the properties of microenvironments could be specifically modulated by light exposure [173]. Previously only small synthetic peptides have been the target of photopatterning approaches because the employed chemical cross-linking or bioconjugation reactions, using nonspecific chemistries, often damage full-length proteins. Photochemical caging strategies have emerged as a means to use light for controlling the temporal presentation of larger biological compounds without impairing their bioactivity.

Reversible presentation of biological entities has been reported based on the combination of two orthogonal, biocompatible wavelength-specific photoreactions, namely thiol-ene reaction for photocoupling and photoscission of an *o*-nitrobenzyl ether for later release from PEG hydrogels [174]. Spatial control of both reactions by controlling the introduction and removal of functional groups was achieved at a subcellular scale in 3D by focusing pulsed laser light within the hydrogel volume with resolution of 1 μm in the *x*-*y* plane and 3–5 μm in the *z*-plane. Mouse embryonic fibroblast (NIH 3 T3) cells were seeded on gels with photopatterned adhesive regions from where they could subsequently be detached by the removal of the adhesive ligand after being first allowed to adhere and spread for 24 h.

The effect of temporal ligand presentation on stem cell phenotype is an important question that could be studied by incorporation photocleavable adhesion molecules. A nitrobenzyl ether-derived moiety was acrylated by a pendant hydroxyl group [photodegradable acrylate (PDA)] and was subsequently attached with a pendant carboxylic acid to PEG-*bis*-amine to create a photocleavable cross-linking diacrylate macromer. The cross-linker was the copolymerized with PEG monoacrylate (PEGA)) by redox-initiated free radical polymerization to create photodegradable hydrogels [175].

Matrix-bound photolabile RGDS peptide was used for investigating the effect of persisting versus temporally modulated RGD environment on hMSC viability and chondrogenic differentiation. Mimicking native chondrogenic differentiation, during which fibronectin is initially produced but subsequently downregulated and replaced by glycosaminoglycans (GAGs) and type II collagen (COLII), was achieved by removing RGD sites after initial culture.

By utilizing multiple modes of cross-linking of acrylated hyaluronic acid in a sequential manner, degradability of 3D matrices could be regulated temporally [176]. During the primary polymerization step hydrogels with adhesive sites and MMP-cleavable dithiol cross-linkers were formed via an addition mechanism, which still left a portion of the acrylate groups unconsumed. At this stage the matrices were permissive to remodeling and migration but by localized light exposure (using a photomask or a focussed laser) could be further cross-linked rendering them unfavorable for such cellular functions. Robust spreading of mesenchymal stem cell was observed within the permissive areas and found to be dependent on the relative amount of each cross-linking mode whereas in highly cross-linked "inhibitory" hydrogels cells remained rounded. Such differences in cellular morphology could be useful for studying signaling mechanisms during spatially controlled differentiation of encapsulated stem cells.

Spatiotemporal regulation of biological compounds in synthetic microenvironments, trapping them in cages and subsequently uncaging them the site of interest, has been shown to allow for a nearly instantaneous manipulation of the bioactive compound concentration [177]. Small signaling molecules and chemically synthesizable peptides have been successfully caged based on chemical modification of the molecules using a photo-removable protective group. This strategy is in most cases not compatible with large proteins, such as growth factors, which require a tailored caging procedure. Also caging is often complicated due to difficulties in achieving site-specific chemical modification.

FXIII cross-linkable TG-PEG hydrogels could be rendered photosensitive by masking the active site of one of the FXIIIa substrates with a photolabile cage group [146], namely nitroveratryloxycarbonyl (Nvoc), which by its broad absorption in ultraviolet/visible around 350 nm is advantageous in terms of penetration depth and minimal DNA and biomolecule damage [177]. Caged Lys-substrates within the polymerized hydrogel network could be subsequently released enabling highly localized enzymatic biomolecule tethering. This system was exploited for light-activated enzymatic gel patterning to manipulate the behavior of live cells within the hydrogel microenvironment. 3D invasion of human MSCs was chosen as a physiologically relevant model, illustrating injury-induced cell recruitment. RGD, the recombinant fibronectin fragment FN_{9-10}, and platelet-derived growth factor B were engineered to contain the TG-peptide for cross-linking into the matrix. Microtissues of MSCs were encapsuled into MMP- and photosensitive TG-PEG hydrogels and a cuboidal pattern of uncaged TG-peptide was then created on one half of the microtissue. The enzymatically immobilized, fluorescently labeled RGD and FN_{9-10} permitted increased MSC migration within the patterned areas.

This demonstrated that light-activated enzymatic gel patterning can be exploited for manipulating the behavior of live cells in three dimensions directly in culture. The same strategy was employed on hyaluronic acid hydrogels [178].

To create a generic retain and release system applicable to any arbitrary protein with an fc-tag, a strategy based on pharmacological cage was employed [144]. The cage was formed by covalently coupling novobiocin to an epoxy-activated agarose matrix via a nucleophilic addition reaction. An adaptor protein consisting of the novobiocin-binding domain of the bacterial protein gyrase subunit B (GyrB) fused to the IgG-binding domain ZZ (derived from Staphylococcus aureus protein A) was used for anchoring proteins via an fc-tag. Protein contained in the cage could be subsequently released by addition of free novobiocin competitively inhibiting the binding between the adapter and the cage. Caging and rapid uncaging were demonstrated by regulating MSC migration out of microtissues in 3D hydrogels by controlled release of caged Fc-PDGF.

Another pharmacochemical approach based on controlling the activity of a growth factor via dimerization was used as a basis for an inducible on–off regulation for cysteine-knot growth factors such as VEGF [179]. The switch consisted of a chimeric protein with an engineered monomeric variant of the protein of interest fused to the inducible dimerization domain of the bacterial protein gyrase B (GyrB). The default state of the switch was off as the monomeric structure prohibits dimerization and thereby activation of the protein receptor. The switch could be turned on upon the addition of coumermycin which binds to GyrB, leading to dimerization of the protein and thus the activation of the receptor and downstream signaling processes. The off state can be restated by the administration of novobiocin, upon which the single coumarin ring of the novobiocin competitively inhibits binding of coumermycin to GyrB, returning the protein to its monomeric state. On–off regulation of the system was demonstrated by controlling the VEGF-induced migration of HUVECs in PEG hydrogels in 3D. As coordination of endothelial cell migration is a key component in angiogenesis, methods to study its regulation are highly valuable for both basic research and tissue engineering.

1.8.2 Mechanically Dynamic Materials

Cells embedded in the ECM of tissue encounter and respond to ECM stiffnesses in the range of 0.2–1 kPa (brain) to 30–45 kPa (osteoid). They actively exert pushing and pulling forces on their surroundings, which results on the activation of intracellular mechanotransduction pathways [180]. For example, vascular endothelial cells experience different types of flow which directs their behavior and stiffening of the ECM in the liver drives liver fibrosis. Mechanics are also tightly coupled with stem cell faith demonstrated by the finding that mesenchymal stem cells are driven towards osteogenesis by a stiffer hydrogel environment and towards adipogenesis by a softer hydrogel environment [181]. Despite the biological relevance of mechanically

dynamic systems, there are only few examples described in the literature and almost none based on synthetic hydrogels. Some work has been done on culturing cells in 2D on mechanically dynamic hydrogels which circumvents cell-induced changes in the matrix properties over time complicating the situation in 3D.

Hydrogel mechanics can be controlled for example by introducing chemical groups that can be cleaved by ultraviolet light leading to matrices that soften upon light exposure [175]. By copolymerizing photocleavable diacrylate macromer cross-linkers with PEG monoacrylate (PEGMA)), using redox-initiated free radical polymerization, photodegradable hydrogels were created. The cross-link density of hydrogel networks could be reduced (by light) in the presence of viable human mesenchymal stem cells allowing their transition from a round to elongated morphology. This same system could be used to direct cell migration by 3D patterning paths for encapsulated cells in real time.

In contrast to dynamically softening hydrogels, matrix stiffening, taking place for example during development and wound healing, might actually be a more biologically relevant phenomenon to mimic as it has been implicated to regulate many cellular processes. A sequential cross-linking approach was used to create dynamically stiffening hyaluronic acid hydrogels [182]. Methacrylate functionalized hyaluronic acid was in the first step cross-linked via a Michael-type addition reaction using dithiothreitol (DTT). The remaining initial hydrogel could be further stiffened by radical polymerization of the remaining methacrylate groups using a photoinitiator and ultraviolet light exposure. The system could be used to investigate cellular response to substrate stiffening in terms of cytoskeletal rearrangement and differentiation, though it was currently only reported on cells grown on top of the hydrogel instead of 3D.

The interaction of GyrB protein with novobiocin and coumermycin was utilized for synthesizing stimulus-responsive PEG hydrogels [145]. Thiol-containing GyrB was covalently grafted to multi-arm PEG-vinylsulfone molecules using a Michael-type addition reaction. Stable hydrogels could be formed by addition of the GyrB-dimerizing substance coumermycin. These hydrogels could again be dissolved in a dose-adjustable manner by the antibiotic novobiocin. This matrix could be used for cell growth either in vivo or in vitro, where the stimulus-responsive characteristics can be used to control the release of growth factors or for dynamic tuning of the matrix mechanical properties.

With the incorporation of RGD motifs the hydrogel could support the adhesion and growth of human primary cells derived from gingival epithelial and connective tissue. No cytotoxic effects could be observed upon gel dissolution with novobiocin, which at 50 μM concentration took place in 4 h. In order to add biological functionality with cell-instructive biomolecules like growth factors, the protein A-derived ZZ-domain was fused to GyrB (ZZ-GyrB), thereby allowing for the immobilization of proteins with an Fc-tag. Fibroblast growth factor 7 (FGF-7), a protein acting in a paracrine manner and being a key player in epithelial tissue regeneration, was used as a model protein. Fc-tagged FGF-7 could be released in a dose and time-dependable manner and it was also shown to retain its activity as demonstrated by the dose-related induction of proliferation of gingival mucosal keratinocyte.

1.9 Outlook and Needs

In the previous sections we have described some of the currently available mostly homogeneously engineered hydrogel systems to control cell function in 3D. However, morphogenetic processes (during tissue formation and regeneration) are highly orchestrated events, mastered by chemotaxis, differentiation, or proliferation of multiple cells from different lineages. These complex spatiotemporally regulated processes are driven by spatially restricted microenvironmental cues, consisting of growth factors, matrix components, and mechanical properties. In order to form 3D tissue mimetics and reproducible organoid culture systems such cues need at least to be partially recapitulated to initiate cell-autonomous tissue morphogenesis. Whereas in biologically derived, complex, and not easily amenable to engineering matrices, impressive tissue formation was observed, for fully defined hydrogels systems, optimal matrix properties for many applications still remain elusive. Clearly, much has to be learned about the function of the native ECM and to integrate more specific integrin ligands into synthetic materials. There will also be a need for more and highly specific, modular building blocks for the selective incorporation of multiple different growth factors, cross-linking elements, degradation sites, and cell adhesion sites.

Nonetheless the many existing, sophisticated materials building blocks generated in recent years provide a growing toolbox for the creation of tailor-made synthetic hydrogels and their integration with biological materials (Fig. 1.5a). Such platforms are an exciting starting point for the assembly of complex 3D structured tissue constructs by combining with emerging, highly sophisticated micromanipulation techniques such as cell and materials printing devices, microfluidics, layer-by-layer assembly (Fig. 1.5b), micromolding techniques, or preventive manufacturing. For manufacturing conditions using gel systems many critical issues will have to be solved, for example, the evaporation of water and the consequent shift in hydrogel properties (due to change in polymer cross-link density caused by increased concentrations) during printing. Also building blocks which are formed individually will likely suffer from different materials properties in the bulk and at the periphery. Such boundaries can largely influence the trafficking of cells and could restrict cell interactions and need to be carefully addressed.

Furthermore, in order to allow temporal, operator controlled, site and individual parameter-specific manipulation of the system, different building blocks would ideally respond highly specific to triggers such as light with different wave length, shift in temperature, or presence of minute quantities of small chemicals (Fig. 1.5c). Of course, improved precision of 3D culture systems must go along with the development of monitoring tools for cells and matrix components. Not only cell-based reporter systems but also high-throughput automated image acquisition and image analysis algorithm systems as well as means to understand the remodeling of the provisional matrix components and the deposition of cell´s own ECM need to be followed.

In conclusion, we believe that “advanced” cell culture models hold great promise for the establishment of physiological meaningful 3D tissue mimetics and the

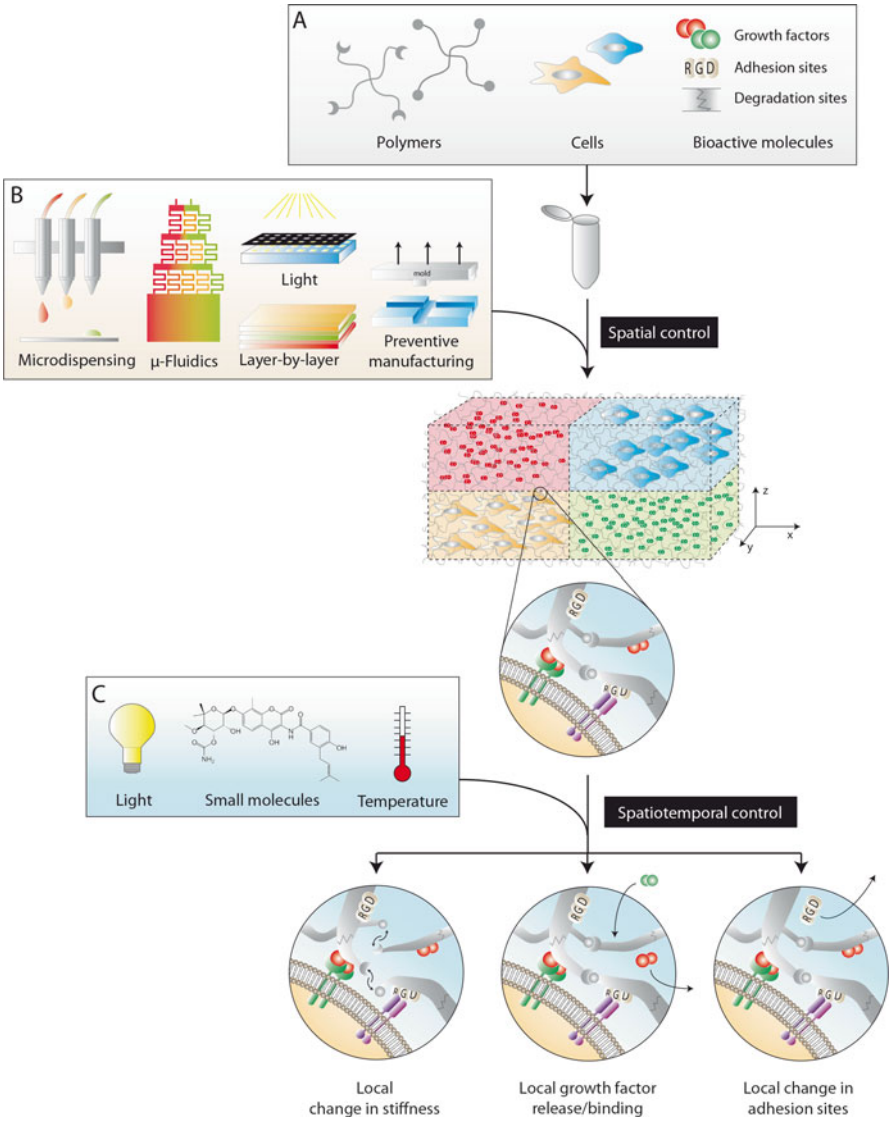

Fig. 1.5 Strategy for creating 3D tissue models starting from (**a**) combining biological elements with synthetic hydrogels, (**b**) structuring these elements, and finally (**c**) eliciting spatiotemporal control over the system

reproducible culture of organoids under highly defined conditions and amenable to investigator-controlled manipulations. Such systems in the future will not only be important intermediates between homogeneous 2D and 3D cultures and in vivo systems and thus could become tools applied to study basic biological questions as well as to validate lead compound during drug screening.

Acknowledgements We would like to express our gratitude to Dr. Philipp Lienemann for producing the illustrations and for helpful discussions.

References

1. Yamada KM, Cukierman E (2007) Modeling tissue morphogenesis and cancer in 3D. Cell 130(4):601–610
2. Griffith LG, Swartz MA (2006) Capturing complex 3D tissue physiology in vitro. Nat Rev Mol Cell Biol 7(3):211–224
3. Friedl P, Brocker EB (2000) The biology of cell locomotion within three-dimensional extracellular matrix. Cell Mol Life Sci 57(1):41–64
4. Eke I, Cordes N (2011) Radiobiology goes 3D: how ECM and cell morphology impact on cell survival after irradiation. Radiother Oncol 99(3):271–278
5. Sethi T, Rintoul RC, Moore SM, MacKinnon AC, Salter D, Choo C et al (1999) Extracellular matrix proteins protect small cell lung cancer cells against apoptosis: a mechanism for small cell lung cancer growth and drug resistance in vivo. Nat Med 5(6):662–668
6. Lee YJ, Sheu TJ, Keng PC (2005) Enhancement of radiosensitivity in H1299 cancer cells by actin-associated protein cofilin. Biochem Biophys Res Commun 335(2):286–291
7. Liu JS, Gartner ZJ (2012) Directing the assembly of spatially organized multicomponent tissues from the bottom up. Trends Cell Biol 22(12):683–691
8. Hynds RE, Giangreco A (2013) Concise review: the relevance of human stem cell-derived organoid models for epithelial translational medicine. Stem Cells 31(3):417–422
9. Frantz C, Stewart KM, Weaver VM (2010) The extracellular matrix at a glance. J Cell Sci 123(Pt 24):4195–4200
10. Cukierman E, Pankov R, Stevens DR, Yamada KM (2001) Taking cell-matrix adhesions to the third dimension. Science 294(5547):1708–1712
11. Kelm JM, Fussenegger M (2010) Scaffold-free cell delivery for use in regenerative medicine. Adv Drug Deliv Rev 62(7–8):753–764
12. Drewitz M, Helbling M, Fried N, Bieri M, Moritz W, Lichtenberg J et al (2011) Towards automated production and drug sensitivity testing using scaffold-free spherical tumor microtissues. Biotechnol J 6(12):1488–1496
13. Rimann M, Graf-Hausner U (2012) Synthetic 3D multicellular systems for drug development. Curr Opin Biotechnol 23(5):803–809
14. Kelm JM, Djonov V, Hoerstrup SP, Guenter CI, Ittner LM, Greve F et al (2006) Tissue-transplant fusion and vascularization of myocardial microtissues and macrotissues implanted into chicken embryos and rats. Tissue Eng 12(9):2541–2553
15. Stevens KR, Ungrin MD, Schwartz RE, Ng S, Carvalho B, Christine KS et al (2013) InVERT molding for scalable control of tissue microarchitecture. Nat Commun 4:1847
16. L'Heureux N, Paquet S, Labbe R, Germain L, Auger FA (1998) A completely biological tissue-engineered human blood vessel. FASEB J 12(1):47–56
17. McAllister TN, Maruszewski M, Garrido SA, Wystrychowski W, Dusserre N, Marini A et al (2009) Effectiveness of haemodialysis access with an autologous tissue-engineered vascular graft: a multicentre cohort study. Lancet 373(9673):1440–1446
18. Gauvin R, Ahsan T, Larouche D, Levesque P, Dube J, Auger FA et al (2010) A novel single-step self-assembly approach for the fabrication of tissue-engineered vascular constructs. Tissue Eng Part A 16(5):1737–1747
19. Bourget JM, Gauvin R, Larouche D, Lavoie A, Labbe R, Auger FA et al (2012) Human fibroblast-derived ECM as a scaffold for vascular tissue engineering. Biomaterials 33(36):9205–9213
20. Guillemette MD, Gauvin R, Perron C, Labbe R, Germain L, Auger FA (2010) Tissue-engineered vascular adventitia with vasa vasorum improves graft integration and vascularization through inosculation. Tissue Eng Part A 16(8):2617–2626

21. Elloumi-Hannachi I, Yamato M, Okano T (2010) Cell sheet engineering: a unique nanotechnology for scaffold-free tissue reconstruction with clinical applications in regenerative medicine. J Intern Med 267(1):54–70
22. Guillaume-Gentil O, Semenov OV, Zisch AH, Zimmermann R, Voros J, Ehrbar M (2011) pH-controlled recovery of placenta-derived mesenchymal stem cell sheets. Biomaterials 32(19):4376–4384
23. Ide T, Nishida K, Yamato M, Sumide T, Utsumi M, Nozaki T et al (2006) Structural characterization of bioengineered human corneal endothelial cell sheets fabricated on temperature-responsive culture dishes. Biomaterials 27(4):607–614
24. Murakami D, Yamato M, Nishida K, Ohki T, Takagi R, Yang J et al (2006) The effect of micropores in the surface of temperature-responsive culture inserts on the fabrication of transplantable canine oral mucosal epithelial cell sheets. Biomaterials 27(32):5518–5523
25. Elloumi Hannachi I, Itoga K, Kumashiro Y, Kobayashi J, Yamato M, Okano T (2009) Fabrication of transferable micropatterned-co-cultured cell sheets with microcontact printing. Biomaterials 30(29):5427–5432
26. Sekine H, Shimizu T, Sakaguchi K, Dobashi I, Wada M, Yamato M et al (2013) In vitro fabrication of functional three-dimensional tissues with perfusable blood vessels. Nat Commun 4:1399
27. Langer R, Vacanti JP (1993) Tissue engineering. Science 260(5110):920–926
28. Couto DS, Hong Z, Mano JF (2009) Development of bioactive and biodegradable chitosan-based injectable systems containing bioactive glass nanoparticles. Acta Biomater 5(1):115–123
29. Peppas NA, Huang Y, Torres-Lugo M, Ward JH, Zhang J (2000) Physicochemical foundations and structural design of hydrogels in medicine and biology. Annu Rev Biomed Eng 2:9–29
30. Lee KY, Mooney DJ (2001) Hydrogels for tissue engineering. Chem Rev 101(7):1869–1880
31. Clevers H, Batlle E (2013) SnapShot: the intestinal crypt. Cell 152(5):1198.e2
32. Vidi P-A, Bissell MJ, Lelièvre SA (2013) Three-dimensional culture of human breast epithelial cells: the how and the why. In: Epithelial cell culture protocols. Springer, New York, pp 193–219
33. Kleinman HK, Martin GR (eds) (2005) Matrigel: basement membrane matrix with biological activity, Seminars in cancer biology. Elsevier, Amsterdam
34. Sato T, Vries RG, Snippert HJ, van de Wetering M, Barker N, Stange DE et al (2009) Single Lgr5 stem cells build crypt villus structures in vitro without a mesenchymal niche. Nature 459(7244):262–265
35. Lanza R, Langer R, Vacanti JP (2011) Principles of tissue engineering. Academic, New York
36. Braziulis E, Diezi M, Biedermann T, Pontiggia L, Schmucki M, Hartmann-Fritsch F et al (2012) Modified plastic compression of collagen hydrogels provides an ideal matrix for clinically applicable skin substitutes. Tissue Eng Part C Methods 18(6):464–474
37. Sabeh F, Shimizu-Hirota R, Weiss SJ (2009) Protease-dependent versus -independent cancer cell invasion programs: three-dimensional amoeboid movement revisited. J Cell Biol 185(1):11–19
38. Boublik J, Park H, Radisic M, Tognana E, Chen F, Pei M et al (2005) Mechanical properties and remodeling of hybrid cardiac constructs made from heart cells, fibrin, and biodegradable, elastomeric knitted fabric. Tissue Eng 11(7–8):1122–1132
39. Smidsrød O (1990) Alginate as immobilization matrix for cells. Trends Biotechnol 8:71–78
40. Rowley JA, Madlambayan G, Mooney DJ (1999) Alginate hydrogels as synthetic extracellular matrix materials. Biomaterials 20(1):45–53
41. Sun J, Tan H (2013) Alginate-based biomaterials for regenerative medicine applications. Materials 6(4):1285–1309
42. Laurent TC, Fraser J (1992) Hyaluronan. FASEB J 6(7):2397–2404
43. Roughley PJ, Lee ER (1994) Cartilage proteoglycans: structure and potential functions. Microsc Res Tech 28(5):385–397
44. Allison DD, Grande-Allen KJ (2006) Review. Hyaluronan: a powerful tissue engineering tool. Tissue Eng 12(8):2131–2140

45. Lesley J, Hyman R, Kincade PW (1993) CD44 and its interaction with extracellular matrix. Adv Immunol 54:271–335
46. Prestwich GD, Marecak DM, Marecek JF, Vercruysse KP, Ziebell MR (1998) Controlled chemical modification of hyaluronic acid: synthesis, applications, and biodegradation of hydrazide derivatives. J Control Release 53(1):93–103
47. van Wachem PB, van Luyn MJ, Olde Damink LH, Dijkstra PJ, Feijen J, Nieuwenhuis P (1994) Tissue regenerating capacity of carbodiimide-crosslinked dermal sheep collagen during repair of the abdominal wall. Int J Artif Organs 17(4):230–239
48. Lorentz KM, Kontos S, Frey P, Hubbell JA (2011) Engineered aprotinin for improved stability of fibrin biomaterials. Biomaterials 32(2):430–438
49. Wissink MJ, Beernink R, Poot AA, Engbers GH, Beugeling T, van Aken WG et al (2000) Improved endothelialization of vascular grafts by local release of growth factor from heparinized collagen matrices. J Control Release 64(1–3):103–114
50. Pike DB, Cai S, Pomraning KR, Firpo MA, Fisher RJ, Shu XZ et al (2006) Heparin-regulated release of growth factors in vitro and angiogenic response in vivo to implanted hyaluronan hydrogels containing VEGF and bFGF. Biomaterials 27(30):5242–5251
51. Sakiyama-Elbert SE, Hubbell JA (2000) Development of fibrin derivatives for controlled release of heparin-binding growth factors. J Control Release 65(3):389–402
52. Sakiyama SE, Schense JC, Hubbell JA (1999) Incorporation of heparin-binding peptides into fibrin gels enhances neurite extension: an example of designer matrices in tissue engineering. FASEB J 13(15):2214–2224
53. Martino MM, Hubbell JA (2010) The 12th–14th type III repeats of fibronectin function as a highly promiscuous growth factor-binding domain. FASEB J 24(12):4711–4721
54. Zisch AH, Schenk U, Schense JC, Sakiyama-Elbert SE, Hubbell JA (2001) Covalently conjugated VEGF–fibrin matrices for endothelialization. J Control Release 72(1–3):101–113
55. Schmoekel HG, Weber FE, Schense JC, Gratz KW, Schawalder P, Hubbell JA (2005) Bone repair with a form of BMP-2 engineered for incorporation into fibrin cell ingrowth matrices. Biotechnol Bioeng 89(3):253–262
56. Lorentz KM, Yang L, Frey P, Hubbell JA (2012) Engineered insulin-like growth factor-1 for improved smooth muscle regeneration. Biomaterials 33(2):494–503
57. Lienemann PS, Lutolf MP, Ehrbar M (2012) Biomimetic hydrogels for controlled biomolecule delivery to augment bone regeneration. Adv Drug Deliv Rev 64(12):1078–1089
58. Sakiyama-Elbert SE, Hubbell JA (2000) Controlled release of nerve growth factor from a heparin-containing fibrin-based cell ingrowth matrix. J Control Release 69(1):149–158
59. Johnson PJ, Parker SR, Sakiyama-Elbert SE (2010) Fibrin-based tissue engineering scaffolds enhance neural fiber sprouting and delay the accumulation of reactive astrocytes at the lesion in a subacute model of spinal cord injury. J Biomed Mater Res Pt A 92(1):152–163
60. Johnson PJ, Tatara A, Shiu A, Sakiyama-Elbert SE (2010) Controlled release of neurotrophin-3 and platelet derived growth factor from fibrin scaffolds containing neural progenitor cells enhances survival and differentiation into neurons in a subacute model of SCI. Cell Transplant 19(1):89
61. Taylor SJ, McDonald JW III, Sakiyama-Elbert SE (2004) Controlled release of neurotrophin-3 from fibrin gels for spinal cord injury. J Control Release 98(2):281–294
62. Taylor SJ, Rosenzweig ES, McDonald JW III, Sakiyama-Elbert SE (2006) Delivery of neurotrophin-3 from fibrin enhances neuronal fiber sprouting after spinal cord injury. J Control Release 113(3):226–235
63. Taylor SJ, Sakiyama-Elbert SE (2006) Effect of controlled delivery of neurotrophin-3 from fibrin on spinal cord injury in a long term model. J Control Release 116(2):204–210
64. Sakiyama-Elbert SE, Das R, Gelberman RH, Harwood F, Amiel D, Thomopoulos S (2008) Controlled-release kinetics and biologic activity of platelet-derived growth factor-BB for use in flexor tendon repair. J Hand Surgery 33(9):1548–1557
65. Thomopoulos S, Zaegel M, Das R, Harwood FL, Silva MJ, Amiel D et al (2007) PDGF-BB released in tendon repair using a novel delivery system promotes cell proliferation and collagen remodeling. J Orthop Res 25(10):1358–1368

66. Wissink M, Beernink R, Scharenborg N, Poot A, Engbers G, Beugeling T et al (2000) Endothelial cell seeding of (heparinized) collagen matrices: effects of bFGF pre-loading on proliferation (after low density seeding) and pro-coagulant factors. J Control Release 67(2):141–155
67. Grieb G, Groger A, Piatkowski A, Markowicz M, Steffens G, Pallua N (2009) Tissue substitutes with improved angiogenic capabilities: an in vitro investigation with endothelial cells and endothelial progenitor cells. Cells Tissues Organs 191(2):96–104
68. Markowicz M, Heitland A, Steffens G, Pallua N (2005) Effects of modified collagen matrices on human umbilical vein endothelial cells. Int J Artif Organs 28(12):1251
69. Steffens G, Yao C, Prevel P, Markowicz M, Schenck P, Noah E et al (2004) Modulation of angiogenic potential of collagen matrices by covalent incorporation of heparin and loading with vascular endothelial growth factor. Tissue Eng 10(9–10):1502–1509
70. Van Wachem P, Plantinga J, Wissink M, Beernink R, Poot A, Engbers G et al (2001) In vivo biocompatibility of carbodiimide-crosslinked collagen matrices: effects of crosslink density, heparin immobilization, and bFGF loading. J Biomed Mater Res 55(3):368–378
71. Wissink M, Beernink R, Pieper J, Poot A, Engbers G, Beugeling T et al (2001) Binding and release of basic fibroblast growth factor from heparinized collagen matrices. Biomaterials 22(16):2291–2299
72. Bladergroen BA, Siebum B, Siebers-Vermeulen KG, Van Kuppevelt TH, Poot AA, Feijen J et al (2008) In vivo recruitment of hematopoietic cells using stromal cell–derived factor 1 alpha–loaded heparinized three-dimensional collagen scaffolds. Tissue Eng Part A 15(7):1591–1599
73. Martino MM, Tortelli F, Mochizuki M, Traub S, Ben-David D, Kuhn GA et al (2011) Engineering the growth factor microenvironment with fibronectin domains to promote wound and bone tissue healing. Sci Transl Med 3(100):100ra89
74. Zhao W, Han Q, Lin H, Sun W, Gao Y, Zhao Y et al (2008) Human basic fibroblast growth factor fused with Kringle4 peptide binds to a fibrin scaffold and enhances angiogenesis. Tissue Eng Part A 15(5):991–998
75. Zhao W, Han Q, Lin H, Gao Y, Sun W, Zhao Y et al (2008) Improved neovascularization and wound repair by targeting human basic fibroblast growth factor (bFGF) to fibrin. J Mol Med 86(10):1127–1138
76. Yang Y, Zhao Y, Chen B, Han Q, Sun W, Xiao Z et al (2009) Collagen-binding human epidermal growth factor promotes cellularization of collagen scaffolds. Tissue Eng Part A 15(11):3589–3596
77. Sun W, Lin H, Xie H, Chen B, Zhao W, Han Q et al (2007) Collagen membranes loaded with collagen-binding human PDGF-BB accelerate wound healing in a rabbit dermal ischemic ulcer model. Growth Factors 25(5):309–318
78. Han Q, Sun W, Lin H, Zhao W, Gao Y, Zhao Y et al (2009) Linear ordered collagen scaffolds loaded with collagen-binding brain-derived neurotrophic factor improve the recovery of spinal cord injury in rats. Tissue Eng Part A 15(10):2927–2935
79. Bentz H, Schroeder J, Estridge T (1998) Improved local delivery of TGF-β2 by binding to injectable fibrillar collagen via difunctional polyethylene glycol. J Biomed Mater Res 39(4):539–548
80. Koch S, Yao C, Grieb G, Prevel P, Noah EM, Steffens GC (2006) Enhancing angiogenesis in collagen matrices by covalent incorporation of VEGF. J Mater Sci Mater Med 17(8):735–741
81. Shen YH, Shoichet MS, Radisic M (2008) Vascular endothelial growth factor immobilized in collagen scaffold promotes penetration and proliferation of endothelial cells. Acta Biomater 4(3):477–489
82. Geer DJ, Swartz DD, Andreadis ST (2005) Biomimetic delivery of keratinocyte growth factor upon cellular demand for accelerated wound healing in vitro and in vivo. Am J Pathol 167(6):1575–1586
83. Zhang G, Nakamura Y, Wang X, Hu Q, Suggs LJ, Zhang J (2007) Controlled release of stromal cell-derived factor-1alpha in situ increases c-kit+cell homing to the infarcted heart. Tissue Eng 13(8):2063–2071

84. Sakiyama-Elbert SE, Panitch A, Hubbell JA (2001) Development of growth factor fusion proteins for cell-triggered drug delivery. FASEB J 15(7):1300–1302
85. Ehrbar M, Djonov VG, Schnell C, Tschanz SA, Martiny-Baron G, Schenk U et al (2004) Cell-demanded liberation of VEGF121 from fibrin implants induces local and controlled blood vessel growth. Circ Res 94(8):1124–1132
86. Ehrbar M, Metters A, Zammaretti P, Hubbell JA, Zisch AH (2005) Endothelial cell proliferation and progenitor maturation by fibrin-bound VEGF variants with differential susceptibilities to local cellular activity. J Control Release 101(1):93–109
87. Ehrbar M, Zeisberger SM, Raeber GP, Hubbell JA, Schnell C, Zisch AH (2008) The role of actively released fibrin-conjugated VEGF for VEGF receptor 2 gene activation and the enhancement of angiogenesis. Biomaterials 29(11):1720–1729
88. Weber CC, Cai H, Ehrbar M, Kubota H, Martiny-Baron G, Weber W et al (2005) Effects of protein and gene transfer of the angiopoietin-1 fibrinogen-like receptor-binding domain on endothelial and vessel organization. J Biol Chem 280(23):22445–22453
89. Zisch AH, Zeisberger SM, Ehrbar M, Djonov V, Weber CC, Ziemiecki A et al (2004) Engineered fibrin matrices for functional display of cell membrane-bound growth factor-like activities: study of angiogenic signaling by ephrin-B2. Biomaterials 25(16):3245–3257
90. Hall H, Djonov V, Ehrbar M, Hoechli M, Hubbell JA (2004) Heterophilic interactions between cell adhesion molecule L1 and αv β3-integrin induce HUVEC process extension in vitro and angiogenesis in vivo. Angiogenesis 7(3):213–223
91. Lühmann T, Hänseler P, Grant B, Hall H (2009) The induction of cell alignment by covalently immobilized gradients of the 6th Ig-like domain of cell adhesion molecule L1 in 3D-fibrin matrices. Biomaterials 30(27):4503–4512
92. Pittier R, Sauthier F, Hubbell JA, Hall H (2005) Neurite extension and in vitro myelination within three-dimensional modified fibrin matrices. J Neurobiol 63(1):1–14
93. Arrighi I, Mark S, Alvisi M, von Rechenberg B, Hubbell JA, Schense JC (2009) Bone healing induced by local delivery of an engineered parathyroid hormone prodrug. Biomaterials 30(9):1763–1771
94. Martino MM, Briquez PS, Guc E, Tortelli F, Kilarski WW, Metzger S et al (2014) Growth factors engineered for super-affinity to the extracellular matrix enhance tissue healing. Science 343(6173):885–888
95. Largo RA, Ramakrishnan VM, Marschall JS, Ziogas A, Banfi A, Eberli D et al (2014) Long-term biostability and bioactivity of "fibrin linked" VEGF(121) in vitro and in vivo. Biomater Sci-Uk 2(4):581–590
96. Ehrbar M, Schoenmakers R, Christen EH, Fussenegger M, Weber W (2008) Drug-sensing hydrogels for the inducible release of biopharmaceuticals. Nat Mater 7(10):800–804
97. Peppas N (2004) Devices based on intelligent biopolymers for oral protein delivery. Int J Pharm 277(1):11–17
98. Schmaljohann D (2006) Thermo-and pH-responsive polymers in drug delivery. Adv Drug Deliv Rev 58(15):1655–1670
99. Chen G, Hoffman AS (1995) Graft copolymers that exhibit temperature-induced phase transitions over a wide range of pH. Nature 373(6509):49–52
100. Bryant SJ, Nuttelman CR, Anseth KS (2000) Cytocompatibility of UV and visible light photoinitiating systems on cultured NIH/3 T3 fibroblasts in vitro. J Biomater Sci Polym Ed 11(5):439–457
101. Fairbanks BD, Schwartz MP, Bowman CN, Anseth KS (2009) Photoinitiated polymerization of PEG-diacrylate with lithium phenyl-2, 4, 6-trimethylbenzoylphosphinate: polymerization rate and cytocompatibility. Biomaterials 30(35):6702–6707
102. Hu B-H, Su J, Messersmith PB (2009) Hydrogels cross-linked by native chemical ligation. Biomacromolecules 10(8):2194–2200
103. Takahashi A, Suzuki Y, Suhara T, Omichi K, Shimizu A, Hasegawa K et al (2013) In situ cross-linkable hydrogel of hyaluronan produced via copper-free click chemistry. Biomacromolecules 14(10):3581–3588

104. Lutolf MP, Lauer-Fields JL, Schmoekel HG, Metters AT, Weber FE, Fields GB et al (2003) Synthetic matrix metalloproteinase-sensitive hydrogels for the conduction of tissue regeneration: engineering cell-invasion characteristics. Proc Natl Acad Sci USA 100(9):5413–5418
105. Deforest CA, Sims EA, Anseth KS (2010) Peptide-functionalized click hydrogels with independently tunable mechanics and chemical functionality for 3D cell CULTURE. Chem Mater 22(16):4783–4790
106. Jung JP, Moyano JV, Collier JH (2011) Multifactorial optimization of endothelial cell growth using modular synthetic extracellular matrices. Integr Biol (Camb) 3(3):185–196
107. Tong X, Yang F (2014) Engineering interpenetrating network hydrogels as biomimetic cell niche with independently tunable biochemical and mechanical properties. Biomaterials 35(6):1807–1815
108. Ehrbar M, Rizzi SC, Schoenmakers RG, Miguel BS, Hubbell JA, Weber FE et al (2007) Biomolecular hydrogels formed and degraded via site-specific enzymatic reactions. Biomacromolecules 8(10):3000–3007
109. Friedl P, Wolf K (2010) Plasticity of cell migration: a multiscale tuning model. J Cell Biol 188(1):11–19
110. Ehrbar M, Sala A, Lienemann P, Ranga A, Mosiewicz K, Bittermann A et al (2011) Elucidating the role of matrix stiffness in 3D cell migration and remodeling. Biophys J 100(2):284–293
111. Bott K, Upton Z, Schrobback K, Ehrbar M, Hubbell JA, Lutolf MP et al (2010) The effect of matrix characteristics on fibroblast proliferation in 3D gels. Biomaterials 31(32):8454–8464
112. Pierschbacher MD, Ruoslahti E (1984) Cell attachment activity of fibronectin can be duplicated by small synthetic fragments of the molecule. Nature 309(5963):30–33
113. Zhu J (2010) Bioactive modification of poly(ethylene glycol) hydrogels for tissue engineering. Biomaterials 31(17):4639–4656
114. Kohn J, Langer R, Ratner B, Hoffman A, Schoen F, Lemons J (1996) Biomaterials science: an introduction to materials in medicine. Academic, San Diego, pp 64–73
115. Patterson J, Hubbell JA (2010) Enhanced proteolytic degradation of molecularly engineered PEG hydrogels in response to MMP-1 and MMP-2. Biomaterials 31(30):7836–7845
116. Patterson J, Hubbell JA (2011) SPARC-derived protease substrates to enhance the plasmin sensitivity of molecularly engineered PEG hydrogels. Biomaterials 32(5):1301–1310
117. Mehta M, Schmidt-Bleek K, Duda GN, Mooney DJ (2012) Biomaterial delivery of morphogens to mimic the natural healing cascade in bone. Adv Drug Deliv Rev 64(12):1257–1276
118. DeLong SA, Moon JJ, West JL (2005) Covalently immobilized gradients of bFGF on hydrogel scaffolds for directed cell migration. Biomaterials 26(16):3227–3234
119. Saik JE, Gould DJ, Keswani AH, Dickinson ME, West JL (2011) Biomimetic hydrogels with immobilized ephrinA1 for therapeutic angiogenesis. Biomacromolecules 12(7):2715–2722
120. Mann BK, Schmedlen RH, West JL (2001) Tethered-TGF- β increases extracellular matrix production of vascular smooth muscle cells. Biomaterials 22(5):439–444
121. Gobin AS, West JL (2003) Effects of epidermal growth factor on fibroblast migration through biomimetic hydrogels. Biotechnol Prog 19(6):1781–1785
122. Saik JE, Gould DJ, Watkins EM, Dickinson ME, West JL (2011) Covalently immobilized platelet-derived growth factor-BB promotes angiogenesis in biomimetic poly (ethylene glycol) hydrogels. Acta Biomater 7(1):133–143
123. He X, Ma J, Jabbari E (2008) Effect of grafting RGD and BMP-2 protein-derived peptides to a hydrogel substrate on osteogenic differentiation of marrow stromal cells. Langmuir 24(21):12508–12516
124. Leipzig ND, Xu C, Zahir T, Shoichet MS (2010) Functional immobilization of interferon-gamma induces neuronal differentiation of neural stem cells. J Biomed Mater Res A 93(2):625–633
125. Zisch AH, Lutolf MP, Ehrbar M, Raeber GP, Rizzi SC, Davies N et al (2003) Cell-demanded release of VEGF from synthetic, biointeractive cell ingrowth matrices for vascularized tissue growth. FASEB J 17(15):2260–2262

126. Seliktar D, Zisch A, Lutolf M, Wrana J, Hubbell J (2004) MMP-2 sensitive, VEGF-bearing bioactive hydrogels for promotion of vascular healing. J Biomed Mater Res A 68(4):704–716
127. Ehrbar M, Rizzi SC, Hlushchuk R, Djonov V, Zisch AH, Hubbell JA et al (2007) Enzymatic formation of modular cell-instructive fibrin analogs for tissue engineering. Biomaterials 28(26):3856–3866
128. Riley CM, Fuegy PW, Firpo MA, Zheng Shu X, Prestwich GD, Peattie RA (2006) Stimulation of in vivo angiogenesis using dual growth factor-loaded crosslinked glycosaminoglycan hydrogels. Biomaterials 27(35):5935–5943
129. Zhao J, Zhang N, Prestwich GD, Wen X (2008) Recruitment of endogenous stem cells for tissue repair. Macromol Biosci 8(9):836–842
130. Hosack LW, Firpo MA, Scott JA, Prestwich GD, Peattie RA (2008) Microvascular maturity elicited in tissue treated with cytokine-loaded hyaluronan-based hydrogels. Biomaterials 29(15):2336–2347
131. Liu Y, Cai S, Shu XZ, Shelby J, Prestwich GD (2007) Release of basic fibroblast growth factor from a crosslinked glycosaminoglycan hydrogel promotes wound healing. Wound Repair Regen 15(2):245–251
132. Cai S, Liu Y, Zheng Shu X, Prestwich GD (2005) Injectable glycosaminoglycan hydrogels for controlled release of human basic fibroblast growth factor. Biomaterials 26(30):6054–6067
133. Tae G, Scatena M, Stayton PS, Hoffman AS (2006) PEG-cross-linked heparin is an affinity hydrogel for sustained release of vascular endothelial growth factor. J Biomater Sci Polym Ed 17(1–2):187–197
134. Freudenberg U, Hermann A, Welzel PB, Stirl K, Schwarz SC, Grimmer M et al (2009) A star-PEG-heparin hydrogel platform to aid cell replacement therapies for neurodegenerative diseases. Biomaterials 30(28):5049–5060
135. Tsurkan MV, Chwalek K, Prokoph S, Zieris A, Levental KR, Freudenberg U et al (2013) Defined polymer-peptide conjugates to form cell-instructive starPEG-heparin matrices in situ. Adv Mater 25(18):2606–2610
136. Zhang L, Furst EM, Kiick KL (2006) Manipulation of hydrogel assembly and growth factor delivery via the use of peptide–polysaccharide interactions. J Control Release 114(2):130–142
137. Yamaguchi N, Kiick KL (2005) Polysaccharide-poly (ethylene glycol) star copolymer as a scaffold for the production of bioactive hydrogels. Biomacromolecules 6(4):1921–1930
138. Nie T, Baldwin A, Yamaguchi N, Kiick KL (2007) Production of heparin-functionalized hydrogels for the development of responsive and controlled growth factor delivery systems. J Control Release 122(3):287–296
139. Yamaguchi N, Zhang L, Chae B-S, Palla CS, Furst EM, Kiick KL (2007) Growth factor mediated assembly of cell receptor-responsive hydrogels. J Am Chem Soc 129(11):3040–3041
140. Benoit DS, Anseth KS (2005) Heparin functionalized PEG gels that modulate protein adsorption for hMSC adhesion and differentiation. Acta Biomater 1(4):461–470
141. Pratt AB, Weber FE, Schmoekel HG, Müller R, Hubbell JA (2004) Synthetic extracellular matrices for in situ tissue engineering. Biotechnol Bioeng 86(1):27–36
142. Lin CC, Anseth KS (2009) Controlling affinity binding with peptide-functionalized poly (ethylene glycol) hydrogels. Adv Funct Mater 19(14):2325–2331
143. Lienemann PS, Karlsson M, Sala A, Wischhusen HM, Weber FE, Zimmermann R et al (2013) A versatile approach to engineering biomolecule-presenting cellular microenvironments. Adv Healthc Mater 2(2):292–296
144. Karlsson M, Lienemann PS, Sprossmann N, Heilmann K, Brummer T, Lutolf MP et al (2013) A generic strategy for pharmacological caging of growth factors for tissue engineering. Chem Commun (Camb) 49(53):5927–5929
145. Gubeli RJ, Laird D, Ehrbar M, Ritter BS, Steinberg T, Tomakidi P et al (2013) Pharmacologically tunable polyethylene-glycol-based cell growth substrate. Acta Biomater 9(9):8272–8278

146. Mosiewicz KA, Kolb L, van der Vlies AJ, Martino MM, Lienemann PS, Hubbell JA et al (2013) In situ cell manipulation through enzymatic hydrogel photopatterning. Nat Mater 12(11):1072–1078
147. Martino MM, Briquez PS, Ranga A, Lutolf MP, Hubbell JA (2013) Heparin-binding domain of fibrin(ogen) binds growth factors and promotes tissue repair when incorporated within a synthetic matrix. Proc Natl Acad Sci 110(12):4563–4568
148. Bentz H, Schroeder JA, Estridge TD (1998) Improved local delivery of TGF-beta2 by binding to injectable fibrillar collagen via difunctional polyethylene glycol. J Biomed Mater Res 39(4):539–548
149. Veronese FM (2001) Peptide and protein PEGylation: a review of problems and solutions. Biomaterials 22(5):405–417
150. Moriyama K, Minamihata K, Wakabayashi R, Goto M, Kamiya N (2013) Enzymatic preparation of streptavidin-immobilized hydrogel using a phenolated linear poly(ethylene glycol). Biochem Eng J 76:37–42
151. Martino MM, Briquez PS, Ranga A, Lutolf MP, Hubbell JA (2013) Heparin-binding domain of fibrin(ogen) binds growth factors and promotes tissue repair when incorporated within a synthetic matrix. Proc Natl Acad Sci USA 110(12):4563–4568
152. Shah RN, Shah NA, Del Rosario Lim MM, Hsieh C, Nuber G, Stupp SI (2010) Supramolecular design of self-assembling nanofibers for cartilage regeneration. Proc Natl Acad Sci USA 107(8):3293–3298
153. Chen AA, Underhill GH, Bhatia SN (2010) Multiplexed, high-throughput analysis of 3D microtissue suspensions. Integr Biol (Camb) 2(10):517–527
154. Xu F, Wu CA, Rengarajan V, Finley TD, Keles HO, Sung Y et al (2011) Three-dimensional magnetic assembly of microscale hydrogels. Adv Mater 23(37):4254–4260
155. Eng G, Lee BW, Parsa H, Chin CD, Schneider J, Linkov G et al (2013) Assembly of complex cell microenvironments using geometrically docked hydrogel shapes. Proc Natl Acad Sci USA 110(12):4551–4556
156. Leong MF, Toh JK, Du C, Narayanan K, Lu HF, Lim TC et al (2013) Patterned prevascularised tissue constructs by assembly of polyelectrolyte hydrogel fibres. Nat Commun 4:2353
157. Fernandez JG, Khademhosseini A (2010) Micro-masonry: construction of 3D structures by microscale self-assembly. Adv Mater 22(23):2538–2541
158. Miller JS, Stevens KR, Yang MT, Baker BM, Nguyen DH, Cohen DM et al (2012) Rapid casting of patterned vascular networks for perfusable engineered three-dimensional tissues. Nat Mater 11(9):768–774
159. Sala A, Hanseler P, Ranga A, Lutolf MP, Voros J, Ehrbar M et al (2011) Engineering 3D cell instructive microenvironments by rational assembly of artificial extracellular matrices and cell patterning. Integr Biol (Camb) 3(11):1102–1111
160. Milleret V, Simona BR, Lienemann PS, Voros J, Ehrbar M (2014) Electrochemical control of the enzymatic polymerization of PEG hydrogels: formation of spatially controlled biological microenvironments. Adv Healthc Mater 3:508–514
161. Chan V, Zorlutuna P, Jeong JH, Kong H, Bashir R (2010) Three-dimensional photopatterning of hydrogels using stereolithography for long-term cell encapsulation. Lab Chip 10(16):2062–2070
162. Wylie RG, Ahsan S, Aizawa Y, Maxwell KL, Morshead CM, Shoichet MS (2011) Spatially controlled simultaneous patterning of multiple growth factors in three-dimensional hydrogels. Nat Mater 10(10):799–806
163. Cosson S, Allazetta S, Lutolf MP (2013) Patterning of cell-instructive hydrogels by hydrodynamic flow focusing. Lab Chip 13(11):2099–2105
164. Cheung YK, Gillette BM, Zhong M, Ramcharan S, Sia SK (2007) Direct patterning of composite biocompatible microstructures using microfluidics. Lab Chip 7(5):574–579
165. Lee H, Choi B, Moon H, Choi J, Park K, Jeong B et al (2012) Chondrocyte 3D-culture in RGD-modified crosslinked hydrogel with temperature-controllable modulus. Macromol Res 20(1):106–111

166. Davis KA, Burke KA, Mather PT, Henderson JH (2011) Dynamic cell behavior on shape memory polymer substrates. Biomaterials 32(9):2285–2293
167. Klouda L, Perkins KR, Watson BM, Hacker MC, Bryant SJ, Raphael RM et al (2011) Thermoresponsive, in situ cross-linkable hydrogels based on N-isopropylacrylamide: Fabrication, characterization and mesenchymal stem cell encapsulation. Acta Biomater 7(4):1460–1467
168. Garbern JC, Hoffman AS, Stayton PS (2010) Injectable pH- and temperature-responsive poly(N-isopropylacrylamide-co-propylacrylic acid) copolymers for delivery of angiogenic growth factors. Biomacromolecules 11(7):1833–1839
169. Fuhrer R, Athanassiou EK, Luechinger NA, Stark WJ (2009) Crosslinking metal nanoparticles into the polymer backbone of hydrogels enables preparation of soft, magnetic field-driven actuators with muscle-like flexibility. Small 5(3):383–388
170. Gubeli RJ, Ehrbar M, Fussenegger M, Friedrich C, Weber W (2012) Synthesis and characterization of PEG-based drug-responsive biohybrid hydrogels. Macromol Rapid Commun 33(15):1280–1285
171. Kim SH, Kiick KL (2010) Cell-mediated delivery and targeted erosion of vascular endothelial growth factor-crosslinked hydrogels. Macromol Rapid Commun 31(14):1231–1240
172. King WJ, Mohammed JS, Murphy WL (2009) Modulating growth factor release from hydrogels via a protein conformational change. Soft Matter 5(12):2399–2406
173. Khetan S, Burdick JA (2011) Patterning hydrogels in three dimensions towards controlling cellular interactions. Soft Matter 7(3):830–838
174. DeForest CA, Anseth KS (2012) Photoreversible patterning of biomolecules within click-based hydrogels. Angew Chem Int Ed Engl 51(8):1816–1819
175. Kloxin AM, Kasko AM, Salinas CN, Anseth KS (2009) Photodegradable hydrogels for dynamic tuning of physical and chemical properties. Science 324(5923):59–63
176. Khetan S, Katz JS, Burdick JA (2009) Sequential crosslinking to control cellular spreading in 3-dimensional hydrogels. Soft Matter 5(8):1601–1606
177. Ellis-Davies GC (2007) Caged compounds: photorelease technology for control of cellular chemistry and physiology. Nat Methods 4(8):619–628
178. Griffin DR, Borrajo J, Soon A, Acosta-Velez GF, Oshita V, Darling N et al (2014) Hybrid photopatterned enzymatic reaction (HyPER) for in situ cell manipulation. Chembiochem 15(2):233–242
179. Karlsson M, Rebmann B, Lienemann PS, Sprossmann N, Ehrbar M, Radziwill G et al (2013) Pharmacologically controlled protein switch for ON-OFF regulation of growth factor activity. Sci Rep 3:2716
180. McBeath R, Pirone DM, Nelson CM, Bhadriraju K, Chen CS (2004) Cell shape, cytoskeletal tension, and RhoA regulate stem cell lineage commitment. Dev Cell 6(4):483–495
181. Engler AJ, Sen S, Sweeney HL, Discher DE (2006) Matrix elasticity directs stem cell lineage specification. Cell 126(4):677–689
182. Guvendiren M, Burdick JA (2012) Stiffening hydrogels to probe short- and long-term cellular responses to dynamic mechanics. Nat Commun 3:792

Chapter 2
Rapid Assembly of Cellular Aggregation Using Micro-Nano Technologies

Taisuke Masuda and Fumihito Arai

Abstract A rapid construction process is necessary for building up numerous cellular aggregations into three-dimensional (3D) tissues that retain the tissue geometries and initial conditions of the cells. In this chapter, we introduce new 3D assembly techniques to fabricate different hollow tissue structures. In cellular self-assembly technique by using the micro-fabricated platform, we discuss a microlumen that facilitates the supply of oxygen and growth factors and the expulsion of waste products and then fabricate a toroid-like tissue by utilizing this assembly technique. In rapid assembly technique by using transfer printing, we discuss the relationship between the 3D transcriptional body of a gel matrix and the developed shape of transferred tissue and then fabricate a hollow tubular tissue by utilizing this assembly technique.

Keywords Microfabrication • Multilayered tissues • Three-dimensional assembly • Toroid cellular aggregate • Tubular tissue

2.1 Micro- and Nano-scale Technologies for Cellular Aggregation

Micro- and nano-scale technologies for the fabrication of cellular micro-aggregation have been successfully integrated into many tissue engineering applications and have allowed for enhanced control of cell behavior and function through control of the cellular microenvironment [1, 2]. Many critical components of the cellular micro-aggregation, such as cell elongation [3, 4], cell differentiation [5, 6], and cell–cell contacts and signaling [7, 8], can all be modulated through control of the microenvironment. Although these cellular micro-aggregation techniques have been shown to be useful, precise control over the geometry of cellular aggregation, as well as over the structure and composition of the microenvironment, which are crucial factors for maintaining tissue structure and function, remains to be achieved.

T. Masuda, Ph.D. (✉) • F. Arai
Department of Micro-Nano Systems Engineering, Graduate School of Engineering, Nagoya University, 1 Furo-cho, Chikusa-ku, Nagoya 464-8603, Japan
e-mail: masuda@mech.nagoya-u.ac.jp

M. Akashi et al. (eds.), *Engineered Cell Manipulation for Biomedical Application*, Nanomedicine and Nanotoxicology,
DOI 10.1007/978-4-431-55139-3_2

Although a recent approach using cell-laden hydrogel matrix does provide extracellular matrix (ECM), a large-scale hollow tubular tissue structure has not yet been achieved because of the module size (>500 μm), uniformity, and throughput limitations. The hollow cellular aggregate formed using 3D microfabrication includes a precise microlumen that facilitates the supply of oxygen and growth factors and expels waste products [9]. By directed assembly of the hollow cellular aggregate, this microlumen can be used as a communication channel for vascularization and neurogenesis. One of the important issues to be solved is a rapid construction process; rapid fabrication of cellular aggregation is necessary to build up numerous cell modules into 3D tissues that retain the tissue geometries.

2.2 Toroid Cellular Aggregate

3D in vitro cell cultures, in which cells grow in environments that more closely mimic native tissue structure and function, have important applications in developmental biology [9], drug screening [10], and regenerative medicine [11, 12]. Consequently, a significant research effort has been recently devoted the development of 3D culture models able to mimic an in vivo microenvironment for research in cell biology especially concerning cell–cell interactions [13, 14]. Spheroid formation is one of the most well-characterized cell models for 3D culture and drug screening due to its simplicity, reproducibility, and similarity to physiological tissues compared to other methods that involve ECM scaffolds and hydrogel systems. The 3D spheroid culture techniques that have been reported employ techniques such as cultivation on nonadhesive surfaces [9], spinner cultures [15], biological macromolecule-based foam scaffolds [5, 16], rotating radial flow bioreactors [17], and hanging drop methods [18]. Although these 3D spheroid culture techniques have shown their importance, precise control over the geometry of cellular aggregation, as well as over the structure and composition of the microenvironment and crucial factors for maintaining tissue structure and function, remains to be achieved.

The greatest successes in tissue engineering have been limited to vascular tissues and thin tissues such as cartilage, skin, and large-scale vasculature, which can survive under conditions where the supply of oxygen and nutrients occurs by simple diffusion without an additional vascular supply. In the case of cultured cellular aggregates in vitro, oxygen transport is limited to a diffusion distance of 150–200 μm from the oxygen source [9]. Insufficient vascularization can lead to improper cell integration or to cell death in larger cellular aggregates. In this study, we have developed a unique multicellular aggregate formation platform that utilizes photolithography. The cellular aggregate formed using this platform has a toroid-like geometry and includes a microlumen that facilitates the supply of oxygen and growth factors and the expulsion of waste products. By utilizing this culture platform, we show that chondrocyte differentiation in toroid cellular aggregates results in distinct physiological responses, significantly differing from those observed by using standard 3D spheroids.

Oxygen supply is important for cell survival in thick tissues. In most cases, cell death within thick tissues is attributable to hypoxia rather than to lack of nutrients.

To improve the supply of oxygen to 3D spheroids, we generated a microlumen within the engineered geometric multicellular aggregate. We then estimated the diffusion of oxygen in the toroid multicellular aggregate based on Fick's diffusion laws [19, 20]. The diffusion of oxygen from the ambient solvent into the toroid multicellular aggregate is given by

$$4\pi^2 rRJ_r = -D\frac{\partial C}{\partial r} \tag{2.1}$$

where r is the cross-sectional radius of the toroid, R is the mean radius of the toroid, J_r is the oxygen flux, D is the oxygen diffusion coefficient of the multicellular aggregate, and C is the oxygen concentration in the medium. In addition, assuming a steady-state system with controlled diffusion, a constant external concentration of oxygen, and a constant oxygen consumption rate (OCR; m), the oxygen consumption (OC) is given by

$$\mathrm{OC} = m2\pi^2 r^2 R \tag{2.2}$$

Because these ratios are equal to each other under equilibrium conditions, this gives

$$4\pi^2 rRD\frac{\partial C}{\partial r} = m2\pi^2 r^2 R \tag{2.3}$$

where, to satisfy the boundary conditions, P_e, the oxygen concentration of the toroid surface in vivo at $r = r_0$, solved this differential equation (2.3).

$$C - P_e = \frac{m}{4D}\left(r^2 - r_0^2\right) \tag{2.4}$$

Thus, when the boundary conditions are $C_{r=0} > 0$ at $r = 0$, the maximum cross-sectional radius of the toroid aggregate for cell survival can be given as follows:

$$r_0 < \left(4P_e\frac{D}{m}\right)^{\frac{1}{2}} \tag{2.5}$$

The cross-sectional diameter of the toroid aggregate was estimated to be 296 μm, calculated using Eq. (2.5), and the proper values of P_e (0.47×10^{-4} mmol/cm^3), D (1.4×10^{-5} cm^2/s), and m (1.2×10^{-5} mmol/cm^3/s) were extracted [20]. Therefore, the diameter and depth of the micro-well were set at less than 300 μm to ensure cell survival.

2.2.1 Microfabrication Technology for 3D Structure

In the past few years, micro-/nanofabrication technology has been applied in the field of tissue engineering, allowing the achievement topographical, spatial, and chemical control over cells, thereby creating more functional tissue engineering constructs [1]. We used polydimethylsiloxane (PDMS; Silpot 184, Dow Corning Toray Corp.

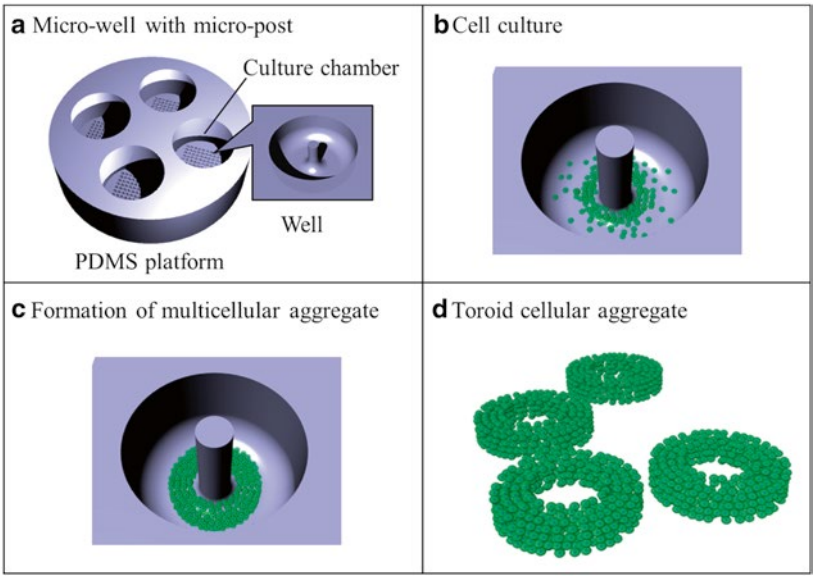

Fig. 2.1 The design concept of the multicellular aggregate formation platform. (**a**) The cellular aggregate formed using this platform has a toroid-like geometry and includes a microlumen that facilitates the supply of oxygen and growth factors and expels waste products. (**b**) By simply seeding cells in the PDMS platform, the cells accumulate around the micro-post because of their low attachment to the platform surface, and (**c**) the toroid multicellular aggregate with a microlumen is thus formed. (**d**) Finally, toroid cellular aggregates are recovered at the end of the culture by inverting the PDMS platform

JAPAN) as the platform material for multicellular aggregate formation, hereafter referred to as the PDMS platform. PDMS is widely used for the fabrication of various microfluidic chips because of its transparency, biocompatibility, superiority over other materials in terms of mechanical properties, and its low production cost [21]. The design concept of the multicellular aggregate formation platform is shown in Fig. 2.1. The designed PDMS platform was constituted by an array of micro-wells showing a horseshoe-shaped bottom and one micro-post. By simply seeding cells in the PDMS platform, they accumulated around the micro-post, due to their low adhesion to the platform surface; the toroid multicellular aggregate with a microlumen was thus formed. Livoti et al. showed that a toroid building unit offers possibilities for building a large tissue construct with a high cell density and open lumen space [22]. However, their results cannot have been achieved by a large tissue with high cell density, due to large open lumen space.

The target of our study was to obtain a cell aggregate with smaller lumens and produce hundreds of such aggregates at a time. Furthermore, an assembled toroid cellular aggregate aimed at resembling a living tissue construct with both a high cell density and a network of communicated microlumens. The developed PDMS platform allowed for efficient formation of uniformly sized toroid multicellular aggregates and for their long-term culture.

Microfabrication was needed to obtain the toroid multicellular aggregate formation platform, in order to provide the platform with micro-wells showing a horseshoe-shaped bottom and one micro-post. Three-dimensional patterns with spatially controlled shapes were fabricated by means of gray-scale lithography.

This technique utilizes locally modulated exposure doses to develop a 3D structure in the photoresist. Differential exposure doses lead to multiple depths of exposed photoresist across the surface. Gray-scale photolithography is a promising technique to achieve spatially controlled 3D structure by modulation of exposure dose, because the profile of the exposure dose can be easily controlled by changing the profile of the contrast of the gray scales. However, gray-scale lithography requires specialized equipment and preparation of photomasks, resulting in a costly and time-consuming process. We therefore incorporated an additional technique based on a maskless exposure system, thus not requiring hard masks [23]. This maskless exposure system achieves synchronous fabrication of the micropattern from the images generated by a PC and displayed through an LCD projector.

2.2.2 Fabrication of Toroid Cellular Aggregate

A mouse chondrogenic cell line ATDC5 aggregated in PDMS platform. With time cell aggregate increased in a nonuniform way with high cell density localized to a central micro-post closer to the lumen rather than the outermost circumference even though spatial capacity in the PDMS platform was uniform. It would be interesting to determine whether cell migration and proliferation vary at these locations. These results indicated that the threshold for the formation of a toroid multicellular aggregate depends on both cell density and spatial capacity. Figure 2.2a, b show light-microscopic images of ATDC5 toroid multicellular aggregates retrieved from the PDMS platform after 3 days of culture. The cells were easily retrieved at the end of the culture by inverting the PDMS platform. Noninvasive recovery of cells from the platform could represent a great advantage for biological applications. Figure 2.2c, d show LIVE/DEAD image of an ATDC5 toroid multicellular aggregate, which indicates that most of the cells in the aggregate (>95 %) were still alive after 3 days of culture. Anada et al. reported that dead cells were present in the center of larger spheroids (>200 μm cross-sectional diameter). Therefore, the large size of viable multicellular aggregates generated by our platform solved this problem. In the case of toroid multicellular aggregate, a cell-dense tissue organized itself, and the control of tissue size was possible. Moreover, the orientation of cell–cell contact can be controlled by the multicellular aggregate with a microlumen.

The organization of cells within a well-defined microenvironment is important in order to obtain a functional resulting tissue. Several techniques such as random assembly [24] or directed assembly [25] have been developed to engineer such tissue organization using, e.g., cells, cell sheets, or 3D cellular spheroids. Random assembly of tissues is rapid and simple, but does not allow control over the final structure of the cellular aggregate. Directed assembly of tissues is another method

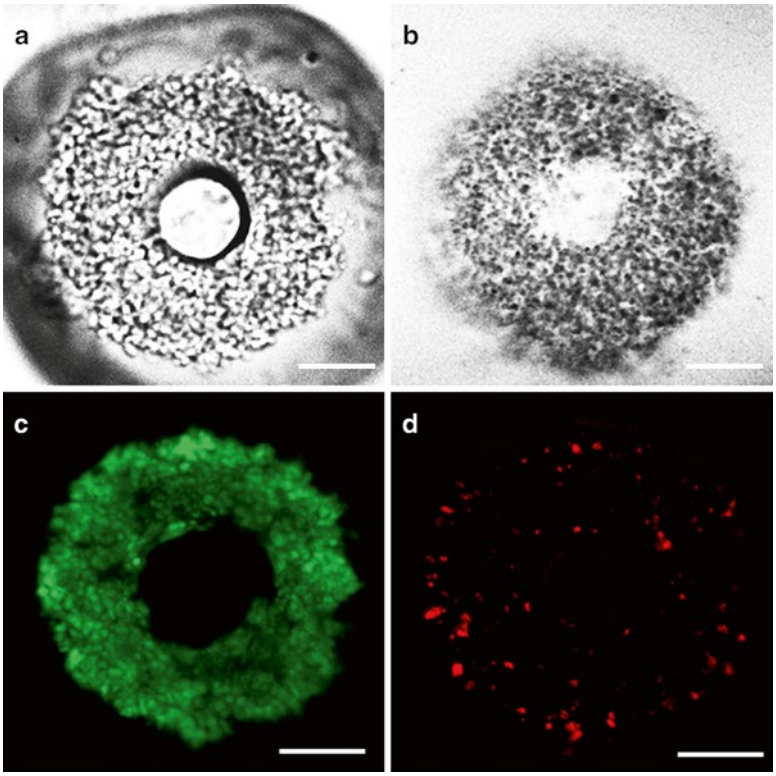

Fig. 2.2 Light-microscopic and fluorescent microscopic images respectively of ATDC5 toroid multicellular aggregates retrieved from the PDMS platform after 3 days of culture. (**a**) Cultured multicellular aggregate in the PDMS platform. (**b**) Retrieved multicellular aggregate from the PDMS platform. (**c** and **d**); LIVE/DEAD assay, which revealed higher proportions of viable cells (*green*) than dead cells (*red*) in ATDC5 toroid multicellular aggregate. All scale bars are 100 μm

for building tissue-like constructs with defined microarchitectures. Advantages of the directed assembly technique include the ability to recapitulate the native tissue architecture. In this study, we addressed the formation of a multicellular aggregate with toroid geometry with a microlumen to supply oxygen and growth factors and to expel waste products. By directed assembly of the toroid multicellular aggregate, this microlumen can be used as a communicating channel for vascularization and neurogenesis. Figure 2.3 shows a fluorescence image of ATDC5 toroid multicellular aggregate in the directed assembly. Each fluorescently labeled toroid multicellular aggregate was accumulated on a glass capillary. A red-labeled (DiI) toroid aggregate was sandwiched between the green-labeled (Calcein-AM). Although this result is preliminary, the fabrication of a communicating channel in the assembled cellular aggregate could be useful to insert other cells and may be potentially useful for fabricating vascular networks or nerve networks to engineer complex tissue

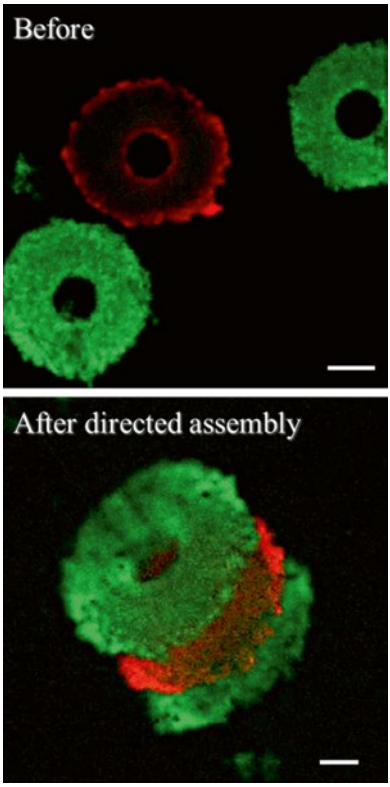

Fig. 2.3 Fluorescent microscopic image of functional tissue by directed assembly of three toroid multicellular aggregate. Each fluorescently labeled toroid multicellular aggregate was accumulated on a glass capillary. All scale bars are 100 μm (*Green*: Calcein-AM, *Red*: DiI)

constructs. These characteristics suggest that the multicellular aggregate has the potential to be used in a wide variety of applications, including drug screening and tissue engineering, as well as in biohybrid robotics, as a component that could enable the integration of complex living tissues in artificial machines.

2.3 Tubular Multilayered Tissue

Controlled cellular alignment plays a crucial role in the microenvironment of many human tissues, dictating their biological and mechanical function [26, 27]. Thus, to effectively study and mimic the biological and mechanical function of many native tissues in vivo, engineered tissues must recapitulate these native 3D microstructures in vitro. Engineered tissue constructs are typically generated by embedding cells in synthetic or biological 3D scaffolds [28, 29]. However, in previous studies, the inability to adequately control cell behavior has often resulted in poor cell and ECM organization within engineered constructs. Such tissue constructs had limited ability to restructure complex tissues characterized by precise cell and ECM alignment [30].

Matsusaki et al. have developed a cell-accumulation technique using highly biocompatible nanofilms and layer-by-layer (LbL) assembly for the rapid construction of thick-layered tissues with a well-controlled layer number and thickness [31, 32]. Fabricated multilayered tissue has been constructed into highly developed blood capillary networks (over 1 cm^2 of layered tissues) by sandwiching endothelial cells between the layered tissues. We proposed a new 3D assembly technique that would enable fabrication of a hollow tubular tissue structure using water transfer printing to manipulate multilayered tissues. By utilizing this assembly technique, we discuss the relationship between the 3D transcriptional body of a hydrogel matrix and a developed shape of transferred tissue and fabricate a hollow tubular tissue. The described technique is applicable to many different cell types and can be used to engineer tissue constructs of user-defined size and shape with microscale control of the cellular organization, which could form the basis for constructing 3D engineered tissues with a hollow tubular tissue in vitro.

2.3.1 Water Transfer Printing for 3D Tubular Tissue

Water transfer printing is a 3D decorating process for generating elaborate graphics, such as wood grain, carbon fiber, camouflage, and geometrical designs [33]. Water transfer printing is extensively used to decorate items that range from the auto body exterior to small items, such as the mobile phones. We applied water transfer printing as a tissue printing technique for the rapid 3D assembly of multilayered tissue. Figure 2.4 shows the design concept of the 3D assembly of multilayered tissues on a curved substrate by water transfer printing. First, a sheet-like multilayered tissue is floated on the water surface, and a 3D alginate hydrogel matrix is raised from the water into the air. The multilayered tissue is transferred to the 3D surface by raising the alginate hydrogel matrix from the water. As a result, the multilayered tissue does not wrinkle and is able to be transferred onto the 3D alginate hydrogel matrix. The multilayered tissue transcribed onto the biodegradable material is returned to the culture medium after fixation after culturing (24 h); the main hydrogel matrix is degraded by using alginate lyase to obtain the multilayered hollow tubular tissue structure.

Multilayered tissues were made by layer-by-layer (LbL) method, a thin film fabrication technique. Using this method, we can obtain uniform thin films having a thickness of only a few nanometers at ordinary temperatures and pressures. The films are formed by depositing alternating layers of oppositely charged materials with wash steps between each deposition step. In this paper, we deposited fibronectin–gelatin (FN-G) nanofilms onto single cell surfaces by the LbL method in order to promote cell–cell interactions, such as those seen in natural ECM. Briefly, cells were alternatively immersed with 0.04 mg/mL fibronectin and gelatin in 50 mM Tris–HCl (pH = 7.4). After each procedure, the cells were washed with 50 mM Tris–HCl (pH = 7.4) to remove unadsorbed polymers. The coated cells were then seeded onto a culture device at an appropriate density. As a result, multilayered tissues were obtained with a shape corresponding to the shape of the bottom of the culture device.

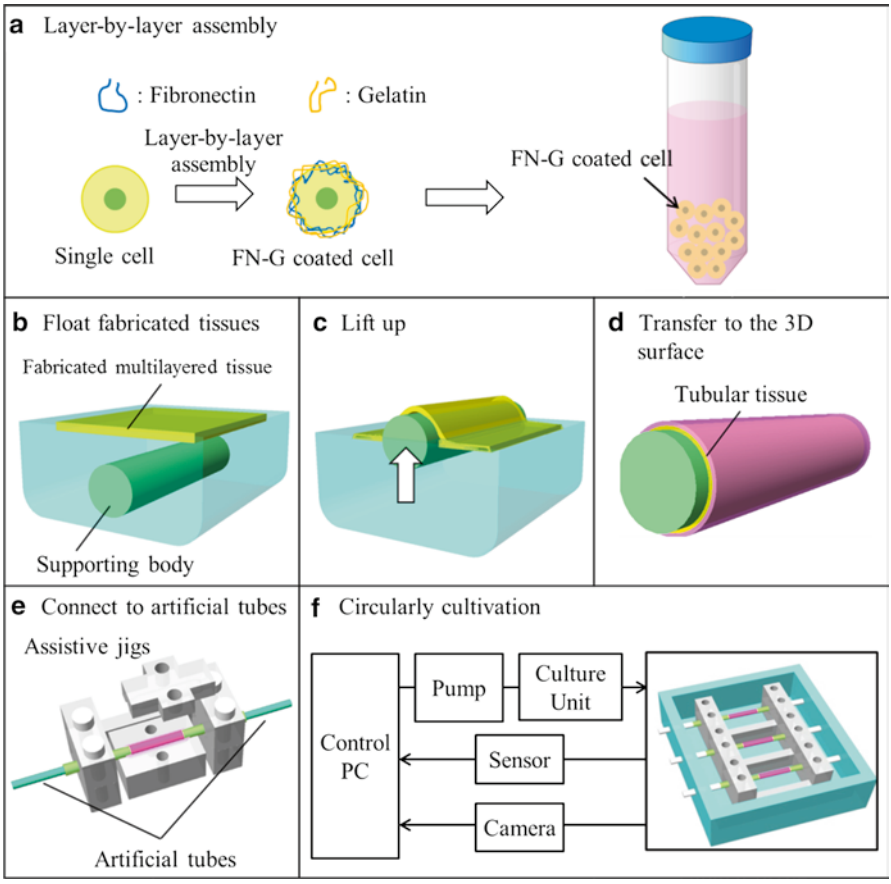

Fig. 2.4 Design concept of the 3D assembly of multilayered tissues on a curved substrate by water transfer printing. (**a**) Layer-by-Layer assembly using FN-G nanofilms on a single cell surface. (**b**) Float fabricated tissues on the surface of water. (**c**) Lift up supporting body from the water to the air. (**d**) Transfer to the 3D surface without wrinkles. (**e**) Coat tissues with collagen and dissolved supporting body. (**f**) To evaluate whether the tissue-engineered tubular models maintain normally mechanical property, tubular tissues are circularly cultured with mechanical and chemical stimulations monitored

The culture device, similar to a commercial culture insert, was made by sandwiching 0.4 μm Nucleporemembrane (GE Healthcare UK Ltd.) between the upper and lower parts.

All cells were cultured in a standard cell culture incubator (Panasonic, Japan) in a 5 % CO_2 atmosphere at 37 °C. Neonatal normal human dermal fibroblasts (NHDFs) were maintained in Dulbecco's modified Eagle medium (DMEM; Sigma-Aldrich, Ireland) supplemented with 10 % fetal bovine serum (FBS) and 1 % penicillin/streptomycin (P/S; GIBCO, USA) and were passaged twice per week. Therefore, to obtain multilayered tissue with a thickness of 50 μm, we seeded

1.9×10^6 cells/well of NHDFs to the culture device. The constructed multilayered tissue was retrieved from the membrane after 4 days of culture. These cells were identified by immunohistochemistry and labeled with green fluorescent dye using the PKH (green) and DAPI (blue) to stain cellular membrane and the nuclei, respectively.

2.3.2 Fabrication of Tubular Multilayered Tissue

To clarify the relationship between 3D transcriptional body of gel matrix and a developed figure of transfer tissue, we evaluated the degree of circularity, surface segmentation, and transcriptional behavior using quasi-multilayered tissue. High circularity of transfer tissue demonstrated excellent transcriptional behavior. These results suggested that the geometry of developed figure is closely related to cut line and the direction of pull-up. Furthermore, we showed that it could assemble in the multisegmentation part. However, multisegmentation requires reduction of parts for using a cell laden, resulting in a time-consuming process. These results indicated that the threshold for accurate assembly by water transfer printing depends on both circularity and segmentation. As the maintained proliferation observed in degradable alginate hydrogel is promising, we evaluated NHDF proliferation in media containing various concentrations of alginate lyase over a 14-day period. The alginate lyase did not affect NHDF proliferation at concentrations as high as 2.0 mg/mL, and only an inhibition of NHDF proliferation was observed at 20 mg/mL. In other words, low-concentration alginate lyase has little effect on the cell proliferation. A concentration of 20 mg/mL far exceeds those required for the following experiments described. So, an alginate lyase has little influence on the proliferation of our tissue.

Figure 2.5 shows a microscopic image of multilayered tissues retrieved from the culture device. The multilayered tissue is transferred to a 1 mm diameter glass capillary dip-coated with alginate hydrogel (thickness of 500 μm). To prepare the intended multilayered tissues, the required size of the culture device was determined to be 10.0-by-6.28 mm. The size of the retrieved multilayered tissues shown in Fig. 2.5a was 9.5-by-6.0 mm. Although contraction of approximately 35 % was observed from the early stages of cultivation, multilayered tissues were wide enough to allow formation of the tubular tissue structure. Figure 2.5b, c show microscopic images of the transcribed multilayered tissue retrieved from the water. The multilayered tissues were uniformly transferred to the 3D alginate hydrogel matrix (Fig. 2.5b). It consisted of two layers and the thickness of the transferred tubular tissue was observed to be 50 μm (Fig. 2.5c).

Enzymatic degradation by alginate lyase of the transcribed hydrogel matrix in a biodegradable hydrogel fabricated a channel with a predetermined 3D hollow tubular structure. The culture device was placed in an incubator (37 °C, 5 % CO_2) for 30 min of incubation for enzymatic degradation of the hydrogel matrix by alginate lyase (2 mg/mL). The multilayered tissue with a hollow tubular structure was capable of connecting both ends of the tube pump and transporting the culture media. In the

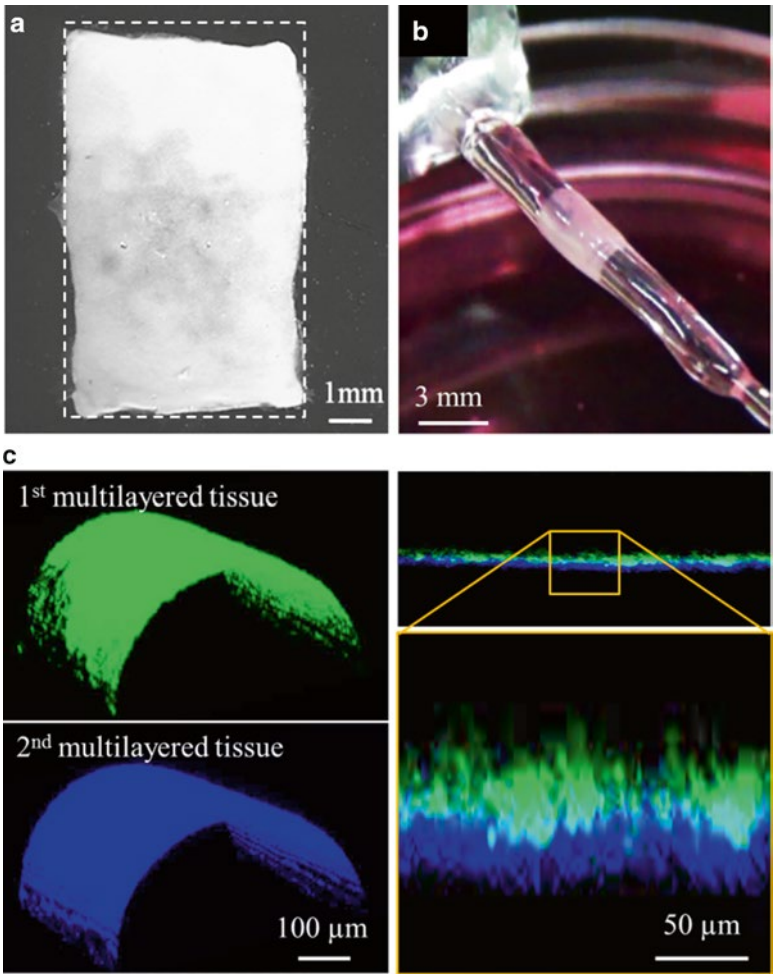

Fig. 2.5 Microscopic images of the transcribed multilayered tissue of the hollow tubular structure formed by water transfer printing. (**a**) Relationship between the retrieved multilayered tissues and the designed multilayered tissues. The *white dashed line* shows the designed shape of the multilayered tissues. (**b**) Multilayered tissue is transferred onto a 3D surface by raising an alginate hydrogel matrix from the water. (**c**) Enzymatic degradation by alginate lyase of the transcribed hydrogel body in a biodegradable gel fabricated a channel with a predetermined 3D hollow tubular structure. NHDFs stained with DAPI (*blue*) and PKH (*green*)

tubular tissue, medium was transported using the flow by the centrifugal pump (Flow rate; 20 µL/min). Furthermore, we measured the mechanical property of tubular tissue by the artificial circulatory system.

Simulation of the 3D environment in which tissues normally develop and function is crucial for the engineering of in vitro models that can be used for the formation of complex tissues. Thus, developing 3D cell-laden constructs will be essential

for creating tissue-engineered organs in vitro with cell volumes similar to those of organs [34]. In this work, we demonstrated that multilayered tissues could rapidly assemble into aligned tubular tissue in the appropriate geometrical conditions using microfabrication. This technique does not require a solid biodegradable scaffold. Therefore, this approach presents the first simple and rapid method to create through the exploitation of the intrinsic potential of cells to assemble into functional 3D tissues in a suitable tubular tissue environment. These artificial hollow tubular tissues could be used as in vitro simulators for drug efficiency evaluation and operative trainings. More in-depth investigation using this circular system could potentially increase our knowledge about complex cell–cell interaction and organization within 3D cell populations in well-defined microarchitectures.

Acknowledgment This research was supported by a Grant-in-Aid from the Ministry of Education, Culture, Sports, Science, and Technology for Scientific Research (23106002 and 24106506) and the Nagoya University Global COE program for Education and the Research of Micro-Nano Mechatronics.

References

1. Khademhosseini A, Langer R, Borenstein J, Vacanti JP (2006) Microscale technologies for tissue engineering and biology. Proc Natl Acad Sci U S A 103:2480–2487
2. Masuda T, Takei N et al (2012) A microfabricated platform to form three-dimensional toroidal multicellular aggregate. Biomed Microdevices 14:1085–1093
3. Chen CS, Mrksich M et al (1997) Geometric control of cell life and death. Science 276:1425–1428
4. McBeath R, Pirone DM et al (2004) Cell shape, cytoskeletal tension, and RhoA regulate stem cell lineage commitment. Dev Cell 6:483–495
5. Fukuda J, Khademhosseini A et al (2006) Micromolding of photocrosslinkable chitosan hydrogel for spheroid microarray and co-cultures. Biomaterials 27:5259–5267
6. Burdick JA, Vunjak-Novakovic G (2009) Engineered microenvironments for controlled stem cell differentiation. Tissue Eng Part A 15:205–219
7. Masuda T, Takahashi I et al (2008) Development of a cell culture system loading cyclic mechanical strain to chondrogenic cells. J Biotechnol 133:231–238
8. Nelson CM, Vanduijn MM et al (2006) Tissue geometry determines sites of mammary branching morphogenesis in organotypic cultures. Science 314:298–300
9. Anada T, Masuda T et al (2010) Three-dimensional cell culture device utilizing thin membrane deformation by decompression. Sens Actuators B 147:376–379
10. Kloss D, Fischer M et al (2008) Drug testing on 3D in vitro tissues trapped on a microcavity chip. Lab Chip 8:879–884
11. Albrecht DR, Underhill GH et al (2006) Probing the role of multicellular organization in three-dimensional microenvironments. Nat Methods 3:369–375
12. Barrila J, Radtke AL et al (2010) Organotypic 3D cell culture models: using the rotating wall vessel to study host–pathogen interactions. Nat Rev Micro 8:791–801
13. Nichol JW, Koshy ST et al (2010) Cell-laden microengineered gelatin methacrylate hydrogels. Biomaterials 31:5536–5544
14. Bartosh TJ, Ylostalo JH et al (2010) Aggregation of human mesenchymal stromal cells (MSCs) into 3D spheroids enhances their antiinflammatory properties. Proc Natl Acad Sci U S A 107(31):13724–13729

15. Wartenberg M, Donmez F et al (2001) Tumor-induced angiogenesis studied in confrontation cultures of multicellular tumor spheroids and embryoid bodies grown from pluripotent embryonic stem cells. FASEB J 15:995–1005
16. Skardal A, Sarker SF et al (2010) The generation of 3-D tissue models based on hyaluronan hydrogel-coated microcarriers within a rotating wall vessel bioreactor. Biomaterials 31: 8426–8435
17. Miyazawa M, Torii T et al (2007) Hepatocyte dynamics in a three-dimensional rotating bioreactor. J Gastroenterol Hepatol 22:1959–1964
18. Tung YC, Hsiao AY et al (2011) High-throughput 3D spheroid culture and drug testing using a 384 hanging drop array. Analyst 136:473–478
19. Metzen E, Wolff M, Fandrey J, Jelkmann W (1995) Pericellular PO_2 and O_2 consumption in monolayer cell cultures. Respir Physiol 100:101–106
20. Mamchaoui K, Saumon G (2000) A method for measuring the oxygen consumption of intact cell monolayers. Am J Physiol Lung Cell Mol Physiol 278:L858–L863
21. Duffy DC, McDonald JC, Schueller OJA, Whitesides GM (1998) Rapid prototyping of microfluidic systems in poly(dimethylsiloxane). Anal Chem 70:4974–4984
22. Livoti CM, Morgan JR (2010) Self-assembly and tissue fusion of toroid-shaped minimal building units. Tissue Eng Part A 16:2051–2061
23. Itoga K, Kobayashi J et al (2008) Second-generation maskless photolithography device for surface micropatterning and microfluidic channel fabrication. Anal Chem 80:1323–1327
24. McGuigan AP, Sefton MV (2006) Vascularized organoid engineered by modular assembly enables blood perfusion. Proc Natl Acad Sci U S A 103:11461–11466
25. Yanagawa F, Kaji H et al (2011) Directed assembly of cell-laden microgels for building porous three-dimensional tissue constructs. J Biomed Mater Res A. doi:10.1002/jbm.a.33034
26. Aubin H, Nichol JW et al (2010) Directed 3D cell alignment and elongation in microengineered hydrogels. Biomaterials 31:6941–6951
27. Papadaki M, Bursac N et al (2001) Tissue engineering of functional cardiac muscle: molecular, structural, and electrophysiological studies. Am J Physiol Heart C 280:H168–H178
28. Khademhosseini A, Vacanti JP, Langer R (2009) Progress in tissue engineering. Sci Am 300:64–71
29. Masuda T, Kawai T et al (2010) Quality of regenerated bone enhanced by implantation of octacalcium phosphate-collagen composite. Tissue Eng Part C Methods 16:471–478
30. Mironov V, Visconti RP et al (2009) Organ printing: tissue spheroids as building blocks. Biomaterials 30:2164–2174
31. Nishiguchi A, Yoshida H, Matsusaki M, Akashi M (2011) Rapid construction of three-dimensional multilayered tissues with endothelial tube networks by the cell-accumulation technique. Adv Mater 23:3506–3510
32. Matsusaki M, Ajiro H et al (2012) Layer-by-layer assembly through weak interactions and their biomedical applications. Adv Mater 24:454–474
33. Ventura CE (2012) Experimental and applied mechanics, vol 4. In: Proceedings of the 2012 annual conference on experimental and applied mechanics. Springer, New York
34. Ochoa ER, Vacanti JP (2002) An overview of the pathology and approaches to tissue engineering. Ann N Y Acad Sci 979:10–26

Chapter 3
Rapid Single Cell Printing by Piezoelectric Inkjet Printer

Ryanto The, Shuichi Yamaguchi, Akira Ueno, Yoshitake Akiyama, and Keisuke Morishima

Abstract Tissue engineering is rapidly developing to assist in the treatment of organ loss or tissue damage. On the other hand, the relatively long process of drug development may also need in vitro fabricated organ for drug testing, which opens up faster door to development process. Several methods and technologies have been introduced as valuable tools for tissue engineering, and inkjet printing stands out as the "scaffold-less" tissue engineering tools starting from the early 2000s, although the scaffold-less feature is still debatable. Furthermore, this technology was also used to encapsulate single cells in the fluid droplet, thus opening up the possibility for isolation of single cells in the open space and better spatiotemporal control of cell printing at individual level. Combined with the high-frequency droplet ejection capability of inkjet printer, high-throughput single cells array and high-speed fabrication of finer detail tissue fabrication may also be possible in the future. This chapter introduced several methods used to deposit cells on arbitrary pattern and explored on the challenge in the implementation of inkjet printing technology to deposit cells and single cells on arbitrary pattern. This chapter also argued several adjustments and limitations for relatively large particles and cell printing, which are in a different size scale compared to ink particles in the commercial inkjet printer.

R. The • K. Morishima (✉)
Department of Mechanical Engineering, Graduate School of Engineering, Osaka University, Suita, Japan

The Center for Advanced Medical Engineering and Informatics
Osaka University, Suita, Japan
e-mail: morishima@mech.eng.osaka-u.ac.jp

S. Yamaguchi
Department of Mechanical Engineering, Graduate School of Engineering, Osaka University, Suita, Japan

Microjet Corporation, Shiojiri, Japan

A. Ueno
Microjet Corporation, Shiojiri, Japan

Y. Akiyama
Department of Mechanical Engineering, Graduate School of Engineering, Osaka University, Suita, Japan

M. Akashi et al. (eds.), *Engineered Cell Manipulation for Biomedical Application*, Nanomedicine and Nanotoxicology,
DOI 10.1007/978-4-431-55139-3_3

Keywords Piezoelectric inkjet printer • Push-pull method • Single cell printing

3.1 Introduction

The benefit of rapid single cell printing lies in two very promising and greatly developing fields, single cell analysis and tissue engineering. In this section, we provide the reader with a brief background in both of these fields and introduction to emerging technologies for cell patterning, including cell printing by inkjet technology.

Tissues and organs consist of complex and large cell population, and each function is performed by cells at individual level. The ability to isolate single cells from heterogeneous cell populations provides enormous advantage in areas such as diagnostics, cell biology, and molecular biology. The understanding of biological process and basic biological concept greatly benefits from single cell analysis. Flow cytometry is a conventional technology capable of quantifying single cell properties. Nevertheless, the analysis only provides snapshot properties of a cell at a given time, and their use requires prior knowledge of cell's characteristics; hence isolation of non-labeled single cell proves to be difficult using this technology. There had been an effort to improve spatiotemporal single cell handling utilizing recent development in nanotechnologies and systems that use a lab-on-a-chip to isolate individual cells [1, 2].

On the other hand, although tissue engineering has been originating since as early as World War II, it just gained momentum in recent years, since the breakthrough work to grow "human ear" shape tissue on a mouse [3] and also the first time "tissue engineering" term appeared in academic literature. Biodegradable scaffold development inspires the construction of more complex tissue structures. Several techniques were developed in recent years for spatiotemporal control of cells, which we will introduce in the following paragraph. The concept of in vitro engineered tissue from individual cells opens several opportunities in clinical medicine, especially organs or tissue transplantation, because shortage of the available donor organ is a common problem.

There are several approaches to position cells on arbitrary pattern. These approaches could be categorized into non-jet-based and noncontact jet based [4]. The non-jet-based approaches range from many manifestations of lithography, which include photolithography and soft lithography. Basically, these techniques are based on the principle of fabricating a predetermined pattern using a mold. On the other hand, noncontact jet-based techniques utilize needles and microfluidic networks for handling of media, which are not in contact with the substrate. The next section will introduce some of the common techniques widely used to position the cells to a certain pattern.

3.1.1 Microcontact Printing

Microcontact printing is a manifestation of soft lithography, which used stamp to pattern extracellular matrix (ECM) of cells [5]. The stamp was commonly fabricated from polydimethylsiloxane (PDMS) using a master stamp, which is fabricated

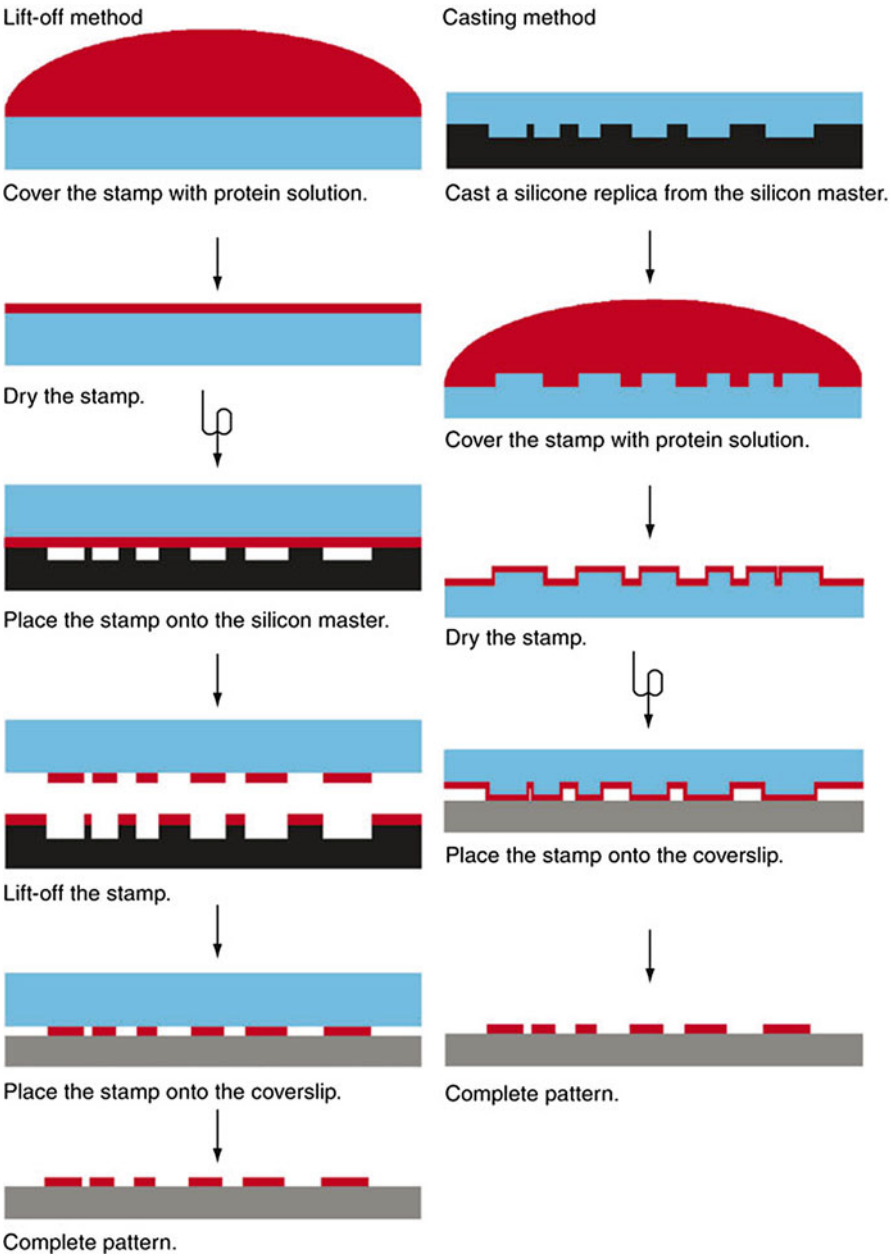

Fig. 3.1 Microcontact printing schematic process (reproduced from von Philipsborn et al. [6])

using traditional photolithography techniques. The ink is then poured over the PDMS stamp for ink patterning over the printing surface. Figure 3.1 shows the common process for microcontact printing [6]. The simplicity of creating pattern over microscale structure, cheap production cost, and non-direct contact with cells are

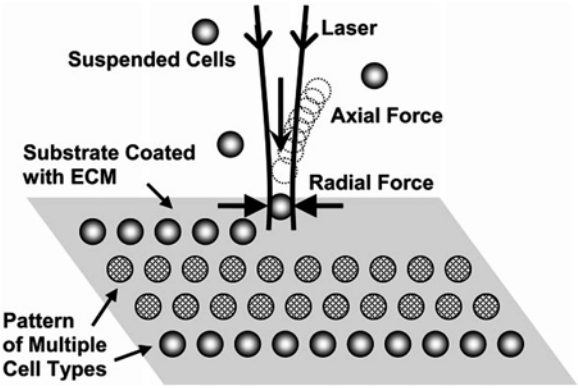

Fig. 3.2 Schematic diagram of laser guidance (reproduced from Pirlo et al. [8])

main advantages of this technology. However, cell patterning is confined on a two-dimensional space, and heterogeneous cell handling proved to be very difficult, therefore severely limiting its use.

3.1.2 Laser-Guided Cell Writing

Laser-guided cell writing is a technology driven by finely tuned lasers, which produce optical forces on radial component capable of guiding individual cells and other microparticles and also on axial component capable of propelling cells and other microparticles along the axis direction. Utilizing this laser guidance principle, a cell deposition system capable of positioning cells with small error margin up to a few μm was successfully developed [7]. Figure 3.2 shows a schematic diagram showing how laser guidance system works [8]. It is considered to be one of the effective tools for studying cell-to-cell interactions and other biological mechanisms at the single cell level, even for 3D tissue engineering [9]. However, slow cell-handling speed severely limited this technology for handling of large cell number and for tissue engineering purpose.

3.1.3 Bio-Electrospraying and Cell Electrospinning

Both bio-electrospraying and cell electrospinning are utilizing the electric field produced between two charged electrodes. Figure 3.3 shows the electrospraying and electrospinning device setup [4]. Liquid media is charged prior to ejection from the orifice, and the ring is connected to the ground electrode. Subsequently, the liquid is exposed to the electric field produced from the potential difference of the charged needle and grounded ring electrode. The column of liquid may form droplet or

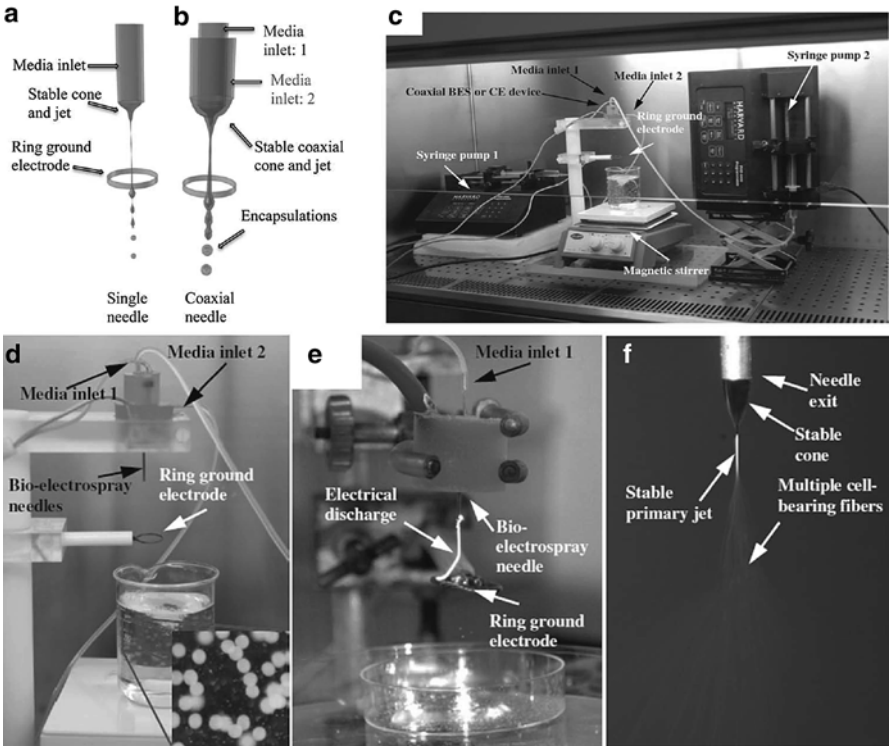

Fig. 3.3 (**a**, **b**) Representative schematic illustrations of a single and coaxial needle electrospray setup. (**c**) Characteristic digital images of a coaxial bio-electrospray system setup in a laminar flow safety hood explored for cell immobilization. (**d**) The *inset* shows the generated beads. (**e**) Single needle BES configuration in which the voltage has been elevated to 30 kV, demonstrating the collection of cell-bearing droplets during electrical discharge. (**f**) Cell electrospinning with a modified counter electrode (reproduced from Poncelet et al. [4])

continuous stream based on the liquid properties. This technique has been widely used across many fields of research, including biotechnology fields, in which this technique provides instrument to precisely position cells in three dimensions. Various studies had evaluated this technique capability for directly handling cells and to transplant the cells in a matrix to construct tissue structure. The disadvantage to this technology is its incapability to handle electrically susceptible cells, therefore limiting its use to certain cell types.

3.1.4 Focused Acoustic Beams

Discrete droplet formation technique which ejected droplets from liquid-air interface with focused acoustic beams was first developed in the late 1980s [10]. Droplet was formed with diameter ranging from 5 to 300 μm. This technique is very similar

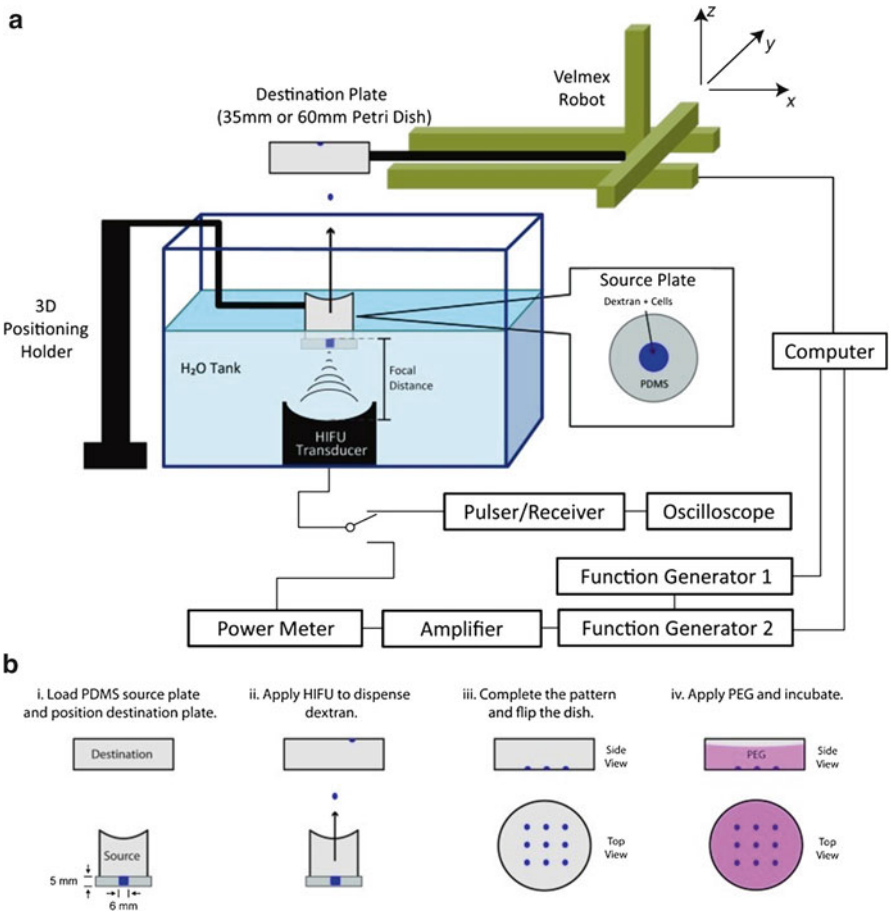

Fig. 3.4 ADE and ATPS setup. (**a**) The source plate containing dextran is positioned above the ultrasound transducer, both immersed in degassed water. The movement of the destination plate is controlled by an automated positioning system synchronized with the ultrasound pulse. (**b**) Two-phase patterning is achieved in four steps. *ADE* acoustic droplet ejection, *ATPS* aqueous two-phase system, *PDMS* polydimethylsiloxane, *PEG* polyethylene glycol, *HIFU* high-intensity focused ultrasound (reproduced from Fang et al. [11])

to the droplet formation by the inkjet printer, but only differs in terms of the actuator. Combining focused acoustic beams and heterogeneous cell printing by using biphasic liquid, the polyethylene glycol (PEG) and dextran (DEX), patterning of heterogeneous cells was studied by a group in the University of Michigan [11]. Figure 3.4 illustrates the schematic diagram and experiment method to print heterogeneous cell. Nozzleless droplet formation reduces the possibility of contamination to the sample. However, constant agitation is necessary, because as time passed cells precipitate to the bottom of the dish.

3.1.5 Inkjet Printing

Inkjet printing is most obviously known for photo- or text printing in household and office use. Various properties of inkjet printing had been investigated in the past years; however, most of the investigation was performed with ink printing as the main objective, and it is mostly unrelated to the bioresearch field. The first work on utilizing inkjet printer for bio-printer was done in 2003 [12, 13]. Household inkjet printer was modified and the ink was replaced with cell suspension. Since the breakthrough work, inkjet printer modification for bio-printer has been rapidly growing, and utilizing inkjet printer's high-speed printing and its open surface properties, the construction of 3-dimensional tissue structure by inkjet printer was also successfully done [14].

Each of those technologies introduced above had its own advantages and disadvantages and may be used interchangeably to maximize their potential. In this chapter, we will focus our discussion on the cell printing by inkjet technology, as this technology has the unique potential for both single cell analysis research and tissue engineering.

3.2 Piezoelectric Inkjet Head Design and Piezoelectric Control Method

Inkjet printer is a noncontact jet-based direct cell-handling technique which encapsulates cells inside micrometer scale liquid droplet produced by microchannel.

Based on the droplet generation method, inkjet printer can be categorized into two types, thermal inkjet printer and piezoelectric inkjet printer. Thermal inkjet printer uses heat element to generate bubble burst near the orifice of the inkjet head, which forces a droplet of liquid out of the inkjet head. Soon after this event, the bubble collapses and ink feed replenishes ejected liquid droplet, thus repeating the cycle. Similar process occurs for the piezoelectric system. Piezoelectric actuator flexes the diaphragm and subsequently generates droplet through the orifice. Figure 3.5 shows the schematic diagram of both the thermal and piezoelectric inkjet printer head.

Pioneer work in cell printing was conducted with the thermal inkjet printer [12, 13]. However, recent work in cell printing mainly utilized piezoelectric inkjet printer, which may be contributed by the following reason. In piezoelectric inkjet printer, pressure was generated without significant heat generation, thus possibly reducing damage to the cells suspended in the liquid. In addition, pressure is also generated without the necessity to form bubble burst. Therefore, piezoelectric inkjet printer can easily produce wider range of pressure pulse and handle wider range of cell suspension liquid.

Piezoelectric inkjet head structure may differ slightly in structure design to one another. A custom design piezoelectric inkjet printer was reported to be capable of deposition of organic polymers and solid particles [16]. A breakthrough study showed piezoelectric inkjet printer potential as a tool to deliver living cells at individual level [17]. Following this study, cell printing based on the piezoelectric inkjet

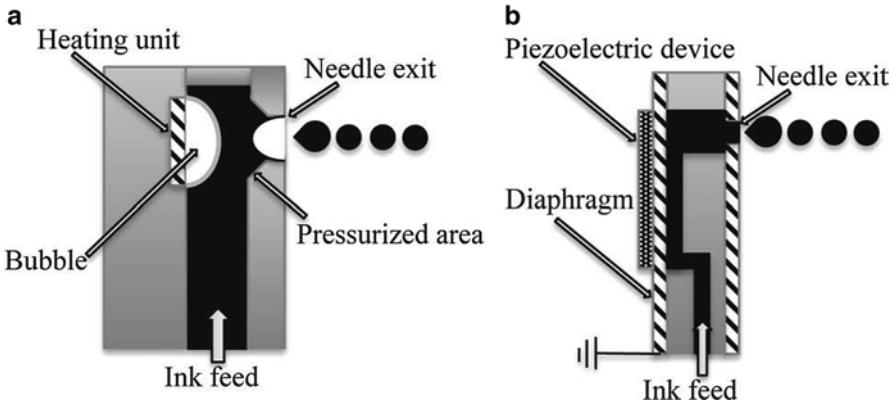

Fig. 3.5 Schematic representations: (**a**) thermal and (**b**) piezoelectric inkjet printing system (reproduced from H. P Le, J [15])

head system was reported in other studies [18, 19]. Study in stem cell patterning and three-dimensional bio-printer was also reported [20].

Piezoelectric inkjet printer showed great potential for rapid cell patterning. Additionally, precise control over the droplet volume, precise control of position where the droplets are ejected, ability to use several types of ink, and its noncontact printing characteristics are advantages of piezoelectric inkjet printer over other cell deposition systems. Nonetheless, piezoelectric inkjet printer has disadvantages, one of them being its incapability to handle individual level of cells. Research to achieve a single cell per droplet printing has been conducted, but only over 87 % of printing efficiency was achieved [21]. Another study to achieve a stable and high-efficiency single cell printing was conducted by another group [22, 23]. The method used in the study of the single cell printing will be elaborated in the next section in this chapter.

3.2.1 Piezoelectric Inkjet Head Structure

In single cell printing, piezoelectric element was used as the actuator of the inkjet head. A glass capillary with the piezoelectric actuator on its side made up the structure of the inkjet head. The movement of the piezoelectric element generates pressure inside the chamber of the inkjet head, thus generating liquid droplet through the orifice. Figure 3.6 shows the schematic structure and the cross-sectional shape of the piezoelectric inkjet head. The study focused on a simple inkjet head structure which only consists of single nozzle to eject droplets instead of a conventional complicated head. In addition, inkjet head was pressed, thus producing the ellipse cross-sectional shape. Glass material and the ellipse cross-sectional shape allow the observation of inkjet head tip, which is critical in accomplishing the single cell printing.

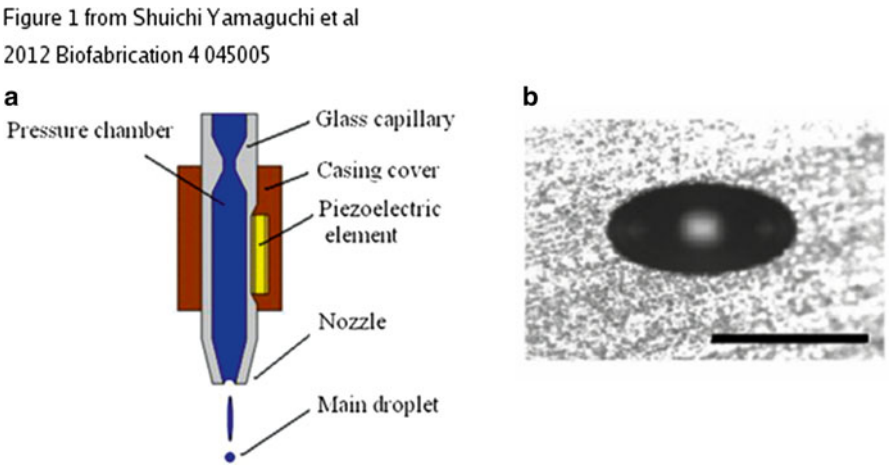

Fig. 3.6 (**a**) Schematic structures of piezoelectric inkjet head for single cell printing. (**b**) Nozzle shape. Scale bar: 50 μm (reproduced from Yamaguchi et al. [22, 23])

3.2.2 Piezoelectric Element Control Method

Methods of controlling piezoelectric element involve the shape of the voltage function. The most conventional voltage function wave is the square wave. The sudden increase and decrease of voltage means the sudden increase and decrease of pressure inside inkjet head chamber, which is indispensable to acquire necessary energy to form a liquid droplet.

Basically, amplitude and pulse width are the only two parameters which decide the shape of a square wave. Voltage amplitude correlates to the pressure change amplitude and thus correlates to droplet speed. On the other hand, pulse width correlates to the timing of the ejection. However, another more important parameter of the piezoelectric driving method is the order of applying the voltage, which leads to two main important ways of driving method, pull-push and push-pull method.

3.2.2.1 Pull-Push Method

In the standby state, voltage is already applied to the piezoelectric element. To produce droplets, voltage amplitude is returned to zero voltage, thus moving the piezoelectric actuator to its original shape and "pulling" the chamber inside inkjet head. This movement creates negative pressure in the chamber, and the liquid-air interface is pulled backward. Afterwards, voltage is applied back to the piezoelectric actuator, thus "pushing" the chamber inside inkjet head and producing droplets. The correct timing of the returning movement correlates to the resonance oscillation of the liquid-air interface layer. Figure 3.7a shows basic piezoelectric movement and (c) stroboscopic photograph of droplet produced by the pull-push method.

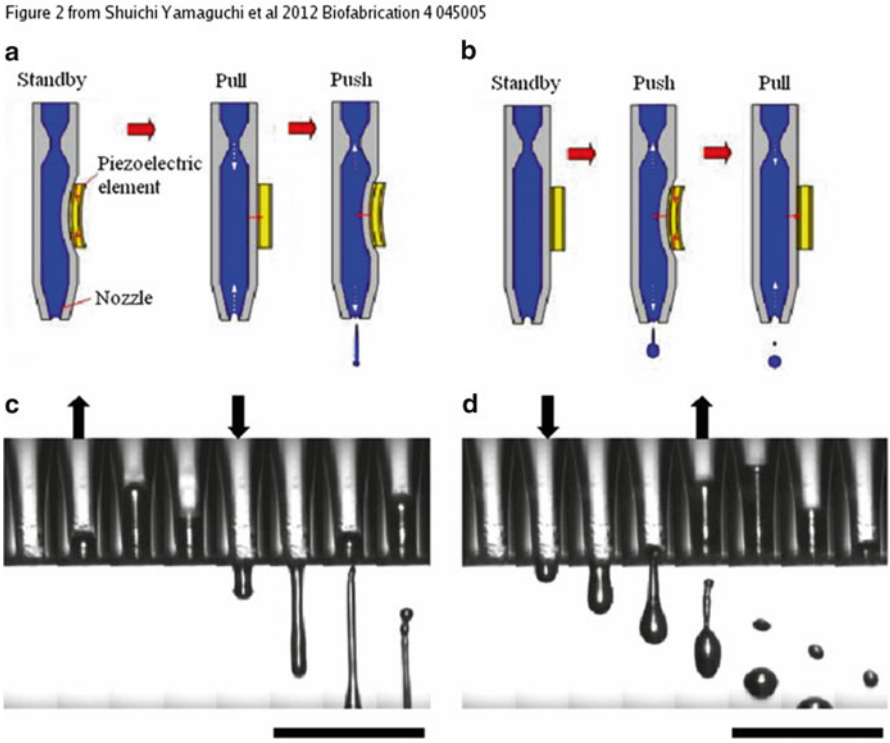

Fig. 3.7 Drive principles of piezoelectric head: (**a**) pull-push method and (**b**) push-pull method. (**c**) 50 μs/frame image of pull-push method ejection and (**d**) 50 μs/frame image of push-pull method ejection. Scale bar: 500 μm (reproduced from Yamaguchi et al. [22, 23])

3.2.2.2 Push-Pull Method

On the other hand, standby mode in push-pull method is the zero voltage. Droplets are produced by applying voltage to the piezoelectric actuator, and the push movement of the push movement of the actuator produces positive pressure inside the inkjet head chamber, thus producing liquid droplet through the nozzle. Figure 3.7b shows basic piezoelectric movement and (d) stroboscopic photograph of droplet produced by the push-pull method.

Push-pull method used to be common wave shape for producing droplets in piezoelectric inkjet technology. However, subsequent research in the field showed that compared to push-pull, the pull-push method produces longer, thinner, and faster droplet. For commercial piezoelectric inkjet printer, smaller and faster droplet is more desirable as smaller and faster droplet leads to higher printing resolution. Therefore, for commercial piezoelectric inkjet printer, pull-push method is used instead of push-pull method. Nevertheless, push-pull driving method was found to be more suitable for cell printing and single cell printing as described in later chapter.

3.3 Stable Particle Ejection

Ejection stability represents the reproducibility of inkjet printer. One way to evaluate ejection stability is by measuring variation in the droplet flight angle. Droplet flight angle is defined as the angle between vertical line and the flight line of the droplet. An inkjet printer capable of producing liquid droplet with the same angle is said to be stable. Commercial inkjet printer requires a highly stable droplet ejection to produce high-quality printing. The same analogy applies to the cell printing. However, compared to ink particles, cells are relatively large, thus causing instability to the droplet ejection. In the following section, the relation between inkjet head size, particle size, and piezoelectric driving method with ejection stability will be explained.

3.3.1 Relation Between Inkjet Head Diameter and Bead Diameters

Figure 3.8 shows a plotted graph, where vertical axis represents the flight angle, while the horizontal axis represents 200-droplet data values. Data from three experiments were plotted in each of the graphs, and each graph was plotted for different inkjet head size. Pull-push method was used as the driving force of the piezoelectric element. Smaller inkjet head diameter produced greater fluctuation of the droplet flight angle. Additionally Table 3.1 shows the evaluated variation in droplet flight angle, which is evaluated with 3σ (σ is standard deviation). Cases marked "–" in the table show the case for halted experiment because results already showed clear trend, while "NG" mark showed that the experiment could not be conducted because clogging occurred, thus preventing droplet ejection. This table shows that lower particle concentration, smaller bead size, and bigger inkjet head size produced more stable droplet.

For pull-push driving method, design for inkjet head size can be based on results showed in the table. When particle size, particle concentration, and largest allowed error in droplet flight angle parameter are fixed, inkjet head size can be easily determined. In the next section, another driving method was applied for large particle printing, and ejection stability was also evaluated with the same process.

3.3.2 Comparison of Pull-Push and Push-Pull Method

Table 3.2 shows the analysis results for the variation of the droplet flight angle for the push-pull method. Push-pull method also showed same trend as the pull-push method. Smaller particle, less particle concentration, and bigger inkjet head diameter led to a more stable ejection. Additionally, the data also showed another trend for comparison between push-pull and pull-push method. Push-pull method showed lower variation in droplet flight angle and higher maximum particle concentration compared to the pull-push method.

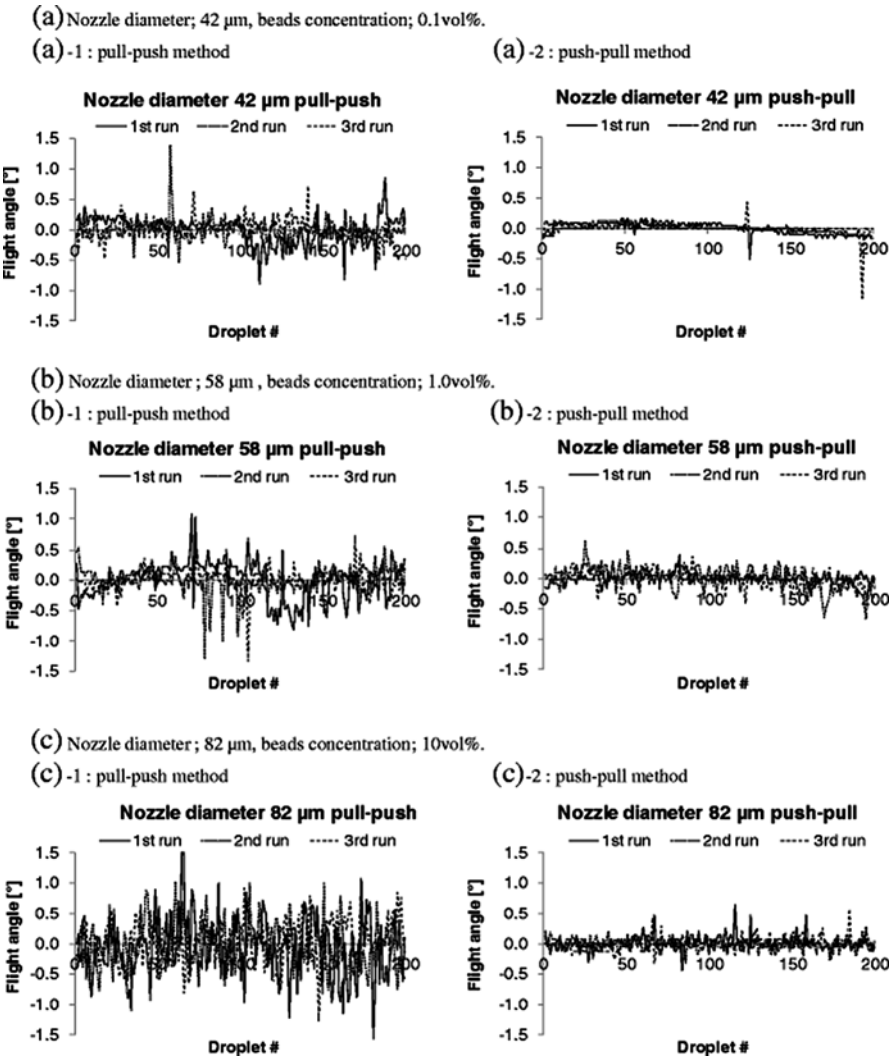

Fig. 3.8 Results of measurement of droplet ejection flight angle for and comparison between pull-push and push-pull methods (reproduced from Yamaguchi et al. [22, 23])

Inkjet head clogging was the most common problem encountered along the development of inkjet printer technology. In particle printing with size as large as living cells, inkjet head clogging also must be avoided. Therefore, for cell printing and large particle suspension, push-pull method was found to be more suitable. In addition, push-pull method also showed more stability; thus it is also more reliable.

In the next section, we will also explore the properties of both pull-push and push-pull method for single cell printing.

Table 3.1 Variation in droplet flight angle (3σ) measurement results for pull-push method (reproduced from Yamaguchi et al. [22, 23])

Bead diameter (μm)	Inkjet head diameter (μm)	Bead concentration					
		No beads	0.1 %	0.5 %	1.0 %	5.0 %	10.0 %
20	42	0.14	0.59	NG	NG	NG	NG
20	58	0.09	0.32	0.47	0.72	1.34	–
20	82	0.10	–	0.15	0.31	0.47	1.14
10	42		0.52	1.00	–	–	–
10	58		0.23	0.49	0.56	0.66	1.03
10	82		–	–	0.29	0.54	0.78

NG, ejection failure due to clogging; –, no test

Table 3.2 Variation in droplet flight angle (3σ) measurement results for push-pull method (Reproduced from Yamaguchi et al. [22, 23])

Bead diameter (μm)	Inkjet head diameter (μm)	Bead concentration					
		No beads	0.1 %	0.5 %	1.0 %	5.0 %	10.0 %
20	42	0.16	0.27	NG	NG	NG	NG
20	58	0.10	–	–	0.25	0.49	0.74
20	82	0.10	–	–	–	0.29	0.33
10	42		–	0.25	0.43	0.92	1.66
10	58		–	—	–	0.30	0.53
10	82		–	–	–	–	0.28

NG, ejection failure due to clogging; –, no test

3.4 Single Cell Printing

In previous section, optimal ejection condition for large particles was established for beads. In this section, capabilities of inkjet printer for single cell printing are explored. Printed cell viability is another important factor for cell printing; thus we will cover the study in the printed cell viability evaluation. At the end of this section, we will cover the most important discussion in this book, the single cell printing by inkjet printer.

3.4.1 Evaluation of Damage to Printed Cells

Various studies on printed cell viabilities had been conducted. One of the study found that inkjet printer showed great potential for cell handling, as printed cells showed low level of apoptosis and showed no difference between normal handling by pipetting and centrifuging [24]. Figure 3.9 also shows another study in the viability of printed cells compared to nonprinted cells. The ratio of living cells after ejection by piezoelectric

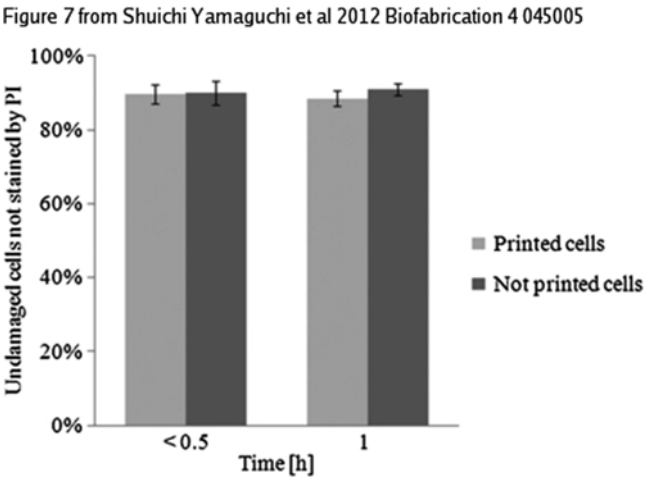

Fig. 3.9 Living cell percentages and elapsed time (reproduced from Yamaguchi et al. [22, 23])

inkjet head and the ratio of living cells by normal handling showed no significant difference. Compared to other matured technologies, recently emerging cell printing by inkjet printer still needs enormous validation for various types; nevertheless two studies discussed above showed the potential of inkjet printer for cell printing with no significant difference with normal handling by pipetting or centrifuging.

3.4.2 Single Cell Printing Principle

Two studies on single cell printing used very simple method which requires observation of inkjet head tip [21, 22]. The observation of the inkjet head allowed the observation of cell number and position inside. Additionally, inkjet head mapping or simulation of inkjet printing gave rough idea of the liquid area which will become a droplet. When single cell presents in this area, inkjet head was moved to the target printing position and the droplet containing single cell was ejected. Otherwise, the droplet is ejected somewhere else. This section covers the method to determine liquid area to become a droplet, inkjet head mapping, and comparison of inkjet head mapping between pull-push and push-pull.

3.4.2.1 Inkjet Head Mapping

Figure 3.10a shows the general idea of inkjet head mapping. First, each cell position near the tip of the inkjet head was recorded. Next, ejection signal was sent to the piezoelectric element to eject one droplet. After the ejection, whether cell had been ejected along with the droplet or not was confirmed. Ejected cell position was

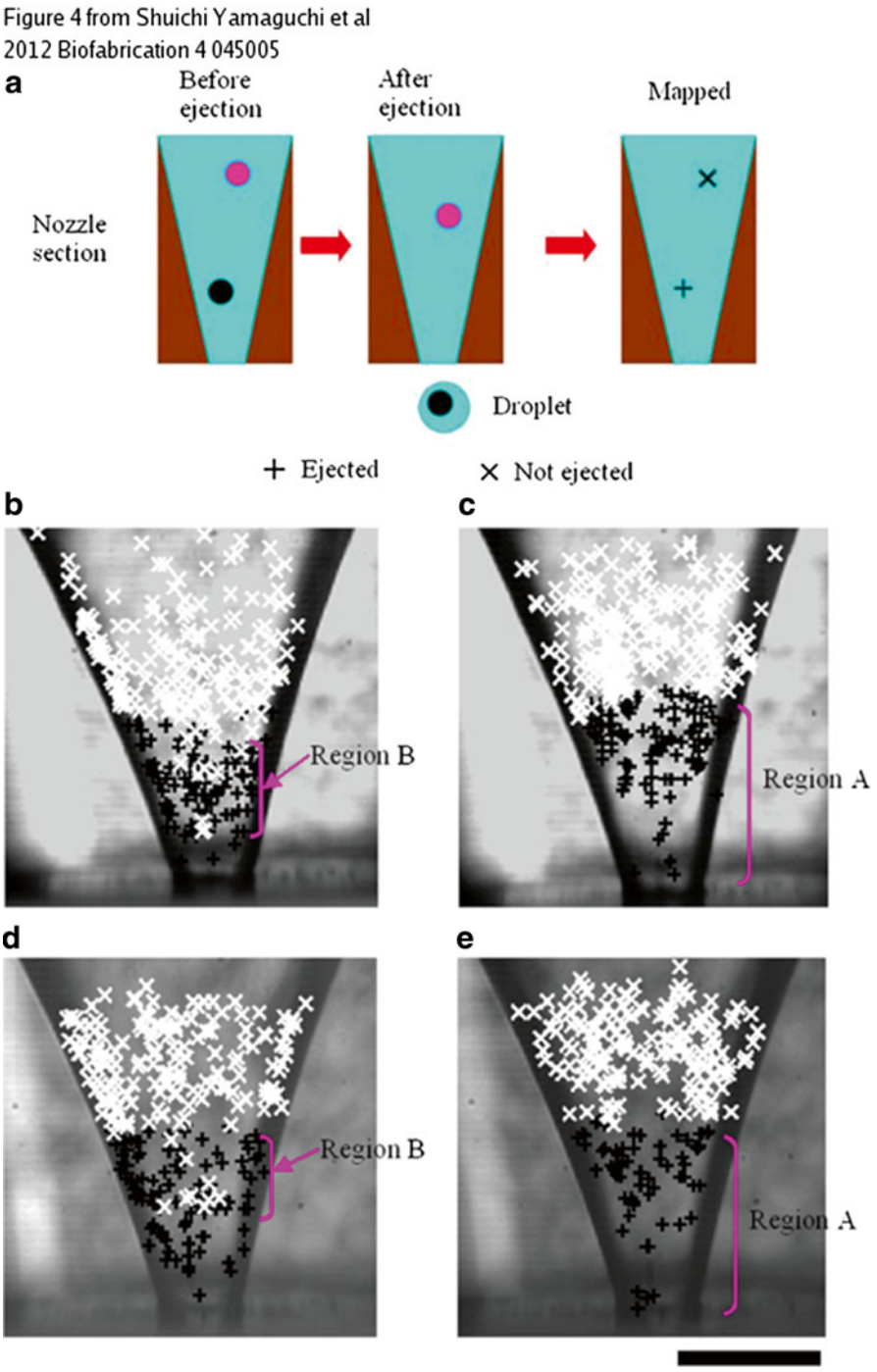

Fig. 3.10 (**a**) Method of inkjet head mapping. For bead suspension, the result of the (**b**) pull-push method and (**c**) push-pull method. And for cell suspension, the results of the (**d**) pull-push and (**e**) push-pull method. Scale bar: 50 μm (reproduced from Yamaguchi et al. [22, 23])

marked with a plus sign (+), and not ejected cell was marked with a cross sign (×). This is repeated for 100 cells and results in Figure 3.10b–e were obtained. Region A was defined as the area with only plus sign, while region B was defined as the area with mixed plus and cross sign.

Region B is undesirable for accurate single cell printing, because with both plus and cross sign at nearby point, cell ejection becomes uncertain. Figure 3.10b–e shows the mapping results for both pull-push and push-pull method. Pull-push method mapping results contained region B, while push-pull method contained none to negligible region B. Therefore, push-pull method was shown to be more suitable for single cell printing. Considering this data and the data from the previous section, push-pull method was found to be more suitable for single cell printing compared to pull-push method.

3.4.2.2 Single Cell per Droplet Ejection

Figure 3.11 shows the cell positioning errors with respect to the target position for single cell printing experiment. All patterned cells were positioned onto the target area with a precision within approximately 100 μm. The average positioning error was approximately 51 μm, and the variation of the positioning error, which is evaluated with the 3σ (σ is the standard deviation), was approximately 75 μm. The positioning error depends on the following three factors: variation of the droplet flight angle, mechanical precision of the device, and the spreading movement of the droplet liquid. In previous section, the variation of the droplet flight angle was 0.26°, which contributes to approximately 5 μm of positioning error.

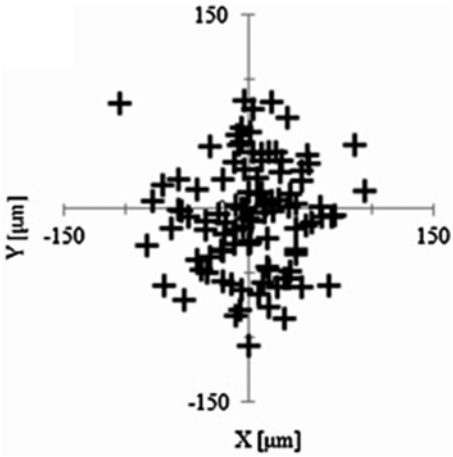

Fig. 3.11 Scatter plot of cell positioning error with respect to the designated location (reproduced from Yamaguchi et al. [22, 23])

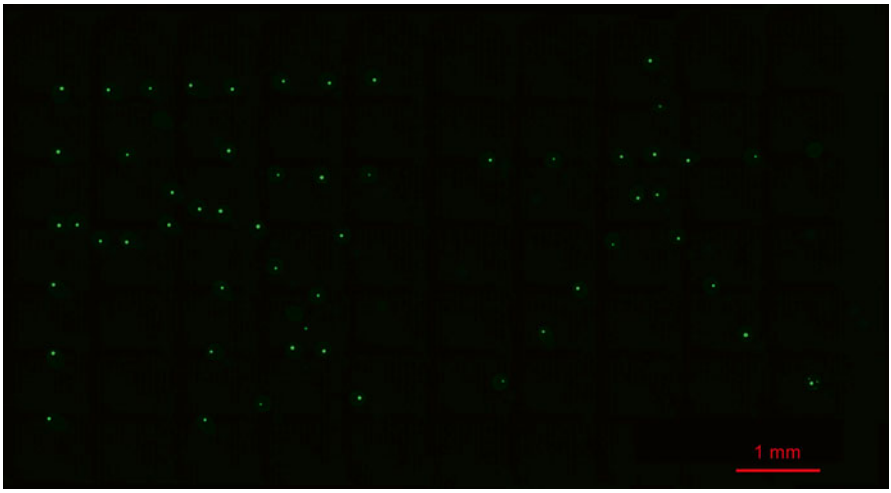

Fig. 3.12 Kanji character of Osaka University patterned with single cell per dot

On the other hand, error from the mechanical robot of the device contributes to approximately 10 μm of positioning error. Thus, it can be concluded that approximately 60 μm of positioning error was the result of the spreading movement of the liquid droplet across the printing surface. Figure 3.12 shows the kanji character of the Osaka University using this cell positioning technology.

3.5 Conclusion

Most commercially available inkjet head and piezoelectric driving method were designed to eject solutions containing functional materials that are either completely dissolved or consist of suspended particles under 1 μm in diameter. In order to achieve stable ejection of large particles by piezoelectric inkjet, inkjet head structure, sizes, and piezoelectric driving method must be adjusted.

Successful adjustment of those parameters resulted in a precise single cell patterning [22], thus showing cell printing potential not only for tissue engineering application but also for single cell analysis. The technology ability for spatiotemporal control of single cells without major damage to cells has enormous implication in various clinical applications. Nevertheless, much effort is still needed for this technology to become the key for future 3D structure printing, such as increasing cell printing resolution and the development of suitable material as the "bio-ink." This technology is still in its early step in the printing of cells; thus vast amount of research is necessary for the development course of this technology. It is fascinating to look into the future where organ transplantation was performed with 3D printed organ.

References

1. Roman GT, Chen Y, Viberg P, Culbertson AH, Culbertson CT (2006) Single-cell manipulation and analysis using microfluidic devices. Anal Bioanal Chem 387:9–12
2. Toner M, Irimia D (2005) Blood-on-a-chip. Annu Rev Biomed Eng 7:77–103
3. Cao Y, Vacanti JP, Paige KT, Upton J, Vacanti CA (1997) Transplantation of chondrocytes utilizing a polymer-cell construct to produce tissue-engineered cartilage in the shape of a human ear. Plast Reconstr Surg 100:297–302, Discussion 303–304
4. Poncelet D, de Vos P, Suter N, Jayasinghe SN (2012) Bio-electrospraying and cell electrospinning: progress and opportunities for basic biology and clinical sciences. Adv Healthc Mater 1:27–34
5. Wilbur JL, Kumar A, Kim E, Whitesides GM (1994) Microfabrication by microcontact printing of self-assembled monolayers. Adv Mater 6:600–604
6. Von Philipsborn AC, Lang S, Bernard A, Loeschinger J, David C, Lehnert D, Bastmeyer M, Bonhoeffer F (2006) Microcontact printing of axon guidance molecules for generation of graded patterns. Nat Protoc 1:1322–1328
7. Odde DJ, Renn MJ (2000) Laser-guided direct writing of living cells. Biotechnol Bioeng 67:312–318
8. Pirlo RK, Dean DMD, Knapp DR, Gao BZ (2006) Cell deposition system based on laser guidance. Biotechnol J 1:1007–1013
9. Nahmias Y, Schwartz RE, Verfaillie CM, Odde DJ (2005) Laser-guided direct writing for three-dimensional tissue engineering. Biotechnol Bioeng 92:129–136
10. Elrod SA, Hadimioglu B, Khuri-Yakub BT, Rawson EG, Richley E, Quate CF, Mansour NN, Lundgren TS (1989) Nozzleless droplet formation with focused acoustic beams. J Appl Phys 65:3441–3447
11. Fang Y, Frampton JP, Raghavan S, Sabahi-Kaviani R, Luker G, Deng CX, Takayama S (2012) Rapid generation of multiplexed cell cocultures using acoustic droplet ejection followed by aqueous two-phase exclusion patterning. Tissue Eng Pt C Methods 18:647–657
12. Boland T, Mironov V, Gutowska A, Roth EA, Markwald RR (2003) Cell and organ printing 2: fusion of cell aggregates in three-dimensional gels. Anat Rec A Discov Mol Cell Evol Biol 272A:497–502
13. Wilson WC, Boland T (2003) Cell and organ printing 1: Protein and cell printers. Anat Rec A Discov Mol Cell Evol Biol 272A:491–496
14. Nishiyama Y, Nakamura M, Henmi C, Yamaguchi K, Mochizuki S, Nakagawa H, Takiura K (2009) Development of a three-dimensional bioprinter: construction of cell supporting structures using hydrogel and state-of-the-art inkjet technology. J Biomech Eng 131:035001
15. Hue PL (1998) Progress and trends in ink-jet printing technology. J. Imaging Sci. Technol. 42:49-62
16. Perçin G, Lundgren TS, Khuri-Yakub BT, (1998) Controlled ink-jet printing and deposition of organic polymers and solid particles. Appl Phys Lett 73:2375–2377
17. Saunders RE, Gough JE, Derby B (2008) Delivery of human fibroblast cells by piezoelectric drop-on-demand inkjet printing. Biomaterials 29:193–203
18. Kim JD, Choi JS, Kim BS, Chan Choi Y, Cho YW (2010) Piezoelectric inkjet printing of polymers: stem cell patterning on polymer substrates. Polymer 51:2147–2154
19. Li EQ, Xu Q, Sun J, Fuh JYH, Wong YS, Thoroddsen ST (2010) Design and fabrication of a PET/PTFE-based piezoelectric squeeze mode drop-on-demand inkjet printhead with interchangeable nozzle. Sensors Actuat Phys 163:315–322
20. Nakamura M, Kobayashi A, Takagi F, Watanabe A, Hiruma Y, Ohuchi K, Iwasaki Y, Horie M, Morita I, Takatani S (2005) Biocompatible inkjet printing technique for designed seeding of individual living cells. Tissue Eng 11:1658–1666
21. Yusof A, Keegan H, Spillane CD, Sheils OM, Martin CM, O'Leary JJ, Zengerle R, Koltay P (2011) Inkjet-like printing of single-cells. Lab Chip 11:2447
22. Yamaguchi S, Ueno A, Akiyama Y, Morishima K (2012) Cell patterning through inkjet printing of one cell per droplet. Biofabrication 4:045005
23. Yamaguchi S, Ueno A, Morishima K (2012) Stable ejection of micro droplets containing microbeads by a piezoelectric inkjet head. J Micro-Nano Mechatronics 7:87–95
24. Cui X, Dean D, Ruggeri ZM, Boland T (2010) Cell damage evaluation of thermal inkjet printed Chinese hamster ovary cells. Biotechnol Bioeng 106:963–969

Chapter 4
Engineering Electrospun Scaffolds to Encourage Cell Infiltration

H. Sakaguchi, N.J. Amoroso, and W.R. Wagner

Abstract Electrospinning has become a popular technique to construct micro-/nanofibrous scaffolds for a broad variety of regenerative medicine applications. Electrospun scaffolds provide an abundant surface area and a densely assembled fiber architecture. However, the small pore sizes common with this technique hinder cellular infiltration and integration with host tissue. In order to address this important limitation, many researchers have proposed methods to create larger pores, to increase porosity, and to integrate cells among the fibers. In this chapter, we survey recent efforts in modifying the electrospinning process to facilitate better cellular infiltration and tissue integration.

Keywords Cell infiltration • Electrospinning • Regenerative medicine • Scaffold

H. Sakaguchi
Advanced Materials Research Laboratories, Toray Industries Inc.,
2-1, Sonoyama 3-chome, Otsu, Shiga 520-0842, Japan

McGowan Institute for Regenerative Medicine, University of Pittsburgh,
Pittsburgh, PA 15219, USA

N.J. Amoroso
McGowan Institute for Regenerative Medicine, University of Pittsburgh,
Pittsburgh, PA 15219, USA

W.R. Wagner (✉)
McGowan Institute for Regenerative Medicine, University of Pittsburgh,
Pittsburgh, PA 15219, USA

Department of Surgery, University of Pittsburgh, Pittsburgh, PA 15219, USA

Department of Bioengineering, University of Pittsburgh, Pittsburgh, PA 15219, USA

Department of Chemical Engineering, University of Pittsburgh, Pittsburgh, PA 15219, USA
e-mail: wagnerwr@upmc.edu

M. Akashi et al. (eds.), *Engineered Cell Manipulation for Biomedical Application*, Nanomedicine and Nanotoxicology,
DOI 10.1007/978-4-431-55139-3_4

4.1 Introduction

In the tissue engineering paradigm, a temporary scaffold is required to structurally and mechanically support cells during tissue repair. In order to successfully perform this function, any tissue engineering scaffold must be biocompatible with sufficient mechanical strength to maintain integrity during extracellular matrix (ECM) elaboration. However it must also possess sufficient surface area and porosity for robust tissue ingrowth. Electrospinning is an attractive technique for the fabrication of fibrous scaffolds which can be employed to meet each of the criteria for a successful tissue engineering scaffold.

Electrospinning is a technique which utilizes coulombic forces in the preparation of ultrathin fibers. This technique was developed over 100 years ago [1]; however it has been the subject of extensive research in the past decade due to its ability to create fibers of 50 nm–10 μm in diameter in comparison to 10–100 μm produced by more conventional extrusion techniques [2]. Such size scales are of particular interest in the medical field, as they encompass the same order of magnitude as the protein fibers which comprise native ECM. This structure was therefore hypothesized to be attractive for supporting viable cells. Indeed, many in vitro studies have demonstrated that living cells thrive on electrospun fibers [3–8] and may be able to maintain a phenotype more similar to that found in vivo when compared with tissue culture polystyrene [9].

4.2 Principle of Electrospinning

In principle, electrospinning is a simple process brought on by electrostatic forces attracting a polymer solution toward a grounded target; however the number of parameters involved makes control of the process quite complex. At its most basic, electrospinning occurs when an electric field is applied to a viscous polymer fluid (solution or melt) in the presence of a grounded or oppositely charged target (Fig. 4.1). Most commonly, but not necessarily, the polymer solution is fed through a charged capillary. The voltage on the capillary perturbs the fluid at the end nearest the target, drawing it into a cone shape known as a "Taylor cone." When the attractive force on the solution applied by the electrostatic field overcomes the surface tension of the fluid, the fluid begins to escape from the tip of the Taylor cone and travels toward the counter electrode. If a sufficient number of polymer chain entanglements exist, the escaping fluid forms a stable, complete jet which will deposit solid fibers onto the target [10, 11]. As the jet travels through the air intramolecular electrostatic repulsions trigger a series of Raleigh instabilities which result in a rapid, chaotic whipping motion. The whipping motion extrudes the jet to such a degree that it is common for fiber diameters upon deposition to be much smaller than the initial size of the jet [12]. The chaotic nature of fiber motion as they deposit upon the target produces a 2D pattern of indeterminate topology. As further fibers deposit on top of the initial layer, a small amount of residual solvent is often present which permits the formation of a bound joint at the intersection between two or

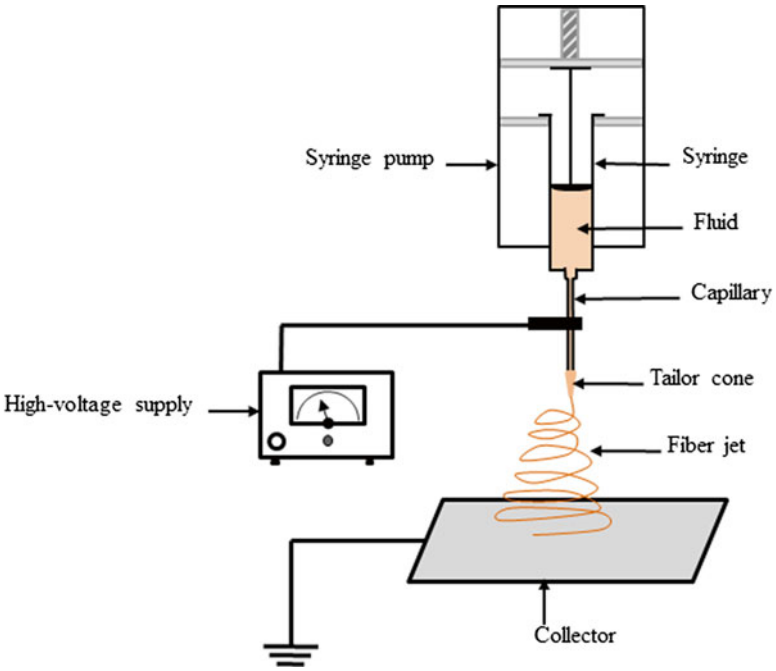

Fig. 4.1 A schematic illustration of an electrospinning technique

more fibers [13]. If no changes are made to the processing parameters over time, the stochastic nature of the process will allow for the formation of a 3D structure in which no two layers are the same, but every layer shares the equivalent structural features on average [14]. The morphology of the fibers deposited onto the target is heavily dependent on the qualities of the polymer solution as well as processing parameters and even ambient conditions (e.g., applied voltage, solvent, concentration and molecular weight of polymer, flow rate, gap distance relative humidity).

4.3 The Challenge of Achieving Cell Infiltration

While many electrospun constructs have been shown to be successful at supporting viable cells on their surface, attempts to encourage cellular infiltration into these scaffolds in vitro have been difficult in terms of producing uniform cellularity throughout the scaffold thickness. Such attempts involve seeding cells on the external surface of the scaffolds and allowing cells to infiltrate during culture. It has been shown that under static culture, cell infiltration is limited to short distances on the order of several micrometers; however perfusion culture can increase these distances [15, 16]. The cause of difficulty with seeding electrospun constructs is the pore size of the scaffolds. Electrospun constructs have been reported to have typical porosity values of approximately 70–80 % [17]. While this value is high, the nature

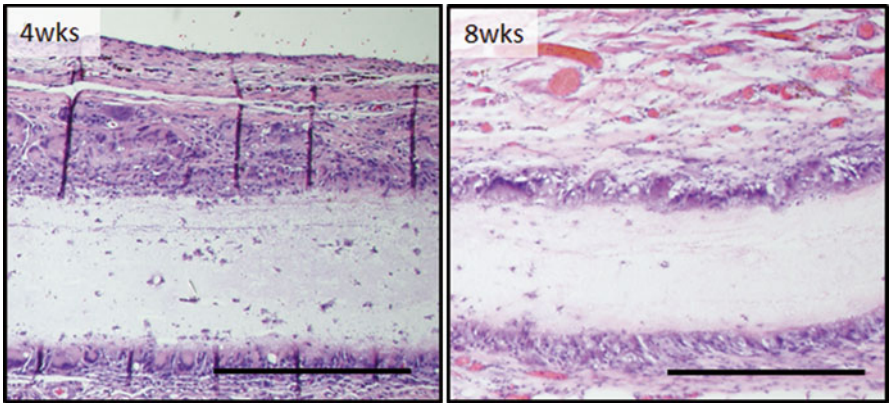

Fig. 4.2 High-magnification image of the borderline of a dense electrospun elastomeric polymer scaffold implanted in the abdominal wall of a rat for 4 (*left*) or 8 (*right*) weeks. Note few infiltrated cells within the bulk of the material, with a dense cell and ECM-rich layer above and below (scale bar: 100 μm)

of the fabrication technique, particularly when fibers are aligned, leads to tightly packed constructs with pore sizes smaller than the typical size of a mammalian cell [18]. Extrapolating from previous studies [19], it can be hypothesized that cells are often hindered from penetrating deeply into scaffolds with small pores. While this resistance to cell infiltration has been used as an advantage in some biomedical applications [20], more often an undesired result occurs when constructs with insufficient pore sizes are implanted in vivo. Rather than infiltrating and integrating the biomaterial with the surrounding tissue, inflammatory cells will stimulate a fibrotic response around such a material. The end result of this process is a dense collagenous capsule that will act to isolate and stiffen even a compliant polymeric scaffold (Fig. 4.2). Further, the lack of cellular infiltration will likely slow the degradation rate of the material.

A wide variety of approaches have been employed, and continue to be developed, to address the challenges of achieving cell integration into electrospun scaffolds [18]. In some cases this has involved placing cells within the scaffolds as they are generated. The following text provides a survey of the different approaches that have been described to facilitate the formation of cell or tissue-integrated scaffolds, attempting to cover the major types of approaches, but necessarily not being able to exhaustively note or describe each variation in this growing literature.

4.3.1 Sparse Fibers to Decrease the Fiber Density

One of the distinct advantages of electrospinning is its amenability to modification. Nearly every fiber-network microstructural feature is controllable, and pore size is no exception. One straightforward technique can be to simply increase the fiber

diameter [7, 21, 22]. However, as the fiber diameter is enlarged, a motivation for using the electrospinning technique may be lost if less favorable cellular response [9] in terms of phenotype and behavior occurs. Several researchers have developed alternative modalities which produce electrospun scaffolds with fundamentally different fiber topologies in 3D in order to produce materials with dramatically lower polymer densities and possibly encourage more substantial cellularity.

Blakeney et al. targeted a jet toward the inner surface of a nonconductive hemispherical dish equipped with an array of electrodes [6]. This technique produced a unique electrostatic field within the hemisphere where no region possessed a preferential attraction for the polymer jet, allowing fiber aggregation in midair—producing a loose "cotton ball-like" construct, which permitted uniform cell infiltration over 7 days. A similar result was achieved by Phipps et al. using a disk-shaped collector with protruding needle electrodes [23]. Scaffolds produced using these methodologies are among the least dense scaffolds that have been made, but are by nature disordered and not well suited for load-bearing applications.

Xie et al. employed a specially designed collector to produce an ordered construct with sufficient pore structures for cell viability [24]. This collector (Fig. 4.3a, b) was designed to mimic the gradients in composition and structure that exist at the native tendon-to-bone insertion and demonstrated the fabrication of poly(D,L-LACTIC-CO-glycolic) acid (PLGA) nanofibrous mats containing both aligned and random fiber regions within the same construct. Tendon fibroblasts seeded on the aligned portion were observed to possess elongated morphology with the main angle of fiber alignment (Fig. 4.3c), while the cells on the random portion were irregularly shaped and randomly oriented.

Liu et al. developed a magnetic-field-assisted electrospinning technique to fabricate the well-ordered nanofibers [25]. Opposing magnetic poles of constant strength were utilized to attract fibers as they deposited, forcing them into alignment across a gap (Fig. 4.3d). Further modification of fiber topology could be achieved by increasing the polymer flow rate, allowing the fibers to become wavy prior to deposition (Fig. 4.3e, f). Two days of mesenchymal stem cell culture on these scaffolds were sufficient to achieve proliferation and elongation in the preferred fiber direction (Fig. 4.3g–i).

In other approaches, Lee et al. developed highly porous scaffolds by using ultrasonication and showed markedly improved cell infiltration in the treated materials [26]. Shabani et al. used an array of halogen lamps to localize heat in the path of the electrospun jet near the collector and developed scaffolds with loosely packed nanofibers [27]. Karchin et al. utilized a degradable polyurethane to fabricate scaffolds with high porosity using melt electrospinning and taking advantage of the thermal properties of the utilized polymer [28]. Farrugia et al. also fabricated scaffolds by melt electrospinning method combined with direct writing mode and produced a scaffold with high porosity and suitable fiber distances to achieve high cell infiltration [29]. Levorson et al. reported a scaffold with high porosity containing two differently scaled fibers to encourage cell infiltration [30]. Jha et al. fabricated highly aligned scaffold with high void volumes by two-pole air gap electrospinning [31]. In that technique a pair of electrodes suspended on pillars was used as a target.

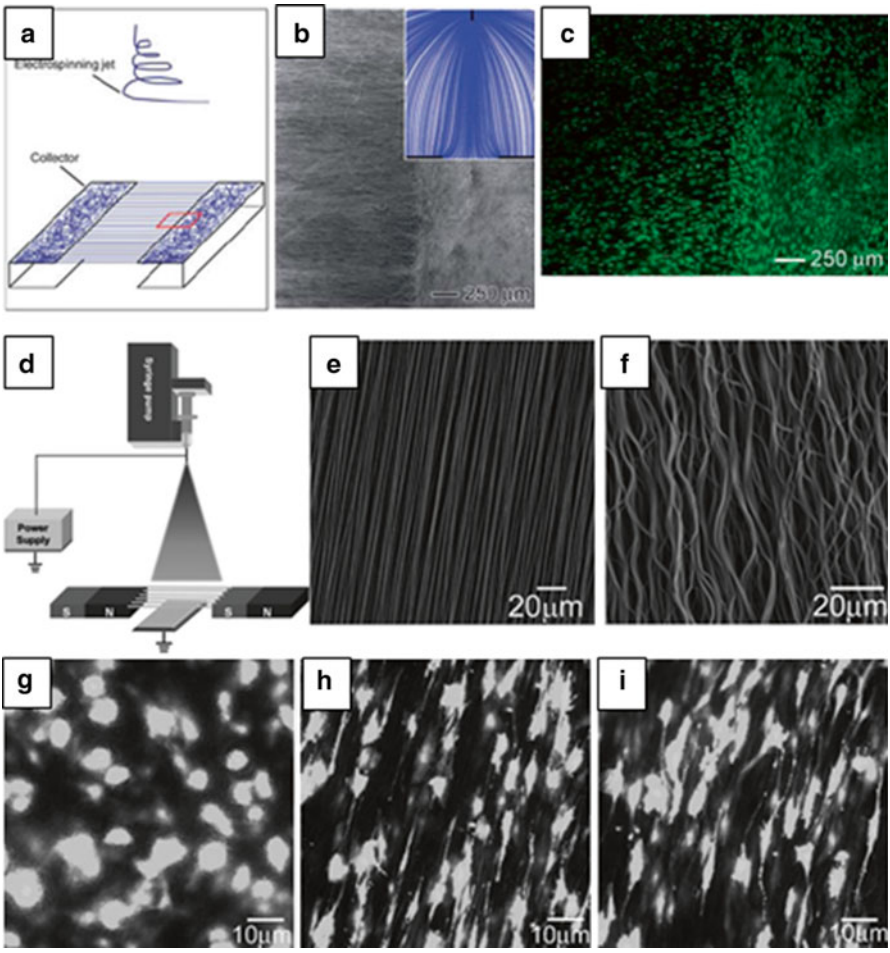

Fig. 4.3 Sparse fibers for fabricating the highly aligned fibers. (**a**) Schematic for the fabrication of aligned-to-random nanofiber scaffolds. (**b**) Scanning electron microscopy (*SEM*) images of the nanofiber scaffolds at the transition region between aligned and random regions. *Inset*: streamline plot of the electric field between the charged capillary and the target. (**c**) Tendon fibroblast cell morphology on aligned-to-random PLGA fiber scaffolds after incubation for 7 days. (**d**) Schematic illustration of the magnetic-field-assisted electrospinning technique. (**e**, **f**) SEM images of electrospun (**e**) straight and (**f**) wavy fiber arrays. (**g–i**) Fluorescent micrographs of stem cells cultured for 2 days on scaffolds consisting of (**g**) random, (**h**) aligned straight, and (**i**) aligned wavy PLGA fibers. (**a–c**) From Xie et al. Copyright The Royal Society of Chemistry 2010, (**d–i**) from Liu et al. Copyright 2010 Wiley-VCH Verlag GmbH & Co. KGaA, Weinheim

The electrospun fiber, drawn to both terminals, whipped in loops and deposited in a loose bundle of parallel fibers. This structure was found to be quite beneficial for peripheral nerve regeneration, as the loose bundles of parallel fibers were able to guide axons from the proximal to distal stumps, as well as regain some degree of function in the short study.

4.3.2 Salt or Ice Crystal Leaching

To fabricate scaffolds having larger pores or higher porosity, porogens (e.g., salt, ice, microspheres) can be deployed during the electrospinning process. After electrospinning is complete, the deposited porogens are leached from within the electrospun sheets. Nam et al. introduced NaCl crystals as a porogen to the poly(ε-caprolactone) (PCL) electrospun fiber network during fabrication [32]. The salt crystals were intermixed among the fibers using a sheath (Fig. 4.4a, b) and dissolved away following fabrication. This technique produced partially delaminated constructs with microscale pores from 100 to 200 μm in diameter (Fig. 4.4c, d). By increasing the pore size using this method, the authors were able to demonstrate cell infiltration up to 4 mm from the seeding surface over 3 weeks compared to 160 μm found with a dense electrospun scaffold.

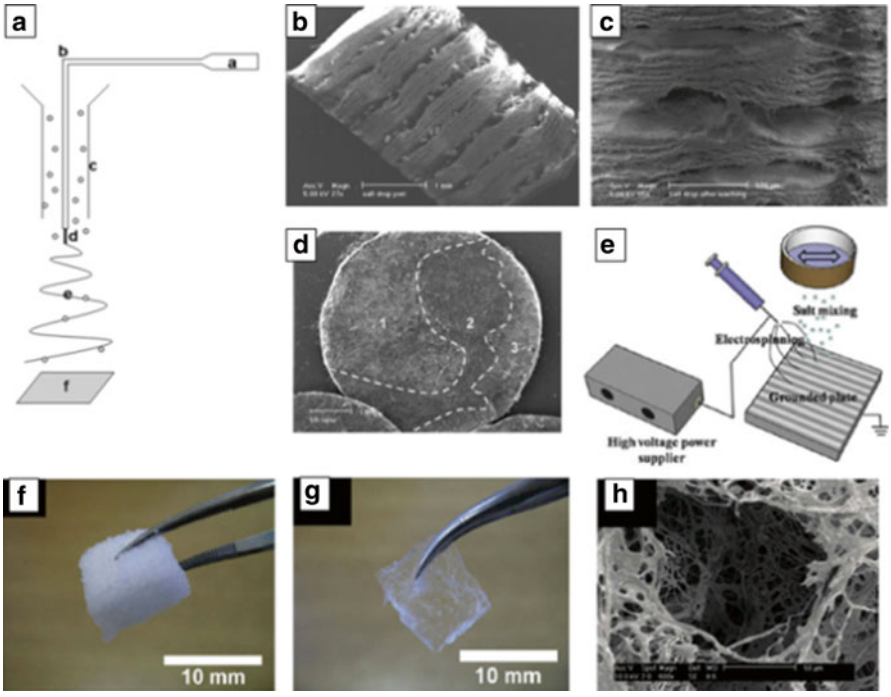

Fig. 4.4 Salt leaching to introduce larger pores into scaffolds. (**a**) Schematic illustration for the fabrication of salt/polymer composite scaffolds. (**b**, **c**) PCL and NaCl multilayered scaffolds (**b**) before and (**c**) after NaCl leaching. (**d**) SEM image of the cross section after 3 weeks of culture (cellular infiltrated areas, regions *1* and *3*; no cellular coverage, region *2*). (**e**) Electrospinning concurrent with salt deposition. (**f**, **g**) Photographs of resultant scaffolds (**f**) before and (**g**) after salt leaching and cross-linking. (**h**) SEM image of scaffold after salt leaching and cross-linking. (**a**–**d**) From Nam et al. Copyright Mary Ann Liebert, Inc., (**e**–**h**) From Kim et al. Copyright 2008 Acta Materialia Inc. Published by Elsevier Ltd

In a related technique, Kim et al. fabricated 3D nanofibrous hyaluronic acid (HA)-based scaffold with pores created by salt leaching [33]. While a mixture of HA and collagen was electrospinning, NaCl crystals were uniformly dropped onto the depositing electrospun fibers (Fig. 4.4e, f). The resultant scaffolds were cross-linked and the included salts were leached away (Fig. 4.4g, h). Though the scaffold shrunk after salt leaching, it maintained its structural integrity and the introduced pores remained.

Porogens can be made up of any readily removable material of a proper size that could be included within a scaffold. Simonet et al. reported a technique where CO_2 ice cooling of the collecting mandrel was used to encourage condensation and ice crystal formation during fabrication (Fig. 4.5a) [34]. When performed at a controlled relative humidity, scaffolds were found to be uniformly less dense with larger interfiber spaces in the *z*-direction, but not along x-y plane (Fig. 4.5b, c). Utilizing a similar technique, Leong et al. demonstrated cryogenic electrospinning under controlled temperature and relative humidity [35]. The collector was chilled to −30 °C, and electrospun fibers were deposited on ice crystals that formed on the collector. After the electrospinning, scaffold was lyophilized and dried (Fig. 4.5d). Pores were significantly enlarged to 10–500 μm, whereas the pore size of conventional electrospun scaffold was less than 5 μm. From in vivo studies, it was shown that cell infiltration in the cryogenic electrospun scaffolds was 100 % of the scaffold thickness (400 μm) at 28 days, while that in the conventional electrospun scaffold was less than 50 % after 56 days (Fig. 4.5e, f) [36].

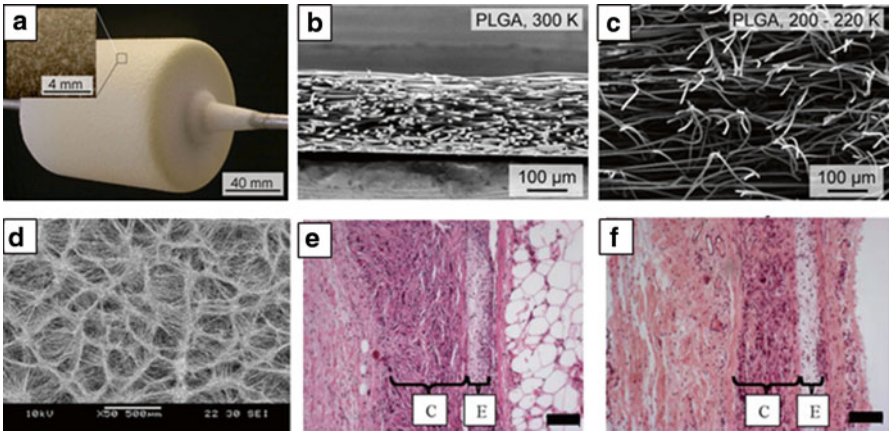

Fig. 4.5 Low-temperature electrospun scaffolds. (**a**) The chilled collector covered with ice crystals and polymer fibers. (**b**, **c**) SEM cross-sectional images of PLGA scaffolds electrospun at (**b**) room and (**c**) low temperature. (**d**) SEM image of scaffold fabricated by cryogenic electrospinning technique. (**e**, **f**) Hematoxylin and eosin (H&E) stained the two-layered (*C*, conventional electrospun layer; *E*, cryogenic electrospun layer) scaffold after implanted for (**e**) 28 days and (**f**) 56 days (scale bar: 100 μm). (**a**–**c**) From Simonet et al. Copyright 2007 Society of Plastics Engineers. (**d**) From Leong et al. Copyright 2008 Wiley Periodicals, Inc. (**e**, **f**) From Leong et al. Copyright 2010 Wiley Periodicals, Inc

4.3.3 UV/Laser Treatment for Creating Microscale Features

Some reports have employed methods to further modify scaffolds following fabrication—for instance, by exposing the scaffold to ultraviolet (UV) or laser radiation. Yixiang et al. utilized UV irradiation to selectively degrade PLGA and poly(L-lactide-co-ε-caprolactone) (P(LLA-CL)) scaffolds using photolithography techniques [37] (Fig. 4.6a, b). After 20 days of culture, cells seeded onto the UV treated P(LLA-CL) scaffolds were able to migrate through the enlarged pores generated by UV irradiation (Fig. 4.6c).

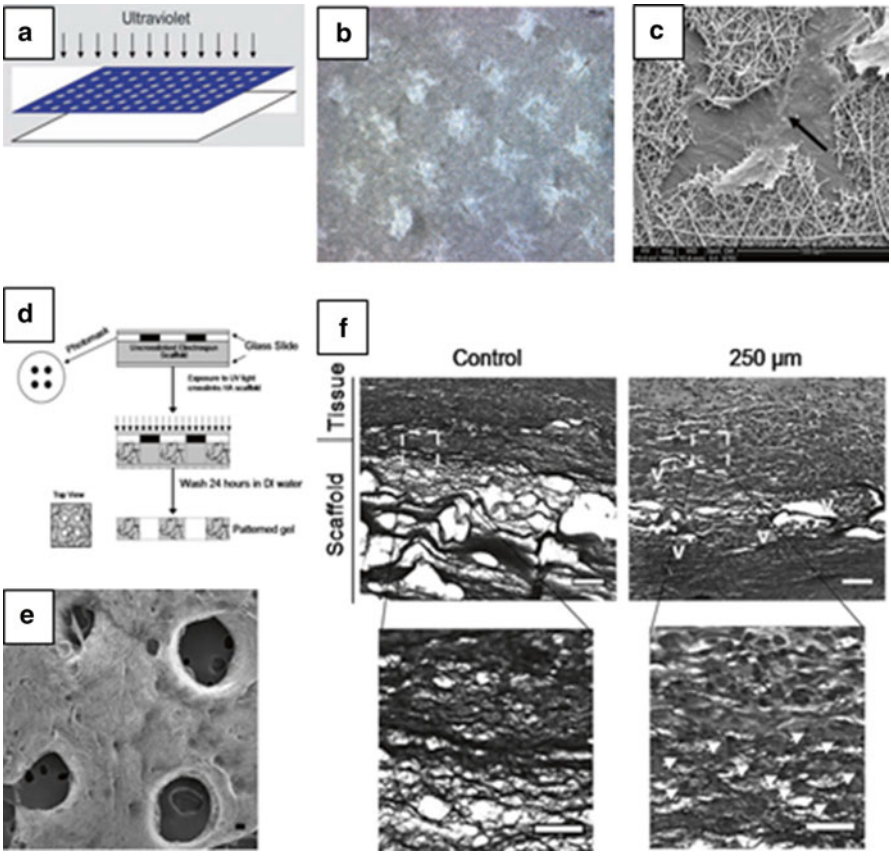

Fig. 4.6 UV treatment to increase the porosity of electrospun scaffolds. (**a**) Schematic of UV photolithography to create porous scaffold. (**b**) P(LLA-CL) scaffold after UV treatment. (**c**) SEM image of UV treated scaffold cultured for 20 days (*black arrow* indicates the cells attached on the coverslip underneath). (**d**) Schematic illustration of technique to provide photopatterned porosity into scaffolds. (**e**) SEM image of HA electrospun scaffold after UV treatment (scale bar: 100 µm). (**f**) Cellular infiltration into scaffold after 1-week implantation period (scale bars in upper and lower image are 200 and 100 µm, respectively) (*V* = vascular structures, *arrows* indicate representative nuclei). (**a**–**c**) From Yixiang et al. Copyright Mary Ann Libert, Inc. (**d**–**f**) From Sundararaghavan et al. Copyright 2010 Wiley-VCH Verlag GmbH & Co. KGaA, Weinheim

Sundararaghavan et al. have combined electrospinning with photopatterning to create multiscale porous scaffolds [38]. After methacrylated hyaluronic acid (MeHA) was co-electrospun with poly(ethylene oxide) (PEO) and a photoinitiator, the electrospun mats were subsequently photocrosslinked using photomasks (Fig. 4.6d). The pores penetrated through the entire scaffold thickness (Fig. 4.6e). After the scaffolds were implanted for 1 week, a high level of cellular infiltration was observed in the patterned scaffolds, while there were acellular regions in the scaffolds fabricated without multiscale porosity (Fig. 4.6f).

Lim et al. reported the formation of patterned microwells generated on the surface of electrospun scaffolds by femtosecond laser ablation (Fig. 4.7a) [39]. The diameter of the microwells could be controlled by adjusting laser pulse energy. After stem cells were cultured in 200 μm diameter microwells for 3 days, it was observed that the cells were confined to their microwells, and the cell proliferation rate in the microwells was faster than that on the flat, as-spun surface (Fig. 4.7b, c). Lee et al. also used the femtosecond laser to ablate and create microscale holes on electrospun scaffolds (Fig. 4.7d) [40]. The diameter and the depth of holes were controllable by the laser energy and the number of laser pulses, respectively. After 2-week implantation, higher cell infiltration was observed in the electrospun

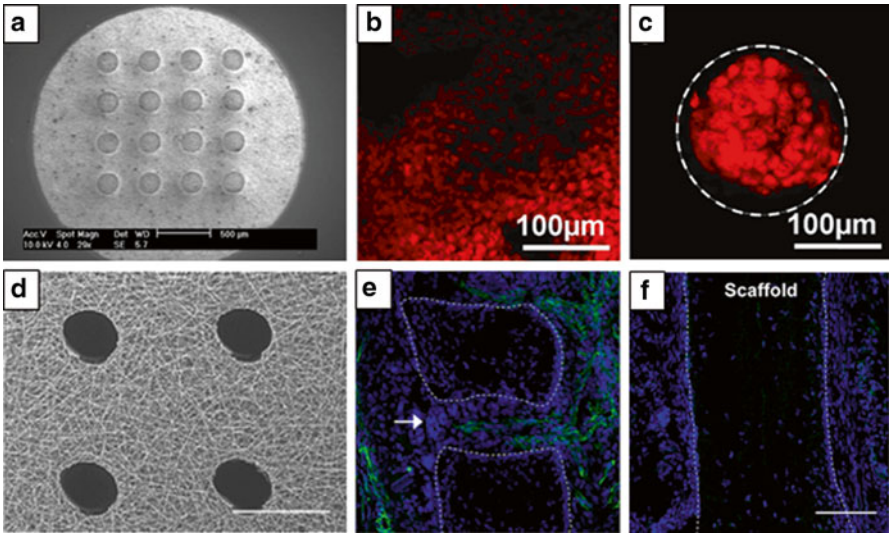

Fig. 4.7 Laser treatment to encourage cellular infiltration. (**a**) Microwells created by laser treatment on PCL/gelatin electrospun scaffold. (**b**, **c**) Fluorescence micrographs showing distributions of stem cells cultured for 3 days on (**b**) the as-spun PCL/gelatin scaffold surface and (**c**) in a microwell. (**d**) SEM image of laser treated PLLA scaffolds with holes (scale bar = 200 μm). (**e**, **f**) Cell infiltration into scaffolds (**e**) with and (**f**) without holes in vivo after 2 weeks (CD31 (*green*) for endothelial cells and 4′,6-diamidino-2-phenylindole (*DAPI*) (*blue*) for cell nuclei). *White dashed line* and *arrow* indicate edges of scaffolds and the hole, respectively (scale bar = 100 μm). (**a**–**c**) From Lim et al. Copyright 2010 Wiley Periodicals, Inc. (**d**–**f**) From Lee et al. Copyright 2012 Acta Materialia Inc. Published by Elsevier Ltd

scaffolds with ablated holes compared to control scaffolds (Fig. 4.7e, f). In similar work, Joshi et al. have reported the use of a CO_2 laser to create micropores for improved cell infiltration in subcutaneous implantation [41]. Keeping the overall porosity constant, and only adjusting pore size, Joshi et al. found that constructs containing the largest pore sizes performed better in terms of enhanced cell infiltration and vascularization.

4.3.4 Sacrificial Fibers

Conceptually similar to the approach of porogen inclusion is the method of enlarging interconnected pores by the inclusion of sacrificial fibers in a composite scaffold. Baker et al. have reported on such an approach [42, 43]. The composites were fabricated with PCL and PEO, with the latter used as the sacrificial fraction due to its water solubility (Fig. 4.8a). After electrospinning, PEO was dissolved from the composite scaffold (Fig. 4.8b, c). The treated scaffolds appeared less dense and had larger interfibrillar voids or pore spaces, but the alignment of PCL fibers remained. After 4-week implantation, cell infiltration into the scaffolds was observed to increase with the sacrificial PEO content (Fig. 4.8d). Similarly, Skotak et al. fabricated highly porous gelatin scaffolds by using PEG microfibers as sacrificial template. Cell infiltration of this scaffold was improved up to 250 μm, while that of non-templated gelatin scaffold was up to a depth of 90 μm [44].

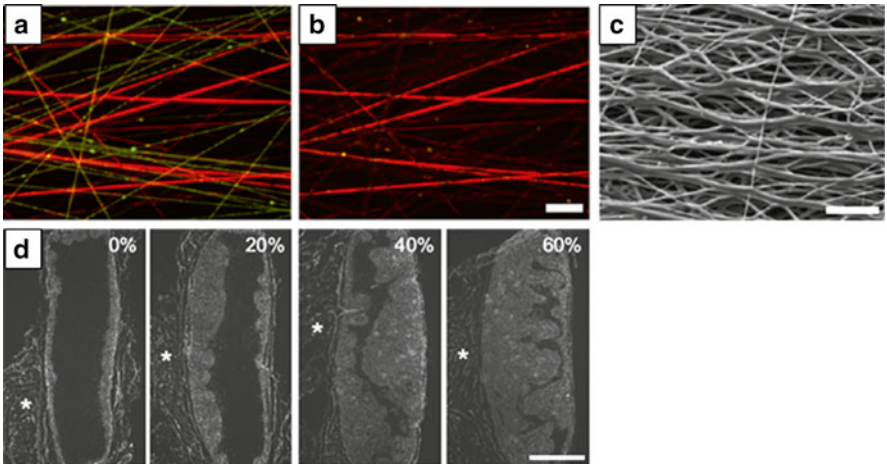

Fig. 4.8 Sacrificial fibers to increase porosity and accelerate cell infiltration. (**a**, **b**) Fluorescent micrographs of electrospun scaffold (**a**) before and (**b**) after removal of PEO fibers (PCL and PEO were fluorescent labeled *red* and *green*, respectively). (**c**) SEM image of scaffold (original PEO content: 60 %) after removal of PEO fibers. Scale bars in (**b**) and (**c**): 10 μm. (**d**) DAPI-stained cross sections of PCL scaffolds after implanted for 4 weeks (*asterisks* indicate adjacent host tissue) (scale bar:1 mm). (**a**–**d**) From Baker et al. Copyright National Academy of Science

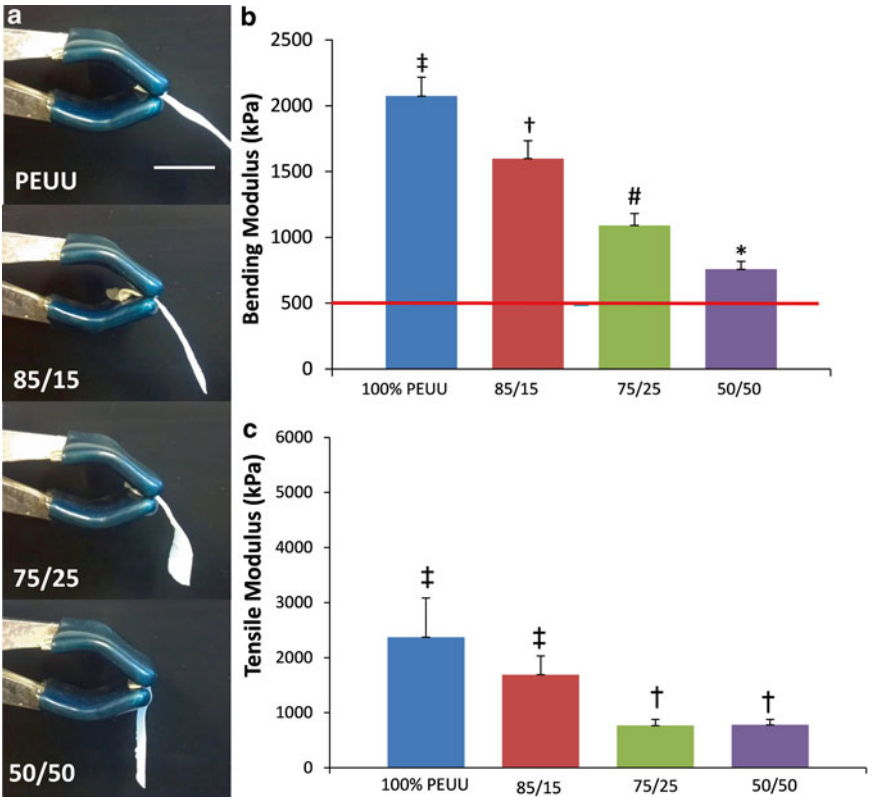

Fig. 4.9 (**a**) Qualitative depiction of constructs originally containing varying amounts of PEO placed in a cantilever position following contact with water. (**b**) Bending modulus of constructs following PEO fiber removal. Reference line indicates the bending modulus of the native pulmonary valve (491 kPa) [46]. (**c**) Tensile modulus of constructs containing varying quantities of PEO following contact with water. Groups with different symbols (*ddagger*, *dagger*, *hash*, *asterisk*) are significantly different from one another ($p < 0.05$). (**a**–**c**) From Amoroso et al. Copyright 2012 Acta Materialia Inc. Published by Elsevier Ltd

Any change in fiber density or topology is likely to also be associated with a change in function under mechanical loads. In examining this effect, Amoroso et al. introduced sacrificial PEO fibers that were later removed from an electrospun poly(ester urethane) urea (PEUU) scaffold at various volume fractions [45]. With increasing PEO content, the elastomeric scaffolds were observed to possess decreasing flexural modulus, which can be understood visually by the scaffold's inability to support its own weight when suspended in a cantilever position (Fig. 4.9). In terms of applications, this may be important in mechanically mimicking heart valve leaflet behavior, where the construct must be sufficiently soft to permit proper motion and therefore proper blood flow.

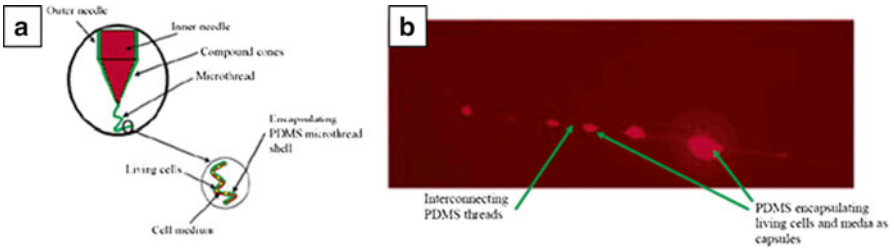

Fig. 4.10 Cells in fibers. (**a**) Schematic illustration of the coaxial cell electrospinning. (**b**) Fluorescent micrograph of cells encapsulated in PDMS fibers. (**a**, **b**) From Townsend-Nicholson et al. Copyright 2006 American Chemical Society

4.3.5 Cells Encapsulated Within Depositing Electrospun Fibers

Townsend-Nicholson et al. demonstrated the capability of encapsulating living cells within electrospun fibers as a method of generating viable biocomposites for tissue engineering or therapeutic delivery applications [47]. In this technique, cells were electrospun in a coaxial arrangement with a polymeric outer fiber shell (Fig. 4.10a). Initial in vitro analysis (Fig. 4.10b) demonstrated that cell viability was approximately 67 %, consistent with the survival of this cell type following standard processing. In vivo subcutaneous evaluation demonstrated that the encapsulated cells remained capable of engraftment with the host [48].

4.3.6 Concurrent Cell Electrospraying for Cell Microintegration

To achieve high cellular density and to accelerate cell infiltration and ECM elaboration, Stankus et al. developed a novel approach to rapidly produce cellularized electrospun tissue constructs in a single step [49]. They achieved this by concurrently electrospraying vascular smooth muscle cells (SMCs) while electrospinning a biodegradable, elastomeric PEUU (Fig. 4.11a, b). SMC viability was found to not be reduced following processing, and cell density within the scaffolds increased with 4 days of perfusion bioreactor culture (Fig. 4.11e, h) compared with 1 and 4 days of static culture (Fig. 4.11c, d, f, g). The PEUU scaffolds microintegrated with SMCs were strong and flexible. When fabricated into a small diameter tube for application as a tissue-engineered blood vessel [50], microintegrated PEUU possessed attractive compliance, burst pressure, sutured retention strength, and demonstrated an ability to maintain patency without hydrostatic support.

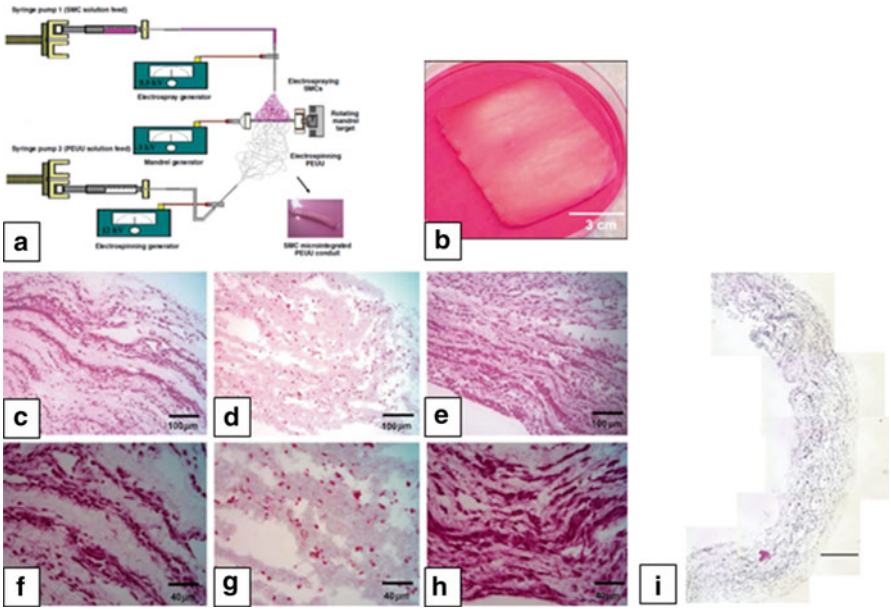

Fig. 4.11 Concurrent cell electrospraying to achieve cellular microintegration. (**a**) Microintegration using a perpendicular capillary configuration for electrospinning PEUU and electrospraying SMCs onto a rotating mandrel moving on a linear stage. (**b**) SMC-microintegrated PEUU scaffold. (**c**–**h**) H&E-stained sections of SMC-microintegrated PEUU constructs after (**c**, **f**) one day of static culture, (**d**, **g**) day 4 of static culture, and (**e**, **h**) day 4 of perfusion culture. ((**c**–**e**) scale bar = 100 mm, (**f**–**h**) scale bar = 40 mm). (**i**) Representative combined H&E-stained images of a half tube after 1 day of static culture (scale bar = 200 mm). (**b**–**h**) From Stankus et al. Copyright 2005 Elsevier Ltd. (**a** and **i**) From Stankus et al. Copyright 2007 Elsevier Ltd

4.3.7 Wet Electrospinning

Hashizume et al. reported on an acellular modification of the microintegration technique for abdominal wall repair [51]. In this technique, a polymer (PEUU) was electrospun concurrently with the electrospraying of an acellular serum-based culture medium, producing a "wet" electrospun scaffold (wet ePEUU) with a more loosely connected fiber network than unmodified electrospinning. Following implantation for 8 weeks in vivo in the abdominal wall, wet ePEUU was found to be largely degraded compared with unmodified PEUU; however the elaborated ECM from the infiltrating cells was sufficient to maintain an appropriate mechanical response throughout healing. Further, wet PEUU was observed to contain a dense cell population and a significantly higher vascular density compared with "dry" ePEUU and commercially available expanded polytetrafluoroethylene (ePTFE) (Fig. 4.12a–e).

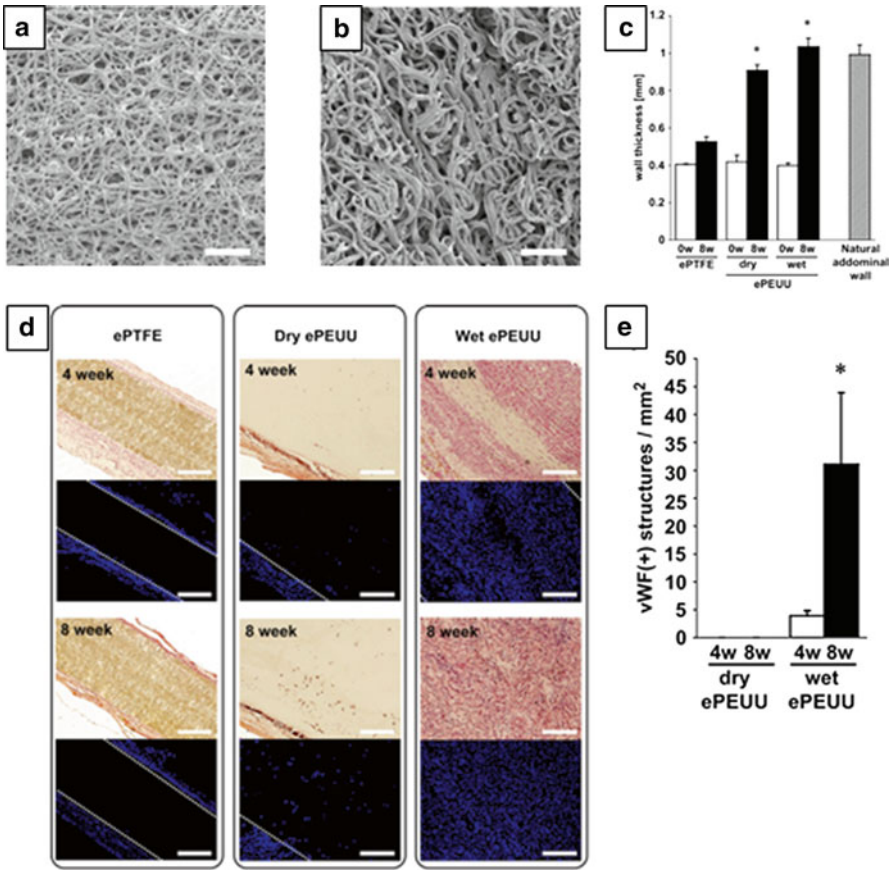

Fig. 4.12 Wet electrospinning to encourage cell infiltration. (**a**, **b**) SEM images of (**a**) dry and (**b**) wet ePEUU patch. (**c**) Wall thickness of patches prior to implant and after 8 weeks in vivo, as well as thickness of the natural rat abdominal wall. $*p<0.01$ compared with ePTFE group at the same time point. (**d**) H&E and nuclear staining for each implanted patch at each time point. (**e**) von Willebrand factor labeled structures in each patch. $*p<0.05$ compared with dry ePEUU group at 8-week point. (**a**–**e**) From Hashizume et al. Copyright 2010 Elsevier Ltd

4.3.8 Biohybrid Electrospun Scaffolds

Decellularized ECM (dECM) has been shown in numerous reports to be highly bioactive and to encourage constructive remodeling in a way that purely synthetic materials are unable to achieve [52]. However, frequently the well-defined and controllable mechanical properties of synthetic elastomers are desired for specific clinical applications. In order to combine the advantages of both classes of materials, Hong et al. developed a biohybrid scaffold consisting of an enzymatically digested

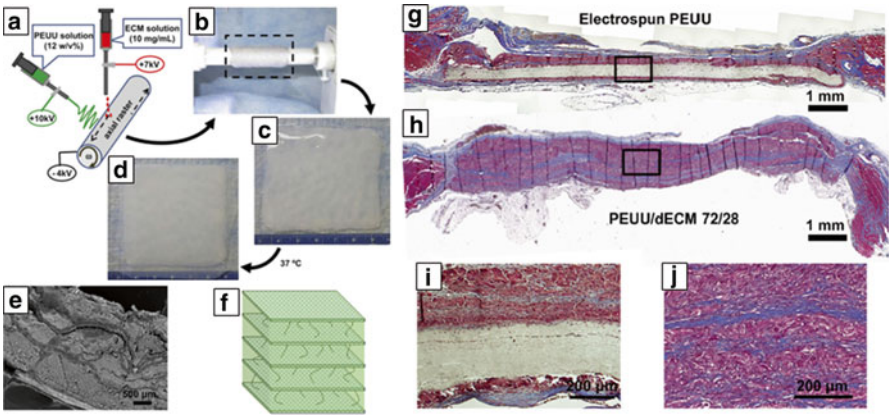

Fig. 4.13 Fabrication of a biohybrid scaffold. (**a**) Concurrent electrospin/electrospray technique for PEUU/dECM biohybrid scaffold fabrication. (**b**) Before and (**c**) after the electrodeposition process. (**d**) Resultant PEUU/dECM hydrogel hybrid scaffold. (**e**) SEM cross-sectional image and (**f**) schematic illustration of PEUU/dECM hydrogel hybrid scaffold. (**g**, **h**) Masson's trichrome-stained cross sections of the explanted (**g**, **i**) PEUU and (**h**, **j**) PEUU/dECM hydrogel biohybrid scaffold. (**a**–**j**) From Hong et al. Copyright 2011 Elsevier Ltd

decellularized ECM gel and synthetic PEUU fibers for soft tissue regeneration [53]. Scaffolds were fabricated by concurrent ECM gel electrospraying with PEUU electrospinning (Fig. 4.13a–f) to produce a cohesive material which possessed sufficient mechanical strength and compliance for good surgical handling, while maintaining bioactivity. After the biohybrid scaffolds were implanted for 4 weeks in an abdominal wall reconstruction procedure, extensive cellular infiltration was observed from the periphery of the material through the entire thickness (Fig. 4.13g–j).

4.3.9 Future Prospects

As techniques for improving the cellular response to electrospun scaffolds diversify and mature, materials have begun to be evaluated in more clinically relevant animal models such as skin wounds [54], blood vessel [55], sciatic nerve [56], spinal cord [57], and long [58] or calvarial [59] bone defects. While early results in the development of fibrous biomaterials based on electrospinning are promising, much work remains to be completed. Just as each application has unique mechanical and biological requirements, each implantation site exposes a material to a unique set of stresses and cellular environment. A cardiac patch will not be subjected to the same loads as a skeletal muscle graft, skin graft, bone graft, or even a heart valve. The host response is different in each local environment as well. The same material may be rapidly cellularized and eroded in the abdomen, but remain largely intact after the same period in the heart. Thus the challenge of designing scaffolds that encourage tissue integration is likely not met with a single solution for every challenge.

Having a broad and effective armamentarium of methods to design appropriate scaffold solutions for various tissue needs thus depends upon further exploration and innovation in scaffold processing. Electrospinning provides a rich and diverse field of options for meeting perceived design requirements.

4.4 Conclusions

Electrospinning has rapidly become one of the most attractive and efficient techniques to fabricate scaffolds with micro- and nanofibrous features for application in regenerative medicine. The initial challenges of achieving cellular infiltration and tissue integration in these scaffolds have been met with a variety of process modifications that overcome this common obstacle. Each technique has its trade-offs in terms of complexity and compromises in structure and function, yet the diversity of approaches provides options that likely will serve at least as a starting point for those designing scaffolds with electrodeposition techniques.

References

1. Greiner A, Wendorff JH (2007) Electrospinning: a fascinating method for the preparation of ultrathin fibers. Angew Chem Int Ed 46(30):5670–5703
2. Lannutti J, Reneker D, Ma T, Tomasko D, Farson D (2007) Electrospinning for tissue engineering scaffolds. Mater Sci Eng C 27(3):504–509
3. Nisbet DR, Rodda AE, Horne MK, Forsythe JS, Finkelstein DI (2009) Neurite infiltration and cellular response to electrospun polycaprolactone scaffolds implanted into the brain. Biomaterials 30(27):4573–4580
4. Kai D, Prabhakaran MP, Jin G, Ramakrishna S (2011) Guided orientation of cardiomyocytes on electrospun aligned nanofibers for cardiac tissue engineering. J Biomed Mater Res Part B Appl Biomater 98B(2):379–386
5. Phipps MC, Clem WC, Catledge SA, Xu Y, Hennessy KM, Thomas V, Jablonsky MJ, Chowdhury S, Stanishevsky AV, Vohra YK, Bellis SL (2011) Mesenchymal stem cell responses to bone-mimetic electrospun matrices composed of polycaprolactone, collagen I and nanoparticulate hydroxyapatite. PLoS One 6(2):e16813
6. Blakeney BA, Tambralli A, Anderson JM, Andukuri A, Lim D-J, Dean DR, Jun HW (2011) Cell infiltration and growth in a low density, uncompressed three-dimensional electrospun nanofibrous scaffold. Biomaterials 32(6):1583–1590
7. Lowery JL, Datta N, Rutledge GC (2010) Effect of fiber diameter, pore size and seeding method on growth of human dermal fibroblasts in electrospun poly(ε-caprolactone) fibrous mats. Biomaterials 31(3):491–504
8. Mei F, Zhong J, Yang X, Ouyang X, Zhang S, Hu X, Ma Q, Lu J, Ryu S, Deng X (2007) Improved biological characteristics of poly(L-lactic acid) electrospun membrane by incorporation of multiwalled carbon nanotubes/hydroxyapatite nanoparticles. Biomacromolecules 8(12):3729–3735
9. Nisbet DR, Forsythe JS, Shen W, Finkelstein DI, Horne MK (2009) A review of the cellular response on electrospun nanofibers for tissue engineering. J Biomater Appl 24(1):7–29
10. McKee MG, Elkins CL, Long TE (2004) Influence of self-complementary hydrogen bonding on solution rheology/electrospinning relationships. Polymer 45(26):8705–8715

11. Shenoy SL, Bates WD, Frisch HL, Wnek GE (2005) Role of chain entanglements on fiber formation during electrospinning of polymer solutions: good solvent, non-specific polymer-polymer interaction limit. Polymer 46(10):3372–3384
12. Rutledge GC, Fridrikh SV (2007) Formation of fibers by electrospinning. Adv Drug Deliv Rev 59(14):1384–1391
13. Feng C, Khulbe KC, Matsuura T (2010) Recent progress in the preparation, characterization, and applications of nanofibers and nanofiber membranes via electrospinning/interfacial polymerization. J Appl Polym Sci 115(2):756–776
14. D'Amore A, Stella JA, Wagner WR, Sacks MS (2010) Characterization of the complete fiber network topology of planar fibrous tissues and scaffolds. Biomaterials 31(20):5345–5354
15. Baker BM, Mauck RL (2007) The effect of nanofiber alignment on the maturation of engineered meniscus constructs. Biomaterials 28(11):1967–1977
16. Kenar H, Kose GT, Toner M, Kaplan DL, Hasirci V (2011) A 3D aligned microfibrous myocardial tissue construct cultured under transient perfusion. Biomaterials 32(23):5320–5329
17. Soliman S, Sant S, Nichol JW, Khabiry M, Traversa E, Khademhosseini A (2011) Controlling the porosity of fibrous scaffolds by modulating the fiber diameter and packing density. J Biomed Mater Res Pt A 96A(3):566–574
18. Rnjak-Kovacina J, Weiss AS (2011) Increasing the pore size of electrospun scaffolds. Tissue Eng Pt B Rev 17(5):365–372
19. van Tienen TG, Heijkants RGJC, Buma P, de Groot JH, Pennings AJ, Veth RPH (2002) Tissue ingrowth and degradation of two biodegradable porous polymers with different porosities and pore sizes. Biomaterials 23(8):1731–1738
20. Soletti L, Hong Y, Guan J, Stankus JJ, El-Kurdi MS, Wagner WR, Vorp DA (2010) A bilayered elastomeric scaffold for tissue engineering of small diameter vascular grafts. Acta Biomater 6(1):110–122
21. Pham QP, Sharma U, Mikos AG (2006) Electrospinning of polymeric nanofibers for tissue engineering applications: a review. Tissue Eng 12(5):1197–1211
22. Milleret V, Hefti T, Hall H, Vogel V, Eberli D (2012) Influence of the fiber diameter and surface roughness of electrospun vascular grafts on blood activation. Acta Biomater 8(12):4349–4356
23. Phipps MC, Clem WC, Grunda JM, Clines GA, Bellis SL (2012) Increasing the pore sizes of bone-mimetic electrospun scaffolds comprised of polycaprolactone, collagen I and hydroxyapatite to enhance cell infiltration. Biomaterials 33(2):524–534
24. Xie J, Li X, Lipner J, Manning CN, Schwartz AG, Thomopoulos S, Xia Y (2010) "Aligned-to-random" nanofiber scaffolds for mimicking the structure of the tendon-to-bone insertion site. Nanoscale 2(6):923–926
25. Liu Y, Zhang X, Xia Y, Yang H (2010) Magnetic-field-assisted electrospinning of aligned straight and wavy polymeric nanofibers. Adv Mater 22(22):2454–2457
26. Lee JB, Jeong SI, Bae MS, Yang DH, Heo DN, Kim CH, Alsberg E, Kwon IK (2011) Highly porous electrospun nanofibers enhanced by ultrasonication for improved cellular infiltration. Tissue Eng Part A 17(21–22):2695–2702
27. Shabani I, Haddadi-Asl V, Seyedjafari E, Soleimani M (2012) Cellular infiltration on nanofibrous scaffolds using a modified electrospinning technique. Biochem Biophys Res Commun 423(1):50–54
28. Karchin A, Simonovsky FI, Ratner BD, Sanders JE (2011) Melt electrospinning of biodegradable polyurethane scaffolds. Acta Biomater 7(9):3277–3284
29. Farrugia BL, Brown TD, Upton Z, Hutmacher DW, Dalton PD, Dargaville TR (2013) Dermal fibroblast infiltration of poly(ε-caprolactone) scaffolds fabricated by melt electrospinning in a direct writing mode. Biofabrication 5(2):025001
30. Levorson EJ, Raman SP, Chennazhi KP, Kasper FK, Nair SV, Mikos AG (2013) Fabrication and characterization of multiscale electrospun scaffolds for cartilage regeneration. Biomed Mater 8(1):014103
31. Jha BS, Colello RJ, Bowman JR, Sell SA, Lee KD, Bigbee JW, Bowlin GL, Chow WN, Mathern BE, Simpson DG (2011) Two pole air gap electrospinning: fabrication of highly aligned, three-dimensional scaffolds for nerve reconstruction. Acta Biomater 7(1): 203–215

32. Nam J, Huang Y, Agarwal S, Lannutti J (2007) Improved cellular infiltration in electrospun fiber via engineered porosity. Tissue Eng 13(9):2249–2257
33. Kim TG, Chung HJ, Park TG (2008) Macroporous and nanofibrous hyaluronic acid/collagen hybrid scaffold fabricated by concurrent electrospinning and deposition/leaching of salt particles. Acta Biomater 4(6):1611–1619
34. Simonet M, Schneider OD, Neuenschwander P, Stark WJ (2007) Ultraporous 3D polymer meshes by low-temperature electrospinning: use of ice crystals as a removable void template. Polym Eng Sci 47(12):2020–2026
35. Leong MF, Rasheed MZ, Lim TC, Chian KS (2009) In vitro cell infiltration and in vivo cell infiltration and vascularization in a fibrous, highly porous poly(D,L-lactide) scaffold fabricated by cryogenic electrospinning technique. J Biomed Mater Res A 91A(1):231–240
36. Leong MF, Chan WY, Chian KS, Rasheed MZ, Anderson JM (2010) Fabrication and in vitro and in vivo cell infiltration study of a bilayered cryogenic electrospun poly(D,L-lactide) scaffold. J Biomed Mater Res A 94A(4):1141–1149
37. Yixiang D, Yong T, Liao S, Chan CK, Ramakrishna S (2008) Degradation of electrospun nanofiber scaffold by short wave length ultraviolet radiation treatment and its potential applications in tissue engineering. Tissue Eng Part A 14(8):1321–1329
38. Sundararaghavan HG, Metter RB, Burdick JA (2010) Electrospun fibrous scaffolds with multiscale and photopatterned porosity. Macromol Biosci 10(3):265–270
39. Lim YC, Johnson J, Fei Z, Wu Y, Farson DF, Lannutti JJ, Choi HW, Lee LJ (2011) Micropatterning and characterization of electrospun poly(ε-caprolactone)/gelatin nanofiber tissue scaffolds by femtosecond laser ablation for tissue engineering applications. Biotechnol Bioeng 108(1):116–126
40. Lee BL-P, Jeon H, Wang A, Yan Z, Yu J, Grigoropoulos C, Li S (2012) Femtosecond laser ablation enhances cell infiltration into three-dimensional electrospun scaffolds. Acta Biomater 8(7):2648–2658
41. Joshi VS, Lei NY, Walthers CM, Wu B, Dunn JCY (2013) Macroporosity enhances vascularization of electrospun scaffolds. J Surg Res 183(1):18–26
42. Baker BM, Gee AO, Metter RB, Nathan AS, Marklein RA, Burdick JA, Mauck RL (2008) The potential to improve cell infiltration in composite fiber-aligned electrospun scaffolds by the selective removal of sacrificial fibers. Biomaterials 29(15):2348–2358
43. Baker BM, Shah RP, Silverstein AM, Esterhai JL, Burdick JA, Mauck RL (2012) Sacrificial nanofibrous composites provide instruction without impediment and enable functional tissue formation. PNAS 109(35):14176–14181
44. Skotak M, Ragusa J, Gonzalez D, Subramanian A (2011) Improved cellular infiltration into nanofibrous electrospun cross-linked gelatin scaffolds templated with micrometer-sized polyethylene glycol fibers. Biomed Mater 6(5):055012
45. Amoroso NJ, D'Amore A, Hong Y, Rivera CP, Sacks MS, Wagner WR (2012) Microstructural manipulation of electrospun scaffolds for specific bending stiffness for heart valve tissue engineering. Acta Biomater 8(12):4268–4277
46. Merryman WD, Huang H-YS, Schoen FJ, Sacks MS (2006) The effects of cellular contraction on aortic valve leaflet flexural stiffness. J Biomech 39(1):88–96
47. Townsend-Nicholson A, Jayasinghe SN (2006) Cell electrospinning: a unique biotechnique for encapsulating living organisms for generating active biological microthreads/scaffolds. Biomacromolecules 7(12):3364–3369
48. Jayasinghe SN, Warnes G, Scotton CJ (2011) Bio-electrosprayed living composite matrix implanted into mouse models. Macromol Biosci 11(10):1364–1369
49. Stankus JJ, Guan J, Fujimoto K, Wagner WR (2006) Microintegrating smooth muscle cells into a biodegradable, elastomeric fiber matrix. Biomaterials 27(5):735–744
50. Stankus JJ, Soletti L, Fujimoto K, Hong Y, Vorp DA, Wagner WR (2007) Fabrication of cell microintegrated blood vessel constructs through electrohydrodynamic atomization. Biomaterials 28(17):2738–2746
51. Hashizume R, Fujimoto KL, Hong Y, Amoroso NJ, Tobita K, Miki T, Keller BB, Sacks MS, Wagner WR (2010) Morphological and mechanical characteristics of the reconstructed rat abdominal wall following use of a wet electrospun biodegradable polyurethane elastomer scaffold. Biomaterials 31(12):3253–3265

52. Gilbert TW, Sellaro TL, Badylak SF (2006) Decellularization of tissues and organs. Biomaterials 27(19):3675–3683
53. Hong Y, Huber A, Takanari K, Amoroso NJ, Hashizume R, Badylak SF, Wagner WR (2011) Mechanical properties and in vivo behavior of a biodegradable synthetic polymer microfiber-extracellular matrix hydrogel biohybrid scaffold. Biomaterials 32(13):3387–3394
54. Uppal R, Ramaswamy GN, Arnold C, Goodband R, Wang Y (2011) Hyaluronic acid nanofiber wound dressing—production, characterization, and *in vivo* behavior. J Biomed Mater Res Part B Appl Biomater 97B(1):20–29
55. Wijeyaratne SM, Kannangara L (2011) Safety and efficacy of electrospun polycarbonate-urethane vascular graft for early hemodialysis access: first clinical results in man. J Vasc Access 12(1):28–35
56. Lee BK, Ju YM, Cho JG, Jackson JD, Lee SJ, Atala A, Yoo JJ (2012) End-to-side neurorrhaphy using an electrospun PCL/collagen nerve conduit for complex peripheral motor nerve regeneration. Biomaterials 33(35):9027–9036
57. Gelain F, Panseri S, Antonini S, Cunha C, Donega M, Lowery J, Taraballi F, Cerri G, Montagna M, Baldissera F, Vescovi A (2011) Transplantation of nanostructured composite scaffolds results in the regeneration of chronically injured spinal cords. ACS Nano 5(1):227–236
58. Ho ST, Hutmacher DW, Ekaputra AK, Hitendra D, Hui JH (2010) The evaluation of a biphasic osteochondral implant coupled with an electrospun membrane in a large animal model. Tissue Eng Part A 16(4):1123–1141
59. Jegal SH, Park JH, Kim JH, Kim TH, Shin US, Kim TI, Kim HW (2011) Functional composite nanofibers of poly(lactide-co-caprolactone) containing gelatin-apatite bone mimetic precipitate for bone regeneration. Acta Biomater 7(4):1609–1617

Chapter 5
The Potential Use of Three-Dimensional Cellular Multilayers as a Blood Vessel Model

Akihiro Nishiguchi, Michiya Matsusaki, and Misturu Akashi

Abstract In this chapter, we described a bottom-up approach for the reconstitution of three-dimensional cellular multilayered tissue for the application of tissue engineering and drug testing models. Based on the technology of polymer chemistry, we performed nanofilm coating with extracellular matrix to living cells by layer-by-layer assembly to induce cell–cell interaction for the adhesion. Using fibronectin–gelatin nanofilms, various cellular multilayers including fibroblast tissues, liver tissues, and blood vessel structures were fabricated. Especially, blood vessel wall models displayed similar structures and functions in vivo and can be used for the analysis of nitric oxide diffusion in the three-dimensional structures. Moreover, blood-capillary models and perfusable blood vessel models were also constructed by nanofilm coating technology and exhibited the possibility for in vitro drug testing. An automatic system using inkjet cell printing allows us to fabricate micrometer-sized tissue arrays and evaluate drug metabolism activity. The promising technologies for the creation of blood vessel models have enormous potential for clinically relevant therapies and drug assessment alternative to animal experiments.

Keywords Blood vessel • Layer by layer • Nanofilm • Three-dimensional tissue

5.1 Introduction

As studies on stem cells such as embryonic stem cell (ES cell) and induced pluripotent stem cell (iPS cell) have progressed, their applications for clinically relevant therapies and drug testing models have been expected [1]. Since ES cells and iPS cells have the capability to differentiate into various types of cells such as chondrocytes, cardiac myocytes, hepatocytes, and neurocytes, they can be employed for cell transplantation therapies [2]. However, the efficiency of cell engraftment is extremely low, resulting in cell death, the formation of tumors, and the diffusion

A. Nishiguchi • M. Matsusaki • M. Akashi (✉)
Department of Applied Chemistry, Graduate School of Engineering, Osaka University,
2-1 Yamada-oka, Suita 565-0871, Japan
e-mail: akashi@chem.eng.osaka-u.ac.jp

M. Akashi et al. (eds.), *Engineered Cell Manipulation for Biomedical Application*, Nanomedicine and Nanotoxicology,
DOI 10.1007/978-4-431-55139-3_5

of the transplanted cells into other organs [3]. To overcome this low engraftment efficiency and organization with host tissues, the concept of tissue engineering was established by Langer and Vacanti [4]. Tissue engineering basically aims to replace a damaged organ with an engineered tissue, which consists of three components: cells, a scaffold, and growth factors. These living tissues possess many types of cells and extracellular matrices (ECM), such as collagen, fibronectin, laminin, and hyaluronic acid, with oriented and hierarchical higher-order structures [5, 6]. To construct them, these tissue structures should mimic the in vivo structure using the three components, and their functions as tissues should be recreated. The in vitro engineering of tissues with structures and functions comparable to living organs would be useful in the field of regenerative medicine. Furthermore these engineered tissues can be used for drug testing models [7]. Normally, a cell monolayer has been employed as the in vitro model in pharmaceutical processes. However, it is difficult to obtain tissue responses from monolayered cell models that do not have a three-dimensional (3D) structure like living tissues. Moreover, alternatives to animal testing have attracted increasing attention [8]. Basically, pharmaceutical assays have been performed by in vivo animal experiments, but the low reproducibility and species differences remain unsolved issues. In particular, animal testing for cosmetics and chemicals has been prohibited under the seventh Amendment to the Cosmetics Directive (Council Directive 76/768/EEC) and REACH (registration, evaluation, authorization, and restriction of chemicals) in the European Union (EU). Taken together, the development of a novel technology for in vitro tissue fabrication is required in the field of tissue engineering and drug assessment.

5.2 A Bottom-Up Approach for 3D Tissue Construction

As described above, all tissues and organs in the body are highly organized in a hierarchical manner. For example, the wall of a blood vessel is multilayered, consisting of three parts: endothelial cells, which are the innermost layer and are in contact with the blood; the middle layers of vascular smooth muscle cells (SMCs); and the outer collagen and elastic fibers extending into the surrounding connective tissue [6]. To recreate this hierarchical structure in vitro, a scaffold which can provide a substrate for cell adhesion is essential [9–14]. Two of the most important properties for the scaffold are how the cells interact with the constituent materials and how cellular functions are affected by these materials [15, 16]. There are many requirements for the scaffold such as biocompatibility, protein adsorption, stiffness, and porosity. For example, protein adsorption depends on the surface characteristics of the material such as hydrophobicity, charge, roughness, and its components [17]. Therefore, the design of scaffold surfaces can control cell behaviors and functions such as adhesion, proliferation, and differentiation. With regard to porosity, topologically controlled scaffolds including nanometer-sized fiber scaffolds constructed by electrospinning [18] or self-assembling amphiphilic peptides [19] have attracted much attention due to their high porosity and the controlled alignment of the fibers.

However, 3D engineered tissues possess precisely controlled cell types and cell alignment, but cell–cell interactions have not been developed yet [15]. The existing tissue models with biodegradable hydrogels and fiber scaffolds seem to have several limitations in satisfying the above requirements. A bottom-up approach using multiple cell types as pieces of tissue can be expected to solve these problems. Currently, various methodologies such as cell sheet engineering [20–22], the cell beads method [23], and magnetic liposomes [24] have been reported in the development of multilayered tissue constructs. Although these methods are intriguing examples for the bottom-up approach, they have limitations due to the complicated manipulation of the fragile cell sheets or remnant magnetite particles inside the cells. A breakthrough in technology for in vitro tissue construction would attract novel methods for regenerative medicine and drug assessment.

5.3 Hierarchical Cell Manipulation Technique

In general cell culture, the cells proliferate on the appropriate substrates in growth media to reach a confluent condition, and the cells stop their growth due to contact inhibition. This is why it has been difficult to obtain 3D multilayered tissues under normal conditions, except for cell lines which can proliferate indefinitely. Moreover, even if the cells were seeded onto adhered cells, they did not adhere and organize completely because of the lack of an ECM on the cell surfaces and electrostatic repulsion between the cells. Therefore, to make 3D tissues in vitro, a proper substrate for cellular adhesion should be employed. Given the cellular adhesion mechanism on substrates, the cells recognize and adhere to the substrates directly as well as the components of the ECM through specific interactions between the ECM proteins and membrane proteins on the cell surface. We assumed that if the direct fabrication of nanometer-sized cell adhesive materials like ECM fibrous scaffolds onto the surface of a cell membrane is possible, then the cells seeded as the second layer may be able to recognize the adhesion substrates and adhere onto the first monolayered cells to generate bilayer structures. Repeating this process would yield 3D multilayered structures in vitro.

To prepare this artificial ECM film onto cells, we focused on layer-by-layer (LbL) assembly, which is an appropriate method to prepare nanometer-sized films on a substrate by alternate immersion into interactive polymer solutions [25, 26]. Researchers have extended LbL assembly to various fields, including biomedical applications for the control of surface properties at the nanometer level [27, 28]. Initially, electrostatic interactions were mainly utilized for LbL assembly, and subsequently other interactions such as covalent bonding [29], hydrogen bonding [30], charge transfer [31], hydrophobicity [32], host–guest [33], and coordination bond [34] interactions have been investigated to facilitate polymer association for ultrathin film deposition. However, most components of the films formed by LbL assembly crucially affect cellular functions like cell viability. In particular, synthetic polymers show strong cytotoxicity, and even natural polymers can impair cellular

functions if they contain cationic polymers which interact strongly with the cells. For example, Rajagopalan et al. constructed a bilayer structure composed of hepatocytes and other cells by preparing a polyelectrolyte (PE) multilayer consisting of chitosan and DNA onto the hepatocyte surface [35]. However, chitosan cannot dissolve in neutral buffer, and the use of PE films as a cell adhesive material was limited due to the cytotoxicity of the polycations [36]. The appropriate choice of natural ECM components for the preparation of nanofilms is important for biocompatibility and stable cellular adhesion on the cell surface.

We selected fibronectin (FN) and gelatin (G) to prepare nano-ECM films on the cell surface. FN is a flexible, multifunctional glycoprotein and plays an important role in cell adhesion, migration, and differentiation [37]. FN can interact not only with a variety of ECM proteins such as collagen (gelatin) and glycosaminoglycan but also with the $\alpha_5\beta_1$ integrin receptor on the cell surface [38]. Even though FN and G have a negative charge under physiological conditions, they interacted with each other through a collagen binding domain ($K_d = 0.6 \sim 5 \times 10^{-6}$ M) in FN, which is a different driving force versus PE films using electrostatic interaction. Thus, FN-G nanofilms are expected to serve as an artificial nano-ECM scaffold to fabricate 3D multilayered tissues by providing a suitable cell adhesive surface similar to the natural ECM without any cytotoxicity. Using FN-G nanofilms on the cell surface, the in vitro fabrication of 3D multilayered tissues can be achieved.

5.3.1 Fabrication of Multilayered Structure by Nano-ECM Coating

A schematic illustration of the hierarchical cell manipulation technique for the construction of 3D multilayered tissues is shown in Fig. 5.1 [39]. The LbL assembly of FN and G onto the cell surface was analyzed quantitatively using a quartz crystal microbalance (QCM) as the assembly substrate and with a phospholipid bilayer membrane as a model cell membrane (Fig. 5.2a). A phospholipid bilayer composed of 1,2-dipalmitoyl-sn-glycero-3-phosphatidylcholine (DPPC) and1,2-dipalmitoyl-sn-glycero-3-phosphate (DPPA) was prepared onto the base layer, a four-step assembly of poly(diallyldimethylammonium chloride) (PDDA) and poly(sodium styrenesulfate) (PSS), according to Krishna's report [40]. The mean thickness of the LbL assembly after 1, 7, and 23 steps was calculated to be 2.3, 6.2, and 21.1 nm, respectively. In addition, we have previously reported FN-based LbL multilayers composed of FN and ECM components, such as gelatin, heparin, and elastin [41]. This FN-G nanofilm was formed on cultured mouse L929 fibroblasts by the alternate immersion of the culture substrate into FN and G solutions. Top and cross sections of confocal laser scanning microscopic (CLSM) 3D merged images indicated a homogeneous assembly of fluorescently labeled FN-G nanofilms on the surface of mouse L929 fibroblasts. Quantifying the fluorescent intensity of the FN-G nanofilms formed on the cell surface by line scanning revealed that the fluorescence intensity of the Rh-FN-G nanofilms increased linearly upon increasing the LbL assembly step number, similar to the frequency shift of the QCM analysis, thus

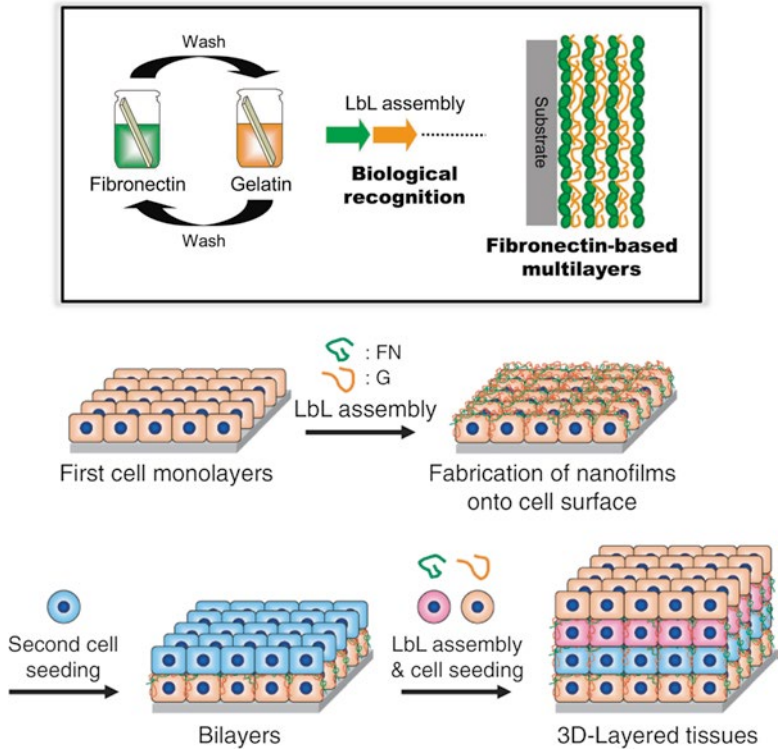

Fig. 5.1 Schematic illustration of hierarchical cell manipulation using the LbL assembly technique. Fibronectin (*FN*) and G were used as components of the LbL assemblies using biological recognition. Reproduced with permission [27, 28]

indicating a clear increase in the film thickness on the cell surface (Fig. 5.2b). These results demonstrated the fabrication of FN-G nanofilms on the cell surface. To check whether FN-G nanofilms can function as adhesion substrates, the overlap of the first and second layer of cells was confirmed by phase and fluorescent microscopic observation (Fig. 5.2c–i). When the seven-step-assembled FN-G nanofilms were prepared on the surface of the first L929 cell layer, the second layer cells were then observed on the first cell layer (Fig. 5.2c, d). However, when the nanofilm was not prepared or the one-step-assembled nanofilm (only FN) was assembled on the first cell layer, then the bilayer architecture was not observed (Figs. 5.2e–h). These results suggest that at least 6-nm-thick FN-G films were required for stable adhesion on the cultured cells, and 2.3-nm films did not work. This was partly because the amount of FN and G deposited where membrane proteins like integrin can bind through biological recognition was involved in stable cellular adhesion.

Four-layered (4L) cellular multilayers were clearly observed after four repetitions of these steps using CLSM and hematoxylin and eosin (HE) staining images (Fig. 5.3a, b). The thickness of the obtained multilayers estimated from 3D reconstructed CLSM images increased linearly with increasing cell layer number

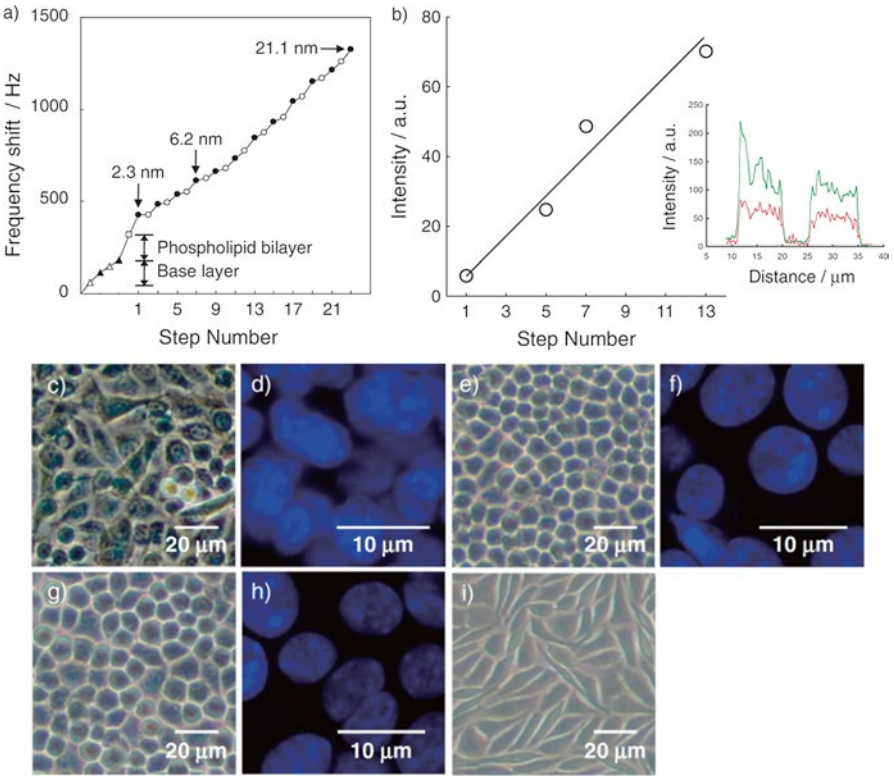

Fig. 5.2 (**a**) QCM analysis of the LbL assembly of FN and G onto a phospholipid bilayer (DPPC/DPPA 4:1). The *open* and *closed circles* show the assembly steps of G and FN, respectively. The base layer was a 4-step assembly of PDDA and PSS. (**b**) Relationship between the LbL assembly step of Rh-FN-G on L929 cells and the fluorescence intensity of the Rh-FN. The *inset* shows the fluorescence intensity of the cells (*green*) and the 7-step-assembled Rh-FN-G nanofilms (*red*) by line scanning. The cells were labeled with cell tracker *green*. (**c**, **e**, **g**) Phase-contrast and (**d**, **f**, **h**) fluorescence microscopic images of L929 fibroblast bilayers (**c**, **d**) with (**e**, **f**) and without a 7-step-assembled or (**g**, **h**) with 1-step-assembled FN-G nanofilms on the surface of the first cell layer. (**i**) Ph image of a L929 cell monolayer as the control. The nuclei were labeled with DAPI. Reproduced with permission [39]

(Fig. 5.3c). This method can be applied to a variety of cells such as myoblast cells (Myo, Fig. 5.3d), cardiac myocytes (CMyo, Fig. 5.3e), SMCs, hepatocytes, and endothelial cells. The obtained 3D cell architectures showed sufficient mechanical strength via the production of ECM and intercellular adhesion to peel off from the substrate easily (Fig. 5.3f). Furthermore, the 3D multilayered fibroblast tissues exhibited high cellular viability and maintained their layered structures even after 28 days of culture (Fig. 5.4) [42]. There was no significant difference in the living cell density from the top to the bottom layers during the 28 days of culture, suggesting that some cells proliferated and replaced the empty spaces left by the dead cells to maintain the density of living cells.

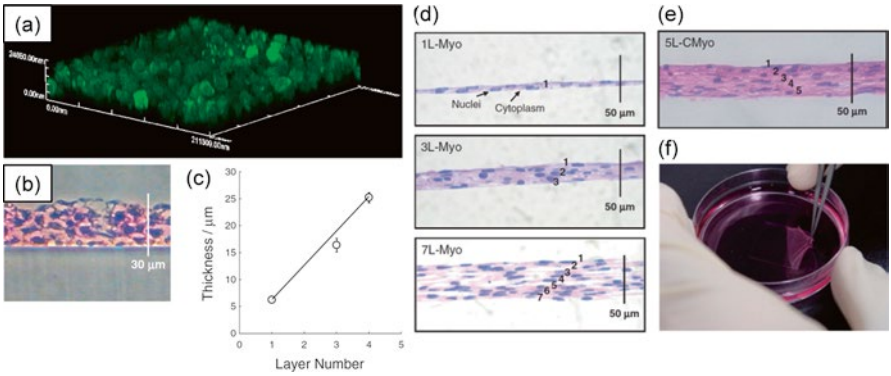

Fig. 5.3 (**a**) 3D reconstructed CLSM cross-sectional image of 4-layered (4L) L929 cells. The cells were labeled with cell tracker *green*. (**b**) HE staining image of 4L-L929 cells. (**c**) Relationship between the L929 cell layer number and the mean thickness estimated from 3D CLSM images ($n=3$). (**d**) HE staining images of 1-, 3-, and 7L-mouse C2C12 Myo. (**e**) HE image of 5L-rat CMyo. (**f**) Photograph of the peeling process of 4L-L929 cells from a cover glass as the substrate. Reproduced with permission [28]

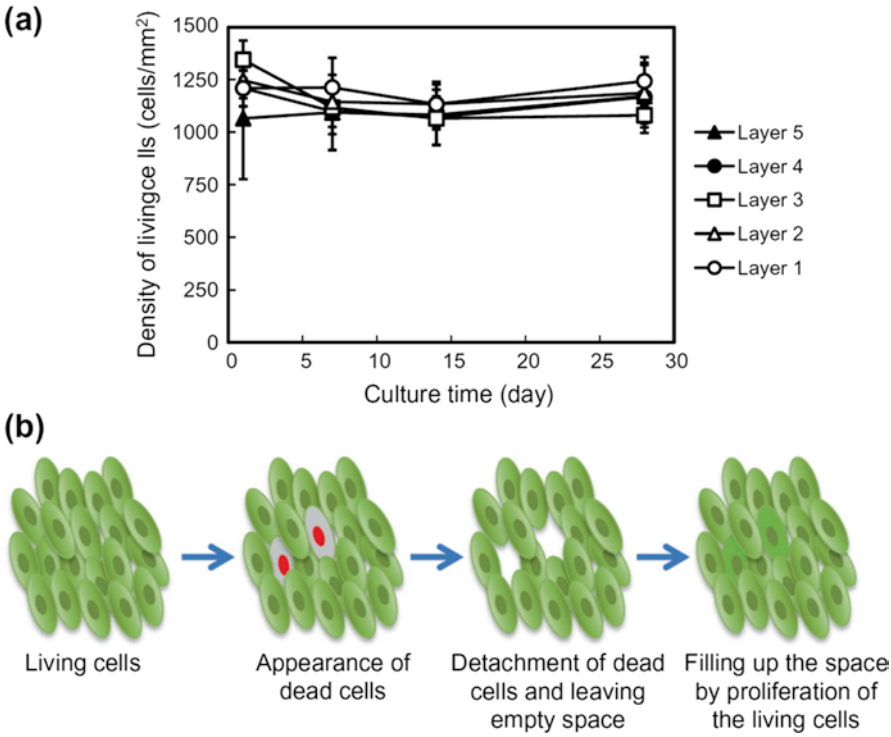

Fig. 5.4 (**a**) Relationship between the living cell density of each layer in 5L-NHDF tissues and the culture time over 1 month. The *error bars* represent the standard deviation ($n=4$–5). (**b**) Schematic illustration of the replacement of the empty spaces by the proliferation of living cells. Reproduced with permission [42]

5.3.2 *Effect of Nanofilms on Cellular Function*

To understand the effects of nanofilms on the cell surface on cellular functions, we confirmed their morphology and fundamental functions after the preparation of various types of PE and FN films (Fig. 5.5). Although cellular functions on various LbL films have been previously reported with regard to adhesion, proliferation, and differentiation [43–45], it is not appropriate to investigate the direct interactions between PE films and the cell membrane because of the adsorption of serum proteins between them during cellular adhesion. Therefore, we focused on the effects of various LbL nanofilms that were prepared on the cells directly on cell functions, including the charge, thickness, composition, and morphology of the LbL films [46]. Table 5.1 summarizes the nanofilm components such as synthetic polymers, polysaccharides, poly(amino acid)s, and proteins and their effects on cellular functions.

As shown in Fig. 5.5a–e, FN-G and FN-dextran sulfate (FN-DS) nanofilms displayed more extended morphologies as compared to PE films. Cells formed on the PE films on the cell membrane had rounded shapes, even though the polymers contained in the PE films did not show any cytotoxicity by themselves (Fig. 5.5f, g). Similarly, PE films drastically affected the cell viability and proliferation upon increasing the thickness of the films. On the other hand, FN films formed through protein–protein recognition exhibited high cytocompatibility, and nanometer-sized meshwork fiber structures were observed after 24 h by scanning electron microscopy (SEM) (Fig. 5.5h). The FN in the films prepared onto the cells transformed their morphologies from films to nano-meshwork fibers, but not the FN in serum, whereas the formation of fiber structures was never observed when PE films were formed (Fig. 5.5i, j). These nano-meshwork morphologies seemed to be similar to the fibrous structure of the natural ECM.

Furthermore, the secretion of interleukin-6 (IL-6) cytokine, which is an inflammatory cytokine, from normal human dermal fibroblasts (NHDFs) with PE films expressed approximately 2.5-fold higher IL-6 per single cell than NHDFs without films (Fig. 5.6) [47]. On the other hand, the FN films did not show any effect on IL-6 production. These results suggested that PE films prepared on the cell surface induced strong inflammation in the cells, probably due to cationic cytotoxicity, leading to cell death or growth arrest dependent on the thickness, cationic charge, or cationic species.

5.3.3 *Control of Cellular Function and Activity in 3D Environments*

An important advantage of this hierarchical cell manipulation technique is to allow the cells to grow in 3D environments composed of layered cells and ECM structures. In general, cells are cultured on a plastic dish, which is a completely different condition from living tissue. If the use of 3D environments which mimic the

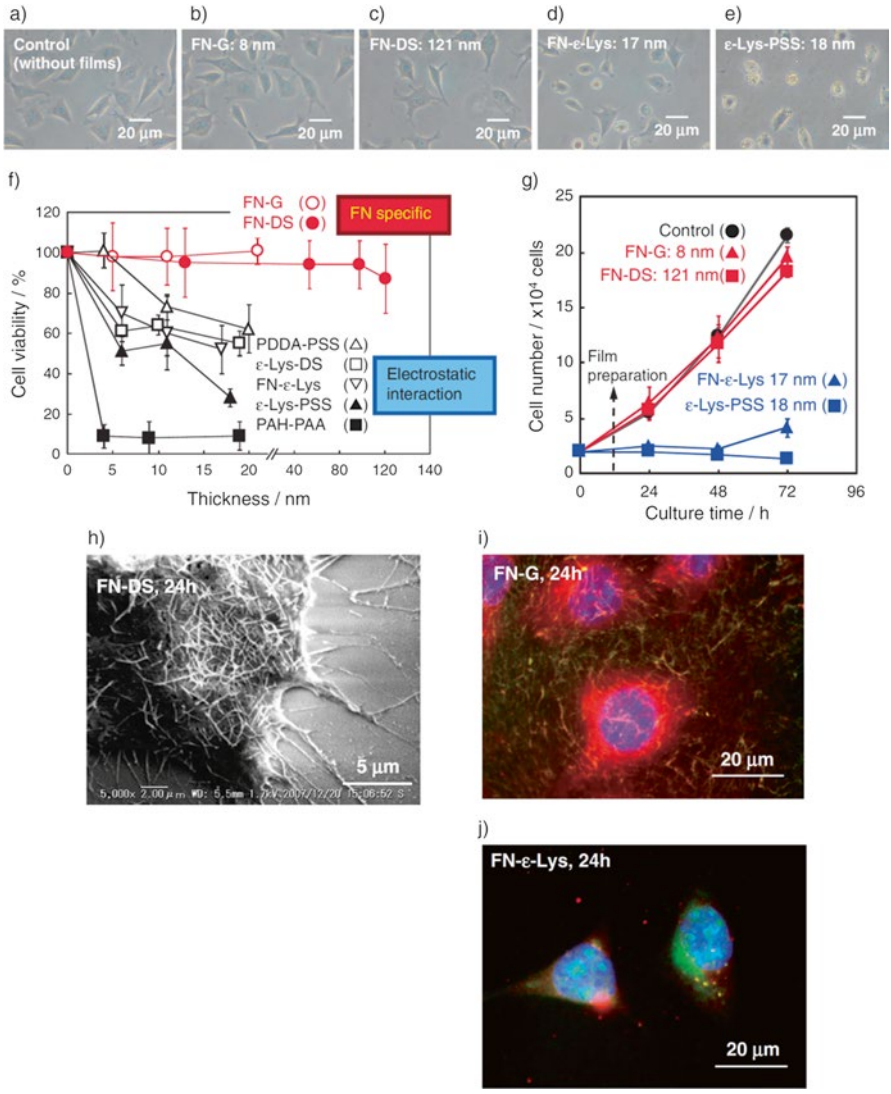

Fig. 5.5 (**a**–**e**) Phase images of L929 fibroblasts (**a**) without or with (**b**) 8-nm-thick FN-G, (**c**) 121-nm-thick FN-DS, (**d**) 17-nm-thick FN-ε-Lys, and (**e**) 18-nm-thick ε-Lys-PSS nanofilms on the cell surfaces after 24 h of incubation. (**f**) Relationship between cell viability and the thickness of various nanofilms prepared on the cell surfaces after 24 h of incubation ($n = 3$). PAH, PAA, and ε-Lys: poly(allylamine hydrochloride), poly(acrylic acid), and ε-poly(lysine hydrochloride), respectively. (**g**) Cell proliferation versus various nanofilms prepared on L929 cell surfaces during 72 h of incubation. (**h**) SEM image of the L929 cells on 121-nm-thick FN-DS films after 24 h of incubation. Fluorescence microscopic images of (**i**) 21-nm-thick Rh-FN-FITC-G and (**j**) 17-nm-thick Rh-FN-FITC-ε-Lys films prepared on L929 cells after 24 h of incubation. Reproduced with permission [28]

Table 5.1 Summary of the nanofilm components and cell types used in this paper

Component 1		Cell viability 1[a] (%)	Component 2 (Charge)	(Species)	Cell viability 2[a] (%)	Total thickness[d] (nm)	Interaction	Nanostructure	Cell type
(Charge)	(Species)								
FN (negative)	Protein	86.3 ± 7.6	G (negative)	Protein	97.7 ± 8.0	8.9 ± 0.9	FN-binding domain interaction	Nanofilm	L929, NHDF, HUVEC, SMC, HAEC, AoSMC
FN (negative)	Protein	86.3 ± 7.6	DS (negative)	Naturally occurring polymer	91.3 ± 2.3	121.1 ± 6.0	FN-binding domain interaction	Nanofilm	L929, NHDF
FN (negative)	Protein	77.0 ± 3.6	ε-Lys (positive)	Naturally occurring polymer	86.3 ± 7.6	11.0 ± 1.3	Electrostatic interaction	Nanofilm	L929, NHDF
ε-Lys (positive)	Naturally occurring polymer	77.0 ± 3.6	DS (negative)	Naturally occurring polymer	91.3 ± 2.3	12.0 ± 0.9	Electrostatic interaction	Nanofilm	L929
ε-Lys (positive)	Naturally occurring polymer	77.0 ± 3.6	PSS (negative)	Synthetic polymer	96.7 ± 9.3	9.1 ± 0.6	Electrostatic interaction	Nanofilm	L929, NHDF
PDDA (positive)	Synthetic polymer	73.3 ± 5.9[b]	PSS (negative)	Synthetic polymer	96.7 ± 9.3	17.2 ± 1.2	Electrostatic interaction	Nanofilm	L929
PAH (positive)[c]	Synthetic polymer	6.5 ± 1.1	PAA (negative)	Synthetic polymer	99.0 ± 7.8	24.4 ± 2.7	Electrostatic interaction	Nanofilm	L929, NHDF
Ca^{2+} (positive)	Ion	94.3 ± 3.2[b]	PO_4^- (negative)	Ion	96.8 ± 5.3[b]	100 ~ 1,000	Electrostatic interaction	Nanocrystal	MSC

Concentration of each solution used for LbL assembly is 0.2 mg/ml in 50 mM Tris–HCl (pH = 7.4)

The living cell percentage was estimated from positive control sample as 100 % in which no treatment was performed

The cell types used for nanofilm or nanocrystal preparation. Abbreviations: *L929* mouse L929 fibroblast, *NHDF* normal human dermal fibroblast, *HUVEC* human umbilical vein endothelial cell, *SMC* smooth muscle cell, *HAEC* human artery endothelial cell, *AoSMC* human aortic smooth muscle cell

[a]Cell viability was determined after immersion in 0.2 mg/ml of each component solution for 15 min by using WST-1 reagent

[b]Concentration of PDDA solution is 0.02 mg/ml in 50 mM Tris–HCl (pH = 7.4) with 0.035 M $CaCl_2$. The concentration of Ca^{2+} and PO_4^- was 10 mM in 50 mM Tris–HCl (pH = 7.4)

[c]PAH is negative control as a cytotoxic component

[d]The total thickness at 13 steps on a phospholipid bilayer prepared on 2.3 ± 0.4 nm of $(PDDA\text{-}PSS)_{1.5}$ base layer is 4.1 ± 1.1 nm. In case of HAp crystal, the values mean crystal sizes

Abbreviations: *FN* fibronectin, *G* gelatin, *DS* sodium dextran sulfate, *ε-Lys* ε-poly(lysine hydrochloride), *PSS* poly(sodium styrenesulfate), *PDDA* poly(diallyldimethylammonium chloride), *PAH* poly(allylamine hydrochloride), *PAA* poly(acrylic acid)

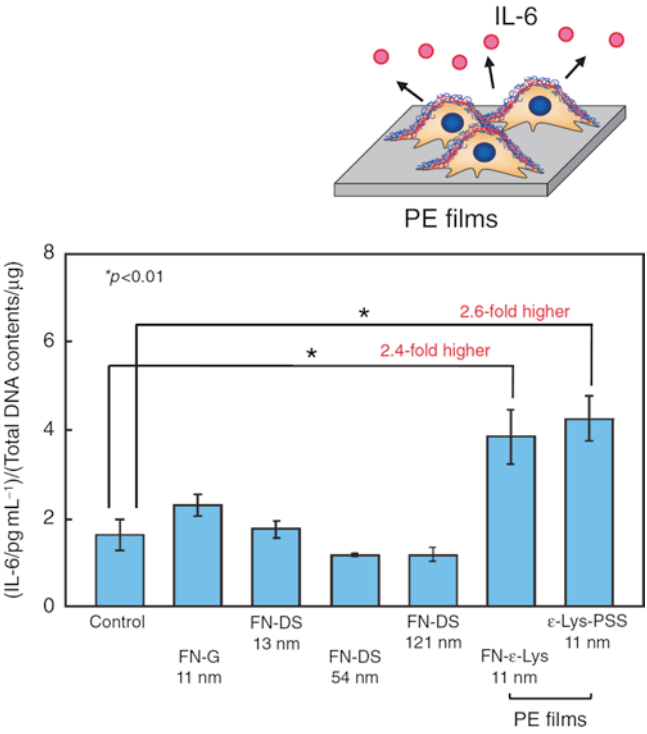

Fig. 5.6 IL-6 secretion versus amount of DNA in normal human dermal fibroblasts (*NHDFs*) without or with FN-based (FN-G and FN-DS) or polyelectrolyte (*PE*) films on the cell surfaces after 24 h of incubation ($n=3$). *Asterisk* denotes a statistically significant difference using a two-sample *t*-test ($*p<0.01$) for each comparison. Reproduced with permission [47]

structures of living tissues can enhance cellular functions and control cell activity, they will be useful tools as compared to cell monolayers, not only for understanding how a 3D environment composed of cells, ECM, and signaling molecules regulates functions similar to natural tissues but also for creating 3D artificial tissues resembling natural tissues. The basic properties induced by 3D cellular structures, such as the layer number or the cell types, have not been clarified yet.

To understand how the 3D environment influences cell behavior and function, we fabricated a layered structure with a human umbilical vein endothelial cell (HUVEC) layer on top of multilayered NHDF tissue (Fig. 5.7a, b) [48]. The two types of layered constructs, 1L-NHDF/1L-HUVEC and 4L-NHDF/1L-HUVEC, were prepared using FN-G nanofilms. To evaluate the general effects of 3D layered structures on cellular stress and inflammation, we purposely fabricated biologically meaningless layered structures consisting of endothelial cells and fibroblasts. Interestingly, the HUVECs adhered homogeneously on the surface of 4L-NHDF tissue at the centimeter scale, whereas heterogeneous HUVEC domain structures were confirmed on the 1L-NHDF tissue (Fig. 5.7c–f). This result suggests that the multilayered structure was able to provide a suitable adhesion scaffold for HUVECs,

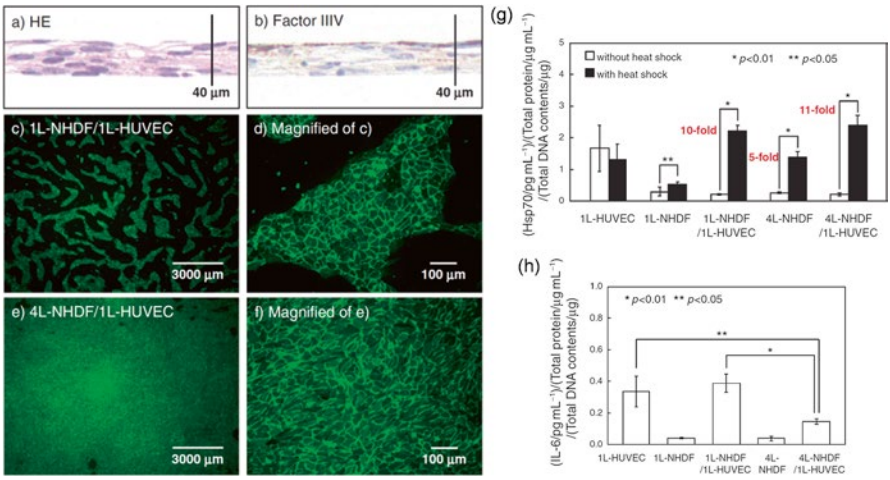

Fig. 5.7 Histological images of 4L-NHDF/1L-HUVEC constructs stained for (**a**) HE and (**b**) factor VIII. Fluorescent immunostaining images of (**c**, **d**) 1L-NHDF/1L-HUVEC and (**e**, **f**) 4L-NHDF/1L-HUVEC constructs immunostained with an anti-CD31 antibody (**g**). Production of Hsp70 versus total protein from non-heat shocked and heat shocked layered constructs composed of NHDFs and HUVECs ($n=4$). The heat shock conditions were 20-min incubation at 45 °C, followed by a 2-h recovery period. (**h**) IL-6 secretion versus total protein from the layered structures ($n=3$). *Asterisk* denotes a statistically significant difference using a two-sample *t*-test ($*p<0.01$, $**p<0.05$) for each comparison. Reproduced with permission [48]

and the HUVECs can recognize their microenvironments such as stiffness, ECM deposition, and cell–cell interactions.

Moreover, when we investigated protein production in layered tissues as a cell function, there were big differences between 1L- and 4L-NHDF tissues with regard to the production of heat shock protein 70 (Hsp70) and IL-6 (Fig. 5.7g, h). The Hsp70 expression of HUVECs decreased after adhesion onto the 4L-NHDF structure as compared with the HUVEC monolayer. Surprisingly, the Hsp70 production response to heat shock increased drastically by approximately tenfold as compared to non-heat shock by 3D structure formation, whereas the monolayer structures showed no change. Moreover, the production of the inflammatory cytokine IL-6 decreased drastically depending on the layer number of NHDFs. These results suggest that 4L-NHDF provided a more favorable environment for HUVECs as compared to a plastic cell culture dish for the induction of high thermosensitivity and for the suppression of inflammatory responses from the substrate.

5.3.4 Permeability Assay of Multilayered Fibrous Tissues

As described above, we found that three-dimensionally cultured cells expressed higher cellular functions and activities as compared to monolayer-cultured cells. In a similar fashion, the 3D structures of cells and the ECM allow for 3D

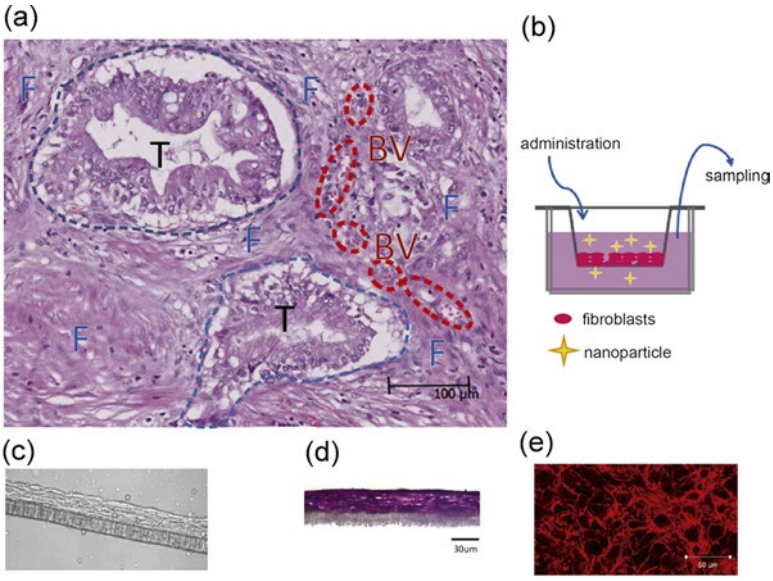

Fig. 5.8 Histological pattern of human pancreatic cancer and the structure of the model. (**a**) HE staining of a pathological specimen of human pancreatic cancer. Most of the tumor tissue is occupied by fibrotic tissue. *T* tumor cells (*inside blue dotted circles*), *BV* blood vessels (*inside red dotted circles*), *F* fibrotic tissue (*other parts*). (**b**) Schematic illustration of the multilayered model for the permeation assay. (**c**) Transmitted light microscopy of the multilayered culture. (**d**) HE staining of the multilayered culture. (**e**) Phalloidin staining of the multilayered culture. For the interpretation of the references to color in this figure legend, the reader is referred to the web version of this article. Reproduced with permission [49]

pharmacokinetic analysis in drug testing such as the permeation, distribution, and accumulation of drugs. Therefore, we performed a permeability assay using multilayered fibrous tissues constructed by the hierarchical cell manipulation technique [49]. We focused on pancreatic cancer, which is known to have an extremely low median survival time for advanced pancreatic adenocarcinoma, approximately 6 months. The reason why treatments against pancreatic cancers have failed despite recent progress with conventional chemotherapies is their hypo-vascular structure and the large amount of fibrous tissues. Histologically, human pancreatic tissue, aside from the tumor cells, shows a large volume of fibrotic tissue with occasional vasculature distal to the tumor cells (Fig. 5.8a). Since the amount of drugs that can be delivered is low and drug permeation is poor due to their structure, drug delivery systems using nanometer-sized carrier (nanoDDS) as a novel therapeutic method have attracted increasing attention to achieve efficient drug delivery and to reduce side effects. However, there are no satisfactory models of drug permeability in fibrotic tissues to design better drug carriers. The permeation of drugs, including nanoparticles, in tissues has been investigated in vitro using endothelial cells or epithelial cells cultured in monolayers [50, 51], but the three-dimensional migration of drugs cannot be analyzed in a monolayer system. Many three-dimensional models have been used to mimic cells, including fibroblasts in an in vivo environment [52],

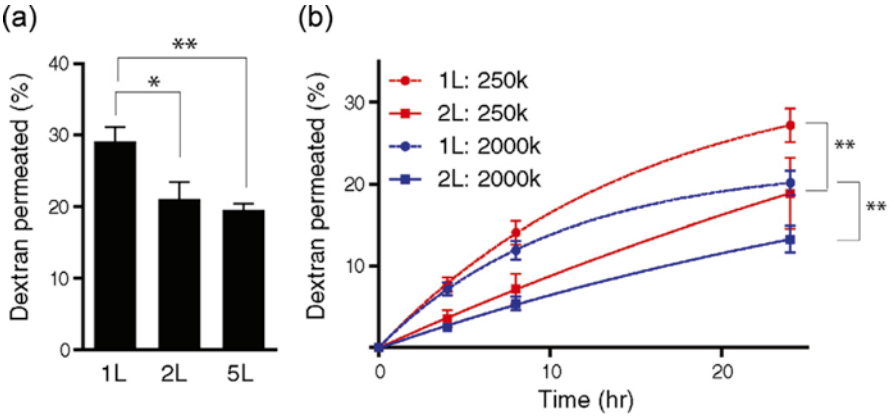

Fig. 5.9 (**a**) Permeation of 20-kDa dextran across 1L-, 2L-, and 5L-K643f tissues after 24 h of incubation. (*Bars*: SD, $p<0.05$, and $p<0.01$. (**b**)) Dextrans of 250 or 2,000 kDa were tested in 1 or 2 layers of K643f culture (*$p<0.01$, **$p<0.05$, $n=3$). Reproduced with permission [49]

but they have not addressed the problem of drug permeability. For example, collagen gel is widely used because it resembles the ECM, but it shrinks after a few days of cell incubation and hence cannot be used to test permeability.

We analyzed the diffusion of dextran molecules as a model drug across engineered fibrotic tissues composed of fibroblasts derived from a murine spontaneous pancreatic tumor (K643f) (Fig. 5.8b). We confirmed the integrity and homogeneity of the structure by transmission light microscopy and HE staining and also observed the fibrous structures by phalloidin staining. Using this multilayered fibrous tissue, the permeation of fluorescently labeled, high-molecular-weight dextran was measured to investigate the delivery of nanoDDS into tumor fibrotic tissue.

First, we tested the relationship between the layer number and permeation using 1L-, 2L-, and 5L-fibrous tissues. As shown in Fig. 5.9a, there were significant differences between the 1L and 2L or 5L tissues, suggesting the permeation of dextran molecules decreased with an increasing number of tissue layers. Next, we confirmed the time-dependent permeation of dextran molecules (Fig. 5.9b). The permeation of 250- and 2,000-kDa dextran molecules, 12 and 31 nm in hydrodynamic diameters, respectively, decreased with an increasing layer number of tissues. These results indicated that the multilayered fibrous tissues can recreate a microenvironment similar to fibrous tissues in vivo better than existing monolayered cell models. Thus, our three-dimensional model will be useful for analyzing the permeation of drugs, including nanoparticles, for diseases such as pancreatic cancer.

5.4 Blood Vessel Wall Model

In physiology and medicine, blood vessels are relevant not only for circulatory diseases and treatments but also for the biological evaluation of drug diffusion into target tissues, the penetration of cancer cells or pathogens, and the control of blood pressure.

A blood vessel is generally composed of three distinct layers: the intima, an inner single layer of endothelial cells (ECs); the media, the middle layers of SMCs; and the adventitia, an outer layer of fibroblast cells [6]. Each layer serves specific functions such as antithrombogenicity and the selective permeation of molecules in the EC layer and mechanical strength in the SMC layer. To construct such a functional tissue in vitro, a hierarchical layered structure composed of EC and SMC layers should be formed. We employed the hierarchical cell manipulation technique for the construction of a blood vessel wall model of human ECs and SMCs with a layered structure [53]. Although long-term culture for several months and additives to promote cell proliferation unnaturally were needed for the construction of multilayered SMC tissues, this method just repeats the FN-G nanofilm formation and cell seeding. Therefore, the obtained blood vessel wall models were expected to display similar structures and functions as living blood vessels.

5.4.1 Construction of Blood Vessel Wall Model

As shown in Fig. 5.10a, the layered structures composed of 4L-SMC and 1L-HUVCEC were confirmed by immunohistological observation, and monolayered HUVECs homogeneously covered the surface of the 4L-SMC layers, as well as the human aorta. Checking whether the HUVEC layer maintained its functions as endothelial cells on the SMC layer by platelet adsorption, the 4L-SMC/1L-HUVEC model suppressed the adsorption and activation of platelets in human platelet-rich plasma (PRP) (Fig. 5.10b, c).

5.4.2 Quantitative 3D Analysis of Nitric Oxide Using Blood Vessel Wall Model

We applied this artificial 3D blood vessel wall model to the biological evaluation of nitric oxide (NO) production from ECs [54]. NO produced from the ECs diffuses into the SMCs through their cell membrane and activates guanylate cyclase to produce intracellular cyclic guanosine monophosphate (cGMP), which induces a signaling pathway mediated by kinase proteins leading to SMC relaxation [55]. Therefore, quantitative, kinetic, and spatial analyses of the extracellular delivery of NO molecules in the blood vessel wall are crucial for pharmaceutical evaluations of hypertension and diabetes. Recently, a significant correlation between NO production and diabetes mellitus was reported; reduced NO production in both type 1 and 2 diabetes [56, 57] and also increased NO production related to improvements in type 2 diabetes were reported [58]. Thus, the development of a convenient and versatile method for the in vitro quantitative and spatial analysis of NO diffusion in the artery wall is important for biological and pharmaceutical applications and as an alternative to animal experiments.

To quantify NO production three dimensionally, NO sensor particles of mesoporous silica were employed in the 3D blood vessel wall model. We reported biocompatible

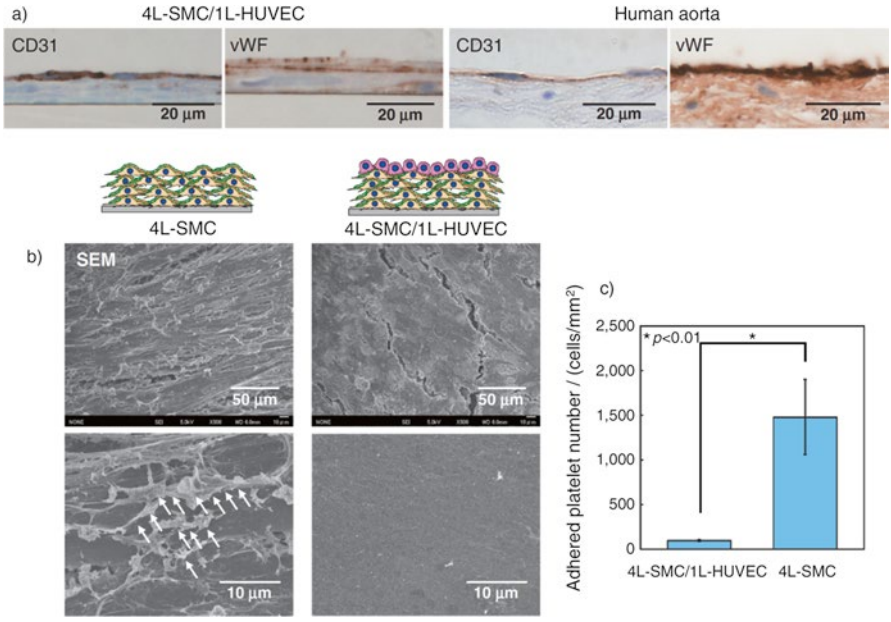

Fig. 5.10 (**a**) Immunohistochemical evaluations of 4L-SMC/1L-HUVEC constructs (*left*) and the human aorta (*right*). The histological image of the human aorta was focused on the inner HUVEC layer for comparison against engineered structures. (**b**) SEM images of the surface of the 4L-SMC and 4L-SMC/1L-HUVEC constructs after immersion into PRP for 15 min at 37 °C. The *arrows* indicate adhered and activated platelets on the surface of the 4L-SMC constructs. (**c**) The number of adhered platelets on 4L-SMC/1L-EC and 4L-SMC counted from SEM images at 120×90 μm areas ($n=3$). The *asterisk* denotes a statistically significant difference using a two-sample *t*-test ($*p<0.01$). Reproduced with permission [28]

and highly sensitive NO sensor particles using LbL assembly. The mesoporous silica microparticles encapsulated 4,5-diaminofluorescein (DAF-2), which is a NO fluorescent indicator dye, by covering the porous surfaces with PE multilayered films composed of chitosan (CT) and DS. The CT-DS films allowed the NO sensor particles (SPs) to retain the dye inside the particles and to exhibit fluorescence in response to the NO molecules. The SPs showed high NO sensitivity at 5,500 nM, which is sufficient to detect NO at concentrations of hundreds of nM (EC production level [59, 60]).

We combined 3D blood vessel wall models with the SP technique for the 3D detection of NO production from ECs (Fig. 5.11). As a model of the blood vessel wall, 3D artery models composed of 4L-human aortic smooth muscle cells (AoSMCs) and 1L-human aortic endothelial cells (HAECs) were constructed by nano-ECM coating as described above. The SPs were seeded into each layer in the tissues at the same time as the cell seeding to obtain layered artery models with homogeneously distributed SPs in the tissues. The amount of NO production from

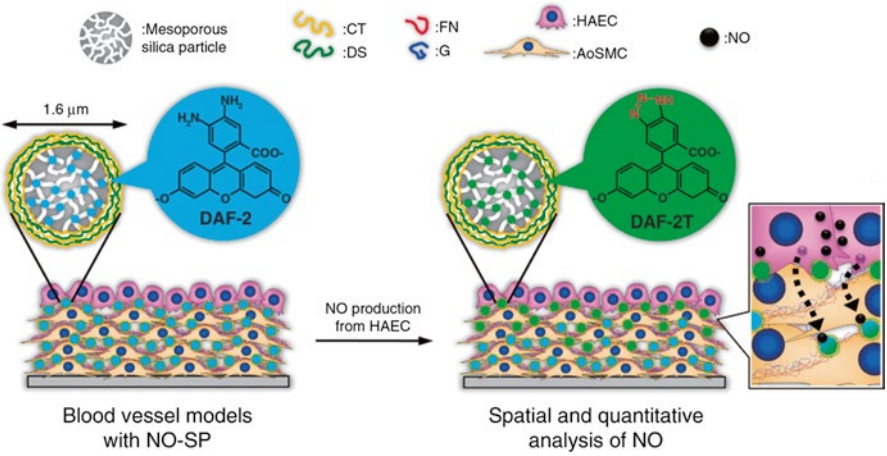

Fig. 5.11 Schematic illustration of the in vitro spatial and quantitative analyses of NO diffusion from the uppermost HAEC layer to the AoSMC layers in a 3D artery model using SPs. The SPs were homogeneously distributed within the 3D layered blood vessel wall model. Reproduced with permission [54]

the ECs was calculated from the fluorescent intensity of SPs obtained by CLSM observation. To evaluate the 3D structural effect of the cellular alignment on localized NO production, the NO concentration at the apical and basal membranes of the HAECs in monolayers or bilayers after 48 h of incubation was analyzed using the SPs (Fig. 5.12a). The NO concentrations at the basal membrane of HAECs in the monolayer and bilayer were 4.5-fold and 2-fold higher, respectively, than those on the HAEC surfaces, suggesting that the NO molecule was more readily produced at the basal membrane than at the apical membrane, independent of the 3D layered structure. This is in agreement with a report by Ortiz and co-workers [61].

Finally, we performed 3D analyses of NO diffusion using 5L-artery wall models by CLSM observation (Fig. 5.12b–d). The first layer is HAECs, and the second to fifth layers were AoSMCs. The fluorescent intensity of SPs with DAF-2 increased in response to NO molecules (green), and the nuclei were stained with DAPI to distinguish each layer. The NO concentrations in first (HAEC) and second (AoSMC) layers were about 530–550 nM and then gradually decreased upon increasing the layer number. The NO concentration reached about 50 % (290 nM) in the fifth layer (32 nm in depth). Although NO diffusion was limited to approximately 60 μm in 3D artery wall models and this value is slightly lower than the reported in vivo NO diffusion distance (approximately 100–200 nm), this might be reasonable considering the NO consumption (approximately 37 % consumption) during the chemical reactions [62]. These results suggest that this technique will be a useful method for in vitro artery assays to replace in vivo animal experiments.

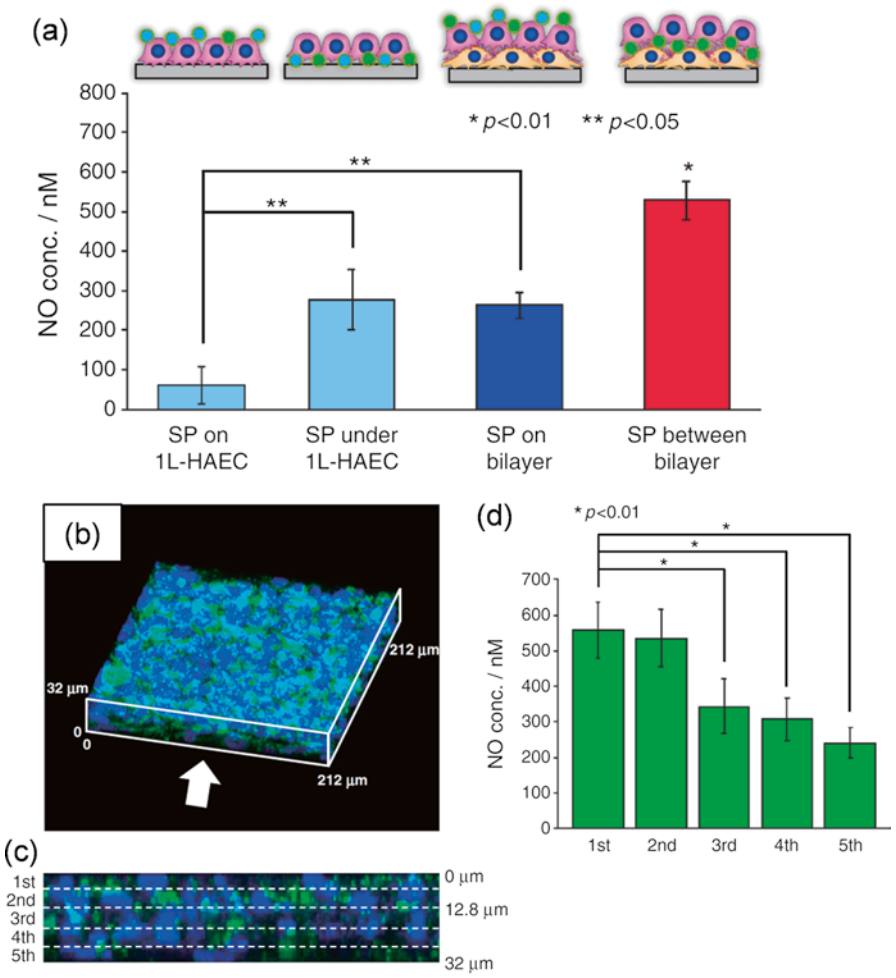

Fig. 5.12 (**a**) Localized NO diffusion in relation to 3D structural effects. The localized NO concentrations were analyzed by SPs on and under the HAECs in monolayers and bilayers after 48 h of incubation. The mean fluorescence intensity of the SPs was measured from CLSM images ($n=3$, over 20 SPs per image), and the NO concentration was estimated from a calibration curve. I_f fluorescence intensity. (**b**) 3D reconstructed CLSM image of a 5L-artery model containing SPs (*green*) in each layer after 48 h of incubation. The first layer is HAECs, and the second to fifth layers are AoSMCs. (**c**) Cross-sectional CLSM image of (**a**) in the *white arrow* direction. The *dashed lines* indicate the brief interfaces of each layer. (**d**) The localized NO concentrations in each cell layer were analyzed using the SPs. The fluorescence intensities of the SPs were measured from each layer in (**c**) ($n=3$, over 20 SPs per image, $^{**}p<0.05$, $^{*}p<0.01$)). Reproduced with permission [54]

5.5 Blood-Capillary Model

Blood capillaries are composed of an endothelial monolayer, pericytes, and fibroblasts and maintain the metabolic activities and functions of organs through the transport of nutrients and oxygen. In the living body, almost all cells and tissues except hypo-vascularized tissues such as cartilage are surrounded with blood capillaries within a perimeter of 100–150 μm [63]. Therefore, cultured cells in vitro need to be supplied with oxygen and nutrients like in vivo, and large tissues over 200 μm in thickness may undergo necrosis without an adequate supply of oxygen and nutrients [64]. That is why the introduction of blood-capillary networks into engineered tissue is a current key challenge in the field of tissue engineering for the development of transplantable thick tissues. To construct functional blood capillaries, many attempts such as a three-dimensional (3D) culture of endothelial cells in hydrogels composed of extracellular matrix (ECM) [65, 66], the fixation of angiogenic factors into scaffolds [67, 68], micro-channel models with flow [69–71], and cell sheet engineering for transplantable tissues [72, 73] have been reported. Although these systems are powerful methods to create vascularized tissues, they need complicated devices and procedures for vascularization and have potential limitations to recreate both the structures and functions of living tissues in vitro. A novel technology to accomplish the in vitro vascularization of tissues would be desirable for applications in not only tissue engineering but also as a tool for biological evaluations such as angiogenesis assays and the analysis of signaling pathways through blood capillaries.

5.5.1 Fabrication of Blood-Capillary Model by Cell-Accumulation Technique

Recently, we developed a powerful method to construct blood-capillary models by improving the hierarchical cell manipulation technique. Although the hierarchical cell manipulation technique allows for exact layered structures with the desired cell types and ECM, it has difficulty in generating thick 3D layered tissues, because a maximum of 2 layers per day was encountered due to stable cell adhesion. Moreover, the introduction of vascular structures has not succeeded. To overcome the problem of this one-by-one method, we performed the rapid construction of thick 3D tissues by the nano-ECM coating of FN-G films onto single cells in dispersion, but not adhered cells, which we called the cell-accumulation technique (Fig. 5.13a) [74]. Since FN-G nanofilms prepared on individual cell surfaces provide an interactive property with the $\alpha_5\beta_1$ integrin receptor of the cell membrane, the cell–cell adhesion of all seeded cells in three dimensions can be induced at the same time (cell-accumulation process).

We began with the formation of FN-G nanofilms onto single cells to confirm the homogeneity and stability of the FN-G nanofilms. The CLSM images showed the successful preparation of FN-G nanofilms on the cell surfaces (Fig. 5.13b).

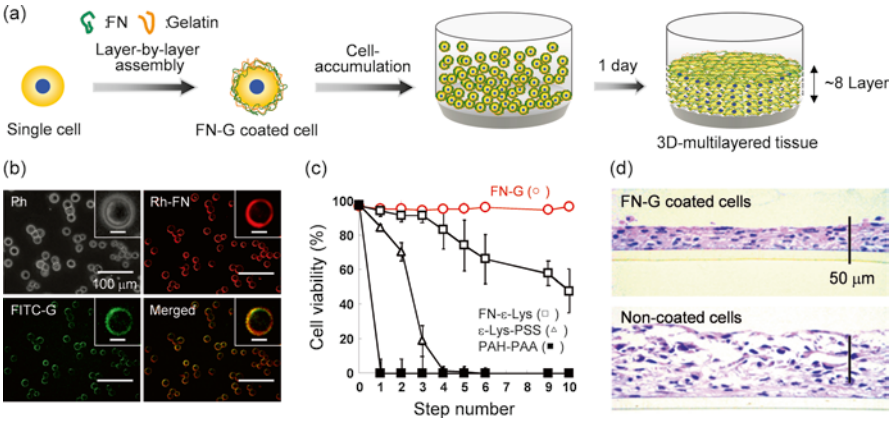

Fig. 5.13 (**a**) Schematic illustration of the rapid construction of 3D multilayered tissues by the cell-accumulation technique using FN-G nanofilms on a single-cell surface. (**b**) Phase and fluorescent microscopic images of L929 mouse fibroblast cells coated with a 9-step assembly of Rh-FN and FITC-G. *Scale bars in the insets* are 10 μm. (**c**) Cell viability of L929 fibroblasts coated with FN-G (*open circles*), FN-ε-Lys (*open squares*), ε-Lys-PSS (*open triangles*), and PAH-PAA (*closed squares*) films at each step of the LbL assembly ($n=3$). (**d**) HE staining images of the obtained layered NHDF constructs with or without the 9-step-assembled FN-G nanofilm. Reproduced with permission [74]

The FN-G nanofilms did not affect fundamental cellular functions such as cell viability (>98 %) or proliferation, whereas other PE-based multilayer films showed higher cytotoxicity depending on the step number and thickness of the films, as well as the results of the film formation on the adhered cell surfaces (Fig. 5.13c) [46]. To test whether FN-G nanofilms prepared onto single cells could function as an adhesion scaffold, cell accumulation was performed. As shown in Fig. 5.13d, the FN-G-coated cells adhered to each other and organized to form layered structures after 1 day of incubation. However, in the case of cells without ECM coating, many defects and detached cells were observed in the tissues. Moreover, we confirmed that the FN-G nanofilms transformed their morphologies from films to fibrous structures, like the natural ECM. These results suggest that FN-G nanofilms formed onto a single cell functioned as a scaffold and promoted the organization of 3D tissues. More importantly, the construction of approximately ten layers per 1 day after only a nanofilm coating within 1 h has never been reported previously, and this approach has tremendous versatility for various cells such as human hepatocellular carcinoma (HepG2).

To apply this cell-accumulation technique to the blood-capillary model, a sandwich culture method was used. Human umbilical vein endothelial cells (HUVECs) with FN-G nanofilms were seeded onto NHDF multilayers constructed by the cell-accumulation technique to obtain tissues with HUVEC layers at the top. Next, FN-G-coated NHDFs were seeded onto the tissues again for the sandwich culture of HUVECs between NHDF multilayers (Fig. 5.14a). During culture, the HUVECs formed tubular structures in the tissues, and highly dense and homogeneous net-

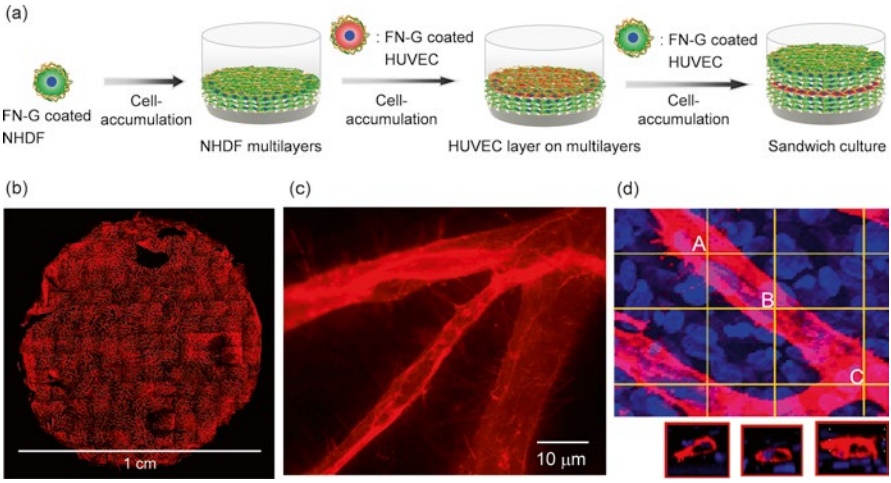

Fig. 5.14 (**a**) Schematic illustration of a sandwich culture of HUVECs between 4L-NHDF tissues. (**b**) Reconstructed fluorescent image of 3D tissues with widespread and dense endothelial tube networks. The HUVECs were immunostained with an anti-CD31 antibody (*red*). This fluorescent image was combined with 150 images at 100× magnification. (**c**) Magnified images of the endothelial tubes. (**d**) CLSM cross-sectional images of the lumenal structures of the endothelial tubes constructed by a sandwich culture of HUVECs between 4L-NHDF layers. The images are shown in the *x*-*z* planes at the A–C positions. Reproduced with permission [74]

works were observed by CLSM observation (Fig. 5.14b). Detailed observations indicated that tip and stalk cell-like structures were formed and seemed to be analogous to blood capillaries in vivo (Fig. 5.14c). Furthermore, these blood capillaries seemed to have clear lumenal structures in many regions (Fig. 5.14d). Therefore, such blood capillaries with a lumen have enormous potential for drug permeability testing or tumor angiogenesis and metastasis assays.

5.5.2 *Application for the Evaluation of the Interaction with Tissues*

To test whether the blood-capillary model constructed by our method can be used as a model for interactions with other tissues, we combined this model with mesenchymal stem cell (MSC) ball-shaped tissues at different differentiation stages [75]. During the process of chondrogenesis, new blood vessel invasion is attenuated in the cartilage tissue at the initial stage of endochondral ossification because of the presence of an anti-angiogenic factor, chondromodulin-I (ChM-I) [76]. On the other hand, vascular invasion into the cartilage tissue occurs during the late stage of ossification. Therefore, the decrease in the expression of ChM-I stimulates blood vessel invasion into the hypertrophic cartilage tissue in the primordial cartilage to supply

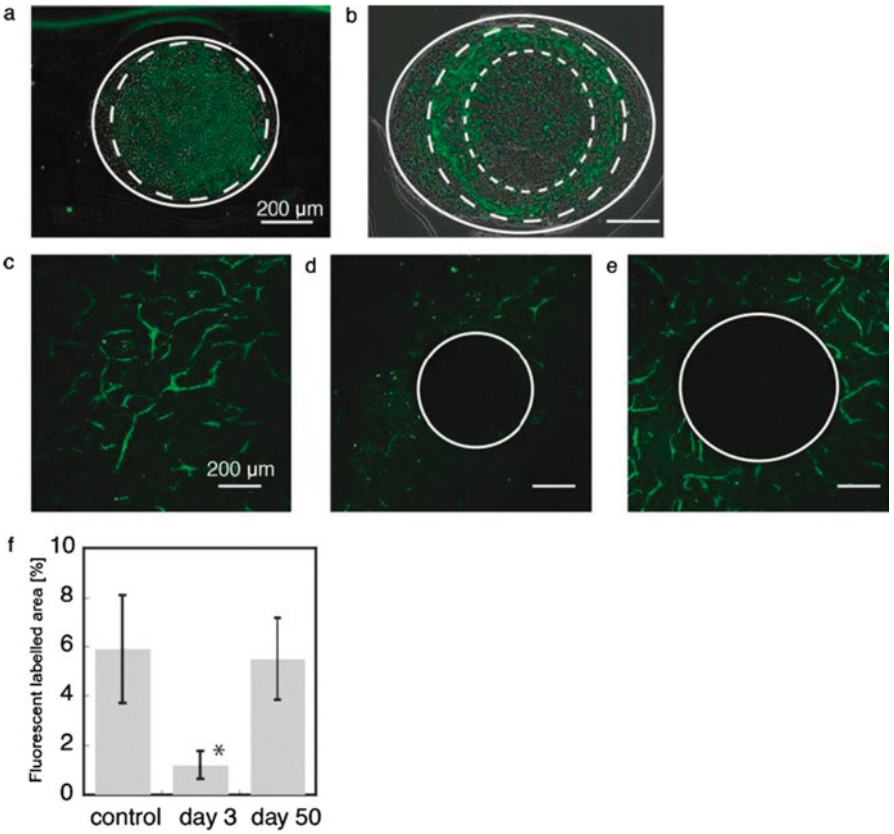

Fig. 5.15 (**a**) ChM-I expression in the cell ball on days 3 and (**b**) 50. Fluorescent microscopic images of capillary networks formed in layered cell sheets (**c**) without cell balls or with (**d**) immature cell balls and (**e**) mature cell balls, which were placed on the tissue directly. (**f**) Ratio of the capillary network area to the total image area (*$p < 0.01$). The *solid curve* indicates the outline of the cell ball, and the *dotted line* indicates the border of the stained region in the cell ball. Reproduced with permission [75]

osteoblastic cells and to convert cartilage into bone. Therefore, we assumed that this blood-capillary model could evaluate the response to engineered MSC tissues, which have properties to promote or suppress vascularization depending on the differentiation stage.

Checking the ChM-I expression in the cell ball, the region of ChM-I expression decreased with increasing culture time (Fig. 5.15a, b). Since joint cartilage tissue keeps on expressing ChM-I to avoid vascularization of the tissue, the thick ChM-I expression region in the 50-day-cultured cell ball has the remaining cartilage tissue phenotype. When these two types of tissues (immature, 3 days of culture; mature, 50 days of culture) were put in the blood-capillary models, the HUVEC tubular networks below the immature MSC ball (3 days of culture) with high ChM-I expression

disappeared after 1 week (Fig. 5.15d). On the other hand, the mature MSC (50 days of culture) with low ChM-I maintained the tubular structures, even after 1 week, as compared to the control (Fig. 5.15c–f). Thus, our system demonstrated that different angiogenic properties responded to the cell ball depending on the culture period and would be useful for testing models and biological evaluations.

5.6 Perfusable Blood Vessel Channel Model

As described above, the in vitro vascularization method can be applied to engineer thick and vascularized tissues by supplying the tissue mass and drug testing model through blood-capillary structures. However, many existing blood-capillary models, including our model, lack blood flow inside the vessels. Therefore, studies have not been performed to directly inject and perfuse a solution from the outside into the blood vessel lumen, except for one example which injected a solution using complicated devices [77]. To solve this problem, micro-fluid systems have attracted increasing attention in the biomedical field, and some reports on the endothelialization of channel-type scaffolds [70, 71] and the connection of two flow channels with endothelial tubes [78] have been recently reported. However, they still have limitations due to structural differences from the living body and the uncontrollable degradability of the scaffolds. Since the surrounding SMCs and pericytes function to support the barrier property [79], structures with pericytes are crucial to study the permeability of drugs, which are involved in the enhanced permeability and retention (EPR) effect and tumor angiogenesis. Furthermore, the uncontrollable degradability of scaffolds like collagen gels and nonbiodegradability should be improved for better stability and the transplantation of these models. If an in vitro drug permeability assay system can be developed using blood-capillary models possessing a controlled layer structure, then it will be a powerful tool for DDS and pharmaceutical applications. Moreover, drug penetration, the metastasis of cancer cells, and pathogen invasion assay systems based on these reconstructed blood capillaries will represent innovative technologies.

We propose for the first time a simple and versatile method to construct multilayered blood capillaries inside biodegradable hydrogels (Fig. 5.16a) [80]. Hydrogels are one of the best candidates to control the permeability of proteins or polymers and to prevent nonspecific adsorption due to their hydrophilic properties. For hydrogel preparation, poly(γ-glutamic acid) (γ-PGA), which has properties to control the network size, high water content, and biocompatibility, was cross-linked via disulfide bonding that was rapidly cleaved to thiol groups (-SH HS-) using biocompatible reductants such as cysteine or glutathione (hydrogel template method) [81, 82]. As shown in Fig. 5.14a, uniaxial micro-channels were prepared inside the hydrogels using silica capillary tubes, and then layered structures composed of HUVECs and human umbilical artery SMCs (UASMCs) were constructed by the hierarchical cell manipulation technique. To elucidate the blood barrier effect of these constructed capillaries, the time-dependent permeation of bovine serum albumin (BSA) of ca.

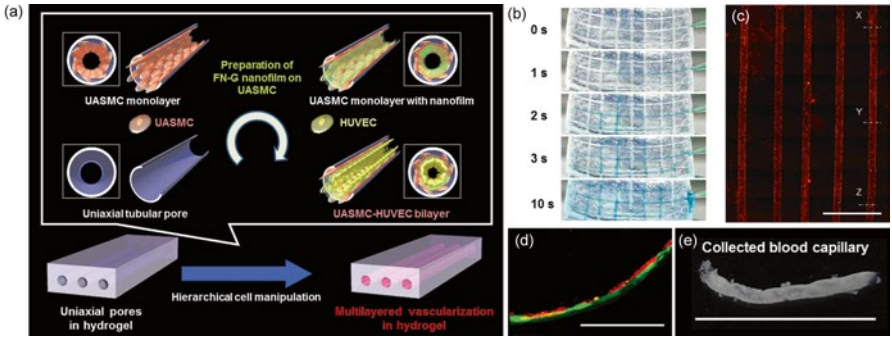

Fig. 5.16 (**a**) Schematic illustration of the in vitro reconstruction of multilayered blood-capillary analogs in biodegradable hydrogels by the hierarchical cell manipulation technique. (**b**) Time-lapse images of the rapid penetration of methylene blue solution into orthogonal-tubular channels of 720-μm diameter in γ-PGA-SS hydrogels constructed by an orthogonal alignment of the silica capillaries. (**c**) Confocal fluorescent images of HUVECs fluorescently labeled with PKH26 in the capillary channels. (**d**) Confocal fluorescent microscopic images of the bilayer morphology of cell tracker *green*-labeled UASMCs as the first layer and PKH26-labeled HUVECs as the second layer. (**e**) Photograph of a blood capillary collected after the decomposition of the hydrogels by 12 h of incubation in culture medium with 10 mML cysteine. The scale bars are 5 mm in (**c**), 100 μm in (**d**), and 1 cm in (**e**). Reproduced with permission [80]

8-nm size was analyzed in detail. This simple and versatile approach will be useful for the in vitro assay of drug permeability through multilayered blood capillaries in the pharmaceutical and biomedical fields.

5.6.1 Construction of Blood Vessel Channel Model in Hydrogel

Uniaxial tubular porous structures in γ-PGA-SS gels were prepared by the hybrid gel formation of γ-PGA and silica capillary tubes of 620-μm diameter and the subsequent extraction of these silica tubes. A γ-PGA polymer solution was mixed with the disulfide cross-linker cystamine plus the GRGDS peptide and water-soluble carbodiimide. The RGD peptide was employed to improve the cell adhesive properties of the γ-PGA gels. The resultant solution was poured between 2 glass plates with a 2-mm silicon spacer and aligned silica tubes. After 3 h, the silica tubes were gently extracted to obtain uniaxial pores in the γ-PGA gels. The channel size was easily controllable depending on the diameter of the silica tubes, and the diameter of the obtained micro-channels was approximately 720 μm. Furthermore, interconnected orthogonal-tubular channels were also fabricated and time-lapse images show the rapid penetration of a methylene blue solution into the tubular channels within 10 s, suggesting complete interconnectivity and usability as a flow culture device (Fig. 5.16b).

To create microvasculatures inside the micro-channels, cell seeding and film preparation were performed by the hierarchical cell manipulation technique.

We began with the preparation of a HUVEC monolayer to check the cell adhesion inside the tubular channels. HUVECs were injected into the channels and cultured for 48 h using rotatory culture conditions at 10 rpm. As shown in Fig. 5.16c, fluorescently labeled HUVECs formed tubular structures with the exact alignment of the channels. Each HUVEC adhered tightly and formed adhesion junctions. To construct a bilayered structure of HUVECs and UASMCs, a UASMC monolayer was formed inside the channels and then the preparation of FN-G films by LbL assembly was performed. HUVECs were injected onto the UASMC monolayer and cultured by rotatory culture to construct the bilayered structure after 48 h. CLSM observation clearly displayed the exact bilayered structure inside the channels (Fig. 5.16d). Furthermore, the engineered blood vessels were successfully collected by the decomposition of the hydrogels by the addition of cysteine. Notably, capillaries of over 1 cm in length were easily obtained, and their diameters and lengths were completely maintained from the tubular channel structures in the hydrogels (Fig. 5.16e). Since we reported high cell viability in these constructs after this hydrogel template method, these collected tubular tissues will be useful as an implantable artificial blood capillaries.

5.6.2 In Vitro Permeability Assay

One of the advantages of this method is for use in permeability assays of drugs and DDS carriers through the surrounding hydrogel networks, which allow for the penetration of macromolecules. To elucidate the network size of the hydrogels, the penetration of fluorescein isothiocyanate-labeled dextran (FITC-dex, $M_w = 200$ kDa) from the tubular channels into the gel networks was evaluated by CLSM observation. As a result, we confirmed the complete diffusion of FITC-dex with a 50-nm hydrodynamic diameter into the gel networks, suggesting that the gel network size is at least 50 nm. This result indicated that major serum proteins such as albumin ($M_w \approx 65$–70 kDa) and globulin ($M_w \approx 100$–150 kDa) can be permeated from the tubular channels into the gel networks, and this model can be used for permeation assays.

We analyzed the barrier effect of the bilayered structures using rhodamine-labeled BSA (Rh-BSA) and compared them to naked tubular channels (Fig. 5.17a, b). The time-lapse fluorescence intensity of Rh-BSA from the channel interface to 300 μm was measured over 60 min by line scanning of the fluorescent images to evaluate the diffusion of albumin. The relative fluorescence intensity of Rh-BSA in the naked channel increased with increasing incubation time, even at 300-μm distance from the channel interface (Fig. 5.17c). On the other hand, the bilayered structures did not show any increase in their fluorescence intensity regardless of the incubation time (Fig. 5.17d). The diffusion rate constant of the naked channels was 7.1-fold higher than that of the bilayer structures, and these results clearly supported a high barrier effect of the bilayer structures, much like a native blood capillary (Fig. 5.17e, f). This technique will be an innovative and versatile approach for in vitro permeability assays of drugs, drug delivery carriers, and cancer cells.

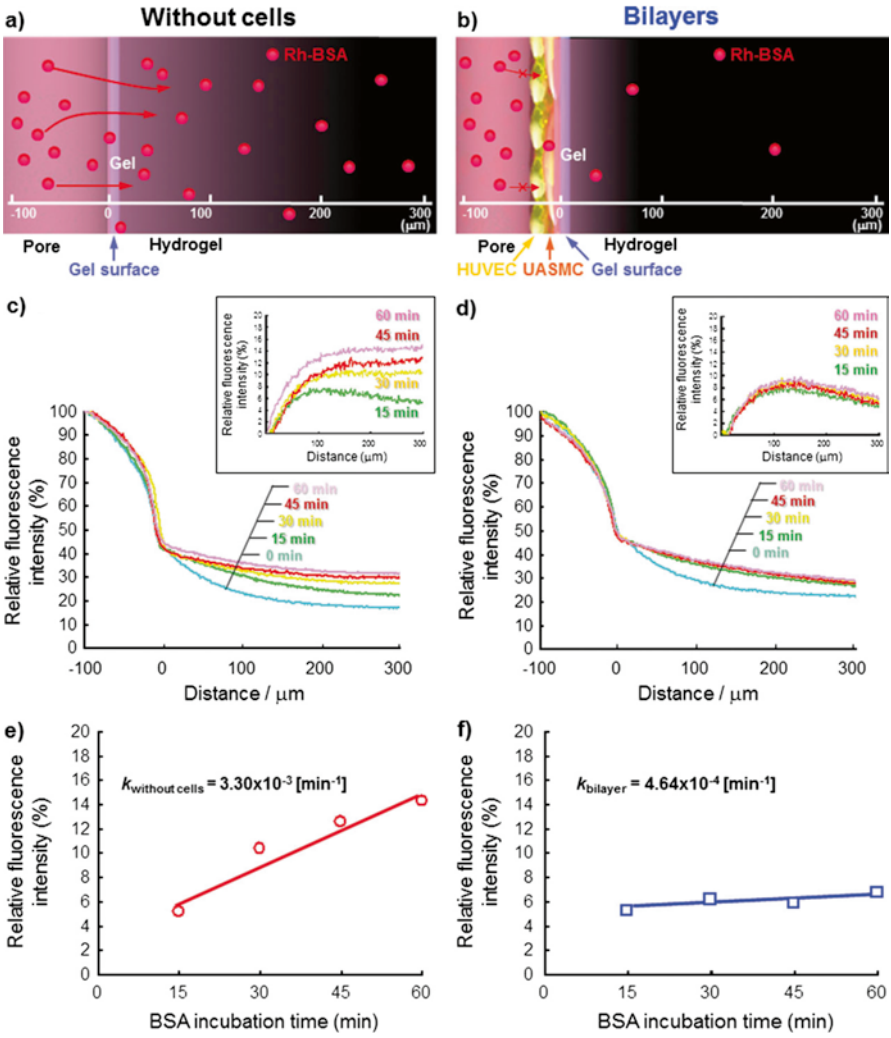

Fig. 5.17 Barrier effect of the blood-capillary analog. Schematic illustration of the BSA permeability of the hydrogels (**a**) without or (**b**) with the bilayers. (**c**, **d**) Fluorescence intensity change in relation to the distance from the inner gel walls. The fluorescence intensity of the line scanning shown in (**a**) and (**b**) was measured every 15 min and normalized against the fluorescence intensity at the −100-μm position (around the center of the channels). The intensity was an average value of over ten replicates. The relative fluorescence intensity compared to the initial intensity (0 min) was plotted in the insets of (**c**) and (**d**). (**e**, **f**) The fluorescence intensity change at a distance of 300 μm and the diffusion rate constant *k*. Reproduced with permission [80]

5.7 Engineering 3D Tissue Chips by Inkjet Cell Printing

For the rapid assessment of drugs, chemicals, and cosmetics, high-throughput assays of human tissue responses using microarrays are valuable. To date, photopolymerized gels with 3D micro-organized cells [83], miniaturized multi-well culture systems [84], and polymeric aqueous two-phase systems [85] have been reported for the fabrication of micro-patterned heterocellular structures. Although these methods are intriguing, they face limitations both in terms of impaired cell–cell contact and in the 3D control of cell positioning at the single-cell level. Therefore, it is still difficult for such a tissue chip to replace the existing monolayered cell model that expresses cell responses but not a tissue response as a drug testing model.

Here, we demonstrate an LbL assembly using the inkjet printing of single cells and ECM to enable the fabrication of 3D human micro-tissue arrays, which are integrated structures of micrometer-sized cellular multilayers controlled at the single-cell layer level. Inkjet printing is a promising technology for noncontact and computer-aided design (CAD) cell printing (Fig. 5.18) [86]. Inkjet cell printing technology allows us to overcome issues regarding low reproducibility and homogeneity of these models because of the well-controlled cell number at the single-cell level and the automatic system. Several approaches have been attempted to make 3D constructs using cell and polymer solution printing, but most fail to reconstitute tissues with cell–cell interactions due to the use of hydrogel encapsulation [87, 88]. We successfully fabricated 440 microarrays of simplified human 3D tissue structures with different layer numbers and cell types by combining our hierarchical cell manipulation with automatic inkjet printing. 3D human tissue chips prepared by this rapid and automatic system will be an innovative technology for in vitro evaluations of drugs, cosmetics, and chemicals, instead of animal testing.

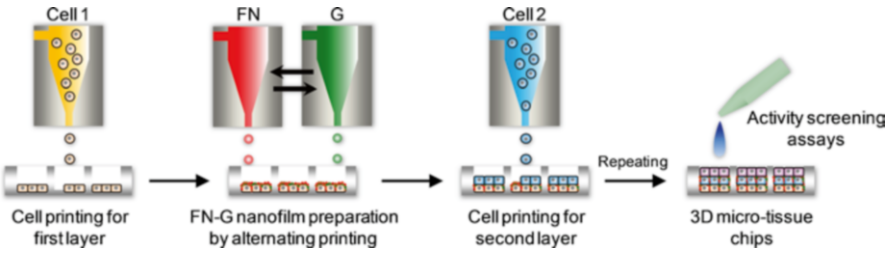

Fig. 5.18 Schematic illustration of the development of 3D micro-tissue arrays by the LbL printing of single cells and ECM proteins. Reproduced with permission [86]

5.7.1 Cell and ECM Printing

Based on inkjet printing technology, the printing conditions of cell and protein solutions should be optimized for the establishment of microarray tissue chips. Boland et al. reported the effect of the solution concentration of *E. coli* on the printed cell number, and approximately 10^7 cells/mL is a suitable concentration for single-cell printing without any defects [89]. We tested the relationship between the drop number and the printed cell number at 10^7 cells/mL. When mammalian C2C12 cells were printed, a good linear correlation was observed from 1 to over 1,000 cells (Fig. 5.19a). Checking the stability and reproducibility of the cell printing, an arbitrary cell number in most spots was confirmed except for the initial 2 spots,

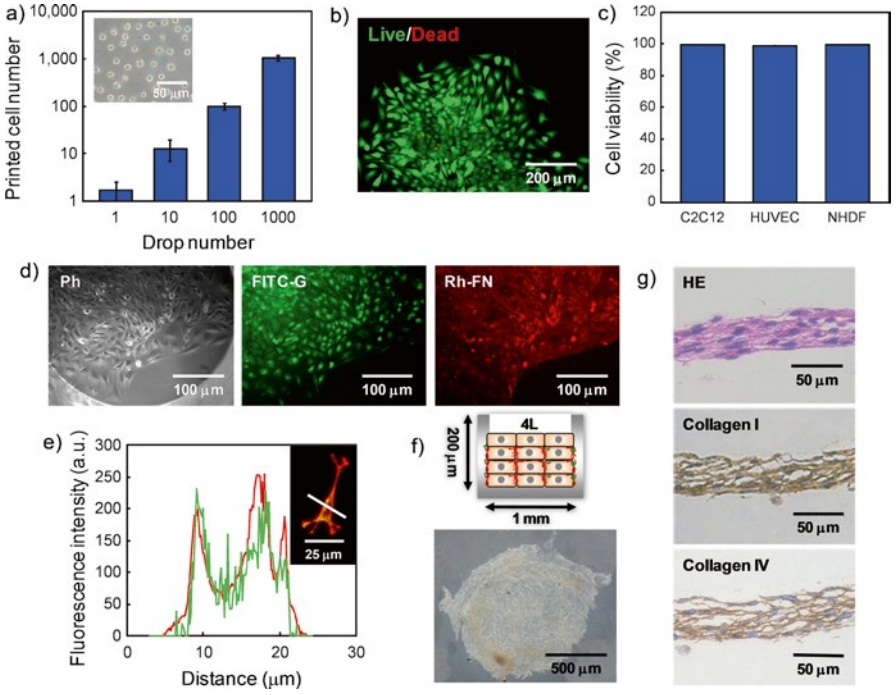

Fig. 5.19 (**a**) Relationship between the drop number and the printed cell number ($n = 3$). The concentration of the cell solution was 1×10^7 cells/ml. The inset shows a phase-contrast image of the printed cells at the 1,000-drop condition. (**b**) Fluorescence microscopic image of printed C2C12 cells labeled with calcein-AM and an ethidium homodimer (EthD-1) after 20 h of culture. The living and dead cells exhibited *green* and *red* colors, respectively (live/dead assay). (**c**) Cell viability of printed C2C12, HUVEC, and NHDF cells after 20 h of culture ($n = 3$). (**d**) Phase-contrast and fluorescence microscopic images of printed C2C12 cells with 10L-FN-G nanofilms prepared by inkjet printing. (**e**) Fluorescence intensity of FITC-G (*green*) and Rh-FN (*red*) from 10L-FN-G nanofilms prepared on printed C2C12 cells by line scanning. (**f**) Illustration (*top*) of four-layered (4L)-C2C12 cells printed in 50-well plates, and a photograph (*bottom*) of 4L-C2C12 constructs peeled off from the wells after 24 h of incubation. (**g**) HE, collagen I, and collagen IV staining histological images of the 4L-C2C12 constructs. Reproduced with permission [86]

indicating stable single-cell printing during the CAD process. Importantly, the cells printed into the well exhibited high viability independent of the cell number and cell types (Fig. 5.19b, c). After incubation, they adhered and extended in each well, and damage in cells was not confirmed. For the observation of the FN-G nanofilms on the printed cells, the inkjet printing of Rh-FN and FITC-G solutions was performed. Fluorescence microscopic images and the intensities of FITC-G and Rh-FN clearly confirmed the preparation of LbL nanofilms on the cell surfaces (Fig. 5.19d, e). To fabricate the 4L-structures of micro-tissue arrays, we continued the inkjet printing of C2C12 myoblasts and FN-G for four times in 50 micro-wells as shown in Fig. 5.19a, accompanied by 24 h of incubation after each cell printing to induce stable cell adhesion. As shown in Fig. 5.19f, g, multilayered C2C12 tissues were fabricated into the micro-well by inkjet cell printing, and they could be easily peeled off from the well. These results clearly proved the successful construction of multilayered micro-tissue arrays by inkjet printing for the first time.

5.7.2 Human Liver Tissue Chips and Liver Function Assay

We applied this inkjet cell printing technology for the use of 3D liver tissue chips. The liver has a variety of crucial functions such as the production and storage of proteins and plays a central role in the metabolism of drugs and toxins. It has hepatic lobule structures composed of liver-specific functional cells such as liver cells and sinusoidal endothelial cells, which account for more than 80 % of the liver's mass. As a liver model cell, human hepatocellular carcinoma cells (HepG2) are one of the candidate cell lines, because their reproducible, inexpensive, and polarized properties are comparable to human primary hepatocytes. However, since they display much lower liver-specific functions at abnormal levels [90], coculture systems with endothelial cells or fibroblasts and spheroid cultures have been performed for drug testing models. These systems allow for the expression of high cellular function in terms of secretion and metabolism, but still structural defects and necrosis inside the tissues were not solved by 2D coculture [91] and the spheroid system, even though actual liver tissue contains hierarchical heterocellular constructs with endothelial cells separated by a thin ECM layer. We fabricated a liver tissue chip, which integrated simplified and multilayered 3D liver structures consisting of HepG2 cells and HUVECs, because the most common cell types in the liver are hepatocytes and endothelial cells, and then evaluated liver functions to understand the most suitable 3D structures for simulating HepG2 functions.

First, to understand the coculture effect of cell types on liver function, albumin secretion was evaluated in the 2L coculture models of HepG2 cells with fibroblasts, myoblasts, and endothelial cells. After 2 days of incubation, the coculture with C2C12 myoblasts showed no consistent enhancement effect, whereas both L929 fibroblasts and NHDFs resulted in a slight increase of albumin secretion as compared to HepG2 cells alone. An obvious 1.4-fold increase was observed for coculture with HUVECs, indicating that hierarchical cocultures with fibroblasts and endothelial cells can yield the highest enhancement effect.

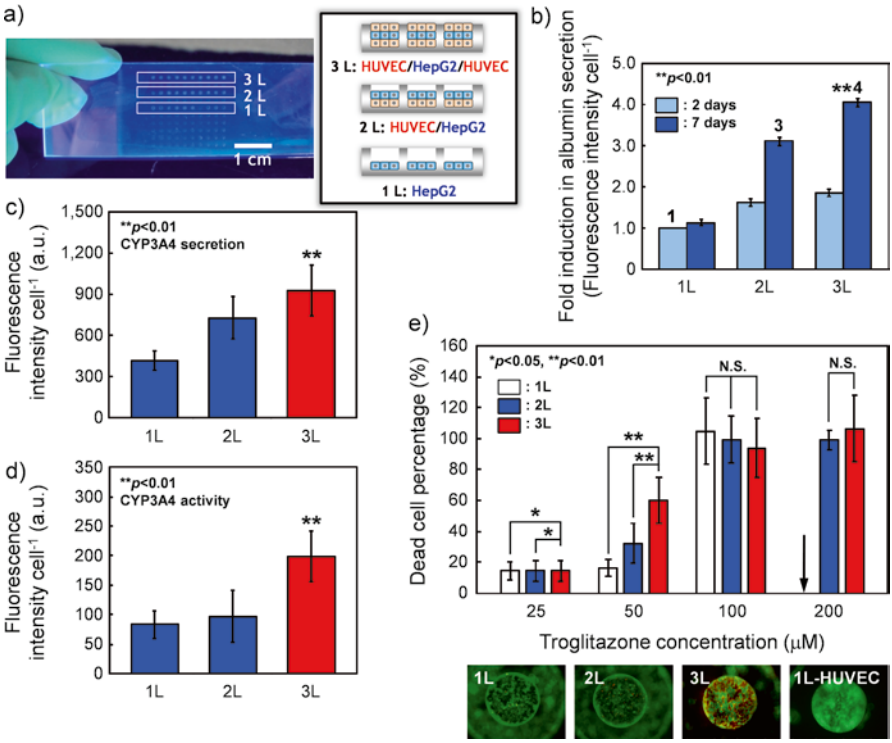

Fig. 5.20 (**a**) Photograph of 1L (HepG2 monolayer), 2L (HUVEC/HepG2), and 3L (HUVEC/HepG2/HUVEC) hepatic layered coculture arrays prepared in 440-micro-well plates under UV light. (**b**) Albumin secretion from HepG2 cells in layered cocultures after 2 or 7 days of incubation ($n=3$, over 10 wells per image). The samples were immunostained with an antihuman albumin antibody. (**c**, **d**) Fluorescence intensity of CYP3A4 secretion and activity from HepG2 cells in layered cocultures after 1 day of incubation ($n=3$, over 10 wells per image). For secretion, the samples were immunostained with an antihuman CYP3A4 antibody. For activity, the fluorescence intensity of resorufin, a metabolite of vivid *red* by CYP3A4, was measured in the micro-wells. (**e**) The layer number and dose-dependent cytotoxicity of troglitazone in coculture after 2 days of incubation ($n=3$, over 10 wells per image). The *bottom fluorescence images* are live/dead images of 1L to 3L constructs and a HUVEC monolayer at 50-μM concentration. The *arrow* indicates undetectable samples due to detachment of the dead cells. All data in (**b–d**) were normalized against blank data (without cells). *,$P<0.05$; **$P<0.01$. N.S.: no significant difference. Reproduced with permission [86]

Next, three types of layers, 1L (HepG2 monolayer), 2L (HUVEC/HepG2), and 3L (HUVEC/HepG2/HUVEC), were constructed in 440-micro-well plates to test the effect of 3D structures in a sandwich culture of HepG2 on cellular activities. Theoretically, 3L structures should induce higher HepG2 cell activities than 2L structures due to the cell–cell interactions at both apical and basal sides, similar to the actual liver structure (Fig. 5.20a). As shown in Fig. 5.20b, albumin secretion from the 3L-sandwich tissue had a fourfold higher increase as compared to 1L-HepG2 tissue and 2L coculture tissue after 7 days of incubation. To assess the

utility of 3D hepatic tissue microarrays for metabolism studies, we characterized phase I cytochrome-P450 (CYP450) enzyme secretion and metabolic activity. As a result, the secretion and activity of CYP3A4, one of the major CYP450 enzymes in the human liver, showed a stepwise increase depending on the layer number, and 3L multilayers showed the highest CYP3A4 secretion and activity (Fig. 5.20c, d). To evaluate practical drug metabolic activity, we employed troglitazone (Rezulin®), which is the first thiazolidinedione antidiabetic agent approved for clinical use in 1997, but was withdrawn from the market in 2000 by the FDA due to serious idiosyncratic hepatotoxicity [92]. Recent toxicological studies have revealed that in the human liver, CYP3A4 plays a major role in the formation of a quinine-type metabolite (M3) from troglitazone, even at a low concentration, and then was further metabolized from M3 induced cytotoxicity [92]. Thus, troglitazone is a suitable candidate to evaluate the practical drug metabolism activity of CYP3A4 using human tissue models but not animal models. Dose-dependent cell death was observed, and the 3L multilayers clearly showed extensive cell death, even at a low concentration, as compared to the 1L and 2L constructs (Fig. 5.20e). These results suggest an approximately 1.5-fold higher CYP3A4 drug metabolism activity. Our results demonstrate for the first time both the development of 3D human tissue chips by an automatic inkjet printing technique and an enhancement of the liver functions of HepG2 cells as 3D human liver chips for drug screening by hierarchical 3L-sandwich structures with HUVECs.

5.8 Conclusions

We introduced several approaches for innovative tissue fabrication technology, focusing on blood vessel models. Using the hierarchical cell manipulation and the cell-accumulation techniques, blood vessel wall models, blood-capillary models, and perfusable blood vessel channel models were successfully fabricated. Furthermore, these bottom-up approaches are valuable for developing 3D cellular organs such as skin, liver, and tumor tissues using multiple types of cells while controlling the location and type of cells. Our techniques would be one of the options for the development of 3D tissue models. However, more precise control of these factors at the single-cell level may be necessary for functional tissue models, which present with human tissue functions comparable to natural tissues. Studies and further developments are ongoing for regenerative medicine and drug testing models.

References

1. Robinton DA, Daley GQ (2012) The promise of induced pluripotent stem cells in research and therapy. Nature 481:295
2. Takahashi K et al (2007) Induction of pluripotent stem cells from adult human fibroblasts by defined factors. Cell 131:861

3. Suzuki K et al (2004) Dynamics and mediators of acute graft attrition after myoblast transplantation to the heart. FASEB J 18:1153
4. Langer R, Vacanti JP (1993) Tissue engineering. Science 260:920
5. Lutolf MP, Hubbell JA (2005) Synthetic biomaterials as instructive extracellular microenvironments for morphogenesis in tissue engineering. Nat Biotechnol 23:47
6. Isenberg BC, Wong JY (2006) Building structure into engineered tissues. Materials Today 9:54
7. Kunz-schughart LA, Freyer JP, Hofstaedter F, Ebner R (2004) The use of 3-D cultures for high-throughput screening: the multicellular spheroid model. J Biomol Screen 9:273
8. Adler S et al (2011) Alternative (non-animal) methods for cosmetics testing: current status and future prospects-2010. Arch Toxicol 85:367
9. Kang HW, Tabata Y, Ikada Y (1999) Fabrication of porous gelatin scaffolds for tissue engineering. Biomaterials 20:1339
10. Lee KY, Mooney DJ (2001) Hydrogels for tissue engineering. Chem Rev 101:1869
11. Shin H, Jo S, Mikos AG (2003) Biomimetic materials for tissue engineering. Biomaterials 24:4353
12. Lee KY, Kong HJ, Larson RG, Mooney DJ (2003) Hydrogel formation via cell crosslinking. Adv Mater 15:1828
13. Lutolf MP, Raeber GP, Zisch AH, Tirelli N, Hubbel JA (2003) Cell-responsive synthetic hydrogels. Adv Mater 15:888
14. Kloxin AM, Kloxin CJ, Bowman CN, Anseth KS (2010) Mechanical properties of cellularly responsive hydrogels and their experimental determination. Adv Mater 22:3484
15. Stevens MM, George JH (2005) Exploring and engineering the cell surface interface. Science 310:1135
16. Place E, Evans N, Stevens M (2009) Complexity in biomaterials for tissue engineering. Nat Mater 8:457
17. Nel AE et al (2009) Understanding biophysicochemical interactions at the nano–bio interface. Nat Mater 8:543
18. Dzenis Y (2004) Spinning continuous fibers for nanotechnology. Science 304:1917
19. Zhang S (2003) Fabrication of novel biomaterials through molecular self-assembly. Nat Biotechnol 21:1171
20. Kushida A et al (1999) Decrease in culture temperature releases monolayer endothelial cell sheets together with deposited fibronectin matrix from temperature-responsive culture surfaces. J Biomed Mater Res 45:355
21. Yang J et al (2005) Cell sheet engineering: recreating tissues without biodegradable scaffolds. Biomaterials 26:6415
22. Nishida N et al (2004) Corneal reconstruction with tissue-engineered cell sheets composed of autologous oral mucosal epithelium. N Engl J Med 251:1187
23. Matsunaga Y, Morimoto Y, Takeuchi S (2011) Molding cell beads for rapid construction of macroscopic 3D tissue architecture. Adv Mater 23:H90
24. Ito A et al (2004) Tissue engineering using magnetite nanoparticles and magnetic force: heterotypic layers of cocultured hepatocytes and endothelial cells. Tissue Eng 10:833
25. Decher G, Hong JD (1991) Buildup of ultrathin multilayer films by a self-assembly process, 1 consecutive adsorption of anionic and cationic bipolar amphiphiles on charged surfaces. Macromol Chem Macromol Symp 46:321
26. Decher G (1997) Fuzzy nanoassemblies: toward layered polymeric multicomposites. Science 277:1232
27. Matsusaki M, Ajiro H, Kida T, Serizawa T, Akashi M (2012) Layer-by-layer assembly through weak interactions and their biomedical applications. Adv Mater 24:454
28. Matsusaki M (2012) Development of three-dimensional tissue models based on hierarchical cell manipulation using nanofilms. Bull Chem Soc Jpn 85:401
29. Feng Z, Wang Z, Gao C, Shen J (2007) Direct covalent assembly to fabricate microcapsules with ultrathin walls and high mechanical strength. Adv Mater 19:3687
30. Stockton WB, Rubner MF (1997) Molecular-level processing of conjugated polymers. 4. Layer-by-layer manipulation of polyaniline via hydrogen-bonding interactions. Macromolecules 30:2717

31. Shimazaki Y, Mitsuishi M, Ito S, Yamamoto M (1997) Preparation of the layer-by-layer deposited ultrathin film based on the charge-transfer interaction. Langmuir 13:1385
32. Xu L, Zhu Z, Sukhishvili SA (2011) Polyelectrolyte multilayers of diblock copolymer micelles with temperature-responsive cores. Langmuir 27:409
33. Crespo-Biel O, Dordi B, Reinhoudt DN, Huskens J (2005) Supramolecular layer-by-layer assembly of 3D multicomponent nanostructures via multivalent molecular recognition. J Am Chem Soc 127:7594
34. Kurth DG, Osterhout R (1999) In situ analysis of metallosupramolecular coordination polyelectrolyte films by surface plasmon resonance spectroscopy. Langmuir 15:4842
35. Rajagopalan P et al (2006) Polyelectrolyte nano-scaffolds for the design of layered cellular architectures. Tissue Eng 12:1553
36. Fischer D, Li Y, Ahlemeyer B, Krieglstein J, Kissel T (2003) In vitro cytotoxicity testing of polycations: influence of polymer structure on cell viability and hemolysis. Biomaterials 24:1121
37. Hynes RO (1990) Fibronectins. Springer, New York
38. Ruoslahti E, Pierschbacher MD (1987) New perspectives in cell adhesion: RGD and integrins. Science 238:491
39. Matsusaki M, Kadowaki K, Nakahara Y, Akashi M (2007) Fabrication of cellular multilayers with nanometer-sized extracellular matrix films. Angew Chem Int Ed 46:4689
40. G. Krishna, T. Shutava, Y. Lvov (2005) Lipid modified polyelectrolyte microcapsules with controlled diffusion. Chem Commun (22):2796
41. Nakahara Y, Matsusaki M, Akashi M (2007) Fabrication and enzymatic degradation of fibronectin-based ultrathin films. J Biomater Sci Polymer Edn 18:1565
42. Chetprayoon P, Kadowaki K, Matsusaki M, Akashi M (2013) Survival and structural evaluations of three-dimensional tissues fabricated by hierarchical cell manipulation technique. Acta Biomater 9:4698
43. Tang Z, Wang Y, Podsiadlo P, Kotov NA (2006) Biomedical applications of layer-by-layer assembly: from biomimetics to tissue engineering. Adv Mater 18:3203
44. Elbert DL, Herbert CB, Hubbell JA (1999) Thin polymer layers formed by polyelectrolyte multilayer techniques on biological surfaces. Langmuir 15:5355
45. Boura C et al (2003) Endothelial cells grown on thin polyelectrolyte multilayered films: an evaluation of a new versatile surface modification. Biomaterials 24:3521
46. Kadowaki K, Matsusaki M, Akashi M (2010) Control of cell surfaces and functions by layer-by-layer nanofilms. Langmuir 26:5670
47. Kadowaki K, Matsusaki M, Akashi M (2012) Control of cellular inflammation by layer-by-layer nanofilms through different driving forces. Chem Lett 41:523
48. Kadowaki K, Matsusaki M, Akashi M (2010) Biochem Biophys Res Commun 402:153
49. Hosoya H et al (2012) Three-dimensional constructs induce high cellular activity: structural stability and the specific production of proteins and cytokines. Biochem Biophys Res Commun 419:32
50. Cooper JA et al (1987) Measurement of albumin permeability across endothelial monolayers in vitro. J Appl Physiol 62:1076
51. Deli MA, Abraham CS, Kataoka Y, Niwa M (2005) Permeability studies on in vitro blood-brain barrier models: physiology, pathology, and pharmacology. Cell Mol Neurobiol 25:59
52. Green JA, Yamada KM (2007) Three-dimensional microenvironments modulate fibroblast signaling responses. Adv Drug Deliv Rev 59:1293
53. Matsusaki M et al (2012) Morphological and histological evaluations of 3D-layered blood vessel constructs prepared by hierarchical cell manipulation technique. J Biomater Sci Polym Ed 23:63
54. Matsusaki M, Amemori S, Kadowaki K, Akashi M (2011) Quantitative 3D-analysis of nitric oxide diffusion in a 3D-artery model using sensor particle. Angew Chem Int Ed 50:7557
55. Alderton WK, Cooper CE, Knowles RG (2001) Nitric oxide synthases: structure, function and inhibition. Biochem J 357:593
56. Zhao G et al (1999) Reduced coronary NO production in conscious dogs after the development of alloxan-induced diabetes. Am J Physiol Heart Circ Physiol 277:H268

57. Kurioka S, Koshimura K, Murakami Y, Nishiki M, Kato Y (2000) Reverse correlation between urine nitric oxide metabolites and insulin resistance in patients with type 2 diabetes mellitus. Endocr J 47:77
58. Nakaya Y et al (2000) Taurine improves insulin sensitivity in the Otsuka Long-Evans Tokushima Fatty rat, a model of spontaneous type 2 diabetes. Am J Clin Nutr 71:54
59. Nakatsubo N et al (1998) Direct evidence of nitric oxide production from bovine aortic endothelial cells using new fluorescence indicators: diaminofluoresceins. FEBS Lett 427:263
60. Amemori S, Matsusaki M, Akashi M (2010) Biocompatible and highly-sensitive nitric oxide sensor particles prepared by layer-by-layer assembly. Chem Lett 39:42
61. Ortiz PA, Hong NJ, Garvin JL (2004) Luminal flow induces eNOS activation and translocation in the rat thick ascending limb. II. Role of PI3-kinase and Hsp90. Am J Physiol Renal Physiol 287:F281
62. Malinski T, Taha Z, Grunfeld S (1993) Diffusion of nitric oxide in the aorta wall monitored in situ by porphyrinic microsensors. Biochem Biophys Res Commun 193:1076
63. Tsai AG, Johnson PC, Intaglietta M (2003) Oxygen gradients in the microcirculation. Physiol Rev 83:933
64. Oishi M et al (2007) Enhanced growth inhibition of hepatic multicellular tumor spheroids by lactosylated poly(ethylene glycol)-siRNA conjugate formulated in PEGylated polyplexes. ChemMedChem 2:1290
65. Folkman J, Haudenschild C (1980) Angiogenesis in vitro. Nature 288:551
66. Madri JA, Williams SK, Wyatt T, Mezzio C (1983) Capillary endothelial cell cultures: phenotypic modulation by matrix components. J Cell Biol 97:153
67. Moon JJ et al (2010) Biomimetic hydrogels with pro-angiogenic properties. Biomaterials 31:3840
68. Levenberg S et al (2005) Engineering vascularized skeletal muscle tissue. Nat Biotechnol 23:879
69. Huh D et al (2010) Reconstituting organ-level lung functions on a chip. Science 328:1662
70. Miller JS et al (2012) Rapid casting of patterned vascular networks for perfusable engineered three-dimensional tissues. Nat Mater 11:768
71. Zheng Y et al (2012) In vitro microvessels for the study of angiogenesis and thrombosis. Proc Natl Acad Sci USA 109:9342
72. Sasagawa T et al (2010) Design of prevascularized three-dimensional cell-dense tissues using a cell sheet stacking manipulation technology. Biomaterials 31:1646
73. Haraguchi Y et al (2012) Fabrication of functional three-dimensional tissues by stacking cell sheets in vitro. Nat Protoc 7:850
74. Nishiguchi A, Yoshida H, Matsusaki M, Akashi M (2011) Rapid construction of three-dimensional multilayered tissues with endothelial tube networks by the cell-accumulation technique. Adv Mater 23:3506
75. Sasaki J et al (2012) In vitro reproduction of endochondral ossification using a 3D mesenchymal stem cell construct. Integrat Biol 4:1207
76. Hiraki Y et al (1997) Identification of chondromodulin I as a novel endothelial cell growth inhibitor. J Biol Chem 272:32419
77. Kobayashi A et al (2007) In vitro formation of capillary networks using optical lithographic techniques. Biochem Biophys Res Commun 358:692
78. Kim S, Lee H, Chung M, Jeon NL (2013) Engineering of functional, perfusable 3D microvascular networks on a chip. Lab Chip 13:1489
79. Armulik A, Genove′ G, Betsholtz C (2011) Pericytes: developmental, physiological, and pathological perspectives, problems, and promises. Dev Cell 21:193
80. Yoshida H, Matsusaki M, Akashi M (2013) Multilayered blood capillary analogs in biodegradable hydrogels for in vitro drug permeability assay. Adv Funct Mater 23:1736
81. Matsusaki M, Yoshida H, Akashi M (2007) The construction of 3D-engineered tissues composed of cells and extracellular matrices by hydrogel template approach. Biomaterials 28:2729
82. Yoshida H, Matsusaki M, Akashi M (2009) Scaffold-mediated 2D-cellular orientations for construction of 3D-engineered tissues composed of cells and ECM. Adv Funct Mater 19:1001

83. Albrecht DR, Underhill GH, Wassermann TB, Sah RL, Bhatia SN (2006) Probing the role of multicellular organization in three-dimensional microenvironments. Nat Methods 3:369
84. Khetani SR, Bhatia SN (2008) Microscale culture of human liver cells for drug development. Nat Biotechnol 26:120
85. Tavana H, Mosadegh B, Takayama S (2010) Polymeric aqueous biphasic systems for non-contact cell printing on cells: engineering heterocellular embryonic stem cell niches. Adv Mater 22:2628
86. Matsusaki M, Sakaue K, Kadowaki K, Akashi M (2013) Three-dimensional human tissue chips fabricated by rapid and automatic inkjet cell printing. Adv Healthc Mater 2:534
87. Mironov V, Boland T, Trusk T, Forgacs G, Markwald RR (2003) Organ printing: computer-aided jet-based 3D tissue engineering. Trends Biotechnol 21:57
88. Calvert P (2007) Printing cells. Science 318:208
89. Xu T et al (2004) Construction of high-density bacterial colony arrays and patterns by the ink-jet method. Biotechnol Bioeng 85:29
90. Wilkening S, Stahl F, Bader A (2003) Comparison of primary human hepatocytes and hepatoma cell line Hepg2 with regard to their biotransformation properties. Drug Metab Dispos 31:1035
91. Bhatia SN, Balis UJ, Yarmush ML, Toner M (1999) Effect of cell–cell interactions in preservation of cellular phenotype: cocultivation of hepatocytes and nonparenchymal cells. FASEB J 13:1883
92. Yokoi T (2010) Compound cytotoxicity profiling using quantitative high-throughput screening. In: Uetrecht J (ed) Adverse drug reactions, vol 196, Handbook of experimental pharmacology. Springer, Berlin

Chapter 6
Engineering Cellular Assembly for Applications in Regenerative Medicine

Christopher Millan and Marcy Zenobi-Wong

Abstract In vitro cell culture methods are undergoing a revolutionary transition towards 3D systems that better imitate the complex microenvironment a cell experiences in the body. Cells must be permitted to participate in an intricate communication network via biochemical and mechanical signaling with neighboring cells and key components of the extracellular matrix, something that is inherently lacking in monolayer cultures using petri dishes or flasks. Over the last 2–3 decades, a number of 3D cell culture techniques have been introduced that rely on cell self-organizing capacity such as hanging drops, centrifuged pellets, and suspension culture. However, more recent approaches have emerged to further control cellular organization in 3D. Methods for engineering a directed assembly of cells will yield 3D models that more closely resemble their organ mimics, which would have significant implications in the field of regenerative medicine.

Keywords 3D cell culture • Chondrogenesis • Microtissue • MSC condensation

6.1 Stem Cell Aggregates and Development

The inner cell mass of a human embryo 9 days after fertilization is a high density cluster of 50–150 cells that will eventually divide and differentiate giving way to form every cell, tissue, and organ in the body [1]. Later on during fetal development, skeletogenesis is initiated by condensation of chondroprogenitor cells into high density micromasses [2]. A myriad of different cues induce behavioral changes among these aggregated stem cells that ultimately determine their differentiated fate—specific genes are up-regulated in various cell subpopulations that define a more specialized function for that group of cells. The end result is a tissue composed of a heterogeneous population of specialized cells which collectively maintain the physiological function of their respective organ.

C. Millan • M. Zenobi-Wong (✉)
Cartilage Engineering+Regeneration, Swiss Federal Institute of Technology,
ETH Zürich, Otto-Stern-Weg 7, 8093 Zürich, Switzerland
e-mail: marcy.zenobi@hest.ethz.ch

M. Akashi et al. (eds.), *Engineered Cell Manipulation for Biomedical Application*, Nanomedicine and Nanotoxicology,
DOI 10.1007/978-4-431-55139-3_6

Embryoid bodies (EBs) are aggregates of embryonic stem cells (ESCs) that are often the basis for studying cues that direct ESC differentiation. Mesenchymal stem cell (MSC) condensation is also simulated in vitro to produce microtissues for studying chondrogenesis. Designing appropriate model systems for investigating stem cell behavior in a more mimetic 3D environment is paramount to harnessing their therapeutic potential and will inform the engineering design strategies in regenerative medicine [3, 4].

6.1.1 Cellular Aggregation and Skeletal Tissue Development

The primordial skeleton appears first as a formation of high density regions of MSCs whose size, shape, and arrangement foreshadow the future skeleton. Between 4 and 5 weeks after fertilization, a rapid and transient upregulation of cell adhesion molecules and specific extracellular matrix proteins facilitates the condensation of chondroprogenitor cells into high density micromasses [2]. Condensation is a requisite step prior to MSC differentiation (Fig. 6.1a), after which mature chondrocytes begin secreting cartilage matrix components primarily consisting of type II collagen and glycosaminoglycans (GAGs) [6]. As a result of signaling gradients in the limb bud, a subpopulation of chondrocytes transition to a hypertrophic phenotype and begin secreting type X collagen which establishes the framework for subsequent calcification, endochondral ossification, and eventual bone formation [7].

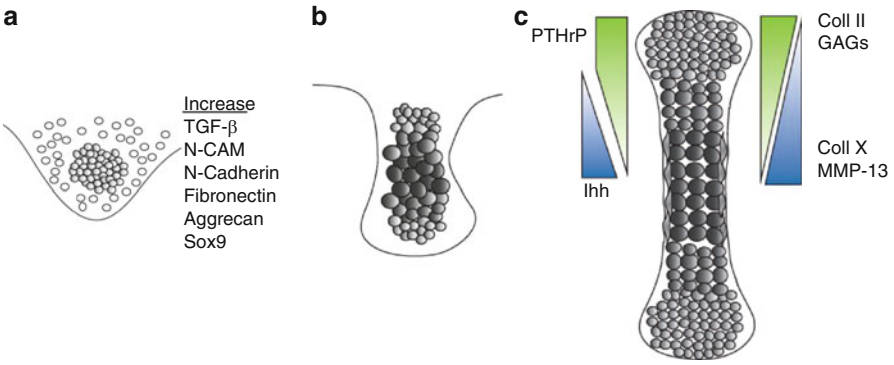

Fig. 6.1 MSC Condensation in the developing limb is a requisite step for chondrogenesis and subsequent endochondral ossification. (**a**) Up-regulation in the expression of N-CAM and N-cadherin plays a major role in increasing cell–cell interactions. (**b**) TGF-β stimulation drives the expression of cartilage specific markers via the Sox9 master transcription factor. (**c**) During maturation and terminal differentiation, chondrocytes in the resting zone at the end of long bones secrete PTHrP which maintains their chondrogenic phenotype, while those outside of this signaling range are under the influence of Ihh which induces hypertrophy (from Studer et al. [3, 5])

6.1.2 Key ECM and Cell–Cell Interaction Molecules in Regulating MSC Condensation

The condensation of MSCs is an active process mediated by a specific and sequential set of differentially regulated extracellular matrix components and proteins. MSCs make initial cell–cell interactions via N-cadherin and neural cell adhesion molecule (N-CAM) membrane receptors (Fig. 6.1a) [8]. Fibronectin secretion additionally aids the formation of a dense aggregate, after which MSCs are stimulated by transforming growth factor-beta (TGF-β) which up-regulates the chondrogenesis master transcription factor Sox-9 and leads to production of type II collagen and proteoglycans such as aggrecan [8, 9].

Hyaluronic acid (HA), the unsulfated GAG present in high quantity in cartilage, also plays a critical role in the initial condensation and subsequent separation of chondroprogenitors during cartilage formation [10]. Via their cell membrane CD44 receptor, MSCs engage in specific binding with HA [11]. In this manner, HA serves as a bridge between neighboring cells that bind the GAG molecule and establish a close proximity. As the HA concentration increases, CD44 binding is saturated eventually establishing cell separation, or cavitation.

The duration of the condensation phase is short, roughly 12 h [6], but it is a requisite step that drives MSC chondrogenesis. Following condensation, maturation of the cartilage coincides with a series of morphological and physical changes. The resting chondrocytes at the end of developing long bones maintain a chondrogenic phenotype due in large part to signaling of the parathyroid hormone-related protein (PTHrP) [12]. Chondrocytes outside of the signaling range of the resting chondrocytes produce Indian hedgehog (Ihh), a potent inducer of hypertrophy (Fig. 6.1c) [13]. Hypertrophic chondrocytes synthesize type X collagen which establishes the framework for eventual calcification and endochondral ossification of the developing bone [5]. MSC condensation is a prime example of a developmental process whereby progenitor cells first coalesce into a high density aggregate leading to differentiation. Researchers have shown that mimicking these conditions in vitro, via culturing a centrifuged pellet of cells in defined induction media, can induce chondrogenic differentiation [14]. However, the phenotype of the differentiated cells shares characteristics of mature chondrocytes as well as hypertrophic chondrocytes, and the deposition levels of cartilage matrix specific components are limited in centrifuged pellets.

6.1.3 In Vitro Differentiation of Pluripotent Stem Cells

Pluripotent stem cells (PSCs) have the capacity to differentiate into any cell in the body. PSCs begin as a cell mass in the developing embryo and in vitro systems for aggregating stem cells aim to mimic this feature to study development [15]. Many systems rely on the self-organizing capacity of PSCs to form spheroids according to

the differential adhesion hypothesis [16]. Examples include culture by gyratory shakers [17], spinner flasks [18], and hanging drop culture [19]. PSCs grown in suspension where cell–substrate interactions are prohibited by nonadhesive plastic have also been shown to spontaneously form embryoid bodies (EBs), or spheres of PSCs, that can differentiate into mature cells of any of the three germ layers [20].

Through temperamental control of exposure of EBs to specific growth factors, their differentiation into intestinal tissue [21], epithelial tissue [22], insulin-responsive pancreatic tissue [23], functional liver tissues [24], and even cerebral tissues [25] has been achieved. These recent successes rely on microtissues formed by inherent characteristics of PSCs. Induced pluripotent stem cells (iPSCs) have recently garnered a great deal of attention as their multipotency has been demonstrated while bypassing ethical concerns raised by working with embryonic cells [26, 27]. Similar to EBs, in vitro work in understanding and controlling differentiation of iPSCs also involves initial culture of cells in spheroids.

Still, limitations for producing embryoid bodies by hanging drop or prolonged suspension culture restrict control of the experimental setup. Certain engineered systems for culturing cells in 3D micromasses may serve to overcome such limitations and further enhance our understanding of, and expand the potential uses for, PSCs in future studies related to development and regenerative medicine.

6.2 Engineered Cell Assembly into Microtissues

A majority of the methods in widespread use for microtissue formation that rely on self-organization of the cells are slow and time consuming, exhibit poor control over size and shape of the microtissue construct, and can vary widely among biological donors [28]. To overcome these pitfalls, tools are rapidly emerging for engineering the assembly process of cells into 3D structures that offer control over microtissue formation featuring various degrees of spatial resolution of the microtissue components [29].

6.2.1 Engineering Cell Surfaces for Directed Adhesion

One approach for control over cell–cell adhesion is to modify the properties of the cell surface. Researchers at UC Berkeley have recently demonstrated the directed assembly of different cell types by coupling complementary single-stranded DNA (ssDNA) to the surfaces of separate cell populations [30]. Hybridization of the ssDNA of one cell type occurs with its complementary strand on the surface of a second cell type forcing the aggregation of cells in a controlled 3D co-culture (Fig. 6.2a). By adjusting the ratio of the two cell types to one another, the cell type in excess formed rosettes surrounding the less abundant cell type. A microtissue dependent upon paracrine signaling between two different cell types for survival was successfully

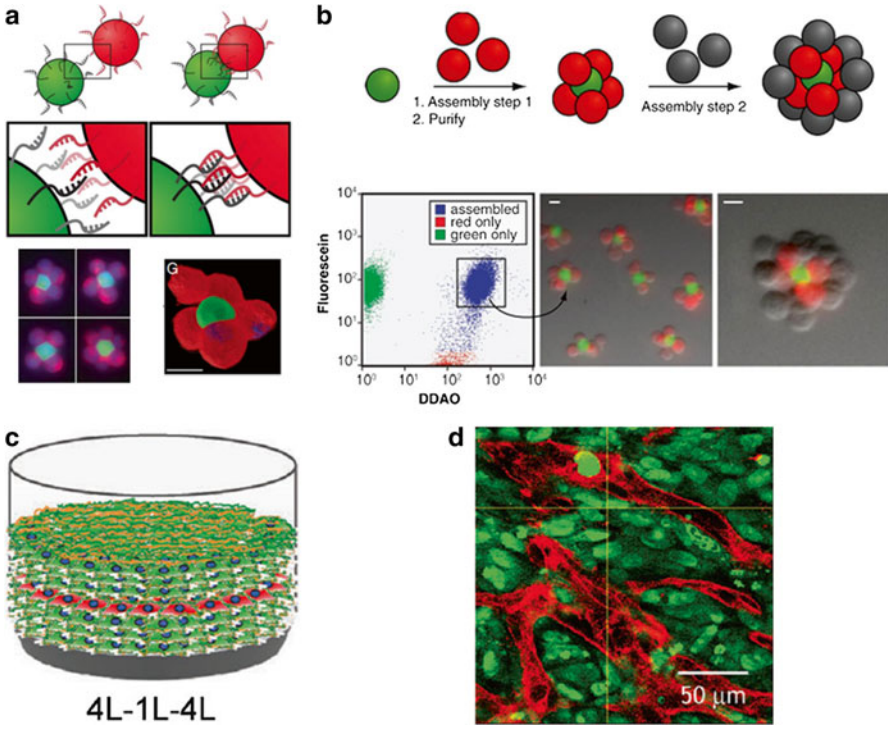

Fig. 6.2 Engineering cell surfaces to control adhesion. Gartner and Bertozzi [30] utilized click chemistry to bind complimentary DNA strands to the surface of different cell populations. Hybridization of the DNA strands adheres one cell type with its ssDNA to another cell type with the complimentary ssDNA (**a**, scale bar = 10 µm). FACS and multistep assembly were utilized to build a microtissue with increasing number of cells per layer (**b**, scale bars = 10 µm). Nishiguchi et al. [31] have developed the "cell accumulation technique" where cells are encapsulated in thin films of fibronectin and gelatin in a layer-by-layer assembly process. Coated cells are seeded at high density and form a compact microtissue where the number of cell layers is defined by the seeding density. In co-culture, 1 layer of HUVEC cells was sandwiched between 2 × 4 layers of fibroblasts (**c**) and a tubular network mimicking vascularization was observed in the microtissue (**d**, scale bar = 50 µm)

constructed between IL-3 expressing CHO cells as the microtissue "nucleus" and IL-3 dependent hematopoietic FL5.12 cells as the rosettes (Fig. 6.2b). In media containing anti-IL-3, only microtissues with both cell types remained viable.

Nishiguchi and co-workers have developed a different cell surface modification involving ligand–receptor binding [31]. Cells were coated with nanofilms of fibronectin and gelatin (FN and G, resp.), two proteins that have binding domains for each other, in a layer-by-layer (LbL) manner by alternate incubation and washing in solutions of the two proteins. Integrin proteins of one cell can therefore bind the fibronectin present in the nanofilm coating of a neighboring cell. FN-G coated cells can then be seeded in high density where they form a compact 3D microtissue structure in a process called the cell accumulation technique. By controlling the number of cells

seeded, microtissues of defined thickness can be constructed, and by alternating the sequence of cell types seeded in this way, microtissues can be fabricated with defined zones for each cell type. For example, a layer of HUVEC cells was sandwiched between 2×4-layer thick zones of fibroblast cells (Fig. 6.2c) resulting in a microtissue bisected with a tubular network that mimicked vascularization (Fig. 6.2d).

6.2.2 Microtissue Manipulation: Arranging Preformed Microtissues into Larger Assembled Constructs

Larger tissues of different cell types can also be fabricated by assembling preformed cell aggregates or cell-laden hydrogels. That is, larger microtissues have been engineered by controlling the assembly of smaller building blocks. Spheroids of different cell types were used as a bio-ink in extrusion-based 3D bioprinting and printed into a hydrogel that was polymerized to retain the printed shape [32]. In another approach, McDevitt and colleagues have harnessed magnetic forces for spatially patterning a large number of separately formed embryoid bodies [33]. Magnetic microparticles (magMPs) were entrapped in the extracellular space around ESCs by first pelleting the cells in AggreWell 400 inserts and mixing magMPs into the wells followed by a second centrifugation step. ESCs were stained with cell tracking molecules in separated populations and embryoid bodies (EBs) were formed. Manipulation of the EBs containing magMPs with a structured magnetic field was successful to form spatially complex microtissue arrangements such as a Venn diagram layout (Fig. 6.3a) or a "bull's-eye" (Fig. 6.3c). Useful strategies have also been developed to organize cell-laden hydrogels into defined orientations. Khademhosseini and co-workers recently introduced the concept of micromasonry whereby cells encapsulated in PEG hydrogels were organized based on their shape in a subsequent polymer solution and "cemented" together by polymerization of the immersion polymer [35]. The PEG hydrogels containing differently labeled fluorescent cells were shape-controlled by formation in PDMS molds so that the gels had complementary shapes and fit together in a "lock-and-key" manner ([34], Fig. 6.3e–i). The time needed for assembly of the form-fitting microgels was reduced by including a hydrophobic solvent layer of perfluorodecalin (PFDC) underneath the gels during the organization process and exposing the system to gentle shaking.

6.3 Schiff-Base Cross-Linking for Microtissue Fabrication: The QuickStick Method

A new method for rapid and controlled fabrication of microtissues, called QuickStick, has recently been developed using modified polysaccharides and Schiff-base cross-linking. A Schiff base is a covalent bond that forms spontaneously between primary amine groups and free aldehyde or ketone groups. Polymers containing the two key reactive groups can be mixed in solution in the presence of cells

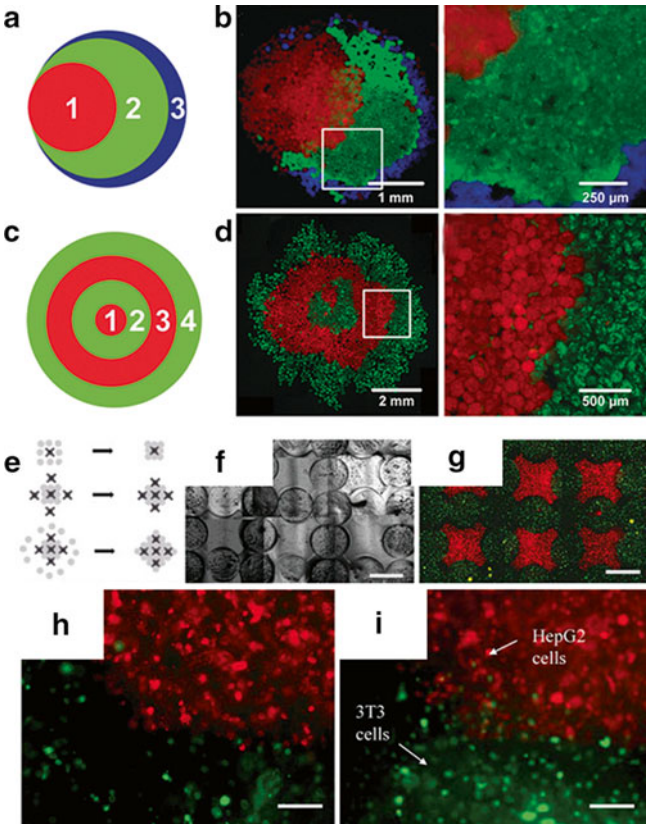

Fig. 6.3 Spatial organization of cellular spheroids (**a**–**d**) and micro-hydrogels of different cell populations (**e**–**i**). Bratt-Leal et al. [33] developed a technique to organize embryoid bodies (*EBs*) labeled with different cell tracking molecules in a highly organized spatial distribution by magnetic manipulation. Magnetic microparticles (*magMPs*) are entrapped within EBs during spheroid formation and exposed to a structured magnetic field to distribute EBs into either a Venn diagram (**a**) or "bull's-eye" (**c**) distribution. Two cell populations were labeled with either cell tracker *red* or cell tracker *green* prior to EB formation and magMP entrapment (**b**, **d** *left*) and higher magnification shows the borders between EBs of the different colors are well defined (**b**, **d** *right*). Zamanian et al. [34] demonstrated a technique termed "micromasonry" where microgels can be molded to fit with each other in a lock-and-key conformation (**e**) and different cell types were labeled and cast in gels of either the lock or key shape. Upon mixing over a hydrophobic surface, the gels self-assemble (**f**-brightfield, **g**-fluorescence, scale bar = 1 mm) defining the interface of the two cell populations in a structured co-culture arrangement (**h**, **i** scale bar = 100 µm)

and will polymerize within minutes forming a polymer network around the cells and releasing water as the by-product of the reaction. Layered co-cultures can be fabricated with spatial control of the different cell populations within the microtissue. In one application, QuickStick microtissues were utilized to mimic MSC condensation and produced constructs with higher degree of chondrogenesis than traditional centrifuged pellets.

6.3.1 QuickStick Polymers and Cross-Linking Chemistry

Two polymer components are necessary to carry out Schiff-base cross-linking—one containing free amino groups in its structure and the second with reactive aldehyde or ketone groups. These basic requirements indicate that many polymer combinations can be utilized in Schiff-base cross-linking chemistries for biomaterial applications [36–39]. In the examples presented here, however, chitosan was selected as the amino-bearing polymer and oxidized alginate as the aldehyde-containing polymer.

Chitosan is a biocompatible polymer that has been studied in detail as an attractive biomaterial for tissue engineering strategies. This is largely due to its structural similarities with various GAGs that are present in many types of extracellular matrix [40]. It has also been previously linked to cell aggregation in cartilage. In a study where chitosan was simply injected into rat knee cartilages, it was shown to significantly increase the density of articular chondrocytes in the tissue [41]. It is an attractive choice as a Schiff pair owing to the high number of free primary amines on almost every saccharide unit of the polymer (depending on the degree of deacetylation), but has very low solubility at physiological pH (Fig. 6.4a). However, partial succinylation of chitosan disrupts crystallinity domains in the structure and allows its solubility at pH 7.4 [42]. The resulting N-succinyl chitosan (sChi) is a molecule that still contains free amino groups for Schiff-base cross-linking and retains cytocompatibility (Fig. 6.4b).

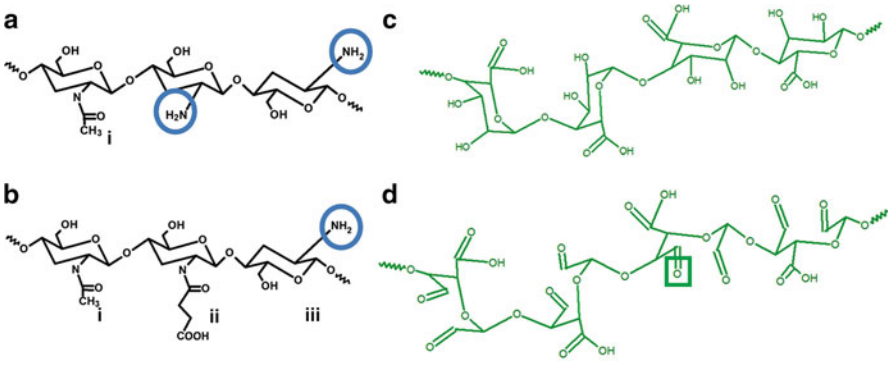

Fig. 6.4 Chemical structures of QuickStick polymers. (**a**) Chitosan is a glucosamine-based polysaccharide. Depending on its deacetylation degree, a number of saccharide units in chitosan still carry the acetyl group (*i*, ≤10 %). The remaining saccharide units have free primary amine groups that can participate in Schiff-base cross-linking (*circled*). (**b**) Chitosan is not soluble at physiological pH, but reaction with succinic anhydride enables solubility at pH 7.4 yielding *N*-succinyl chitosan (*sChi*). The succinyl groups form bonds with a number of free amines necessary for cross-linking, but a degree of 40 % *N*-substitution is sufficient to enable solubility and provide sufficient amines for Schiff-base polymerization (*i* = 10 %, *ii* = 40 %, *iii* = 50 %). (**c**) Alginate contains copolymer blocks of α-L-guluronic acid (I) and (1,4)-linked β-D-mannuronic (II). (**d**) Oxidation of vicinal hydroxyl groups by sodium periodate in the saccharide units results in formation of oxidized alginate (*oxAlg*) with free aldehyde groups for Schiff-base polymerization (*green square* indicates one free aldehyde as an example)

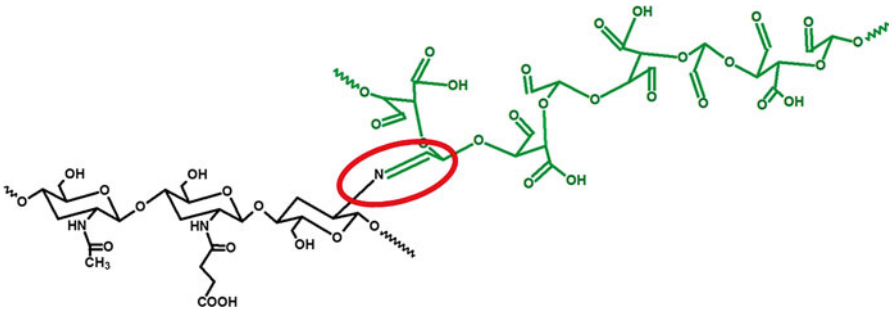

Fig. 6.5 Schiff-base formation (*red circle*) between a free amine group in sChi and a free aldehyde of oxAlg. The resulting Schiff base, or imine bond, is susceptible to hydrolysis over time. This can be tuned to coincide with matrix depositions by cells in the QuickStick microtissue

Alginate is another polysaccharide widely used for biomaterial applications owing to its inert characteristic and cytocompatibility [43]. It is composed of linear unbranched copolymer blocks of (1,4)-linked β-D-mannuronic acid and α-l-guluronic acid (Fig. 6.4c). Physical cross-linking of alginate occurs in the presence of divalent cations through interactions between carboxylic groups between two G-blocks of adjacent polysaccharide chains. The alginate structure must be slightly modified to permit its participation in Schiff-base cross-linking. This is accomplished by oxidization of the vicinal hydroxyl groups with sodium periodate [44]. The resulting oxidized alginate (oxAlg) molecule contains two free aldehyde groups per saccharide unit (Fig. 6.4d), which can cross-link with the free amino groups in sChi (Fig. 6.5).

6.3.2 QuickStick Microtissue Formation

QuickStick microtissues are formed by entrapping cells in an intercalating network of sChi and oxAlg in a rapid cross-linking reaction. Cells are suspended in sChi at a relatively high density and subsequently transferred to droplets of oxAlg (Fig. 6.6a). A covalent bond is formed between free primary amines in sChi and aldehydes in oxAlg in a 30 min Schiff-base cross-linking reaction. The cells are trapped in the hydrogel network and form a microtissue that can immediately be manipulated and transferred with fine-tipped forceps (Fig. 6.6b). Because the Schiff base (or imine bond) is unstable, the QuickStick polymers are eventually hydrolyzed over time during culture. This effect can be tuned by adjusting the reactive groups by either altering the degree of substitution of NH_2 groups in the sChi by succinic anhydride or by changing the degree of oxidation of the oxAlg. Ideally, the polymer is degraded over a time frame that coincides with synthesis and deposition of extracellular matrix by the entrapped cells that replaces the adhesive network.

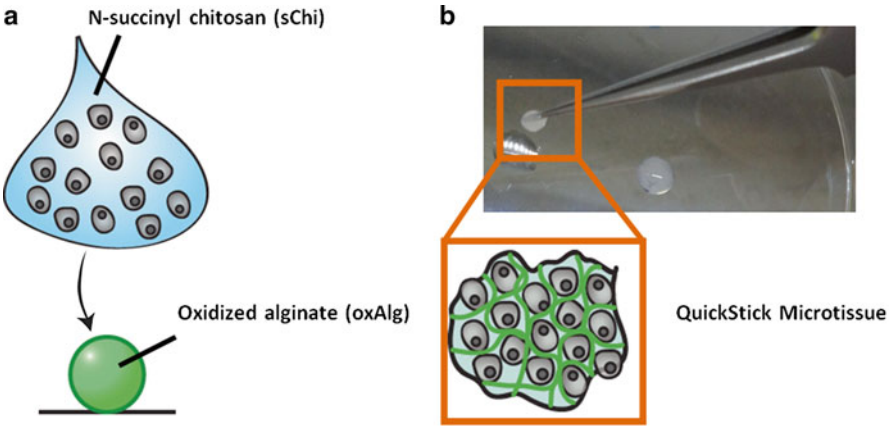

Fig. 6.6 QuickStick microtissues are formed by pipetting a droplet of sChi with high cell density in a droplet of oxAlg (**a**). After a 30 min cross-linking reaction, the microtissue is formed with an intercalating polymer structure and can immediately be handled with fine-tipped forceps (**b**)

6.3.3 QuickStick Microtissue Architecture

The initial makeup of a QuickStick microtissue is composed of the two polymers, sChi and oxAlg, along with the cells which are entrapped in their network. In order to analyze the architectural structure of such microtissues, sChi containing the fluorescent tag fluorescein isothiocyanate (sChi-FITC) was synthesized. FITC, as an isothiocyanate, readily reacts with primary amines in a slightly basic carbonate buffer to form a stable thiourea molecule. Therefore, in order to couple the fluorescent molecule to the sChi polymer backbone, Schiff-base-ready amine groups must be "given up" in the sChi-FITC synthesis. It is essential to ensure that the final sChi-FITC molecule is adequately labeled to be visualized under fluorescence while leaving as many primary amines free as possible to be available for cross-linking with the aldehyde groups of the oxAlg (Fig. 6.7a). Following a successful synthesis of a cross-linkable and fluorescently tagged sChi-FITC, QuickStick microtissues are fabricated using the labeled polymer together with oxAlg in the manner described previously. The polymer distribution is observed in microtissues that are snap frozen in OCT and processed by cryosectioning. The polymer network remains intact and the fluorescent label remains clearly visible (Fig. 6.7b) following cryosectioning. Alternatively, microtissues can be visualized in situ via confocal laser scanning microscopy (Fig. 6.7c). In both cases, it is clear that the polymer component of the microtissue architecture forms an intercalating network around cells which may temporarily isolate individual cells or individual clusters of cells from direct contact with their neighbors. Synthesis of the sChi-FITC molecule and its use in QuickStick microtissue fabrication has become a useful tool for understanding the polymer's role in the microtissue structure.

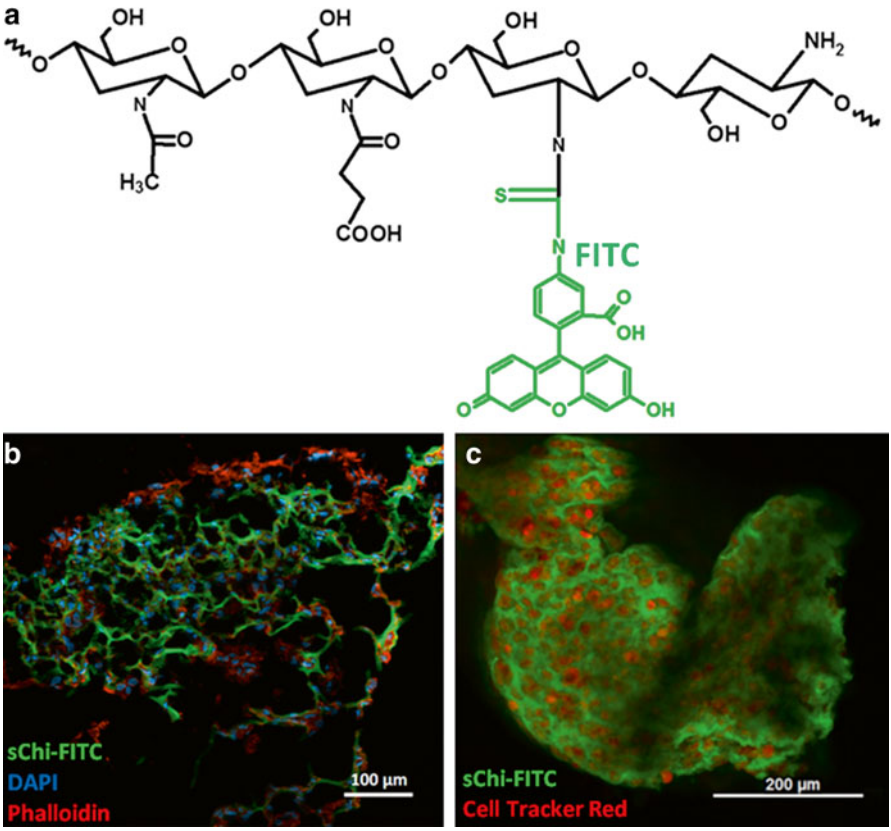

Fig. 6.7 QuickStick microtissue architecture can be visualized with a fluorescently labeled sChi-FITC. Because FITC is also grafted to the polysaccharide via amine modification, the sChi-FITC molecule must be tailored to contain sufficient FITC labeling for visualization while leaving enough free amine groups for Schiff-base cross-linking (**a**). The fluorescence is retained after QuickStick microtissue cryosectioning and staining (**b**) and can be visualized in situ via confocal laser scanning microscopy (**c**). The polymer network intercalates the cells in the QuickStick microtissue structure

6.3.4 Directing Organized Assembly of Cells into Microtissues Using the QuickStick Method

One limitation of self-organizing microtissue structures is the lack of spatial control for cell distribution in the final construct, which severely limits their versatility for use in experiments involving multiple cell types. The majority of tissues in the body are composed of different cell types whose interaction with one another is fundamental for the tissue's function. Co-culture studies offer researchers the ability to probe the relationship between different types of cells. Utilizing the QuickStick

method for microtissue formation, different populations of cells can readily be organized in 3D during seeding of the microtissue. In proof of concept experiments, we separated two populations of human bone marrow stem cells (hMSCs) and labeled them with cell tracker red and cell tracker green molecules, respectively. Cells from each population were again suspended at a high density of 20×10^6 cells/mL in sChi, and 5 μL oxAlg spots were made on a slightly hydrophobic surface. Simply by sequentially pipetting from the different cell solutions, it was possible to create microtissues demonstrating a high level of organization for the two cell populations. The cross-linking is rapid enough to retain one population of cells and yet slow enough to allow interactions between the two cell types at the interface of their populations (Fig. 6.8).

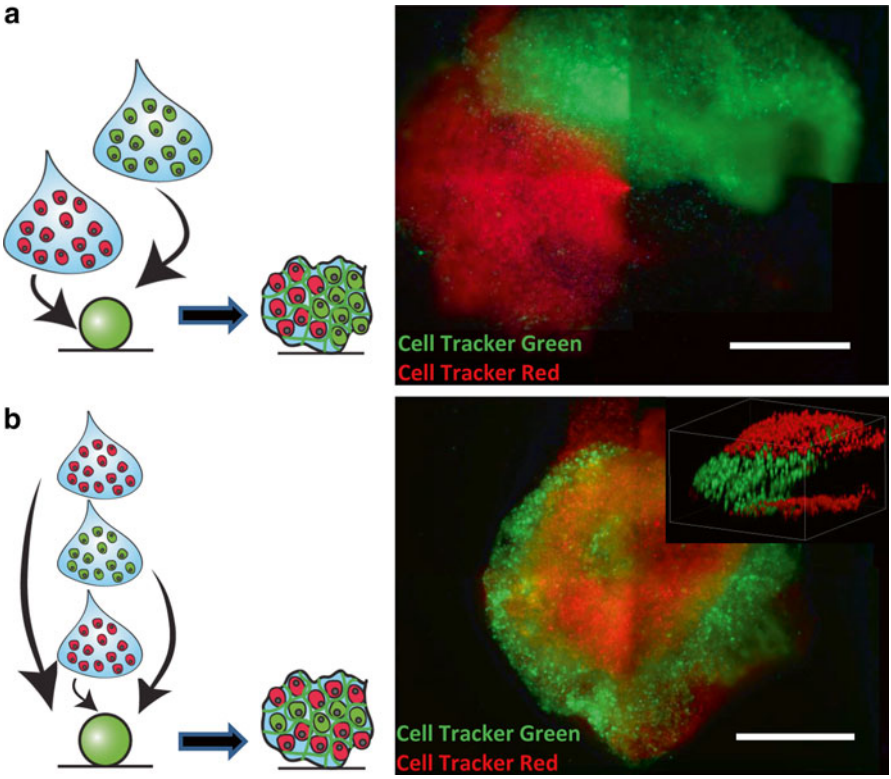

Fig. 6.8 Organized 3D assembly of QuickStick microtissues. Different cell populations were labeled with cell tracker *red* or cell tracker *green*. By pipetting the sChi droplets containing cells of the different populations in a sequential manner, microtissues could be formed with distinct spatial organizations of the two cell populations. Proof of concept experiments were performed with hMSCs using two successive droplets (**a**) or three successive droplets of *red*, then *green*, and then *red* labeled cells (**b**). QuickStick microtissues were imaged just 30 min after seeding and maximum intensity projections through a Z-stack are depicted (**a**, **b** *right*, scale = 500 μm) and 3D projection of the 1-1-1 microtissue is included (**b**, *right*, insert, scale = 1 × 1 mm × 500 μm)

6.3.5 *QuickSticks for Tissue Engineering: Cartilaginous Microtissues*

Chondrogenesis of MSCs is initiated in vivo by cellular condensation. In vitro chondrogenic induction of MSCs is typically carried out by centrifuging cells and culturing them as micromass pellets in defined chondrogenic media. MSC condensations can be engineered in vitro using Schiff linkages by first suspending cells in a solution with amino-containing sChi and pipetting these cells into a droplet of a solution of aldehyde containing oxidized alginate (oxAlg) (Fig. 6.9).

Bone marrow-derived hMSCs were cultured as centrifuged pellets or QuickStick microtissues for 21 days in chondrogenic induction media and then snap frozen for cryosectioning. Alcian blue histological stain shows deposition of GAGs, a component of native tissue architecture vital to the tissue's ability to withstand high compressive loads. Alcian blue staining was compared between centrifuged pellets and QuickStick microtissue taking a cartilage biopsy for reference. The cartilage biopsy shows even GAG distribution and cells (counterstained with nuclear fast red) dispersed and isolated throughout the tissue. The histology of the centrifuged pellet shows very little staining for GAGs, and cells remain very densely packed. In the QuickStick microtissue, cells appear evenly dispersed within the microtissue and the GAG deposition is much more similar to native tissue.

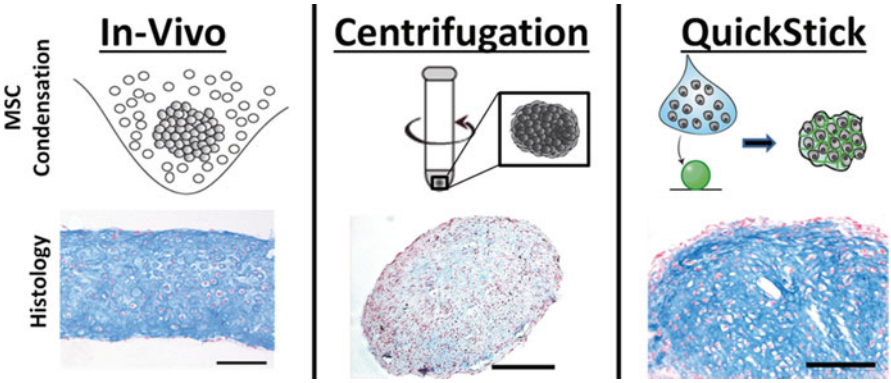

Fig. 6.9 Application of QuickStick microtissues to cartilage tissue engineering. MSC condensation is the first step towards chondrogenesis in vivo. This is often mimicked in vitro by centrifugation and culture of cells in a micromass pellet. Glycosaminoglycans (*GAGs*) are a critical component of the cartilage extracellular matrix, responsible for retaining water in the tissue and providing resistance to compressive loads. Histological staining for GAGs by Alcian blue and cell nuclei counterstained with nuclear fast red of the cartilage biopsy (*bottom left*) shows an even GAG distribution and cells dispersed as single cells throughout the tissue. The histology of the centrifuged pellet (*bottom middle*) shows very little staining for GAGs, but in the QuickStick microtissue GAG deposition bears striking similarity to native tissue (*bottom right*). Scale = 250 μm

Acknowledgments Work was funded by the Swiss National Science Foundation (CR32I3-146338/1), the European Union Seventh Framework Programme (FP7/2007–2013) under grant agreement n^0 NMP4-SL-2009-229292, and an AO Foundation startup grant (S-11-60Z).

References

1. Larsen WJ, Sherman LS, Potter SS, Scott WJ (2001) Human embryology. Churchill Livingstone, Philadelphia
2. Holtzer H (1964) Control of chondrogenesis in the embryo. Biophys J 4:239–250
3. Battler A, Leor J (2007) Stem cell and gene-based therapy: frontiers in regenerative medicine. Springer, New York
4. Carlson BM (2011) Principles of regenerative biology. Elsevier, Amsterdam
5. Studer D, Millan C, Ozturk E, Maniura-Weber K, Zenobi-Wong M (2012) Molecular and biophysical mechanisms regulating hypertrophic differentiation in chondrocytes and mesenchymal stem cells. Eur Cell Mater 24:118–135
6. Hall BK, Miyake T (1995) Divide, accumulate, differentiate: cell condensation in skeletal development revisited. Int J Dev Biol 39:881–894
7. Cancedda R, Castagnola P, Cancedda F, Dozin B, Quarto R (2000) Developmental control of chondrogenesis and osteogenesis. Int J Dev Biol 44:707–714
8. Oberlender SA, Tuan RS (1994) Expression and functional involvement of N-cadherin in embryonic limb chondrogenesis. Development 120:177–187
9. Ichinose S, Tagami M, Muneta T, Sekiya I (2005) Morphological examination during in vitro cartilage formation by human mesenchymal stem cells. Cell Tissue Res 322:217–226
10. Underhill C, Dorfman A (1978) The role of hyaluronic acid in intercellular adhesion of cultured mouse cells. Exp Cell Res 117:155–164
11. Underhill C (1992) CD44: the hyaluronan receptor. J Cell Sci 103:293–298
12. Vortkamp A, Lee K, Lanske B, Segre GV, Kronenberg HM, Tabin CJ (1996) Regulation of rate of cartilage differentiation by Indian hedgehog and PTH-related protein. Science 273:613–622
13. Lanske B, Karaplis AC, Lee K, Luz A, Vortkamp A, Pirro A et al (1996) PTH/PTHrP receptor in early development and Indian hedgehog–regulated bone growth. Science 273:663–666
14. Johnstone B, Hering T, Caplan A, Goldberg V, Yoo J (1998) In vitro chondrogenesis of bone marrow-derived mesenchymal progenitor cells. Exp Cell Res 238:265
15. Moscona A (1961) Rotation-mediated histogenetic aggregation of dissociated cells: a quantifiable approach to cell interactions in vitro. Exp Cell Res 22:455–475
16. Foty R, Steinberg M (2005) The differential adhesion hypothesis: a direct evaluation. Dev Biol 278:255
17. Shacoori V, Khan N, Saiag B, Rault B (1995) Rat pineal cell aggregates: ultrastructural and functional characteristics. Brain Res Bull 38:215–220
18. Cameron C, Hu WS, Kaufman DS (2006) Improved development of human embryonic stem cell-derived embryoid bodies by stirred vessel cultivation. Biotechnol Bioeng 94:938–948
19. Yoon BS, Yoo SJ, Lee JE, You S, Lee HT, Yoon HS (2006) Enhanced differentiation of human embryonic stem cells into cardiomyocytes by combining hanging drop culture and 5-azacytidine treatment. Differentiation 74:149–159
20. Itskovitz-Eldor J, Schuldiner M, Karsenti D, Eden A, Yanuka O, Amit M et al (2000) Differentiation of human embryonic stem cells into embryoid bodies comprising the three embryonic germ layers. Mol Med 6:88–95
21. Spence JR, Mayhew CN, Rankin SA, Kuhar MF, Vallance JE, Tolle K et al (2010) Directed differentiation of human pluripotent stem cells into intestinal tissue in vitro. Nature 470:105–109
22. D'Amour KA, Agulnick AD, Eliazer S, Kelly OG, Kroon E, Baetge EE (2005) Efficient differentiation of human embryonic stem cells to definitive endoderm. Nat Biotechnol 23:1534–1541

23. Kroon E, Martinson LA, Kadoya K, Bang AG, Kelly OG, Eliazer S et al (2008) Pancreatic endoderm derived from human embryonic stem cells generates glucose-responsive insulin-secreting cells in vivo. Nat Biotechnol 26:443–452
24. Rambhatla L, Chiu C-P, Kundu P, Peng Y, Carpenter MK (2003) Generation of hepatocyte-like cells from human embryonic stem cells. Cell Transplant 12:1–11
25. Lancaster MA, Renner M, Martin C-A, Wenzel D, Bicknell LS, Hurles ME et al (2013) Cerebral organoids model human brain development and microcephaly. Nature 501:373–379
26. Yu J, Vodyanik MA, Smuga-Otto K, Antosiewicz-Bourget J, Frane JL, Tian S et al (2007) Induced pluripotent stem cell lines derived from human somatic cells. Science 318:1917–1920
27. Takahashi K, Yamanaka S (2006) Induction of pluripotent stem cells from mouse embryonic and adult fibroblast cultures by defined factors. Cell 126:663–676
28. Kelm J, Timmins N, Brown C, Fussenegger M, Nielsen L (2003) Method for generation of homogeneous multicellular tumor spheroids applicable to a wide variety of cell types. Biotechnol Bioeng 83:173
29. Rimann M, Graf-Hausner U (2012) Synthetic 3D multicellular systems for drug development. Curr Opin Biotechnol 23:803–809
30. Gartner ZJ, Bertozzi CR (2009) Programmed assembly of 3-dimensional microtissues with defined cellular connectivity. Proc Natl Acad Sci U S A 106:4606–4610
31. Nishiguchi A, Yoshida H, Matsusaki M, Akashi M (2011) Rapid construction of three-dimensional multilayered tissues with endothelial tube networks by the cell-accumulation technique. Adv Mater 23:3506–3510
32. Jakab K, Norotte C, Marga F, Murphy K, Vunjak-Novakovic G, Forgacs G (2010) Tissue engineering by self-assembly and bio-printing of living cells. Biofabrication 2:022001
33. Bratt-Leal AM, Kepple KL, Carpenedo RL, Cooke MT, McDevitt TC (2011) Magnetic manipulation and spatial patterning of multi-cellular stem cell aggregates. Integr Biol 3:1224–1232
34. Zamanian B, Masaeli M, Nichol JW, Khabiry M, Hancock MJ, Bae H et al (2010) Interface-directed self-assembly of cell-laden microgels. Small 6:937–944
35. Fernandez JG, Khademhosseini A (2010) Micro-masonry: construction of 3D structures by microscale self-assembly. Adv Mater 22:2538–2541
36. Tan H, Chu CR, Payne K, Marra KG (2009) Injectable in situ forming biodegradable chitosan-hyaluronic acid based hydrogels for cartilage tissue engineering. Biomaterials 30:2499
37. Wang D-A, Varghese S, Sharma B, Strehin I, Fermanian S, Gorham J et al (2007) Multifunctional chondroitin sulphate for cartilage tissue–biomaterial integration. Nat Mater 6:385–392
38. Bhattacharjee M, Miot S, Gorecka A, Singha K, Loparic M, Dickinson S et al (2012) Oriented lamellar silk fibrous scaffolds to drive cartilage matrix orientation: towards annulus fibrosus tissue engineering. Acta Biomater 8:3313–3325
39. Pescosolido L, Piro T, Vermonden T, Coviello T, Alhaique F, Hennink WE et al (2011) Biodegradable IPNs based on oxidized alginate and dextran-HEMA for controlled release of proteins. Carbohydr Polym 86:208–213
40. Francis Suh JK, Matthew HWT (2000) Application of chitosan-based polysaccharide biomaterials in cartilage tissue engineering: a review. Biomaterials 21:2589–2598
41. Xi Lu J, Prudhommeaux F, Meunier A, Sedel L, Guillemin G (1999) Effects of chitosan on rat knee cartilages. Biomaterials 20:1937–1944
42. Kato Y, Onishi H, Machida Y (2004) N-succinyl-chitosan as a drug carrier: water-insoluble and water-soluble conjugates. Biomaterials 25:907–915
43. Augst AD, Kong HJ, Mooney DJ (2006) Alginate hydrogels as biomaterials. Macromol Biosci 6:623–633
44. Li X, Kong X, Zhang Z, Nan K, Li LL, Wang XH et al (2012) Cytotoxicity and biocompatibility evaluation of N,O-carboxymethyl chitosan/oxidized alginate hydrogel for drug delivery application. Int J Biol Macromol 50:1299–1305

Chapter 7
Hepatic Differentiation of Human Embryonic Stem Cells and Induced Pluripotent Stem Cells by Two- and Three-Dimensional Culture Systems In Vitro

Maiko Higuchi and Hiroyuki Mizuguchi

Abstract Hepatocytes differentiated from human embryonic stem cells (hESCs) or induced pluripotent stem cells (hiPSCs) have a wide range of potential applications in biomedical research, drug discovery, and the treatment of liver disease. In this review, we provide an up-to-date overview of the wide variety of hepatic differentiation protocols. Moreover, we discuss the application of these protocols to three-dimensional culture systems in an attempt to induce hepatocyte-like cells with high hepatic functions.

Keywords Differentiation • ES cells • Hepatocytes • iPS cells • Three-dimensional culture

7.1 Hepatocytes in Cell-Based Therapy and Drug Discovery

The incidence of liver disease such as viral hepatitis, autoimmune hepatic disorders, fatty liver disease, and hepatic carcinoma is increasing worldwide [1]. Although the optimal treatment for end-stage liver disease is orthotopic liver transplantation, the

M. Higuchi
Laboratory of Biochemistry and Molecular Biology, Graduate School of Pharmaceutical Sciences, Osaka University, Osaka 565-0871, Japan

H. Mizuguchi (✉)
Laboratory of Biochemistry and Molecular Biology, Graduate School of Pharmaceutical Sciences, Osaka University, Osaka 565-0871, Japan

Laboratory of Hepatocyte Differentiation, National Institute of Biomedical Innovation, Osaka 567-0085, Japan

The Center for Advanced Medical Engineering and Informatics, Osaka University, Osaka 565-0871, Japan

iPS Cell-Based Research Project on Hepatic Toxicity and Metabolism, Graduate School of Pharmaceutical Sciences, Osaka University, Osaka 565-0871, Japan
e-mail: mizuguch@phs.osaka-u.ac.jp

M. Akashi et al. (eds.), *Engineered Cell Manipulation for Biomedical Application*, Nanomedicine and Nanotoxicology,
DOI 10.1007/978-4-431-55139-3_7

major limitation of such treatment is the shortage of donor livers. The liver is composed of several types of cells, including hepatocytes, endothelial cells, Kupffer cells, stellate cells, and hematopoietic cells. Of these cells, hepatocytes play the most important role in major liver functions. Hepatocytes have many functions, including carbohydrate metabolism, glycogen storage, lipid metabolism, urea synthesis, drug detoxification, production of plasma proteins, and destruction of erythrocytes [2]. Therefore, the transplantation of hepatocytes has been considered an effective treatment alternative to orthotopic liver transplantation [3]. However, such a treatment requires an unlimited source of hepatocytes. Hepatocytes are useful for not only regenerative medicine but biomedical research and drug discovery. They are particularly useful for drug screenings, such as for the determination of metabolic and toxicological properties of drug compounds in in vitro models. Primary human hepatocytes are the current standard in vitro model, but isolated hepatocytes lose their functions rapidly even under optimized culture conditions [4, 5]. The use of human hepatocytes is limited by the scarcity of primary tissue from healthy donors. Donor-to-donor and batch-to-batch variations are also significant problems. Moreover, human hepatocytes can no longer proliferate in in vitro culture [6]. These are crucial issues for various applications, and new and unlimited sources of human hepatocytes are urgently required to address them.

7.2 Hepatic Differentiation of hESCs/hiPSCs in Two-Dimensional Culture

hESCs and hiPSCs could be established as promising new resources for obtaining human hepatocytes. Abe et al. [7] and Levinson-Dushnik et al. [8] demonstrated that mouse ESCs (mESCs) were capable of differentiating into endodermal cells. Hamasaki et al. [9] reported that hepatocyte-like cells were induced from mESCs by using humoral factors. Rambhatla et al. demonstrated the differentiation of hESCs into hepatocyte-like cells for the first time [10]. Since then, many studies have been initiated to enhance the hepatic differentiation efficiency and the functional qualities of the hepatocyte-like cells [11–16].

Hepatic differentiation from hiPSCs has been achieved using similar protocols as for hESCs [17–20]. iPSCs were generated from somatic cells as a result of the overexpression of four reprogramming factors (Oct3/4, Sox2, Klf-4, and c-Myc) [21, 22]. Consequently, hiPSCs provide the opportunity to generate individual-specific hepatocyte-like cells. For example, drug metabolism capacity differs among individuals [23], and thus it is difficult to make a precise prediction of drug toxicity by using hepatocytes isolated from a single donor or hESC-derived hepatocytes. A hepatotoxicity screening utilizing hiPSC-derived hepatocyte-like cells would allow the investigation of individual drug metabolism capacity. Moreover, hiPSC-derived hepatocytes generated from patients suffering from a particular disease could provide a source for the disease study and disease modeling [24, 25]. These application would be expected to lead to the discovery of novel drugs.

7.2.1 *Stepwise Hepatic Differentiation from hESCs/hiPSCs*

The general strategy for hepatic differentiation from hESCs/hiPSCs is a stepwise culture with the addition of growth factors or cytokines [11, 20] (Fig. 7.1), which mimics the in vivo microenvironment during liver development [26, 27] (Fig. 7.2).

Gastrulation of the vertebrate embryo starts with the formation of three germ layers: the ectoderm, mesoderm, and endoderm. The endoderm differentiates into various organs, including the liver, pancreas, lungs, intestine, and stomach. To examine the molecular mechanisms of endoderm specification during early embryogenesis, endoderm differentiation from ESCs has been widely investigated as an in vitro model [28].

In definitive endoderm (DE) differentiation, it is well known that nodal signaling, which involves members of the transforming growth factor-β super family, plays a crucial role and induces the expression of endoderm-related genes [29]. Activin A, a member of the nodal family, is a ligand of the type II activin receptor and can transmit a downstream signal by using Smad adaptor proteins [30–32]. D'Amour et al. accomplished the differentiation of hESCs to DE by using activin A [32]. Recently, protocols using the combination of activin A with other factors such as fibroblast growth factor (FGF) 2 or Wint3a have been also applied to efficiently induce the DE [33, 34, 14].

Hepatic differentiation from the DE is divided into two steps: hepatic specification and hepatic maturation. In the hepatic specification step, the DE differentiates into hepatoblasts that express alpha-fetoprotein (AFP), transthyretin, and albumin (ALB) [35–37]. At this stage, the interaction of FGFs with bone morphogenetic

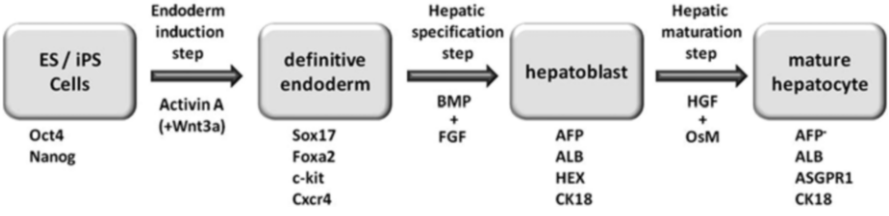

Fig. 7.1 In vitro hepatic differentiation from hESCs/hiPSCs

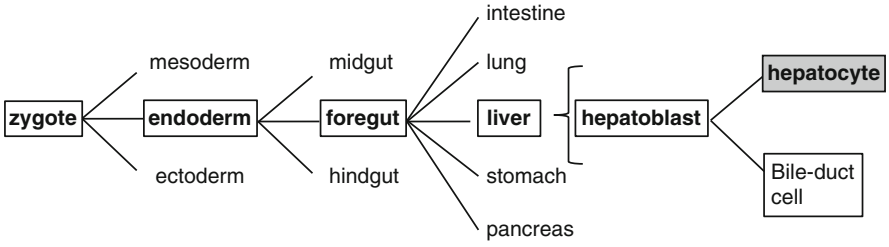

Fig. 7.2 The cell lineage steps during hepatic development

protein (BMP) 2 or BMP4 is important for the induction of hepatocyte-related genes [27, 38]. The combination of FGF4 and BMP2 promotes hepatic specification from human ESC-derived DE cells [13]. Similar results were obtained by using the combinations of aFGF and BMP4, bFGF and BMP4, or FGF4 and BMP4 [13, 33].

It is known that hepatoblasts differentiate into two distinct lineages, hepatocytes and cholangiocytes. During the fetal hepatic maturation, growth factors that are secreted by surrounding non-parenchymal liver cells, such as hepatocyte growth factor (HGF) and oncostatin M (OsM), are essential for hepatic maturation [39]. HGF enhances hepatocyte proliferation but inhibits biliary differentiation by blocking notch signaling [40]. Although HGF is widely used for inducing hepatic phenotypes (e.g., ALB and dipeptidyl peptidase IV expression) [16, 41, 42], this is not enough to induce functional mature hepatocytes [42, 43]. OsM, which is expressed in hematopoietic cells in the fetal liver [43, 44], promotes the hepatic differentiation from hepatoblast cells [39, 40, 45]. Furthermore, supplementation of the culture medium with dexamethasone, a glucocorticoid hormone, induces the production of mature hepatocyte-specific proteins and also supports the maturation process of the hepatocytes together with OsM [14, 15, 18].

7.2.2 Hepatic Differentiation from hESCs/hiPSCs by Transduction of Hepatic Lineage-Specific Transcription Factors

DE differentiation methods using growth factors are useful strategies for generating a DE with the ability to differentiate into hepatic or pancreatic lineages; however, these methods are not sufficient for generation of homogenous DE populations [46, 47]. To improve the efficiency of DE differentiation, several groups have attempted the modulation of expression levels in endoderm-related transcription factors. It has been demonstrated that overexpression of SOX17, which is an integral transcription factor for DE formation, promotes DE differentiation, resulting in an efficiency of DE differentiation of over 80 % based on the estimation of c-KIT/CXCR4 double-positive cells [47, 48]. The FOXA2 transcription factor also functions as a crucial regulator of the initial intracellular signaling pathways in DE differentiation [49, 50]. Overexpression of FOXA2 also enhances the efficiency of DE differentiation [51–53].

Several studies have demonstrated that, in the hepatic lineage specification stage, homogeneous hepatoblast populations can be generated by modulating the expression levels of hepatocyte-lineage-specific transcription factors as in the DE differentiation stage. Overexpression of HEX, which is an integral transcription factor for hepatic specification, has been shown to promote hepatic specification, resulting in enhanced expression levels of ALB and AFP in the HEX-transduced cells [54–56].

To generate functional hepatocyte-like cells which have characteristics similar to primary human hepatocytes, transduction of HNF4α genes, which are central regulators of liver development, in hESC-/hiPSC-derived hepatoblasts has been shown to successfully induce mature hepatocyte-like cells that have characteristics similar to

primary human hepatocytes [57]. Furthermore, the combination of overexpression of FOXA2 and HNF1α also could effectively induce mature hepatocyte-like cells [52]. The transduction of differentiation-related genes into hESCs/hiPSCs would be a powerful strategy to generate mature hepatocyte-like cells.

7.2.3 Hepatic Differentiation from hESCs/hiPSCs by a Co-culture System

In order to facilitate maturation of the hESC-/hiPSC-derived hepatocyte-like cells and to enhance the efficiency of hepatic differentiation, development of a differentiation system that more closely mimics progenitor development in vivo will be needed. The normal culture conditions of hepatocytes in vitro differ substantially from the environment in vivo. Cell–cell interactions are important in embryogenesis and organogenesis. In particular, heterotypic cell–cell interactions in the liver, such as interactions of parenchymal cells with non-parenchymal cells, play a fundamental role in liver function [58, 59]. Moreover, it is known that cell–cell interactions between the embryonic cardiac mesoderm and definitive endoderm are essential for liver development [60]. Transcription factors that are critical for hepatic development have been identified from these cell–cell interactions [60]. ES cells co-cultured with cardiac mesoderm showed spontaneous differentiation into hepatocyte-like cells [61]. It seems that the growth factors, including FGF and BMP, secreted from the cardiac mesoderm facilitate differentiation into hepatocyte-like cells. These results suggest that the combined differentiation methods, such as addition of soluble factors into the culture medium, transduction of differentiation-related genes, or co-cultivation with other lineage cells, may further enhance the differentiation and maturation efficiency of hepatocyte-like cells.

7.3 Hepatic Differentiation of hESCs/hiPSCs in Three-Dimensional Culture

Recently, numerous three-dimensional (3D) culture methods have been reported. Among these, the spheroid culture methods, which include the hanging-drop method and the float-culture method using culture dishes coated with non-adherent polymer, have been widely used to culture primary hepatocytes in vitro [62, 63] (Fig. 7.3). Spheroid culture methods allow better maintenance of the liver function of primary hepatocytes compared to two-dimensional (2D) culture [64, 65]. Moreover, various micro-patterned substrates, employing both surface engineering and synthetic polymer chemistry for utilizing spheroid culture, have been reported [66, 67] (Fig. 7.3). One of these technologies uses a nanopillar plate with an arrayed μm-scale hole structure at the bottom of each well and nanopillars that are aligned at the bottom of the respective holes. The seeded cells evenly drop into the holes,

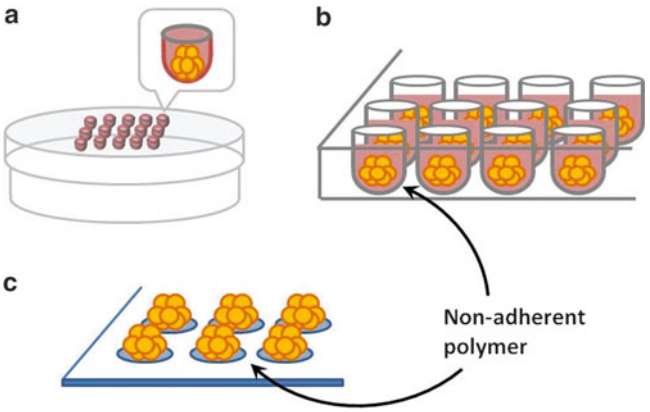

Fig. 7.3 The various spheroid culture methods: (**a**) the hanging-drop method, (**b**) the float-spheroid culture method using culture plate coated with non-adherent polymer, and (**c**) the spheroid culture method on micro-patterned plate

then migrate and aggregate on the top surface of the nanopillars, and thereby tend to form uniform spheroids in each hole. 3D spheroid culture systems using a nanopillar plate of hepatocyte-like cells have been used to promote hepatocyte maturation [68].

As a large-scale culture system of primary hepatocytes, the bioreactor methods have been used. By employing various optimized conditions, including flow conditions [69] and cell densities [70], the bioreactor method has been shown to have advantages for maintaining the functions of primary hepatocytes in vitro in comparison with 2D culture [71, 72] and also for achieving effects of spontaneous differentiation from hESCs into hepatocytes [73]. It has been reported that 3D culture using a bioreactor induces more functional hepatocyte-like cells differentiated from hESCs than in the case of 2D culture [73]. The 3D culture methods using polymer scaffold systems have also demonstrated effectiveness both in culturing primary hepatocytes [74, 75] and in differentiation from ESCs into hepatocyte-like cells in vitro [76–78]. These data showed that hepatocyte-like cells could be differentiated from hESCs on a polymer scaffold.

Furthermore, cell-sheet engineering has recently been reported [79, 80]. Cell-sheet culture was performed by using a culture dish coated with a temperature-responsive polymer, poly (*N*-isopropylacrylamide) [81–83]. Several groups have adopted culture methods with a combination of 3D culture and co-culture (3D co-culture) and showed that the liver function of primary hepatocytes could be maintained at a higher level and for longer than without the coculture conditions [84–86]. Furthermore, the hepatic maturation of hESC-/hiPSC-derived hepatocyte-like cells by stratification of a Swiss 3T3 cell sheet using cell-sheet engineering was demonstrated. The hESC-/hiPSC-derived hepatocyte-like cells in the 3D co-culture system showed significantly up-regulated ALB expression in comparison with the case of 2D culture [87]. A 3D co-culture system would be expected to enhance the degree of maturation compared with a 2D culture.

In the last decade, the hepatic differentiation from hESCs/hiPSCs has been subjected to numerous challenges. Many groups have been struggling to develop the best differentiation protocols from hESCs/hiPSCs to hepatocyte-like cells. The hepatic differentiation efficiency, which is the population of ALB-positive cells, of over 80 % has been achieved in vitro from hESCs/hiPSCs. However, several hepatic functions, including expression levels of cytochrome P450 enzyme, of hESCs-/hiPSCs-derived hepatocyte-like cells are still lower than freshly isolated hepatocytes. New approaches that generate more effective and more functional hepatocyte-like cells may be developed in the near future. The hESC-/hiPSC-derived hepatocyte-like cells are expected to be a useful source of cells not only for drug discovery but also for the treatment of liver disease in the future medicine.

References

1. Yang JD, Roberts LR (2010) Hepatocellular carcinoma: a global view. Nat Rev Gastro Hepatol 7:448–458
2. Michalopoulos GK, Defrances MC (1997) Liver regeneration. Science 276:60–66
3. Ito M, Nakata H, Miyagawa S, Fox IJ (2009) Review of hepatocyte transplantation. J Hepatol Panc Surg 16:97–100
4. Hewitt NJ, Lecho MJ, Houston JB, Hallifax D, Brown HS, Maurel P, Kenna JG, Gustavsson L, Lohmann C, Skonberg C, Gullouzo A, Tuschl G, Li AP, LeCluyse E, Groothuis GM, Hengstler JG (2007) Primary hepatocytes: current understanding of the regulation of metabolic enzymes and transporter proteins, and pharmaceutical practice for the use of hepatocytes in metabolism, enzyme induction, transporter, clearance, and hepatotoxicity studies. Drug Metab Rev 39:159–234
5. LeCluyse EL, Alexandre E, Hamilton GA, Viollon-Abadie C, Coon DJ, Jolley S, Richert L (2005) Isolation and culture of primary human hepatocytes. Methods Mol Biol 290:207–229
6. Safinia N, Minger SL (2009) Generation of hepatocytes from human embryonic stem cells. Methods Mol Biol 481:169–180
7. Abe K, Niwa H, Iwase K, Taniguchi M, Mori M, Abe S, Abe K, Yamamura K (1996) Endoderm-specific gene expression in embryonic stem cells. Exp Cell Res 229:27–34
8. Levinson-Dushnik M, Benvensty N (1997) Involvement of hepatocyte nuclear factor 3 in endoderm differentiation of embryonic stem cells. Mol Cell Biol 17:3817–3822
9. Hamazaki T, Iiboshi Y, Oka M, Papst PJ, Meacham AM, Zon LI, Terada N (2001) Hepatic maturation in differentiating embryonic stem cells in vitro. FEBS Lett 497:15–19
10. Rambhetla L, Chiu CP, Kundu P, Peng Y, Carpenter MK (2003) Generation of hepatocyte-like cells from human embryonic stem cells. Cell Transplant 12:1–11
11. Lavon N, Yanuka O, Benvenisty N (2004) Differentiation and isolation of hepatic-like cells from human embryonic stem cells. Differentiation 72:230–238
12. Shirahashi H, Wu J, Yamamoto N, Catana A, Wege H, Wager B, Okita K, Zern MA (2004) Differentiation of human and mouse embryonic stem cells along a hepatocyte lineage. Cell Transplant 13:197–211
13. Cai J, Zhao Y, Liu Y, Ye F, Song Z, Meng S, Chen Y, Zhou R, Song X, Guo Y, Ding M, Deng H (2007) Directed differentiation of human embryonic stem cells into functional hepatic cells. Hepatology 45:1229–1239
14. Hay DC, Fletcher J, Payne C, Terrace JD, Gallagher RC, Snoeys J, Black JR, Wojtacha D, Samuel K, Hannoun Z, Pryde A, Filippi C, Currie IS, Forbes SJ, Ross JA, Newsome PN, Iredale JP (2008) Highly efficient differentiation of hESCs to functional hepatic endoderm requires ActivinA and Wnt3a signaling. Proc Natl Acad Sci USA 105:12301–12306

15. Agarwal S, Holton KL, Lanza R (2008) Efficient differentiation of functional hepatocytes from human embryonic stem cells. Stem Cells 26:1117–1127
16. Duan Y, Ma X, Zou W, Wang C, Bahbahan IS, Ahuja TP, Tolstikov V, Zern MA (2010) Differentiation and characterization of metabolically functioning hepatocytes from human embryonic stem cells. Stem Cells 28:674–686
17. Si-Tayeb K, Noto FK, Nagaoka M, Li J, Battle MA, Duris C, North PE, Dalton S, Duncan SA (2010) Highly efficient generation of human hepatocyte-like cells from induced pluripotent stem cells. Hepatology 51:297–305
18. Song Z, Cai J, Liu Y, Zhao D, Yong J, Duo S, Song X, Guo Y, Zhao Y, Qin H, Yin X, Wu C, Che J, Lu S, Ding M, Deng H (2009) Efficient generation of hepatocyte-like cells from human induced pluripotent stem cells. Cell Res 19:1233–1242
19. Sullivan GJ, Hay DC, Park IH, Fletcher J, Hannoun Z, Payne CM, Dalgetty D, Black JR, Ross JA, Samuel K, Wang G, Daley GQ, Lee JH, Church GM, Forbes SJ, Iredale JP, Wilmut I (2010) Generation of functional human hepatic endoderm from human induced pluripotent stem cells. Hepatology 51:329–335
20. Chen YF, Tseng CY, Wang HW, Kuo HC, Yang VW, Lee OK (2012) Rapid generation of mature hepatocyte-like cells from human induced pluripotent stem cells by an efficient three-step protocol. Hepatology 55:1193–1203
21. Takahashi K, Yamanaka S (2006) Induction of pluripotent stem cells from mouse embryonic and adult fibroblast cultures by defined factors. Cell 126:663–676
22. Takahashi K, Tanabe K, Ohnuki M, Narita M, Ichisaka T, Tomoda K, Yamanaka S (2007) Induction of pluripotent stem cells from adult human fibroblasts by defined factors. Cell 131:861–872
23. Xie HG, Kim RB, Wood AJ, Stein CM (2001) Molecular basis of ethnic differences in drug disposition and response. Annu Rev Pharmacol Toxicol 41:815–850
24. Ghodsizadeh A, Taei A, Totonchi M, Seifinejad A, Gourabi H, Pournasr B, Aghdami N, Malekzadeh R, Almadani N, Salekdeh GH, Baharvand H (2010) Generation of liver disease-specific induced pluripotent stem cells along with efficient differentiation to functional hepatocyte-like cells. Stem Cell Rev Rep 6:622–632
25. Rashid ST, Corbineau S, Hannan N, Marciniak SJ, Miranda E, Alexander G, Huang-Doran I, Griffin J, Ahrlund-Richter L, Skepper J, Semple R, Weber A, Lomas DA, Vallier L (2010) Modeling inherited metabolic disorders of the liver using human induced pluripotent stem cells. J Clin Invest 120:3127–3136
26. Kinoshita T, Miyajima A (2002) Cytokine regulation of liver development. Biochim Biophys Acta 1592:302–312
27. Zaret KS, Grompe M (2008) Generation and regeneration of cells of the liver and pancreas. Science 322:1490–1494
28. Murry CE, Keller G (2008) Differentiation of embryonic stem cells to clinically relevant populations: lessons from embryonic development. Cell 132:661–680
29. Sulzbacher S, Schroeder IS, Truong TT, Wobus AM (2009) Activin A-induced differentiation of embryonic stem cells into endoderm and pancreatic progenitors-the influence of differentiation factors and culture conditions. Stem Cell Rev 5:159–173
30. Tam PP, Kanai-Azuma M, Kanai Y (2003) Early endoderm development in vertebrates: lineage differentiation and morphogenetic function. Curr Opin Genet Dev 13:393–400
31. Chen YG, Wang Q, Lin SL, Chang CD, Chuang J, Ying SY (2006) Activin signaling and its role in regulation of cell proliferation, apoptosis, and carcinogenesis. Exp Biol Med 231:534–544
32. D'Amour KA, Agulnick AD, Eliazer S, Kelly OG, Kroon E, Baetge EE (2005) Efficient differentiation of human embryonic stem cells to definitive endoderm. Nat Biotechnol 23:1534–1541
33. Brolen G, Sivertsson L, Bjorquist P, Eriksson G, Ek M, Semb H, Johansson I, Andersson TB, Ingelman-Sundberg M, Heins N (2010) Hepatocyte-like cells derived from human embryonic stem cells specifically via definitive endoderm and a progenitor stage. J Biotechnol 145:284–294

34. Na J, Furue MK, Andrews PW (2010) Inhibition of ERK1/2 prevents neural and mesendodermal differentiation and promotes human embryonic stem cell self-renewal. Stem Cell Res 5:157–169
35. Gualdi R, Bossard P, Zheng M, Hamada Y, Coleman JR, Zaret KS (1996) Hepatic specification of the gut endoderm in vitro: cell signaling and transcriptional control. Genes Dev 10:1670–1682
36. Jung J, Zheng M, Goldfarb M, Zaret KS (1999) Initiation of mammalian liver development from endoderm by fibroblast growth factors. Science 284:1998–2003
37. Asgari S, Moslem M, Bagheri-Lankarani K, Pournasr B, Miryounesi M et al (2013) Differentiation and transplantation of human induced pluripotent stem cell-derived hepatocyte-like cells. Stem Cell Rev 9:493–504
38. Gouon-Evans V, Boussemart L, Gadue P, Nierhoff D, Koehler CI, Kubo A, Shafritz DA, Keller G (2006) BMP-4 is required for hepatic specification of mouse embryonic stem cell–derived definitive endoderm. Nat Biotechnol 24:1402–1411
39. Si-Tayeb K, Lemaigre FP, Duncan SA (2010) Organogenesis and development of the liver. Dev Cell 18:175–189
40. Snykers S, De Kock J, Rogiers V, Vanhaecke T (2009) In vitro differentiation of embryonic and adult stem cells into hepatocytes: state of the art. Stem Cells 27:577–605
41. Kumashiro Y, Teramoto K, Shimizu-Saito K, Asahina K, Teraoka H, Arii S (2005) Isolation of hepatocyte-like cells from mouse embryoid body cells. Transplant Proc 37:299–300
42. Zhou QJ, Xiang LX, Shao JZ, Hu RZ, Lu YL, Yao H, Dai LC (2007) In vitro differentiation of hepatic progenitor cells from mouse embryonic stem cells induced by sodium butyrate. J Cell Biochem 100:29–42
43. Kuai XL, Cong XQ, Li XL, Xiao SD (2003) Generation of hepatocytes from cultured mouse embryonic stem cells. Liver Transplant 9:1094–1099
44. Yoshimura A, Ichihara M, Kinjyo I, Moriyama M, Copeland NG, Gilbert DJ, Jenkins NA, Hara T, Miyajima A (1996) Mouse oncostatin M: an immediate early gene induced by multiple cytokines through the JAK-STAT5 pathway. EMBO J 15:1055–1063
45. Kamiya A, Kinoshita T, Miyajima A (2001) Oncostatin M and hepatocyte growth factor induce hepatic maturation via distinct signaling pathways. FEBS Lett 492:90–94
46. Morrison GM, Oikonomopoulou I, Migueles RP, Soneji S, Livigni A, Enver T, Brickman JM (2008) Anterior definitive endoderm from ESCs reveals a role for FGF signaling. Cell Stem Cell 3:402–415
47. Seguin CA, Draper JS, Nagy A, Rossant J (2008) Establishment of endoderm progenitors by SOX transcription factor expression in human embryonic stem cells. Cell Stem Cell 3:182–195
48. Takayama K, Inamura M, Kawabata K, Tashiro K, Katayama K et al (2011) Efficient and directive generation of two distinct endoderm lineages from human ESCs and iPSCs by differentiation stage-specific SOX17 transduction. PLoS One 6:e21780
49. Hallonet M, Kaestner KH, Martin-Parras L, Sasaki H, Betz UA et al (2002) Maintenance of the specification of the anterior definitive endoderm and forebrain depends on the axial mesendoderm: a study using HNF3beta/Foxa2 conditional mutants. Dev Biol 243:20–33
50. Gifford CA, Ziller MJ, Gu H, Trapnell C, Donaghey J, Tsankov A, Shalek AK, Kelley DR, Shishkin AA, Issner R, Zhang X, Coyne M, Fostel JL, Holmes L, Meldrim J, Guttman M, Epstein C, Park H, Kohlbacher RJ, Gnirke A, Lander ES, Bernstein BE, Meissner A (2013) Transcriptional and epigenetic dynamics during specification of human embryonic stem cells. Cell 153:1149–1163
51. Ishizaka S, Shiroi A, Kanda S, Yoshikawa M, Tsujinoue H, Kuriyama S, Hasuma T, Nakatani K, Takahashi K (2002) Development of hepatocytes from ES cells after transfection with the HNF-3beta gene. FASEB J 16:1444–1446
52. Takayama K, Inamura M, Kawabata K, Sugawara M, Kikuchi K, Higuchi M, Nagamoto Y, Watanabe H, Tashiro K, Sakurai F, Hayakawa T, Furue MK, Mizuguchi H (2012) Generation of metabolically functioning hepatocytes from human pluripotent stem cells by FOXA2 and HNF1α transduction. J Hepatol 57:628–636

53. Kanda S, Shiroi A, Ouji Y, Birumachi J, Ueda S, Fukui H, Tatsumi K, Ishizaka S, Takahashi Y, Yoshikawa M (2003) In vitro differentiation of hepatocyte-like cells from embryonic stem cells promoted by gene transfer of hepatocyte nuclear factor 3 beta. Hepatol Res 26:225–231
54. Kubo A, Kim YH, Irion S, Kasuda S, Takeuchi M, Ohashi K, Iwano M, Dohi Y, Saito Y, Snodgrass R, Keller G (2010) The homeobox gene Hex regulates hepatocyte differentiation from embryonic stem cell-derived endoderm. Hepatology 51:633–641
55. Inamura M, Kawabata K, Takayama K, Tashiro K, Sakurai F, Katayama K, Toyoda M, Akutsu H, Miyagawa Y, Okita H, Kiyokawa N, Umezawa A, Hayakawa T, Furue MK, Mizuguchi H (2011) Efficient generation of hepatoblasts from human ES cells and iPS cells by transient overexpression of homeobox gene HEX. Mol Ther 19:400–407
56. Kawabata K, Inamura M, Mizuguchi H (2012) Efficient hepatic differentiation from human iPS cells by gene transfer. Methods Mol Biol 826:115–124
57. Takayama K, Inamura M, Kawabata K, Katayama K, Higuchi M, Ashiro K, Nonaka A, Sakurai F, Hayakawa T, Furue MK, Mizuguchi H (2012) Efficient generation of functional hepatocytes from human embryonic stem cells and induced pluripotent stem cells by HNF4α transduction. Mol Ther 20:127–137
58. Bhatia SN, Balis UJ, Yamush ML, Toner M (1999) Effect of cell–cell interactions in preservation of cellular phenotype: co-cultivation of hepatocytes and non-parenchymal cells. FASEB J 134:1883–1900
59. Malik R, Selden C, Hodgson H (2002) The role of non-parenchymal cells in liver growth. Semin Cell Dev Biol 13:425–431
60. Zaret KS (2000) Liver specification and early morphology. Mech Dev 92:83–88
61. Fair JH, Cairns BA, LaPaglia M, Wang J, Meyer AA, Kim H, Hatada S, Smithies O, Pevny L (2003) Induction of hepatic differentiation in embryonic stem cells by co-culture with embryonic cardiac mesoderm. Surgery 134:189–196
62. Li AP, Colburn SM, Beck DJ (1992) A simplified method for the culturing of primary adult rat and human hepatocytes as multicellular spheroids. In Vitro Cell Dev Biol 28A:673–677
63. Tong JZ, Sarrazin S, Cassio D, Gauthier F, Alvarez F (1994) Application of spheroid culture to human hepatocytes and maintenance of their differentiation. Biol Cell 81:77–81
64. Miranda JP, Leite SB, Muller-Vieira U, Rodrigues A, Carrondo MJT, Alves PM (2009) Towards an extended functional hepatocyte in vitro culture. Tissue Eng Part C Methods 15:157–167
65. Wu F, Friend J, Remmel R, Cerra F, Hu W (1999) Enhanced cytochrome P450 1A1 activity of self assembled rat hepatocyte spheroids. Cell Transplant 8:233–246
66. Jones CN, Tuleuova N, Lee JY, Ramanculov E, Reddi AH (2009) Hepatocyte growth factor microarrays induce and maintain differentiated phenotype in primary rat hepatocytes. Biomaterials 30:3733–3741
67. Otsuka H, Hirano A, Nakasaki Y, Okano T, Horiike Y, Kataoka K (2004) Two-dimensional multiarray formation of hepatocyte spheroids on a microfabricated PEG-brush surface. Chembiochem 5:850–855
68. Takayama K, Kawabata K, Nagamoto Y, Kishimoto K, Tashiro K, Sakurai F, Tachibana M, Kanda K, Hayakawa T, Furue MK, Mizuguchi H (2013) 3D spheroid culture of hESC/hiPSC-derived hepatocyte-like cells for drug toxicity testing. Biomaterials 34:1781–1789
69. Fiegel HC, Havers J, Kneser U, Smith MK, Moeller T, Kluth D, Mooney DJ, Rogiers X, Kaufmann PM (2004) Influence of flow conditions and matrix coatings on growth and differentiation of three-dimensionally cultured rat hepatocytes. Tissue Eng 10:165–174
70. Ring A, Gerlach J, Peter G, Pazin BJ, Minervini CF, Turner ME, Thompson RL, Triolo F, Gridelli B, Miki T (2010) Hepatic maturation of human fetal hepatocytes in four-compartment three-dimensional perfusion culture. Tissue Eng Part C 16:835–845
71. Kiyota A, Matsushita T, Ueoka R (2007) Induction and high density culture of human hepatoblasts from fetal hepatocytes with suppressing transformation. Bio Pharm Bull 30:2308–2311
72. Garlach JC (1997) Long-term liver cell cultures in bioreactors and possible application for liver support. Cell Biol Toxicol 13:349–355

73. Miki T, Ring A, Gerlach J (2011) Hepatic differentiation of human embryonic stem cells is promoted by three-dimensional dynamic perfusion culture conditions. Tissue Eng Part C 17:557–568
74. Bierwolf J, Lutgehetmann M, Feng K, Erbes J, Deichmann S (2011) Primary rat hepatocyte culture on 3D nanofibrous polymer scaffolds for toxicology and pharmaceutical research. Biotech Bioeng 108:141–150
75. Baharvand H, Hashemi SM, Ashtiani SK, Farrokhi A (2006) Differentiation of human embryonic stem cells into hepatocytes in 2D and 3D culture systems in vitro. Int J Dev Biol 50:645–652
76. Liu T, Zhang S, Chen X, Li G, Wang Y (2010) Hepatic differentiation of mouse embryonic stem cells in three-dimensional polymer scaffolds. Tissue Eng Part A 16:1115–1122
77. Lee H (2003) Effect of implantation site on hepatocytes heterotopically transplanted on biodegradable polymer scaffolds. Tissue Eng 9:1227–1232
78. Matsumoto K, Mizumoto H, Nakazawa K, Ijima H, Funatsu K (2008) Differentiation of mouse embryonic stem cells in a three-dimensional culture system using polyurethane foam. J Biosci Bioeng 105:350–354
79. Yang J, Yamato M, Kohno C, Nishimoto A, Sekine H, Fukai F, Okano T (2005) Cell sheet engineering: recreating tissues without biodegradable scaffolds. Biomaterials 26:6415–6422
80. Shimizu T, Yamamoto M, Isoi Y, Akutsu T, Setomaru T, Abe K, Kikuchi A, Umezu M, Okano T (2002) Fabrication of pulsatile cardiac tissue grafts using a novel 3-dimensional cell sheet manipulation technique and temperature-responsive cell culture surfaces. Circ Res 90:e40–e48
81. Yamada N, Okano T, Sakai H, Karikusa F, Sawasaki Y (1990) Thermo-responsive polymeric surfaces; control of attachment and detachment of cultured cells. Macromol Chem Rapid Commum 11:571–576
82. Okano T, Yamada N, Sakai H, Sakurai Y (1993) A novel recovery system for cultured cells using plasma-treated polystyrene dishes grafted with poly (*N*-isopropylacrylamide). J Biomed Mater Res 27:1243–1251
83. Hirose M, Kwon OH, Yamato M, Kikuchi A, Okano T (2000) Creation of designed shape cell sheets that are noninvasively harvested and moved onto another surface. Biomacromolecules 1:377–381
84. Lu H, Chua K, Zhang P, Lim W, Ramakrishna S et al (2005) Three-dimensional co-culture of rat hepatocyte spheroids and NIH/3T3 fibroblasts enhances hepatocyte functional maintenance. Acta Biomater 1:399–410
85. Thomas RJ, Bhandari R, Barret DA, Benett AJ, Fry JR, Powe D, Thomson BJ, Shakesheff KM (2005) The effect of three-dimensional co-culture of hepatocytes and hepatic stellate cells on key hepatocyte functions in vitro. Cell Tissue Org 181:67–79
86. Xiong A, Austin TW, Lagasse E, Uchida N, Tamaki S, Bordier BB, Weissman IL, Glenn JS, Millan MT (2008) Isolation of human fetal liver progenitors and their enhanced proliferation by three-dimensional coculture with endothelial cells. Tissue Eng Part A 14:995–1006
87. Nagamoto Y, Tashiro K, Takayama K, Ohashi K, Kawabata K, Sakurai F, Tachibana M, Hayakawa T, Furue MK, Mizuguchi H (2012) Promotion of hepatic maturation of human pluripotent stem cells in 3D co-culture using type I collagen and Swiss 3T3 cell sheets. Biomaterials 33:4526–4534

Chapter 8
Reconstruction of Elastic Fibers in Three-Dimensional Smooth Muscle Cells

Utako Yokoyama and Yoshihiro Ishikawa

Abstract Proper elastic fiber formation is required to maintain sufficient blood flow and smooth muscle cell function, but elastic fiber formation is impaired with age and by health conditions including aneurysms and atherosclerosis. Despite considerable progress in the understanding of elastogenesis and degradation of elastic fibers using the planar culture system and animals with genetic modifications, it remains difficult to restore elastic fibers in diseased vessels. To further study the molecular mechanisms and the development of therapeutic strategies, a new experimental tool for vascular biology is required. Using a hierarchical cell manipulation technique, we developed three-dimensional cellular multilayers (3DCMs) that exhibited layered elastic fiber formation within 7 days of being in a static culture condition. In this vascular model, the formation of elastic fibers was disturbed by BAPN, an inhibitor of elastin cross-linking. Furthermore, gene expression profiles of smooth muscle cell phenotypic markers suggested that smooth muscle cells show more contractile phenotypes in 3DCMs than in smooth muscle cells of 2D culture. In conclusion, the 3DCMs have the potential to serve as a new vascular experimental platform in which the spatial and temporal regulation of vascular remodeling can be studied.

Keywords 3D vascular model • Elastic fiber • Smooth muscle cells

8.1 Structure and Functions of Arteries

In order to explore the molecular mechanisms of vascular elastic fiber formation and the diagnostic and therapeutic strategies for disordered elastic fiber metabolism, understanding of some of the distinctive anatomic and functional characteristics of vascular structures is required.

U. Yokoyama (✉) • Y. Ishikawa
Cardiovascular Research Institute, Yokohama City University School of Medicine,
3-9 Fukuura Kanazawaku, Yokohama City 236-0004, Japan
e-mail: utako@yokohama-cu.ac.jp

M. Akashi et al. (eds.), *Engineered Cell Manipulation for Biomedical Application*, Nanomedicine and Nanotoxicology,
DOI 10.1007/978-4-431-55139-3_8

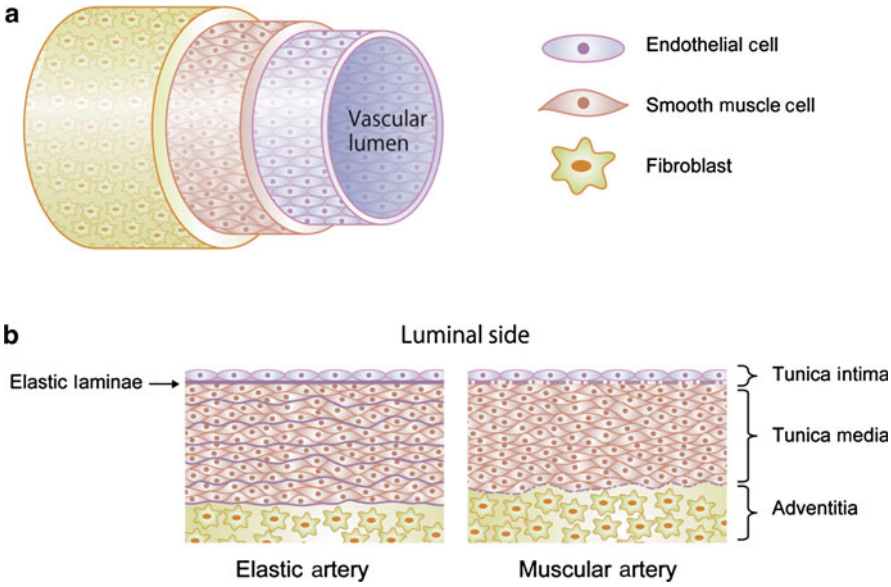

Fig. 8.1 Structure of arterial wall. (**a**) The arterial wall is composed of three concentric tunics, the tunica intima, tunica media, and tunica adventitia, divided by distinct elastic laminae. The main cellular components of these tunics are endothelial cells, SMCs, and fibroblasts. (**b**) Arteries are classified as elastic or muscular arteries based on elastic fiber content in their tunica media. Large arteries such as the aorta and pulmonary artery contain well-organized elastic fibers interpenetrating SMCs and are thus termed elastic arteries. On the other hand, relatively small arteries including the coronary artery are called muscular arteries. In muscular arteries elastic fiber is scarce and dispersed

Arteries are composed of three concentric tunics [1] as shown in Fig. 8.1a. The tunica intima forms the innermost lining, consisting of a monolayer of endothelial cells with their underlying subendothelial connective tissues. Endothelial cells regulate vascular tone, platelet activity, leukocyte adhesion, and angiogenesis by producing nitric oxide and other regulatory factors [2]. The outer limit of the tunica intima is demarcated by a longitudinally dispersed layer of elastic fibers. The tunica media is primarily composed of a dense population of concentrically organized smooth muscle cells (SMCs) and elastic fibers (Fig. 8.1b). The tunica adventitia forms the extra layer and produces the collagenous extracellular matrix (ECM) in which nerve fibers, fibroblasts, and small, thin-walled nutrient vessels known as the vasa vasorum are dispersed. The primary content of the ECM is collagen (types I and III). Under physiological conditions, the tunica media is poorly vascularized, and the inner smooth muscle layers depend largely on direct diffusion from the vessel lumen for their nutritional needs.

8.1.1 Arterial Elastic Fiber Formation

The major mechanical properties related to blood vessel function are tensile stiffness, elasticity, and compressibility [3]. Elastic fibers provide elasticity, proteoglycans contribute to compressibility, and collagen provides the tensile stiffness, contributing to resistance against rupture [4]. Elastic fibers are the largest structures in the ECM in blood vessels. Beginning with the onset of pulsatile blood flow in the developing aorta and pulmonary artery, SMCs in the vessel wall produce a complex ECM that ultimately determines the mechanical properties that are critical for proper function of the neonatal and adult vascular system [3]. As such, hemodynamics and mechanical stress are considered to be the main regulators of the formation of the vascular elastic fiber system during development [5].

In elastic arteries, such as the aorta and its largest branches, including the brachiocephalic, common carotid, subclavian, and iliac arteries, SMCs synthesize elastin and other specific molecules, which are incorporated into elastic fibers [3] and arranged into concentric rings of elastic lamellae around the arterial media (Fig. 8.1b) [4]. In large elastic arteries, condensed elastic fibers allow the artery to maintain sufficient blood pressure even during variations in hemodynamic stress. In muscular arteries, however, the elastic lamellae are poorly defined. Elastic fibers are compacted into a discrete internal elastic lamina in large arteries, while this is less obvious in muscular arteries.

8.1.2 Process of Elastic Fiber Formation

Elastin imparts the property of elasticity to tissues including blood vessels [6]. In the first process of elastic fiber assembly, soluble elastin precursors (tropoelastin) are deposited on microfibrils [3, 7]. Tropoelastins from various species share a characteristic domain arrangement of hydrophobic sequences alternating with lysine-containing cross-linking motifs [6]. The hydrophobic domains are necessary for the self-aggregation of tropoelastin via coacervation, which is thought to concentrate and align tropoelastin molecules for cross-linking [8]. They are then cross-linked by lysyl oxidase, which confers elastic properties to elastic fibers [9] (Fig. 8.2). Inactivation of the elastin or lysyl oxidase gene is known to cause structural alterations in the arterial walls, leading to cardiovascular abnormalities [3, 10].

Microfibrils, made up of fibrillins and microfibril-associated glycoproteins, are thought to serve as a scaffold that guides elastin deposition [11]. Fibulin-4 and fibulin-5 are also known to associate with elastic fibers [7, 12–15]. The deposition of fibulin-5 on microfibrils also promotes the coacervation and alignment of tropoelastins on microfibrils and facilitates the cross-linking of tropoelastin by tethering lysyl oxidase-like 1, 2, and 4 enzymes [14]. Fibulin-4 interacts with lysyl oxidase and recruits lysyl oxidase to elastin monomers as well [15].

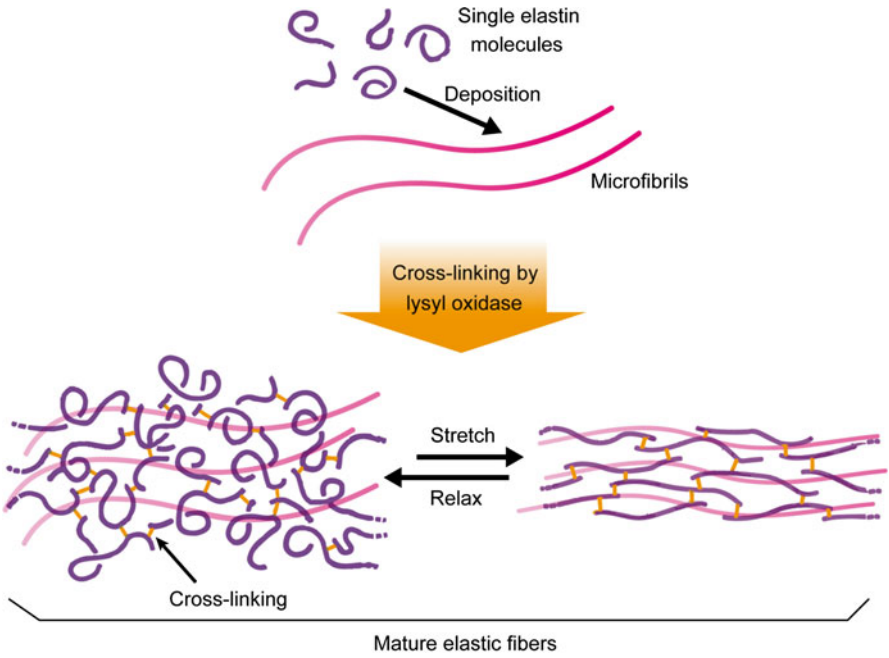

Fig. 8.2 Process of elastic fiber formation. In the process of elastic fiber assembly, tropoelastin molecules are deposited on microfibrils which are made up of fibrillins and microfibril-associated glycoproteins. After the self-aggregation of tropoelastin via coacervation, tropoelastins are then cross-linked by lysyl oxidase, which confers elastic properties to the elastic fibers

Recently, it has been reported that the fibronectin meshwork is required for the assembly of microfibrils, such as fibrillin-1 [16, 17]. Inactivation of genes encoding fibrillin-1, fibrillin-2, fibulin-4, or fibulin-5 individually has revealed that each may be dispensable for elastogenesis [3, 7, 18, 19].

8.1.3 Elastic Fiber Metabolism and Diseases

Despite recent discoveries relating to the molecular mechanisms of elastic fiber formation, vascular diseases associated with elastic fiber disorders, such as aneurysms and atherosclerosis, remain the leading cause of mortality and morbidity in the developed world [20]. No pharmacological strategy to restore the elastic fiber assemblies in diseased vessels or to inhibit the progression of elastin-related diseases is currently available.

The hallmarks of abdominal aortic aneurysms are the presence of an inflammatory infiltration within the vascular walls, which is followed by proteolytic degradation of elastic fibers and collagens [21] (Fig. 8.3). Because human aortic elastin

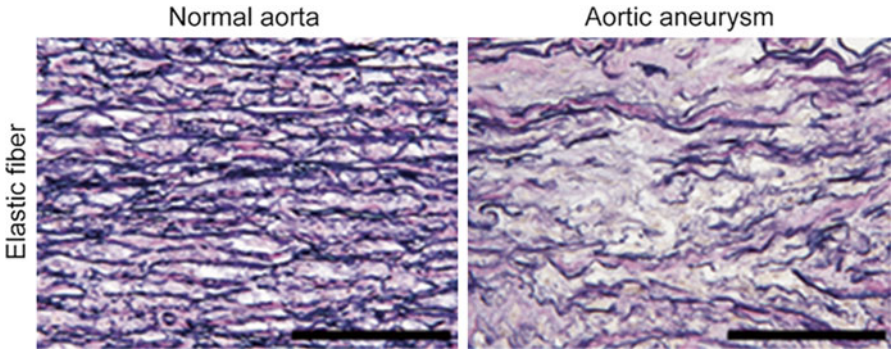

Fig. 8.3 Elastic fibers in abdominal aortic aneurysm. Elastic fibers visualized by Elastica van Gieson stain were disrupted in the tissues from patients with abdominal aortic aneurysm compared to normal aortic tissues. Scale bars: 100 μm

represents 50 % of the total dry weight of the aorta and the lamellae of elastin are important in providing the elastomeric properties of the larger arteries, promoted degradation of elastic fibers results in arterial dilation. Ultrasonographic screening studies of men over 60 years of age have shown that a small abdominal aortic aneurysm, i.e., 3–5 cm in diameter, is present in 4–5 % [22, 23]. When patients with abdominal aortic aneurysm were followed for up to 6 years, the aortic diameter had increased in 55 % of patients. The diameter of the abdominal aortic aneurysm had expanded to 6 cm in 9 % of patients, at which point the risk of rupture significantly increases [23]. After rupture occurs, the probability of mortality is greater than 60 % [24]. Although abdominal aortic aneurysms typically continue to expand, increasing the likelihood of rupture and consequent mortality, no effective pharmacological therapy to prevent the progression of abdominal aortic aneurysms is currently available.

Elastic fiber formation may be a key factor in the pathophysiology of atherosclerotic vascular remodeling. Atherosclerosis is associated with local accumulation of lipid and inflammatory cells. Areas of atherosclerotic plaque commonly show abnormality of elastic fiber formation [25]. During atherogenesis, macrophage-derived proteinases, such as matrix metalloproteinase, promote the degradation of elastic fibers, which promotes calcification through an increase of elastin polarity and elastin affinity for calcium [25]. Moreover, it has been suggested that low-density lipoproteins (LDLs) bind to elastin proteins and abnormal cholesterol deposition in vascular elastic fibers is associated with alterations in the amino acid composition of elastin and cross-linking of elastin molecules [25]. The deposition of LDLs in intima elastic fibers is also thought to promote SMC migration toward the intima. These data suggest that degradation of elastic fibers in atherosclerotic lesions contributes to the progression of atherosclerosis. In addition to the mechanical responsiveness of elastin, elastin is a potent autocrine regulator of vascular physiology and the proper regulation of vascular physiology is important for preventing pathological vascular remodeling.

8.1.4 Phenotypic Changes of Smooth Muscle Cells

SMCs exhibit diverse phenotypic states in response to the external environment and stimuli [26]. Under physiological conditions, SMCs exhibit a quiescent contractile phenotype by which they control the dilation and constriction of blood vessels to regulate blood flow. Under pathological conditions including atherosclerosis, however, they convert to a synthetic and noncontractile phenotype [27], which results in their proliferation and increased matrix production in the tunica media (Fig. 8.4).

Contractile SMCs have tightly bundled myofilaments and show extremely low proliferation rates and migration. Contractile SMCs exhibit a mature contractile apparatus, including α-smooth muscle actin (α-SMA), smooth muscle myosin heavy chains SM1 and SM2, calponin, h-caldesmon, and smoothelin [26]. On the other hand, a synthetic phenotype is correlated with SMC proliferation, with the number

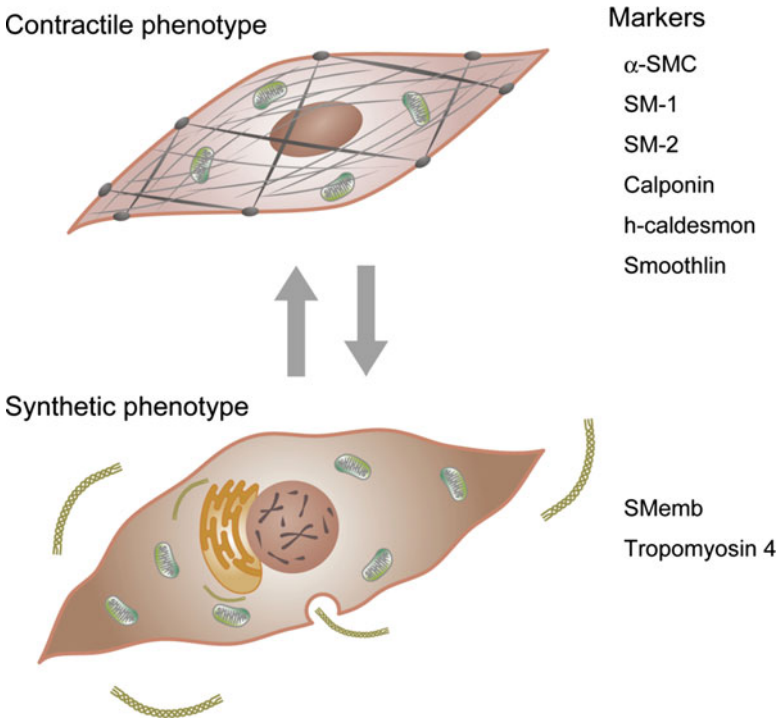

Fig. 8.4 Phenotypic changes of smooth muscle cells (*SMCs*). The phenotype continuum is modulated by various stimuli and environmental conditions. SMCs of the contractile phenotype have abundant expression of myofilament proteins and minimal rough endoplasmic reticulum and/or Golgi. Contractile SMCs show extremely low proliferation rates and migration. SMCs in pathologic conditions or in culture conditions exhibit synthetic phenotypes characterized by enhanced proliferation, migration, and ECM production

of S-phase-cultured SMCs increasing from 3–5 % to 40–60 % during primary culture and pathologies such as intimal hyperplasia [28]. There are several markers of the synthetic SMC phenotype, such as the nonmuscle myosin heavy chain (SMemb) and tropomyosin 4. These genes are known to be expressed in atherosclerotic vascular lesions [27, 29, 30]. Relative expression of these and other marker proteins can be used to localize SMCs on the contractile-synthetic continuum [28].

Interestingly, elastin expression and SMC proliferation are coupled tightly and inversely. It has been reported that elastin is expressed maximally at the G_0 and minimally at the G_2/M phase during the cell cycle [25, 31]. It has also been reported that potent inhibitors of SMC proliferation, including retinoic acid and heparin, enhance elastin expression, while stimulators of SMC proliferation, including endothelial growth factor, angiotensin II, and endothelin-1, significantly inhibit elastin expression [25, 32, 33]. These data suggest that phenotypic changes in SMCs greatly affect elastin expression and elastic fiber formation.

8.2 Three-Dimensional Cellular Multilayers: A New Experimental Model for Vascular Research

There are multiple approaches to combat and treat atherosclerosis and aortic aneurysms, including lipid-lowering pharmacological strategies and controlling blood pressure. Despite considerable progress in the understanding of elastogenesis and phenotypic changes in SMCs using the planar culture system and animals with genetic modifications, the regulation and restoration of proper elastic fiber formation and the SMC phenotype in diseased vessels are not currently possible. To obtain further insights into elastic fiber formation, we created a new experimental vascular model designed specifically for vascular elastic fiber research, in which SMC phenotypes can be also examined [34].

8.2.1 3DCMs of Vascular SMCs

Recent advances in tissue-engineered blood vessels free from synthetic scaffolds have enabled the assembly of multiple layers of SMCs and the production of elastic fiber deposition in vitro [35]. These techniques provide excellent mechanical properties for implantable vascular constructs but require an excessively long culturing time and/or an in vivo bioreactor, neither of which is practical for ex vivo experimental vascular models. Setting tissue-engineered blood vessels aside, Matsusaki et al. recently developed a hierarchical cell manipulation technique for the construction of three-dimensional cellular multilayers (3DCMs) [36]. In this technique, fibronectin-gelatin nanofilms were prepared on the surfaces of cellular layers to provide a cell-adhesive nano-scaffold to hold the next layer of cells.

The recent proteomics approach has enabled the study of comprehensive molecular interactions in elastic fiber assemblies and revealed that fibronectin and microfibril fibrillin play a central role [37]. Kinsey et al. and Sabatier et al. demonstrated that, in addition to expression, fibronectin assemblies are a prerequisite for fibrillin assembly [16, 17]. It has been noted that the fibronectin assembly and subsequent fibrillin assembly in vitro were observed within a couple of days of static culture [16, 17]. Other in vitro studies have demonstrated that fibronectin is critical for the deposition of the latent transforming growth factor β-binding protein-1 (LTBP-1), which is associated with microfibrils [38], and that the fibronectin assembly promotes lysyl oxidase activation [39]. Because the 3DCM reported by Matsusaki et al. demonstrated that pericellular fibronectin fibers were observed in 3DCMs within 24 h of culture [40], the rapid elastic fiber formation in 3DCMs is thought to be possible. On the basis of this evidence, we adopted fibronectin nanofilms placed on the surface of SMCs. These have not been used in other tissue-engineered blood vessels and 3DCMs for hierarchical cell manipulation and the rapid induction of elastic fiber formation.

8.2.2 Construction of 3DCMs

We optimized culture conditions and found that 3DCMs consisting of fibronectin-gelatin-coated neonatal rat aortic SMCs cultured in 1 % FBS/DMEM exhibited layered elastic fiber formation within 7 days of culture and that the amount of newly synthesized insoluble elastic fibers was significantly greater in 3DCMs than in 2D-SMCs cultured in the same medium [34].

Most elastic fiber proteins are expressed in the second half of development and increase throughout the early postnatal period [41]. This is followed by a decreased expression to the low levels that persist through adulthood [42]. Consistent with this in vivo evidence, it has been suggested that neonatal rat SMCs produce a greater amount of elastin and elastic fibers compared to adult rat SMCs [43, 44]. We confirmed that the mRNA expression levels of elastic fiber-related genes, such as tropoelastin, fibrillin-1, fibulin-4, fibulin-5, lysyl oxidase, and lysyl oxidase-like 1, are significantly greater in the neonatal rat aorta (1 day old) than in the adult rat aorta (4–5 months old) [34]. In our study, 3DCMs using adult human aortic SMCs did not produce elastic fibers, even if the same fibronectin coating and culture conditions were applied [34]. On the basis of these data, we used neonatal rat SMCs to fabricate 3DCMs as ex vivo vascular constructs. Construction of 3DCMs was performed as previously described [36] with some modification suitable for elastic fiber formation (Fig. 8.5) [34].

A cell disk LF (Sumitomo Bakelite, Tochigi, Japan) was rinsed with 50 mM Tris–HCl buffer solution (pH 7.4) for 15 min and coated with fibronectin (0.2 mg/ml) for 30 min at 37 °C. SMCs were cultured on the cell disk (11×10^4 cells/cm^2) and incubated for 12 h in 10 % fetal bovine serum (FBS)/Dulbecco's modified eagle

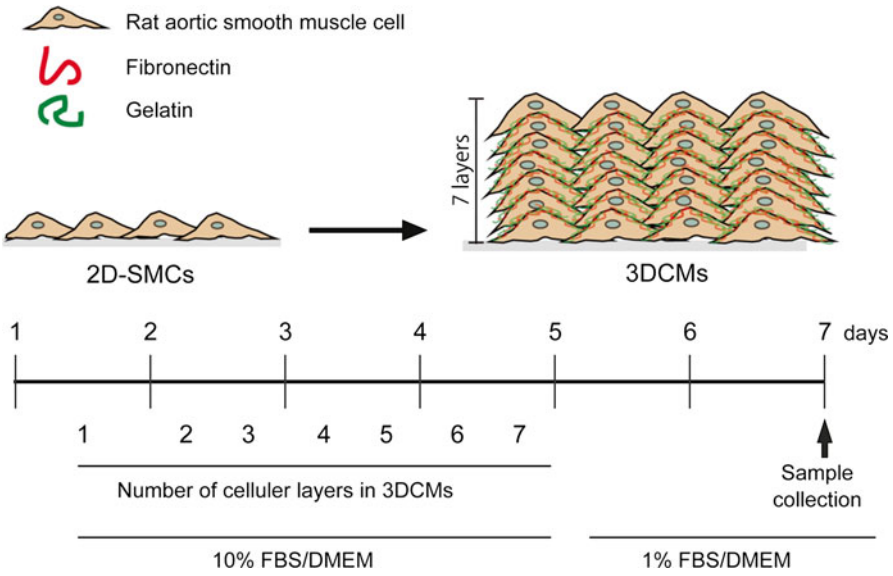

Fig. 8.5 Experimental design of 3DCM construction. Neonatal rat aortic SMCs were plated on a cell disk coated with fibronectin. Fibronectin-gelatin coating and subsequent cell seeding were repeated six times to construct seven-layered 3DCMs. After 4 days of 3DCM construction, it was incubated in 1 % FBS/DMEM for 48 h until sample collection

medium (DMEM). The monolayered SMCs were then immersed alternatively in a solution of fibronectin (0.2 mg/ml) and gelatin (0.2 mg/ml). After nine steps of layer-by-layer assembly with fibronectin and gelatin, a second cell layer was seeded on the first cell layer (11×10^4 cells/cm^2) and incubated for 6–12 h at 37 °C. The cycles of layer-by-layer nanofilm assembly and subsequent cell seeding were repeated six times in 4 days to construct seven-layered 3DCMs. During the first 4 days, the medium was refreshed daily. Twelve hours after the seeding of the last layer, the culture media was changed to 1 % FBS/DMEM. After the 3DCMs were incubated for an additional 48 h, 3DCM samples were collected (Fig. 8.6).

8.2.3 Layered Elastic Fiber Formation in 3DCM

For culture of 3DCMs, we tested four different culture media, including DMEM and DMEM F-12, because DMEM F-12 includes proline, one of the major amino acids that constitutes elastin protein, and copper, which enhances lysyl oxidase activity [45]. Contrary to expectations, viability was better in the 3DCMs cultured in DMEM than in DMEM F-12 containing either 10 % or 1 % FBS. We then compared elastic fiber formation using Elastica van Gieson stain in 3DCMs cultured in

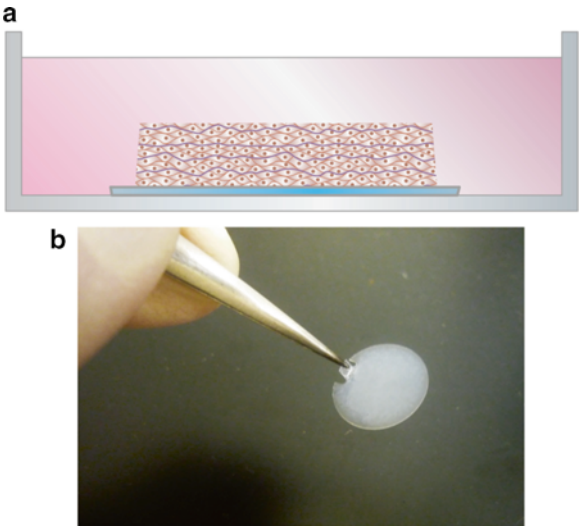

Fig. 8.6 3DCMs on the cell disk. (**a**) An illustration of 3DCMs incubated on the cell disk. (**b**) An image of 3DCMs on the cell disk at sample collection

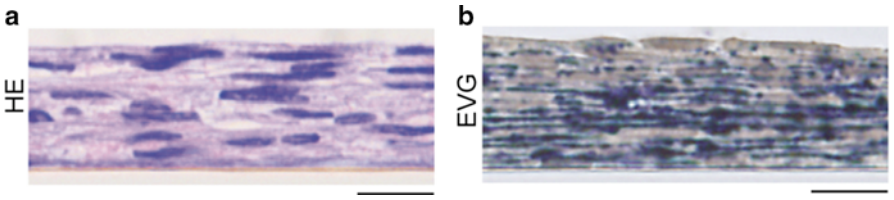

Fig. 8.7 Elastic fibers in 3DCMs. (**a**) Seven SMC layers in 3DCMs. Hematoxylin-eosin stain (*HE*). (**b**) Elastic fibers are visualized by Elastica van Gieson stain (*EVG*) in 3DCMs. Scale bars: 10 μm

DMEM containing 10 % or 1 % FBS. We found that 3DCMs cultured in 1 % FBS/DMEM exhibited layered elastic fiber formation (Fig. 8.7). Although the 3DCM culture in 10 % FBS/DMEM exhibited a certain amount of positive stain of elastic fibers, no layered elastic fiber formation was clearly detected. In 3DCMs cultured in 1 % FBS/DMEM, abundant protein expressions of tropoelastin, lysyl oxidase, fibrillin-1, and fibrillin-2 were also observed. Furthermore, the expression levels of tropoelastin and fibrillin-2 mRNAs were greater in 3DCMs cultured in 1 % FBS/DMEM than in 10 % FBS/DMEM. In accordance with previous reports, these data suggest that serum withdrawal likely induces an enhancement of the expression of tropoelastin and fibrillin-2, resulting in elastic fiber formation.

To quantify the amount of mature (i.e., cross-linked) elastic fibers in 3DCMs, we metabolically labeled newly synthesized elastin with [^{3}H]valine and measured the

incorporation of [^{3}H]valine in the NaOH-insoluble fraction of these cells, which reflects the amount of newly synthesized mature elastic fibers [12]. The 3DCMs cultured with 1 % FBS/DMEM exhibited a significant increase in the incorporation of [^{3}H]valine into the insoluble fraction compared to 2D-SMCs cultured in the same culture medium but not coated with fibronectin [34]. These data also support our belief that the pericellular fibronectin meshwork on SMCs contributes to elastic fiber assembly in 3DCMs.

These data suggest that 3DCMs consisting of rat neonatal aortic SMCs cultured in 1 % FBS/DMEM produce layered elastic fibers in vitro.

8.2.4 Characterization of SMC Phenotype in 3DCMs

Since the differentiated status of SMCs varies according to developmental stage and under pathological conditions, including atherosclerosis and vascular injury [46], an understanding of the differentiation status of SMCs in 3DCMs is important in vascular biology research. Under physiological conditions, the majority of SMCs in the medial layer of the artery are considered to be in a differentiated (contractile) state that is hardly retained in planar cell culture [47]. Since layered elastic fiber formation was achieved in 3DCMs cultured in 1 % FBS/DMEM, we further examined SMC differentiation in this culture system in comparison to the conventional planar culture of SMCs by monitoring the expression of genes for vascular smooth muscle skeletal and contractile proteins and found that vascular SMCs in 3DCMs partly regained differentiated phenotypes, but those in 2D-SMCs did not [34].

The mRNA expression level of smooth muscle myosin heavy chain isoform SM1, an SMC differentiation marker [47], was greater in 3DCMs than in 2D-SMCs, although SM1 expression in 3DCMs did not seem to reach the SM1 expression level of neonatal rat aorta (Fig. 8.8a). Consistent with these results, the expression levels of an SMC dedifferentiation marker nonmuscle myosin heavy chain (SMemb) [47] in 3DCMs were significantly lower than that in 2D-SMCs and were similar to that of neonatal rat aorta (Fig. 8.8b). The expression of SM2, which is a myosin heavy chain isoform expressed in adult vessels but rarely seen in neonatal vessels [47], was subtle in both 3DCMs and 2D-SMCs. The serum response factor coactivator gene myocardin, which is required for the expression of many SMC differentiation marker genes and for the initial differentiation of SMCs [47], was expressed similarly in both 3DCMs and 2D-SMCs. The high molecular weight isoform of caldesmon (h-caldesmon), an SMC differentiation marker [47], was also expressed similarly in both 3DCMs and 2D-SMCs. In the 3DCM system, at least in part, SMCs exhibited more differentiated phenotypes than in the 2D culture system.

These data suggest that the special arrangement of SMCs seems to affect phenotypic changes in 3DCMs, although SMCs in 3DCMs were not fully differentiated compared to native vascular tissues.

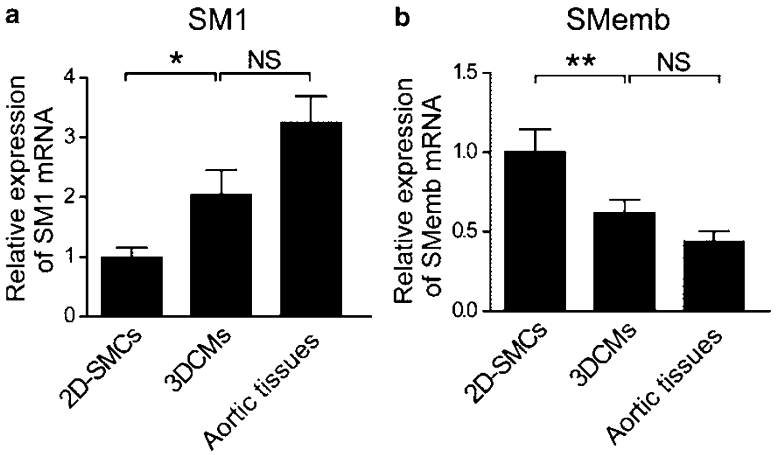

Fig. 8.8 Smooth muscle cells exhibited contractile-like phenotypes in 3DCMs. Expressions of myosin heavy chain isoforms were compared between 2D smooth muscle cells (*2D SMCs*), 3DCMs, and native tissue of rat neonatal aorta. Tissues were cleansed of adventitia and endothelial cells. (**a**) The contractile smooth muscle cell marker SM1 was more strongly expressed in 3DCMs than in 2D SMCs. (**b**) The synthetic phenotype marker SMemb was less strongly expressed in 3DCMs. $n = 4$–8, $^{*}p < 0.05$; $^{**}p < 0.01$; *NS* not significant

8.2.5 Pharmacological Manipulation of Elastic Fiber Formation in 3DCMs

To examine the molecular mechanisms of the elastogenesis and degradation of elastic fibers and to explore new therapeutic strategies to prevent and treat elastic fiber formation disorders, pharmacological manipulation of 3DCMs is essential. However, in conventional in vivo studies using systemic drug administration, drug metabolism profoundly affects their efficacy, and their indirect effects cannot be discriminated. Although there have been recent advances in drug delivery systems, such as nanoparticles and antibody-drug conjugates that enable tissue-specific targeting strategies, these techniques remain impractical for initial drug screening [48].

Thus, we examined whether elastic fiber formation in 3DCMs was regulated by a drug that inhibits the cross-linking of elastin monomers to form insoluble elastic fibers [3, 45]. When β-aminopropionitrile (BAPN), an inhibitor of lysyl oxidase, was applied to 3DCMs for the last 2 days of culture, elastic fiber formation was significantly inhibited (Fig. 8.9).

LOX expression is known to be markedly responsive to a variety of pathological states, including development, wound repair, aging, and tumorigenesis [49, 50]. In particular, strong evidence exists regarding the involvement of a reduction in LOX activity in the pathogenesis of vascular diseases characterized by destructive remodeling of the arterial wall. Previous reports demonstrated that aortic aneurysms and coronary dissections were related to a disturbance in LOX expression in animal models and humans [51, 52]. Therefore, the regulation of LOX expression is considered

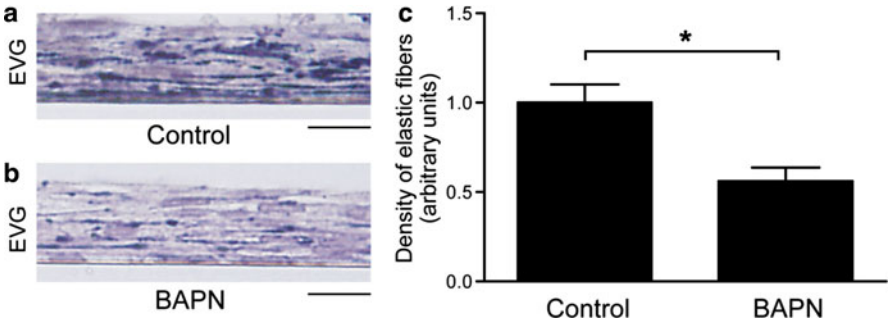

Fig. 8.9 Elastic fiber formation inhibited by a lysyl oxidase inhibitor in 3DCMs. (**a**, **b**) Elastica van Gieson stain (*EVG*) of 3DCMs cultured in 1 % FBS/DMEM in the presence (control) of BAPN. (**c**) Quantification of the density of elastic fibers in (**a**) and (**b**) using color extraction method. $n=5$. $^*p<0.05$. Scale bars: 10 μm

an attractive therapeutic target. Since elastic fiber formation in 3DCMs was disturbed by a lysyl oxidase inhibitor, it appears that pharmacological manipulation can be applied in 3DCMs. 3DCMs may offer a new strategy to examine the direct effects of various drugs on vascular elastic fiber formation and phenotypic changes of SMCs.

8.3 Conclusions

Although the exact mechanisms of the rapid induction of elastic fibers in 3DCMs are not fully clear, several factors, such as the type of SMC, the ECM coated on the cells, and the culture media components, allow the formation of layered elastic fibers in static culture conditions, even in short time periods. Since the regulation of vascular elastic fiber formation and phenotypic changes of SMCs can be examined in 3DCMs, 3DCMs may be useful for exploring pharmacological therapeutic strategies to treat or prevent disordered elastic fiber homeostasis, such as atherosclerotic and aneurismal vascular diseases for which no pharmacological treatment is currently available.

In the previous study by Matsusaki et al., 3DCMs composed of four layers of human umbilical artery SMCs and one layer of human umbilical vascular endothelial cells showed a structure analogous to that of native arteries and tight interactions between each cellular layer. Furthermore, a tight junction was formed between the uppermost endothelial cells, which inhibited platelet adhesion to the 3DCM [40]. In addition to elastic fiber formation, combination with lipids and inflammatory cells in 3DCMs could expand the application of the new experimental vascular models to the examination of pathological conditions including atherosclerosis.

In conclusion, 3DCMs have the potential to serve as a new vascular experimental platform in which the spatial and temporal regulation of vascular remodeling can be studied.

Acknowledgments This work was supported by grants from the Ministry of Education, Culture, Sports, Science and Technology of Japan (UY and YI), a Grant-in-Aid for Scientific Research on Innovative Areas (UY, 23116514 and 25116719; YI, 22136009), the Yokohama Foundation for Advanced Medical Science (UY), and the Takeda Science Foundation (UY and YI).

References

1. Ross R, Glomset JA (1976) The pathogenesis of atherosclerosis (first of two parts). N Engl J Med 295:369–377
2. Vita JA (2011) Endothelial function. Circulation 124:e906–e912
3. Wagenseil JE, Mecham RP (2009) Vascular extracellular matrix and arterial mechanics. Physiol Rev 89:957–989
4. Patel A, Fine B, Sandig M, Mequanint K (2006) Elastin biosynthesis: the missing link in tissue-engineered blood vessels. Cardiovasc Res 71:40–49
5. Wagenseil JE, Ciliberto CH, Knutsen RH, Levy MA, Kovacs A, Mecham RP (2010) The importance of elastin to aortic development in mice. Am J Physiol Heart Circ Physiol 299:H257–H264
6. Mithieux SM, Weiss AS (2005) Elastin. Adv Protein Chem 70:437–461
7. Nakamura T, Lozano PR, Ikeda Y, Iwanaga Y, Hinek A, Minamisawa S, Cheng CF, Kobuke K, Dalton N, Takada Y, Tashiro K, Ross J Jr, Honjo T, Chien KR (2002) Fibulin-5/DANCE is essential for elastogenesis in vivo. Nature 415:171–175
8. Vrhovski B, Jensen S, Weiss AS (1997) Coacervation characteristics of recombinant human tropoelastin. Eur J Biochem 250:92–98
9. Rodriguez C, Martinez-Gonzalez J, Raposo B, Alcudia JF, Guadall A, Badimon L (2008) Regulation of lysyl oxidase in vascular cells: lysyl oxidase as a new player in cardiovascular diseases. Cardiovasc Res 79:7–13
10. Maki JM, Rasanen J, Tikkanen H, Sormunen R, Makikallio K, Kivirikko KI, Soininen R (2002) Inactivation of the lysyl oxidase gene Lox leads to aortic aneurysms, cardiovascular dysfunction, and perinatal death in mice. Circulation 106:2503–2509
11. Kielty CM, Sherratt MJ, Shuttleworth CA (2002) Elastic fibres. J Cell Sci 115:2817–2828
12. Hirai M, Horiguchi M, Ohbayashi T, Kita T, Chien KR, Nakamura T (2007) Latent TGF-beta-binding protein 2 binds to DANCE/fibulin-5 and regulates elastic fiber assembly. EMBO J 26:3283–3295
13. Nakamura T, Ruiz-Lozano P, Lindner V, Yabe D, Taniwaki M, Furukawa Y, Kobuke K, Tashiro K, Lu Z, Andon NL, Schaub R, Matsumori A, Sasayama S, Chien KR, Honjo T (1999) DANCE, a novel secreted RGD protein expressed in developing, atherosclerotic, and balloon-injured arteries. J Biol Chem 274:22476–22483
14. Hirai M, Ohbayashi T, Horiguchi M, Okawa K, Hagiwara A, Chien KR, Kita T, Nakamura T (2007) Fibulin-5/DANCE has an elastogenic organizer activity that is abrogated by proteolytic cleavage in vivo. J Cell Biol 176:1061–1071
15. Horiguchi M, Inoue T, Ohbayashi T, Hirai M, Noda K, Marmorstein LY, Yabe D, Takagi K, Akama TO, Kita T, Kimura T, Nakamura T (2009) Fibulin-4 conducts proper elastogenesis via interaction with cross-linking enzyme lysyl oxidase. Proc Natl Acad Sci USA 106:19029–19034
16. Kinsey R, Williamson MR, Chaudhry S, Mellody KT, McGovern A, Takahashi S, Shuttleworth CA, Kielty CM (2008) Fibrillin-1 microfibril deposition is dependent on fibronectin assembly. J Cell Sci 121:2696–2704
17. Sabatier L, Chen D, Fagotto-Kaufmann C, Hubmacher D, McKee MD, Annis DS, Mosher DF, Reinhardt DP (2009) Fibrillin assembly requires fibronectin. Mol Biol Cell 20:846–858
18. Pereira L, Andrikopoulos K, Tian J, Lee SY, Keene DR, Ono R, Reinhardt DP, Sakai LY, Biery NJ, Bunton T, Dietz HC, Ramirez F (1997) Targeting of the gene encoding fibrillin-1 recapitulates the vascular aspect of Marfan syndrome. Nat Genet 17:218–222

19. Chaudhry SS, Gazzard J, Baldock C, Dixon J, Rock MJ, Skinner GC, Steel KP, Kielty CM, Dixon MJ (2001) Mutation of the gene encoding fibrillin-2 results in syndactyly in mice. Hum Mol Genet 10:835–843
20. Lloyd-Jones D, Adams RJ, Brown TM, Carnethon M, Dai S, De Simone G, Ferguson TB, Ford E, Furie K, Gillespie C, Go A, Greenlund K, Haase N, Hailpern S, Ho PM, Howard V, Kissela B, Kittner S, Lackland D, Lisabeth L, Marelli A, McDermott MM, Meigs J, Mozaffarian D, Mussolino M, Nichol G, Roger VL, Rosamond W, Sacco R, Sorlie P, Thom T, Wasserthiel-Smoller S, Wong ND, Wylie-Rosett J (2010) Heart disease and stroke statistics–2010 update: a report from the American Heart Association. Circulation 121:e46–e215
21. Freestone T, Turner RJ, Coady A, Higman DJ, Greenhalgh RM, Powell JT (1995) Inflammation and matrix metalloproteinases in the enlarging abdominal aortic aneurysm. Arterioscler Thromb Vasc Biol 15:1145–1151
22. Collin J, Araujo L, Walton J, Lindsell D (1988) Oxford screening programme for abdominal aortic aneurysm in men aged 65 to 74 years. Lancet 2:613–615
23. Scott RA, Ashton HA, Kay DN (1991) Abdominal aortic aneurysm in 4237 screened patients: prevalence, development and management over 6 years. Br J Surg 78:1122–1125
24. Annambhotla S, Bourgeois S, Wang X, Lin PH, Yao Q, Chen C (2008) Recent advances in molecular mechanisms of abdominal aortic aneurysm formation. World J Surg 32:976–986
25. Seyama Y, Wachi H (2004) Atherosclerosis and matrix dystrophy. J Atheroscler Thromb 11:236–245
26. Owens GK (1995) Regulation of differentiation of vascular smooth muscle cells. Physiol Rev 75:487–517
27. Aikawa M, Sivam PN, Kuro-o M, Kimura K, Nakahara K, Takewaki S, Ueda M, Yamaguchi H, Yazaki Y, Periasamy M et al (1993) Human smooth muscle myosin heavy chain isoforms as molecular markers for vascular development and atherosclerosis. Circ Res 73:1000–1012
28. Beamish JA, He P, Kottke-Marchant K, Marchant RE (2010) Molecular regulation of contractile smooth muscle cell phenotype: implications for vascular tissue engineering. Tissue Eng Part B Rev 16:467–491
29. Kuro-o M, Nagai R, Nakahara K, Katoh H, Tsai RC, Tsuchimochi H, Yazaki Y, Ohkubo A, Takaku F (1991) cDNA cloning of a myosin heavy chain isoform in embryonic smooth muscle and its expression during vascular development and in arteriosclerosis. J Biol Chem 266:3768–3773
30. Abouhamed M, Reichenberg S, Robenek H, Plenz G (2003) Tropomyosin 4 expression is enhanced in dedifferentiating smooth muscle cells in vitro and during atherogenesis. Eur J Cell Biol 82:473–482
31. Wachi H, Seyama Y, Yamashita S, Tajima S (1995) Cell cycle-dependent regulation of elastin gene in cultured chick vascular smooth-muscle cells. Biochem J 309(Pt 2):575–579
32. Ichiro T, Tajima S, Nishikawa T (1990) Preferential inhibition of elastin synthesis by epidermal growth factor in chick aortic smooth muscle cells. Biochem Biophys Res Commun 168:850–856
33. Tokimitsu I, Kato H, Wachi H, Tajima S (1994) Elastin synthesis is inhibited by angiotensin II but not by platelet-derived growth factor in arterial smooth muscle cells. Biochim Biophys Acta 1207:68–73
34. Ishiwata R, Yokoyama U, Matsusaki M, Asano Y, Kadowaki K, Ichikawa Y, Umemura M, Fujita T, Minamisawa S, Shimoda H, Akashi M, Ishikawa Y (2014) Three-dimensional multilayers of smooth muscle cells as a new experimental model for vascular elastic fiber formation studies. Atherosclerosis 233:590–600
35. Peck M, Gebhart D, Dusserre N, McAllister TN, L'Heureux N (2012) The evolution of vascular tissue engineering and current state of the art. Cells Tissues Organs 195:144–158
36. Matsusaki M, Kadowaki K, Nakahara Y, Akashi M (2007) Fabrication of cellular multilayers with nanometer-sized extracellular matrix films. Angew Chem Int Ed Engl 46:4689–4692
37. Cain SA, McGovern A, Small E, Ward LJ, Baldock C, Shuttleworth A, Kielty CM (2009) Defining elastic fiber interactions by molecular fishing: an affinity purification and mass spectrometry approach. Mol Cell Proteomics 8:2715–2732

38. Dallas SL, Sivakumar P, Jones CJ, Chen Q, Peters DM, Mosher DF, Humphries MJ, Kielty CM (2005) Fibronectin regulates latent transforming growth factor-beta (TGF beta) by controlling matrix assembly of latent TGF beta-binding protein-1. J Biol Chem 280:18871–18880
39. Fogelgren B, Polgar N, Szauter KM, Ujfaludi Z, Laczko R, Fong KS, Csiszar K (2005) Cellular fibronectin binds to lysyl oxidase with high affinity and is critical for its proteolytic activation. J Biol Chem 280:24690–24697
40. Matsusaki M, Kadowaki K, Adachi E, Sakura T, Yokoyama U, Ishikawa Y, Akashi M (2012) Morphological and histological evaluations of 3D-layered blood vessel constructs prepared by hierarchical cell manipulation. J Biomater Sci Polym Ed 23:63–79
41. Kelleher CM, McLean SE, Mecham RP (2004) Vascular extracellular matrix and aortic development. Curr Top Dev Biol 62:153–188
42. Wagenseil JE, Mecham RP (2007) New insights into elastic fiber assembly. Birth Defects Res C Embryo Today 81:229–240
43. McMahon MP, Faris B, Wolfe BL, Brown KE, Pratt CA, Toselli P, Franzblau C (1985) Aging effects on the elastin composition in the extracellular matrix of cultured rat aortic smooth muscle cells. In Vitro Cell Dev Biol 21:674–680
44. Long JL, Tranquillo RT (2003) Elastic fiber production in cardiovascular tissue-equivalents. Matrix Biol 22:339–350
45. Kagan HM, Li W (2003) Lysyl oxidase: properties, specificity, and biological roles inside and outside of the cell. J Cell Biochem 88:660–672
46. Aikawa M, Yamaguchi H, Yazaki Y, Nagai R (1995) Smooth muscle phenotypes in developing and atherosclerotic human arteries demonstrated by myosin expression. J Atheroscler Thromb 2:14–23
47. Owens GK, Kumar MS, Wamhoff BR (2004) Molecular regulation of vascular smooth muscle cell differentiation in development and disease. Physiol Rev 84:767–801
48. Lobatto ME, Fuster V, Fayad ZA, Mulder WJ (2011) Perspectives and opportunities for nanomedicine in the management of atherosclerosis. Nat Rev Drug Discov 10:835–852
49. Smith-Mungo LI, Kagan HM (1998) Lysyl oxidase: properties, regulation and multiple functions in biology. Matrix Biol 16:387–398
50. Yokoyama U, Minamisawa S, Shioda A, Ishiwata R, Jin MH, Masuda M, Asou T, Sugimoto Y, Aoki H, Nakamura T, Ishikawa Y (2014) Prostaglandin E2 inhibits elastogenesis in the ductus arteriosus via EP4 signaling. Circulation 129:487–496
51. Nakashima Y, Sueishi K (1992) Alteration of elastic architecture in the lathyritic rat aorta implies the pathogenesis of aortic dissecting aneurysm. Am J Pathol 140:959–969
52. Sibon I, Sommer P, Lamaziere JM, Bonnet J (2005) Lysyl oxidase deficiency: a new cause of human arterial dissection. Heart 91:e33

Chapter 9
Building Experimental System Modeling Fibrotic Tissue in Human Pancreatic Cancer by Three-Dimensional Layer-by-Layer Culture

Mitsunobu R. Kano

Abstract Pancreatic adenocarcinoma, which accounts for 90 % of cancers arising from the pancreas, is especially notorious for its poor prognosis. However, the reason why the cancer is so refractory to therapy has not yet been fully elucidated. We hypothesize that the characteristic of the "route" via which antitumor drugs reach the tumor cells is the factor responsible for the refractoriness. This factor should presumably be more critical for drugs with larger sizes, especially those of nanometer order. Microscopic observation reveals that the major component of the pancreatic adenocarcinoma tissue is fibrotic tissue, whereas tumor cells are minor in terms of number and area. Any antitumor drug, however potent it may be against naked cultured tumor cells, is only effective when it reaches the tumor cells within the human body. To treat pancreatic adenocarcinoma, drugs need to travel through the systemic circulation towards the tumor microcirculation and across the fibrotic tissue, before reaching the tumor cells. The tumor vasculature in pancreatic adenocarcinoma is embedded in the fibrotic tissue. Therefore, we need a new experimental system that models the microscopic structures that the drugs encounter en route to tumor cells. We discuss in this paper our novel system which models the thickness of fibrotic tissue as a first step in modeling the microenvironment of pancreatic adenocarcinoma.

Keywords Desmoplasia • Fibrotic tissue • Pancreatic cancer • Three-dimensional culture

M.R. Kano, M.D., Ph.D. (✉)
Department of Pharmaceutical Biomedicine, Graduate School of Medicine, Dentistry, and Pharmaceutical Sciences, Okayama University, Okayama, Japan
e-mail: Mikano-tky@umin.net

M. Akashi et al. (eds.), *Engineered Cell Manipulation for Biomedical Application*, Nanomedicine and Nanotoxicology,
DOI 10.1007/978-4-431-55139-3_9

9.1 Introduction

Pancreatic cancer is notorious for its poor prognosis. Especially, the prognosis of pancreatic adenocarcinoma, which accounts for 90 % of pancreatic cancer, is extremely poor: median life expectancy is only around 6 months if the tumor is deemed unresectable. Healthcare professionals feel helplessness in front of such patients. A major way to treat unresectable tumor is chemotherapy; therefore inadequacy in treatment for such tumor can be rooted in the ineffectiveness of anticancer drugs.

While extensive investigation based on molecular biology has tried to elucidate the reason for this poor prognosis, we have adopted a morphological viewpoint. Microscopic observation of tissue specimens of human pancreatic adenocarcinoma reveals a pattern characterized by a predominance of fibrotic component, as if nests of tumor cells are scattered in a broad field of fibrosis. The percentage of fibrotic tissue is reported to be almost 80 %. To summarize, the tissue of human pancreatic adenocarcinoma, a devastating cancer, consists of (1) predominant fibrotic tissue, (2) scattered nests of tumor cells, and (3) some other components including vasculature embedded in fibrotic tissue (Fig. 9.1).

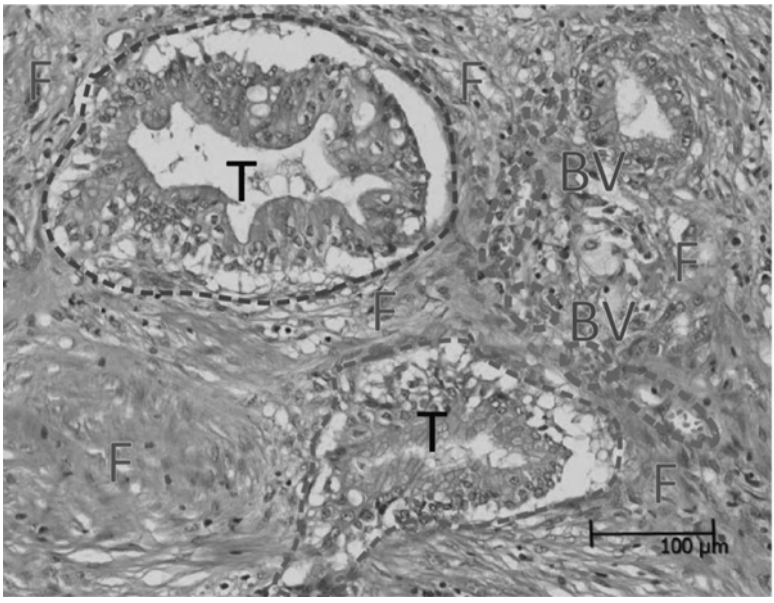

Fig. 9.1 Microscopic observation of human pancreatic adenocarcinoma (from Hosoya et al. [1]). *T* stands for tumor nests, *F* for fibrotic tissue, and *BV* for blood vessels (*inside gray dotted circles*)

9.2 Factors to Consider in Developing Effective Chemotherapy for Pancreatic Adenocarcinoma

Chemotherapy for pancreatic adenocarcinoma, with tissue structure as described, has been developed using conventional methods in oncology: developing potential antitumor compounds and testing their effect with tumor cell lines derived from human tumors. Tumor cell lines are either cultured in monolayer in a culture dish or xenografted in animals. Clinical studies are designed based on the results of these experiments. However, flat monolayer culture of tumor cells alone cannot model the complicated structure of tumor tissue. Even the tissue of xenografts in animals generally consists of abundant tumor cells as a major component supported by leaky tumor vessels, but lacks fibrotic tissue or other components, even if cell lines from pancreatic adenocarcinoma are used.

As a consequence, antitumor drugs, however potent in conventional experimental systems, may fail to show effectiveness in the real human diseases: unresectable pancreatic adenocarcinoma in particular [2]. For example, gemcitabine, the first-line anticancer drug for pancreatic adenocarcinoma used in the clinical setting, exhibits potent cytotoxicity against BxPC3 cell line in flat monolayer culture, while the drug hardly inhibits tumor growth when the same cell line is xenografted. In humans, the drug was clinically approved first in 1995 due to significant "clinical benefits" in patients with advanced pancreatic adenocarcinoma, albeit a modest 0.5-month elongation of median survival versus patients treated with 5-FU. "Clinical benefit" is an endpoint designed to quantitatively measure the effect of gemcitabine on patients' overall quality of life.[1]

Why, then, do results differ between the experimental systems: flat monolayer cultures, xenografts in animals, and human tumors? The cause of the difference has not been fully elucidated. According to a viewpoint based on tumor cell autonomous mechanisms, the discrepancy is attributed to cancer stem cells, metastasis of tumor cells, changes in tumor cell drug sensitivity/resistance, or others. Our previous studies meanwhile suggest that the discrepancy may also arise from the characteristics of tumor tissue structure which determines the route the drugs must take to reach tumor cells, as described above. Administered drugs, especially those of larger size of nanometers in diameter, for example, first get into the systemic circulation, including the vasculature in the tumor foci, and gradually get out of the vasculature into the interstitial space around. The drug may act directly against the target tumor cells if the cells exist adjacent to the vasculature.

[1] http://www.cancernetwork.com/articles/odac-recommends-full-approval-gemzar-pancreatic-cancer (viewed on 10 Jan, 2014)

However, if a large mass of fibrotic tissue separates the tumor cells from the vasculature, the drug may not easily be able to affect the target cells. The vasculature in pancreatic adenocarcinoma actually is embedded in the fibrotic tissue, not in the tumor nests. Moreover, the vasculature is less in number and less in leakiness in pancreatic adenocarcinoma, which only worsens the situation. In summary, for drugs to reach target cancer cells in pancreatic adenocarcinoma, the drugs need to pass through the less dense vasculature with less leakiness in the cancer tissue and furthermore get across the fibrotic tissue. In colon cancer, in comparison, density and leakiness of the vasculature are more, and tumor cells exist right next to the vasculature: the drugs may have far less obstacles to get to the target cells.

9.3 Developing an Experimental System Reflecting the Tissue Structure of Pancreatic Adenocarcinoma

The conventional method, culture of tumor cells in a plate, is a relevant model of human disease for hematologic malignancies such as leukemic and lymphoma cells or colon cancer. These cancers are relatively well treated with conventional chemotherapy. Culture medium mimics human blood, with 10 % serum, oxygen, and nutrients. All cells contact the culture medium and attach to stable scaffold in a culture dish. This resembles for example colon cancer, in which tumor cells have good contact with dense tumor vasculature with high leakiness. Suspension culture of tumor cells more resembles leukemic cells.

In the case of pancreatic adenocarcinoma, as described above, the circumstance for the tumor cells is largely different from this conventional culture system. We therefore need a novel experimental system especially to investigate drug delivery. There are almost no appropriate systems available, either in vivo or in vitro, only except for an in vitro system using a mesh-like apparatus to culture various kinds of cells on both sides of the mesh. Investigators can observe permeation of molecules through the mesh with cells cultured: the system is appropriately named “transwell.” The transwell system can be used to investigate permeability, by culturing vascular endothelial cells on the transwell and applying an alternating electric field (a method named transepithelial electric resistance: TEER), for example. However, the existence of fibrotic tissue cannot be modeled even with this method.

Of course various three-dimensional (3D) culture methods have meanwhile been attempted using materials derived from extracellular matrices, such as collagen or Matrigel. These models however have not been used for the investigation of drug delivery. 3D culture of fibroblasts in collagen gel results in shrinkage of the whole gel mixture and is thus not appropriate for the present purpose. In addition, fibrotic tissue within pancreatic adenocarcinoma seems to consist mostly of fibroblasts according to microscopic observation. Therefore, we need more cell density in the experimental system than in the conventional 3D culture system using collagen gel for it to be appropriate for investigating drug delivery in pancreatic adenocarcinoma.

9.4 3D Culture of Fibroblasts Based on Layer-by-Layer Culture

Layer-by-layer (LbL) 3D culture method was established by Matsusaki and Akashi et al., by creating on the cell surface a coat comprising fibronectin and gelatin of approximately 6 nm. We can now culture cells vertically in multiple layers with this method. We examined permeation of nanomaterials using multilayered fibroblasts cultured by this method (Fig. 9.2). Here we used fluorescent-labeled dextran molecule of 250 and 2,000 kDa, the latter of which has an estimated hydrodynamic diameter of 50 nm.

A difference was observed when comparing models using fibroblasts derived from a mouse model of pancreatic cancer, K643f, and normal fibroblasts NIH3T3. Comparing permeation of dextran of 250 and 2,000 kDa in both models, the number of layers is affected more on permeation in the model using K643f cells, whereas the size of dextran molecule is affected more in the NIH3T3 model. This difference suggests that the choice of cells to use is an important issue.

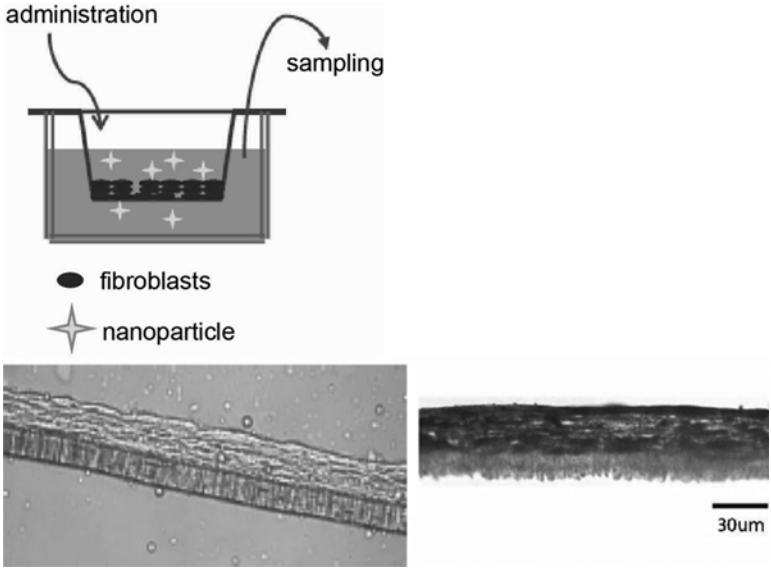

Fig. 9.2 An experimental system to model fibrotic tissue in pancreatic adenocarcinoma using layer-by-layer 3D culture of fibroblasts (from Hosoya et al. [1]). Fibroblasts are cultured in multilayer on commercially available transwell. We examined the amount of nanomaterial permeating from the medium in the upper chamber to the lower. Two photographs in the *lower row* show a cross section of the layer-by-layer culture of fibroblasts

9.5 Choice of Fibroblasts to Use

How can we make the right choice of fibroblasts to use? One possibility is to use cells expressing functionally important molecular markers. To determine such a marker, let us share our recent result.

Known prognostic markers for pancreatic adenocarcinoma are staging of the tumor (tumor-node-metastasis or TNM classification), lymphatic invasion (abbreviated as "Ly"), and others. We have shown, in addition to these, that the expression level of PDGF beta receptor (PDGFRβ) in fibroblasts, but not in tumor cells, significantly correlates with prognosis. PDGFRβ is a signaling molecule known to be important in the activation and proliferation of activated fibroblasts ([3] and Fig. 9.3a). Meanwhile, the expression level of another marker of activated fibroblasts, smooth muscle actin (SMA), does not correlate with prognosis (Fig. 9.3b). SMA functions in the contraction of cells.

These results suggest that fibrotic tissue causes difficulty in the treatment of pancreatic adenocarcinoma and that an experimental system modeling such fibrotic tissue is important. Although isolation and culture of cells from fibrotic tissue in pancreatic adenocarcinoma are not common yet, we need to continue trying to establish a clinically relevant model of fibrotic tissue to realize effective medical treatment against pancreatic adenocarcinoma, which remains a devastating disease.

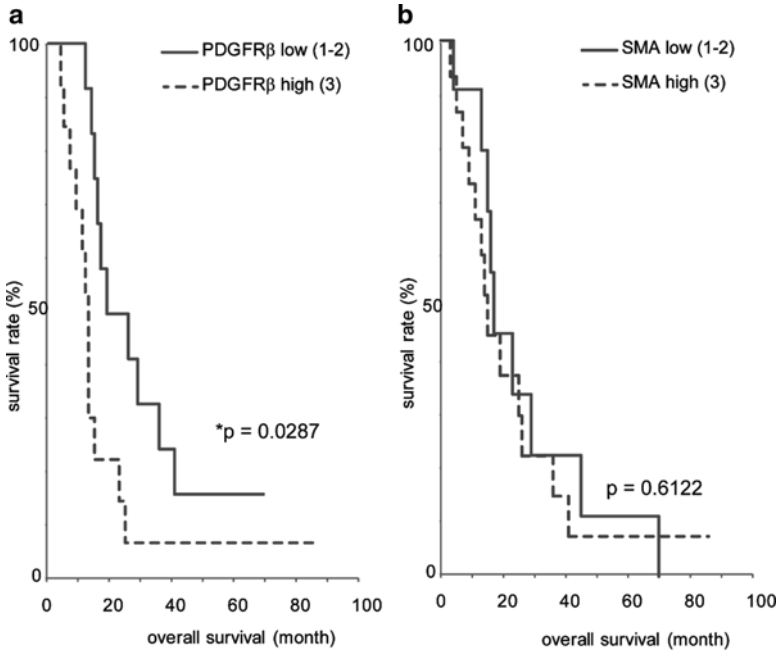

Fig. 9.3 Molecular markers in fibrotic tissue and its correlation with prognosis (from Yuzawa et al. [2]). Although both PDGFRβ (**a**) and SMA (**b**) are molecular markers of activated fibroblasts, only PDGFRβ is shown to correlate with prognosis

9.6 Summary

We discussed the importance of the layer-by-layer culture technique in investigating the "route" of drug delivery in the disease foci, a viewpoint largely unnoticed but nonetheless important in developing effective medical treatment of pancreatic tumor. We hope that we can treat currently intractable diseases in the future through this kind of investigation.

Acknowledgments The author would like to thank Dr. Hiroyoshi Y. Tanaka for his critical reading of the manuscript. This work was supported by JSPS KAKENHI Grants, Health Labor Sciences Research Grants, grants from the Japan Foundation for Applied Enzymology, and the Funding Program for World-Leading Innovative R&D on Science and Technology (FIRST program) from the Japan Society for the Promotion of Science (JSPS).

References

1. Hosoya H, Kadowaki K, Matsusaki M, Cabral H, Nishihara H, Ijichi H, Koike K, Kataoka K, Miyazono K, Akashi M, Kano MR (2012) Engineering fibrotic tissue in pancreatic cancer: a novel three-dimensional model to investigate nanoparticle delivery. Biochem Biophys Res Commun 419(1):32–37
2. Kano MR, Bae Y, Iwata C, Morishita Y, Yashiro M, Oka M, Fujii T, Komuro A, Kiyono K, Kaminishi M, Hirakawa K, Ouchi Y, Nishiyama N, Kataoka K, Miyazono K (2007) Improvement of cancer-targeting therapy, using nanocarriers for intractable solid tumors by inhibition of TGF-beta signaling. Proc Natl Acad Sci USA 104(9):3460–3465
3. Yuzawa S, Kano MR, Einama T, Nishihara H (2012) PDGFRb expression in tumor stroma of pancreatic adenocarcinoma as a reliable prognostic marker. Med Oncol 29(4):2824–2830

Chapter 10
Human Living Skin Equivalents as a Promising Model for Skin Grafts

Satoshi Hirakawa, Yuji Shirakata, and Koji Hashimoto

Abstract The recent progress of bioengineered technology enabled to generate the three-dimensional living skin equivalents from human materials. This scientific proceeding was initially developed by the fundamental knowledge of biology in epidermal keratinocytes. The human skin induces terminal differentiation in the epidermis which overlays the dermis, a major extracellular matrix component in the skin. Importantly, the sub-epidermal basement membranes promote the cell fate, indicating that the biological interaction of the epidermis with extracellular matrix molecules essentially promotes the physiological development in the skin. Therefore, human living equivalents are composed of cultured epidermal keratinocytes upon dermal fibroblasts, leading the materials to feasible ex vivo models involving the assessment of chemical compounds for drug screening. Furthermore, the human living skin equivalents are currently available for clinical application to those who undergo skin defects due to burn or congenital bullous disease. Future direction of the human skin living equivalents involves the induction of skin appendages such as hair follicles and sweat glands. Finally, the integration of other cell types such as blood or lymphatic endothelial cells may lead the living skin equivalents to a suitable graft for severe skin defects. Thus, the human living skin equivalents directly contribute to benefit the patients as well as the pharmaceutical assessment.

Keywords Keratinocytes • Fibroblasts • Endothelial cells • Growth factors • Clinical application

S. Hirakawa (✉)
Department of Dermatology, Hamamatsu University School of Medicine, Hamamatsu, Japan
e-mail: hirakawa@hama-med.ac.jp

Y. Shirakata • K. Hashimoto
Department of Dermatology, Ehime University Graduate School of Medicine, Toon, Japan

M. Akashi et al. (eds.), *Engineered Cell Manipulation for Biomedical Application*, Nanomedicine and Nanotoxicology,
DOI 10.1007/978-4-431-55139-3_10

10.1 Introduction

Skin is one of the major organs that have been extensively investigated by scientists in medicine as well as in biology. Mammalian skin is characterized by the thin structure which differentiates internal body from the environment outside. Mammalian body is predominantly composed of water. Therefore, one of the major functions of the skin is to inhibit water loss from the inside. Furthermore, mammals hold stable body temperature for efficient activity. Therefore, the other function of mammalian skin is to protect the loss of body temperature from the internal organs in physiological condition. Moreover, mammalian skin is exposed to the environment which encloses several types of pathogenic bacteria and virus to the animals. Thus, the key function of the skin is to protect the body from bacterial or viral infection by consisting barriers and recruiting immune cells for inflammatory tissue response.

Organ transplantation is currently available for internal organs such as liver and kidney, whereas the skin is not feasible for the organ transplantation from a donor to a recipient. It is because the immune system of the recipient is highly responsive to the skin from donors, resulting in the rejection of the skin graft from others. Meanwhile, adults may die due to the loss of human skin by 30 % in pathologic conditions such as burn because those patients might undergo dehydration or bacterial infection Therefore, the biological characteristics of the skin should be clarified in order to develop the skin equivalents suitable for clinical usage.

Recent progress and maturation of biological research raised the fundamental issue whether animal experiments can be replaced by ex vivo protocols. To challenge the crucial topic, three-dimensional skin equivalents are widely accepted to monitor the physiological events in the skin. Furthermore, three-dimensional skin equivalents are a feasible model to assess the biological effect of chemical mediators and compounds potentially upon human skin. Therefore, in this chapter, we first introduce the fundamental knowledge of human skin so that one can better understand the structure of the skin. Moreover, we demonstrate the recent progress of three-dimensional skin equivalents by bioengineered technology. Finally, we summarize the future direction of skin equivalents which can be modified for clinical settings as well as for drug screening.

10.2 Biological Importance of the Skin

The skin covers the whole surface of animal body except eyeballs. The thin nature of the skin indicates the minimal function of living tissue as compared with other organs such as liver. However, the exact function of skin is multifaceted depending on the multilayered structure by the epidermis, dermis, and subcutaneous tissue. The outer surface of mammalian skin is exposed to the air which is dry on the surface of the earth, whereas the humidity may be increased depending on the weather.

Furthermore, the condition of the environment may be changed by wind and temperature as well as sunlight. Therefore, the outer surface of the mammalian skin is tolerable to different conditions of the environment. Meanwhile, the inner surface of the mammalian skin is adjacent to the body which is predominantly comprised of water and further maintained by stable temperature. Therefore, the outer and inner surface of the mammalian skin is exposed to a totally different condition. Therefore, these two surfaces of the skin show different functions, contributing to the tissue homeostasis of the mammalian body.

10.3 Structure and Function in the Epidermis

The epidermis comprises four functional layers. The outer surface of the skin is covered by the cornified layer, whereas the basal layer is composed of basal keratinocytes as well as melanocytes (Fig. 10.1). The majority of epidermal keratinocytes develops spinous layer sealing the basal layer in the epidermis. The spikes are

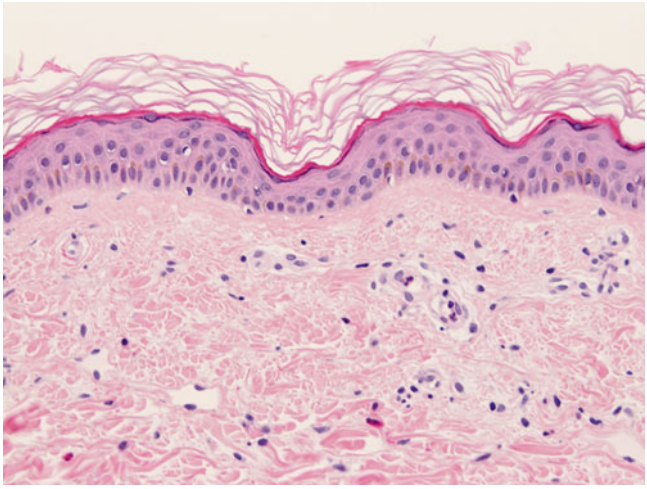

Fig. 10.1 Representative image of normal human skin by histological analysis. Hematoxylin and eosin stains demonstrate the epidermis by multiple cell layers with terminal differentiation by keratinocytes. Furthermore, a small number of melanocytes are found in the basal layer of the epidermis. The cornified layer is shown in *red to pink*, overlying the surface of the skin. The granular layer is shown in *dark purple*, reflecting the enlargement of keratohyaline granules. Furthermore, the microscopic image reveals a bundle of sweat glands as a representative skin appendage. The dermis is shown in *pink to purple*, underlying the epidermis. Note that the prominent network of collagen fibers comprises the fundamental architecture in the dermis. Small-sized vessels are found in the upper dermis with a moderate infiltration of immune cells surrounding the vessels

necessary for keratinocytes to generate stable cell adhesion together with the adjacent cells, contributing to the barrier formation in the epidermis. These keratinocytes are living in the whole epidermis, whereas the cornified layer is composed of dead cells without nuclei. Microscopic analysis shows that keratinocytes underneath the cornified layer generate a large number of granules within the keratinocytes, leading to the aggregation of cytoskeleton and terminal differentiation. Those granules are called keratohyaline granules which contain a prominent amount of profilaggrin, the high molecular weight precursor (Fig. 10.1). Profilaggrin is physiologically processed into several monomers which are further digested to amino acids, leading to the potential moisturization of the skin.

10.4 Dermis as a Major Component in the Skin

Extracellular matrix composes the fundamental structure of respective organs involving skin. Dermis is predominantly composed of extracellular matrix molecules such as type I collagen which is a representative type of fibrillar collagens. Furthermore, the dermis is enriched by proteoglycans as well as hyaluronan which shows extremely hydrophilic feature. Thus, the dermal complex of the extracellular matrix molecules efficiently serves to tolerate physical tension and pressure from outside the body.

The dermis is a scaffold of the epidermis which is comprised of keratinocytes and other cell types. The basement membranes of the epidermis regulate the fate of epidermal keratinocytes and melanocytes. Furthermore, the physiological interaction of the dermis and epidermis induces hair follicle development. Therefore, the dermis is an essential component in the skin during physiological development. The extracellular matrix molecules are produced by fibroblasts in the dermis. Furthermore, neural and vascular networks are prominent in the dermis. Sensory nerve endings and blood capillaries are common in the upper dermis. Blood capillaries physiologically leak plasma from endothelial cell barriers, contributing to the sufficient supply of oxygen and nutrients to the epidermis. Meanwhile, the blood stream is efficiently transported by arteries and veins which are covered by pericytes. Cutaneous blood vascular endothelial cells express platelet endothelial cell adhesion molecule-1 and plasmalemmal vesicle-associated protein (PV)-1 as blood vessel-specific markers in the plasma membranes [1], whereas pericytes express α-smooth muscle actin in the cytoplasm. Once the blood stream is altered by pathological conditions such as thrombi, the ischemia may induce hypoxia in the epidermis as well as the dermis, leading to the formation of cutaneous necrosis. Thus, blood vessels are necessary for tissue homeostasis in the skin.

Cutaneous lymphatic vessels are found in the dermis. The initial lymphatic vessels are blunt ended and characterized by the endothelial cell flaps. This architecture is called “button-like junction” which enables the initial lymphatic vessels to absorb interstitial fluids and immune cells to traffic into the vessels. Furthermore, the initial

lymphatic vessels are connected to collecting lymphatic vessels which are larger in diameter. Lymphatic endothelial cells in the initial lymphatic vessels express lymphatic vessel endothelial hyaluronan receptor (LYVE)-1 as well as podoplanin, a specific receptor for CLEC-2 in the platelets, whereas lymphatic endothelium in the collectors exclusively expresses podoplanin [2]. The endothelial cell junction of the collecting lymphatic vessels is tight as compared with the "button-like junction" in the initial lymphatic vessels [3]. The distinct endothelial cell junction of the collecting lymphatic vessels is called "zip-like junction," which enables the collectors to transport lymph efficiently. Moreover, collecting lymphatic vessels are characterized by valves and pericytes which allow the lymphatic flow in a unidirection.

10.5 Living Skin Equivalents as a Feasible Instrument for Basic Research

Human skin is composed of multiple cell layers in the epidermis. Furthermore, the spatiotemporal interaction of the epidermis and dermis induces the terminal differentiation in the epidermis and physiologically develops highly differentiated structures such as hair follicles. Based on the background, the combination of primary cultured human epidermal keratinocytes and dermal fibroblasts represents a feasible model to gain insights into the biological function of the skin, leading to the reconstitution of living skin equivalents for clinical settings (Fig. 10.2).

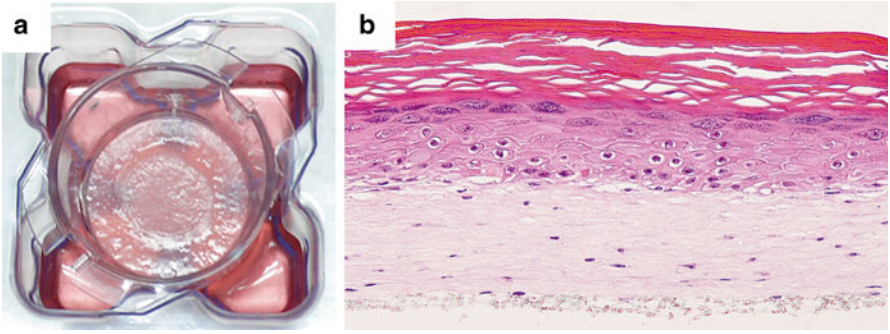

Fig. 10.2 Human living skin equivalents as a feasible model for cutaneous biology. A macroscopic appearance of living skin equivalents shows cultured epidermal keratinocytes in white to slightly *brown* (**a**). Histological analysis shows the development of the epidermis on cultured fibroblasts in the dermis (**b**). Hematoxylin and eosin stains reveal the terminal differentiation in the epidermis, whereas no skin appendages or melanocytes are found in the experimental model

Living skin equivalents are utilized for patients who undergo skin defects such as burns, chronic ulcers, or congenital blistering disease. Several growth factors and cytokines are induced during the wound healing process. Among endogenous growth factors, epidermal growth factor (EGF) plays a crucial role in promoting keratinocyte proliferation and migration in the wounds. Epidermal keratinocytes express EGF and activate their proliferation via an autocrine manner. Meanwhile, dermal fibroblasts express potent growth factors such as basic fibroblast growth factor (bFGF). Recombinant bFGF is commercially available in Japan and is currently applied for several types of cutaneous ulceration in human patients. Ectopic stimulation of epidermal keratinocytes by recombinant bFGF promotes the epidermal differentiation and suppresses the proliferation of cultured keratinocytes in human living skin equivalents [4]. Therefore, the biological interaction of the dermis and epidermis is mediated by the mesenchymal-derived growth factors such as bFGF and further responsible for physiological differentiation of the epidermis.

Cutaneous extracellular matrix is a key component that regulates cell fate, leading to the differentiation of epidermal keratinocytes as well as dermal fibroblasts [5]. Among the extracellular matrix, subepidermal basement membranes induce the physiological function of adjacent cells, leading to the regulation of growth factors and cytokines. Amnion, a sac for embryonic development, is composed of extracellular matrix components such as basement membranes. Amnion induces a physiological condition in human living skin equivalents [6]. Human living skin equivalents show the marked induction of transforming growth factor (TGF)-β in cultured epidermal keratinocytes. Meanwhile, in the presence of amnion, cultured epidermal keratinocytes decrease the expression levels of TGF-β, which is negatively regulated in normal human epidermis. Of particular importance, dermal fibroblasts underlying the epidermis suppress the expression levels of α-SMA in response to the decrease of TGF-β from the epidermis. Therefore, the extracellular matrix components such as basement membranes regulate the interaction of epidermal keratinocytes and dermal fibroblasts in human living skin equivalents leading to the maintenance of the three-dimensional culture in physiological condition [7].

Blood vessels develop the vascular network as well as lymphatic vessels in the dermis, whereas no blood vessels were supplied in human living skin equivalents. Recent studies showed that cultured blood vascular endothelial cells induce capillary-like tube formation on dermal fibroblasts in three-dimensional dermal equivalents [8, 9] (Fig. 10.3). Furthermore, human living skin equivalents maintain the fundamental architecture of lymphatic vessels as well as blood vessels in the bioengineered skin graft on immunoincompetent rats [10]. Importantly, these bioengineered lymphatic vessels functionally anastomose to preexisting lymphatic vessels in the recipients. Therefore, the reconstruction of vascular network may represent a promising application of human living skin equivalents from experimental models to clinical settings.

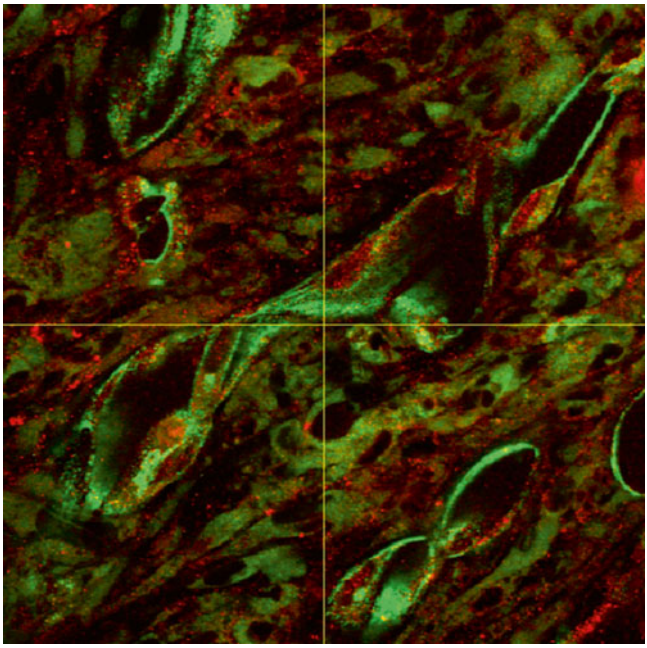

Fig. 10.3 Cultured human dermal microvascular endothelial cells on fibroblasts. Double immunofluorescence analysis for PV-1 in *green* and for α-smooth muscle actin in red shows the characteristic formation of capillary-sized tubelike structures by blood vascular endothelial cells. Underlying fibroblasts express α-smooth muscle actin, indicating the biological interaction of cultured fibroblasts to endothelial cells

10.6 Perspectives

Human living skin equivalents are enabled to gain insights into the biological regulation of epidermal differentiation and dermo-epidermal interaction in cutaneous biology. The living skin equivalents are applicable to recipients because the physiological nature of the graft is relevant to human skin. Meanwhile, the living skin equivalents lack their appendages such as hair follicles and sweat glands. Therefore, the skin equivalents may serve as a biological material which provides crucial information to develop the unique and highly differentiated structure in the skin. Furthermore, the living skin equivalents can be subjected to clarify the other types of epidermal cells such melanocytes or Langerhans cells. Photoinduced skin damage is quantitatively assessed by human living skin equivalents. Thus, the biological significance of melanocytes may be clarified by the skin equivalents, leading to the protection of photoaging and tumor progression in the skin. Future studies to integrate respective cell types in a living skin equivalent contribute to reconstitute a three-dimensional skin, which is identical to human skin and ideal for the patients.

Acknowledgment We thank Mr. Akihiro Nishiguchi for providing the image of cultured dermal microvascular endothelial cells on fibroblasts.

References

1. Keuschnigg J, Tvorogov D, Elima K, Salmi M, Alitalo K, Salminen T et al (2012) PV-1 is recognized by the PAL-E antibody and forms complexes with NRP-1. Blood 120(1):232–235
2. Hirakawa S (2011) Regulation of pathological lymphangiogenesis requires factors distinct from those governing physiological lymphangiogenesis. J Dermatol Sci [Research Support, Non-US Govt Review] 61(2):85–93
3. Baluk P, Fuxe J, Hashizume H, Romano T, Lashnits E, Butz S et al (2007) Functionally specialized junctions between endothelial cells of lymphatic vessels. J Exp Med 204(10): 2349–2362
4. Yang L, Hashimoto K, Tohyama M, Okazaki H, Dai X, Hanakawa Y et al (2012) Interactions between myofibroblast differentiation and epidermogenesis in constructing human living skin equivalents. J Dermatol Sci 65(1):50–57
5. Yang L, Hashimoto K, Shirakata Y (2012) Epidermogenesis in a skin wound deep through the basement membrane contributes to scar formation. J Dermatol Sci 65(3):224–226
6. Yang L, Shirakata Y, Tokumaru S, Xiuju D, Tohyama M, Hanakawa Y et al (2009) Living skin equivalents constructed using human amnions as a matrix. J Dermatol Sci 56(3):188–195
7. Fleischmajer R, Utani A, MacDonald ED, Perlish JS, Pan TC, Chu ML et al (1998) Initiation of skin basement membrane formation at the epidermo-dermal interface involves assembly of laminins through binding to cell membrane receptors. J Cell Sci 111(Pt 14):1929–1940
8. Nishiguchi A, Yoshida H, Matsusaki M, Akashi M (2011) Rapid construction of three-dimensional multilayered tissues with endothelial tube networks by the cell-accumulation technique. Adv Mater 23(31):3506–3510
9. Nishiguchi A, Matsusaki M, Asano Y, Shimoda H, Akashi M (2014) Effects of angiogenic factors and 3D-microenvironments on vascularization within sandwich cultures. Biomaterials 35(17):4739–4748
10. Marino D, Luginbuhl J, Scola S, Meuli M, Reichmann E (2014) Bioengineering dermo-epidermal skin grafts with blood and lymphatic capillaries. Sci Transl Med 6(221):221ra14

Part II
Cell Manipulation for Control of Cell Function for Drug Delivery System

Chapter 11
Particulate and Immunity

Etsushi Kuroda, Cevayir Coban, and Ken J. Ishii

Abstract It is known that some particulates and crystals stimulate the immune system to induce inflammatory responses. Nanometer- to micrometer-sized crystal, sphere, and hydrogel forms of aluminum salts (referred to as "alum") have been used as vaccine adjuvants to enhance antibody responses in animals and humans. Conversely, several particulate pollutants, such as diesel particles and sand dust, induce pulmonary inflammation and allergic asthma. In particular, most of particulates including alum and silica induce type-2 immune responses in vivo, which are characterized by the accumulation of eosinophils and the elevation of serum immunoglobulin (Ig)E. However, the basis for the adjuvanticity of particulates and the mechanisms by which they elicit immune responses remain poorly understood. In this chapter, we will discuss the molecular and immunological mechanisms of action of particulate in immune responses.

Keywords Adjuvant • DAMPs • Particulate • Type-2 immune response

---

The original version of this chapter was revised. An erratum to this chapter can be found at DOI 10.1007/978-4-431-55139-3_16

E. Kuroda
Laboratory of Vaccine Science, WPI Immunology Frontier Research Center (IFReC), Osaka University, Suita, Osaka 565-0871, Japan

C. Coban
Laboratory of Malaria Immunology, IFReC, Osaka University, Suita, Osaka 565-0871, Japan

K.J. Ishii (✉)
Laboratory of Vaccine Science, WPI Immunology Frontier Research Center (IFReC), Osaka University, Suita, Osaka 565-0871, Japan

Laboratory of Adjuvant Innovation, National Institute of Biomedical Innovation, Ibaraki, Osaka 567-0874, Japan
e-mail: kenishii@biken.osaka-u.ac.jp

M. Akashi et al. (eds.), *Engineered Cell Manipulation for Biomedical Application*, Nanomedicine and Nanotoxicology,
DOI 10.1007/978-4-431-55139-3_11

11.1 Immune Responses

Immune responses are categorized into two types: innate and adaptive (Fig. 11.1). Innate immunity is mediated by macrophages and dendritic cells (DCs), which engulf and kill microbes. In contrast, adaptive immunity involves antigen-specific responses mediated by T cells, B cells, and memory cells. Adaptive immunity is further divided into type-1 (cellular) immunity and type-2 (humoral) immunity. It had long been believed that the innate immune response functions as a temporal defense system against infection until the adaptive immune response can be elicited. However, recent studies have demonstrated that innate immunity is essential for the effective induction of adaptive immunity (Fig. 11.1) [1–3].

Some particulates and crystals stimulate the immune system to induce antigen-specific (adaptive) immune responses. Substances that enhance adaptive immune responses are called "adjuvant." Most well-known particulate adjuvant is alum and it has been clinically used as vaccine adjuvants for a long time [4–6]. An adjuvant is thought to be an activator of innate immunity. In general, innate immune cells recognize pathogen-derived factors (pathogen-associated molecular patterns (PAMPs)) and thorough pattern-recognition receptors (PRRs) and induce inflammatory responses. There are four classes of PRRs: Toll-like receptors (TLRs), Nod-like receptors (NLRs), RIG-I-like receptors (RLRs), and C-type lectin receptors (CLRs) [7–10]. These receptors recognized PAMPs, transduce activating signals into cells,

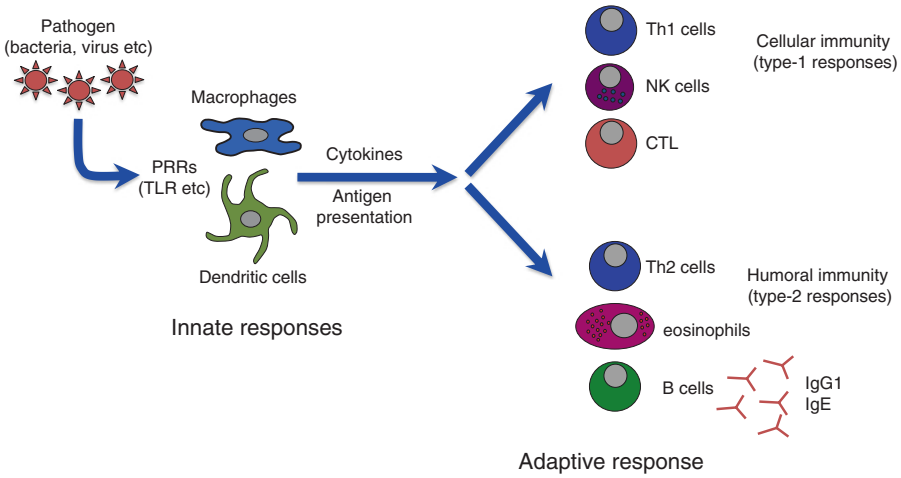

Fig. 11.1 Innate immunity triggers adaptive immunity. When pathogens attack the body, innate immune cells are activated, engulf, and kill microbes. Activated innate cells such as dendritic cells act as antigen-presenting cells and trigger adaptive immunity. Antigen (pathogen)-specific T and B cells are activated, and the resulting antibody and T cells attack pathogens. *PRR* pattern-recognition receptor, *TLR* toll-like receptor, *Th1* helper T cell type 1, *Th2* helper T cell type 2, *NK* natural killer, *CTL* cytotoxic T lymphocyte

and trigger adaptive immunity against pathogens. Not only PAMPs, factors released from dying or stressed cells, what we call damage-associated molecular patterns (DAMPs), also contribute to the induction of adaptive immune responses. DAMPs include lipids, sugars, metabolites, nucleic acid, and cytokines. PRRs also recognized DAMPs and induce inflammatory responses. Therefore, the ligands for PRRs, such as PAMPs and DAMPs, exhibit potent adjuvant properties that elicit adaptive immunity, and PRRs are considered to be receptors for adjuvants (Fig. 11.1) [1, 11].

An increasing number of particulates and nanoparticles have been reported to exhibit adjuvant activity. The mechanisms of induction of adaptive immunity by alum or a particulate adjuvant are also unclear even though alum has been used as a human vaccine adjuvant for more than 80 years. The induction of adaptive immunity requires innate immunity. Hence, it has been proposed that particulates can activate innate cells and that this action is accompanied by the induction of cytokines, chemokines, and other factors.

11.2 Particulates That Have Adjuvant Effect

Several particulates are known to exhibit adjuvant effects in immune responses. Alum selectively stimulates type-2 immune responses, which are characterized by the production of interleukin (IL)-4 and IL-5, the accumulation of eosinophils at the site of injection, and the induction of immunoglobulin (Ig)E [4–6]. Crystalline silica is known to cause a pulmonary fibrosis referred to as "silicosis." This particulate also induces type-2 immune responses and antigen-specific IgE [12]. Many reports have shown that synthesized particles, such as poly(lactic-co-glycolic acid) (PGLA), polystyrene particles, nickel oxide nanoparticles, carbon nanotubes, and particle pollutants, induce type-2 immune responses, especially antigen-specific production of IgE [13–20]. In addition to artificial particulates, several crystals generated in the body induce inflammatory responses and possess adjuvant activity. Monosodium urate (MSU) crystals are formed if the concentration of uric acid released from damaged cells reaches saturation. MSU crystals also act as an adjuvant that induces type-2 immune responses [21–25]. The bio-crystalline substance hemozoin is a hemin detoxification by-product of malaria parasites. Hemozoin exhibits a potent adjuvant effect and induces antigen-specific immune responses [26]. Chitin particles, which are biopolymers of *N*-acetyl-D-glucosamine found in fungi, helminthes, and insects, induce the accumulation of IL-4-producing eosinophils and basophils and are associated with allergy [27]. In general, PAMPs such as lipopolysaccharide (LPS) and CpG oligodeoxynucleotides are known to induce type-1 immune responses; however these reports indicate that almost all particulates preferentially elicit type-2 immune responses and the induction of IgE. Therefore, it has been hypothesized that the specific signals evoked by particulates in innate cells are involved in triggering adaptive (type-2) responses. Table 11.1 shows the summary of the characteristics of particulate adjuvant in immune responses.

Table 11.1 Summary of characteristics of particulate in immune responses

Particulate	Property	Adjuvant activity	References
Aluminum salt (Alum)	Vaccine adjuvant	Type-2 responses IgE induction	[4–6]
Crystalline silica	Lung disease (silicosis)	Type-2 responses IgE induction	[12]
MSU	Causative agent of gout	Type-2 responses IgE induction	[21–25]
Hemozoin	Hemin detoxification by-product of malaria parasites	Strong adjuvant activity IgG1 induction	[26]
PLGA	Candidate of vaccine adjuvant	IgG1 induction	[13]
Polystyrene particle	Micro-sized particle	IgG1, IgE induction	[14]
Carbon nanotubes	Allotropes of carbon with a cylindrical nanostructure	IgG1, IgE induction	[16, 17]
Nickel oxide	A catalyst of chemical reaction	Pulmonary inflammation IgG1, IgE induction	[15]
Chitin particle	A biopolymer of *n*-acetylglucosamine	Eosinophil activation IL-4 induction	[27]
Diesel exhaust particle	Particle in automobile exhaust	Pulmonary inflammation IgE induction	[18, 19]
Sand dust	Sand dust particles from desert	Pulmonary inflammation IgE induction	[20]

11.3 Particle Size and Immune Responses

Particle size is thought to affect particulate-induced immune responses, and nanometer-sized particulates are believed to display strong adjuvant activity. Several papers have reported that particulates (polystyrene particles or silica crystals) measuring between 430 nm and 1 μm are engulfed and activate macrophage and DCs efficiently to produce cytokines in vitro [13, 28]. In addition, it is reported that hemozoin particles measuring between 50 and 200 nm exhibited a stronger adjuvant effect compared with larger (2–20 μm) and smaller (<50 nm) particles in vivo [26, 29]. These in vitro and in vivo results suggest that particles measuring between 200 nm and 1 μm are the optimal size for phagocytosis and the stimulation of adaptive immune responses.

11.4 The Molecular Mechanisms of Induction of Adaptive Immunity by Particulates

So far, the basis for the adjuvanticity of particulates and the mechanisms by which they elicit adaptive immune responses remain poorly understood. However, recently several papers have demonstrated the molecular mechanisms of induction of adaptive immunity by particulates, especially focusing on alum's effect.

11.4.1 Depot Effect

First, Glenny et al. reported that antigen persistence and prolonged release, an effect referred to as the "depot effect," were responsible for the adjuvanticity of alum [30]. Depot effect has been believed to be the main effect of alum since then. However, a recent report demonstrated that the removal of the injection site 2 h after the administration of antigen/alum had no effect on antigen-specific antibody and T cell responses [31]. This study suggests that the antigen depot does not play an important part in alum adjuvanticity and that alum exhibits additional effects that account for its adjuvant properties.

11.4.2 Inflammasome

In 2008, several reports focused on the discovery that alum adjuvants activate the NLRP3 inflammasome [28, 32]. The inflammasome is a PRR, and there are four classes of inflammasome [8]. The NLRP3 inflammasome is one of best characterized inflammasomes and is activated by particulates and alum [13, 28, 32–37]. As described above, PRRs are considered to be receptor for adjuvant and they are important for the induction of adaptive immunity. In addition, these reports were clearly showing that alum directly activated innate immunity though PRR, and activated NLRP3 inflammasome promoted the secretion of inflammatory cytokines such as IL-1β and IL-18. Interestingly, alum-induced antigen-specific IgG1 responses are significantly reduced in NLRP3 inflammasome-deficient mice in vivo [32, 38]. Similar to alum, most particulate adjuvants are considered to have an adjuvant effect via inflammasome activation because silica, asbestos, PLGA, MSU, and chitin act as activators of the NLRP3 inflammasome. However, other reports have shown that the NLRP3 inflammasome is not required for the induction of adaptive immunity by alum in vivo [26, 39–41]. In addition, the signal transduction triggered by IL-1β and IL-18, which are released by the activation of inflammasomes, is reported to be dispensable for alum adjuvanticity [42, 43]. These results indicate that the NLRP3 inflammasome may participate in adjuvant activity through IL-1β- and IL-18-independent mechanisms, but the role of the NLRP3 inflammasome in the induction of adjuvant activity remains unclear (Fig. 11.2).

11.4.3 MSU Crystal

Uric acid is a purine catabolite that is released from dying or stressed cells. Uric acid forms MSU crystals if the concentration of uric acid is saturated. It is reported that MSU crystals act as DAMPs and stimulate innate immunity to induce the maturation and activation of cells [44]. In addition, similar to alum, MSU crystals are known to activate type-2 immune responses [21–25]. Interestingly, it is reported

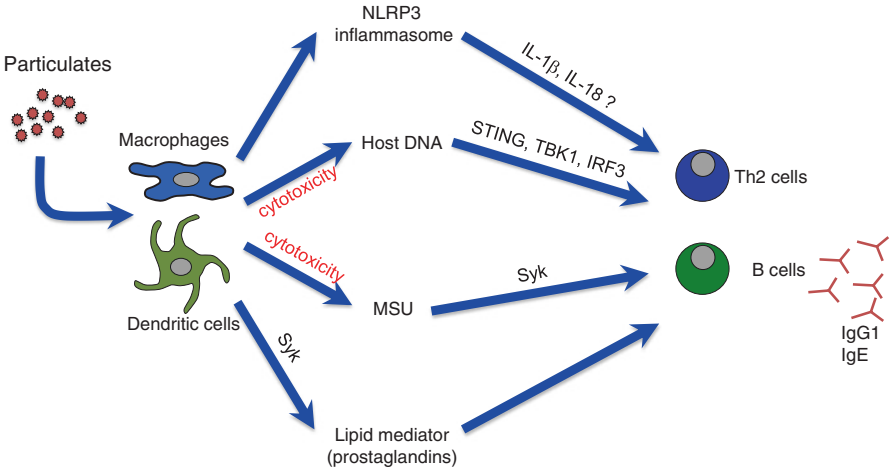

Fig. 11.2 Proposed models of the mechanisms of action of particulate (alum). Initially, particulates are engulfed by phagocyte such as macrophage and dendritic cells. Then particulates stimulate cells to activate NLRP3 inflammasome. Activated inflammasome promotes IL-1β and IL-18 release. Particulates also induce prostaglandin synthesis by the activation of Syk and prostaglandins are generated. Some particulates have cytotoxic activities and induce cell death. Dead cell-derived factors (DAMPs) such as host genomic DNA and MSU stimulate immune cells via specific signal transducer. These factors are involved in the induction of type-2 immune responses. *MSU* monosodium urate, *IRF3* interferon regulatory factor 3, *TBK1* TANK-binding kinase 1, *STING* stimulator of IFN genes, *Syk* the spleen tyrosine kinase

that uric acid is released in the peritoneal cavity after the injection of alum and that alum-induced adaptive immune responses were abolished after uricase treatment [21]. This result indicates that MSU crystals induced by alum cytotoxicity appear to contribute to alum adjuvanticity. Similar to alum and silica, MSU crystals have been reported to activate the NLRP3 inflammasome [34], and this finding is suspected to be linked to the adjuvant activity through the activation of the NLRP3 inflammasome. However, it has been reported that IL-1β, IL-18, and the NLRP3 inflammasome are dispensable for uric acid-dependent adjuvant activity. Interestingly, spleen tyrosine kinase (Syk) was reported to be required for the induction of type-2 immune response by MSU crystal [24]. Syk is a non-receptor tyrosine kinase and a key mediator of immunoreceptor signaling in immune cells. It has been demonstrated that Syk is involved in particulate-mediated innate cell activation [15, 35, 45]. The relationship between MSU crystal-induced adaptive immune responses and Syk is interesting; however the underlying mechanism of Syk activation by particulates is unclear (Fig. 11.2).

Recently, several studies demonstrated the unique recognition mechanisms of particulates. The analysis of the recognition of MSU crystals by DCs using atomic force microscopy is reported. MSU crystals were shown to interact with DCs via receptor-independent mechanisms by directly engaging cell surface lipids (mainly cholesterol) [46]. The aggregation of lipid rafts triggers the recruitment and activation of

Syk, and ultimately, Syk activates phagocytosis and cytokine secretion. Another report has indicated that alum also binds to the surface of DCs, leading to lipid sorting that is similar to MSU crystal-mediated activation of Syk. However, the uptake of alum is not required, and activated DCs interact with T cells via binding with cell surface molecules [47]. Syk appears to be a key molecule for the activation of DCs via lipid sorting, but the mechanisms of Syk activation by MSU or alum are unclear.

11.4.4 Lipid Mediator

Recently, other unique mechanisms for the activation of innate immune cells have been reported. This report demonstrated that alum and silica particulates stimulate innate immunity (macrophages) to produce prostaglandins (PGs) in a similar way to the secretion of IL-1β and IL-18 via NLRP3 activation [15]. In addition to pro-inflammatory cytokines, lipid mediators such as PGs are involved in the induction of inflammatory responses. The well-characterized pro-inflammatory lipid mediator PGE_2 is a metabolite of arachidonic acid that is produced by various types of cells, including antigen-presenting cells, and exhibits various functions in the regulation of immune responses [48].

Silica and alum stimulate innate cells to produce IL-1β, IL-18, and PGE_2. The PGE_2 productions induced by silica and alum have been shown to be independent of the NLRP3 inflammasome because inflammasome-deficient macrophages produced normal levels of PGE_2 in response to silica and alum. Treatment with a Syk inhibitor or the knockdown of Syk using small interfering RNA (siRNA) molecules markedly suppressed the production of PGE_2 after stimulation with silica and alum, demonstrating that Syk regulates particulate-induced PGE_2 production. In this case, the mechanisms of Syk activation by alum and silica are unclear. However, several reports (including those involving studies on MSU crystals) have demonstrated that particulates stimulate innate immune cells via Syk activation. Therefore, Syk may be a key molecule for particulate-induced immune responses (Fig. 11.2).

PGE_2 synthesis is regulated by cyclooxygenase (COX) and PGE synthase (PTGES) [49]. PTGES-deficient macrophages do not produce detectable amounts of PGE_2 after stimulation with silica or alum. In addition, PTGES-deficient mice display reduced amounts of antigen-specific IgE after immunization with alum and silica. In contrast, the levels of antigen-specific IgG are normal in PTGES-deficient mice. These results indicate that particulate-induced PGE_2 is involved in IgE production in vivo [15].

Many particulates that exhibit adjuvant activity, such as MSU crystals, PLGA, chitin particles, nickel oxide, amorphous silica, and carbon nanotubes, stimulate macrophages to produce inflammasome-dependent IL-1β and inflammasome-independent PGE_2. In addition, we have found that, similar to the release of uric acid, increased amounts of PGE_2 are released from damaged cells, suggesting that PGE_2 also works as a DAMP (Kuroda et al., unpublished data). These findings suggest that PGE_2 is a useful marker for the screening of particulate adjuvants.

11.4.5 Nucleic Acids from Host Cells

The activation of innate immunity by DAMPs appears to be a critical mechanism for adjuvant activity. Recently, it was reported that the DNA released from host cells mediates the adjuvant activity of alum [50]. In this study, alum induced the local accumulation of host DNA at the injection site during alum-induced cell death and, interestingly, treatment with DNase I decreased the antigen-specific antibody responses in mice immunized with ovalbumin (OVA) in alum. Purified genomic DNA mixed with OVA induced OVA-specific IgG1 and IgE responses as efficiently as the alum adjuvant. These results indicate that the alum-induced release of host DNA triggers initial innate immune responses. These responses are not dependent on TLRs, RLRs, or inflammasomes, and the mechanisms by which the host DNA triggers the immune response are unclear. However, interferon regulatory factor 3 (IRF3) and TANK-binding kinase 1 (TBK1) are required for the adjuvant activity of alum. In addition, recent report indicated the importance of stimulator of IFN genes (STING) in alum adjuvanticity. It has been reported that antigen-specific IgE responses, but not IgG1 responses, are significantly reduced in IRF3-deficient, TBK1/tumor necrosis factor (TNF)-double-deficient, and STING-deficient mice. Inflammatory DCs (derived from inflammatory monocytes) were identified as the cells responsible for the induction of type-2 immune responses (Fig. 11.2).

IgG1 and IgE responses are uncoupled, i.e., the TBK1-IRF3 axis is required only for only the IgE responses. It is believed that the IgE and IgG1 are regulated by identical mechanisms, which are type-2 immune responses. As described above, PGE_2 is only involved in IgE production, not IgG1 production. Although the mechanisms of the regulation of IgE and IgG1 production and the relationship between IRF3 and PGE_2 remain unclear, the investigation of these mechanisms may help to improve the adjuvants currently in use clinically.

11.5 Prospect of Particulate Adjuvant

Particulate matters can be processed according to their size, shape, electric charge, surface modification, and so on. In addition, many particulates exhibit strong adjuvant activities. For that reason, particulate adjuvants could be promising candidate as adjuvants for new human vaccines, yet no specific receptor(s) is identified. However, as described above, particulate adjuvants elicit type-2 immunity and stimulate the production of IgE and are not efficient in raising cellular immune responses. IgE is known to be a mediator for allergic responses and anaphylaxy shock. The mechanisms that type-2 immune responses are induced by alum are still unclear; however several reports indicated that IgG1 and IgE responses are uncoupled as described above [15, 50]. In addition, recently, the combination adjuvant composed of alum and the TLR ligand monophosphoryl lipid A (MPLA) is used in licensed vaccine. This combination adjuvant has been reported to induce a stronger antibody

response and a shift type-2 to type-1 responses in murine model [51, 52]. These results indicate that particulate adjuvant which does not induce IgE might be developed in the future.

11.6 Conclusion

Particulate adjuvants (including alum) induce adaptive immunity. The development and modulation of adaptive immunity is regulated by innate immunity. However, the basis for the adjuvanticity of particulates and the mechanisms by which particulates activate innate immunity are not fully understood. Alum has been used as a safe vaccine adjuvant in humans, but the limitations of alum include local reactions and the augmentation of IgE antibody responses [4, 53]. These limitations reflect the need for continuing research, and these limitations may be overcome by elucidation of the mechanisms of the effect of particulate adjuvants on immune responses. Advances in adjuvant research could open new possibilities for the treatment of not only infectious diseases but also allergic inflammation and cancer (**This is a modified review based on ref. 54*).

Acknowledgments Etsushi Kuroda was supported in part by Regional Innovation Strategy Support Program and Grant-in-Aid for Scientific Research from the Ministry of Education, Culture, Sports, Science and Technology of Japan (grant number 24591145). Cevayir Coban and Ken J Ishii are supported by a Health and Labour Sciences Research Grant "Adjuvant database Project" of the Japanese Ministry of Health, Labour and Welfare."

Declaration of Interest The authors have no conflict of interest to declare. The authors alone are responsible for the content and writing of this article.

Abbreviations

CLR	C-type lectin receptor
COX	Cyclooxygenase
CTL	Cytotoxic T lymphocyte
DAMP	Damage-associated molecular pattern
DC	Dendritic cell
Ig	Immunoglobulin
IL	Interleukin
IRF3	Interferon regulatory factor 3
KO	Knockout
LPS	Lipopolysaccharide
MPLA	Monophosphoryl lipid A
MSU	Monosodium urate
NK	Natural killer
NLR	Nod-like receptor

OVA	Ovalbumin
PAMP	Pathogen-associated molecular pattern
PG	Prostaglandin
PGLA	Poly(lactic-co-glycolic acid)
PRR	Pattern-recognition receptor
PTGES	PGE synthase
RLR	RIG-I-like receptor
siRNA	Small interfering RNA
STING	Stimulator of IFN genes
Syk	The spleen tyrosine kinase
TBK1	TANK-binding kinase 1
Th1	Helper T cell type 1
Th2	Helper T cell type 2
TLR	Toll-like receptor
TNF	Tumor necrosis factor
WT	Wild type

References

1. Akira S (2011) Innate immunity and adjuvants. Philp Trans R Soc B 366:2748–2755
2. Iwasaki A, Medzhitov R (2010) Regulation of adaptive immunity by the innate immune system. Science 327:291–295
3. Coquerelle C, Moser M (2010) DC subsets in positive and negative regulation of immunity. Immunol Rev 234:317–334
4. Gupta RK (1998) Aluminum compounds as vaccine adjuvants. Adv Drug Deliv Rev 32:155–172
5. Aimanianda V, Haensler J, Lacroix-Desmazes S, Kaveri SV, Bayry J (2009) Novel cellular and molecular mechanisms of induction of immune responses by aluminum adjuvants. Trends Pharmacol Sci 30:287–295
6. Marrack P, McKee AS, Munks MW (2009) Towards an understanding of the adjuvant action of aluminium. Nat Rev Immunol 9:287–293
7. Kawai T, Akira S (2011) Toll-like receptors and their crosstalk with other innate receptors in infection and immunity. Immunity 34:637–650
8. Elinav E, Strowig T, Henao-Mejia J, Flavell Richard A (2011) Regulation of the antimicrobial response by NLR proteins. Immunity 34:665–679
9. Loo Y-M, Gale M (2011) Immune signaling by RIG-I-like receptors. Immunity 34:680–692
10. Osorio F, Reis e Sousa C (2011) Myeloid C-type lectin receptors in pathogen recognition and host defense. Immunity 34:651–664
11. Desmet CJ, Ishii KJ (2012) Nucleic acid sensing at the interface between innate and adaptive immunity in vaccination. Nat Rev Immunol 12:479–491
12. Mancino D, Buono G, Cusano M, Minucci M (1983) Adjuvant effects of a crystalline silica on IgE and IgG1 antibody production in mice and their prevention by the macrophage stabilizer poly-2-vinylpyridine N-oxide. Int Arch Allergy Appl Immunol 71:279–281
13. Sharp FA, Ruane D, Claass B, Creagh E, Harris J, Malyala P et al (2009) Uptake of particulate vaccine adjuvants by dendritic cells activates the NALP3 inflammasome. Proc Natl Acad Sci U S A 106:870–875
14. Nygaard UC, Aase A, Lovik M (2005) The allergy adjuvant effect of particles – genetic factors influence antibody and cytokine responses. BMC Immunol 6:11

15. Kuroda E, Ishii Ken J, Uematsu S, Ohata K, Coban C, Akira S et al (2011) Silica crystals and aluminum salts regulate the production of prostaglandin in macrophages via NALP3 inflammasome-independent mechanisms. Immunity 34:514–526
16. Inoue K, Koike E, Yanagisawa R, Hirano S, Nishikawa M, Takano H (2009) Effects of multi-walled carbon nanotubes on a murine allergic airway inflammation model. Toxicol Appl Pharmacol 237:306–316
17. Nygaard UC, Hansen JS, Samuelsen M, Alberg T, Marioara CD, Lovik M (2009) Single-walled and multi-walled carbon nanotubes promote allergic immune responses in mice. Toxicol Sci 109:113–123
18. Ichinose T, Takano H, Miyabara Y, Yanagisawa R, Sagai M (1997) Murine strain differences in allergic airway inflammation and immunoglobulin production by a combination of antigen and diesel exhaust particles. Toxicology 122:183–192
19. Lovik M, Hogseth AK, Gaarder PI, Hagemann R, Eide I (1997) Diesel exhaust particles and carbon black have adjuvant activity on the local lymph node response and systemic IgE production to ovalbumin. Toxicology 121:165–178
20. Hiyoshi K, Ichinose T, Sadakane K, Takano H, Nishikawa M, Mori I et al (2005) Asian sand dust enhances ovalbumin-induced eosinophil recruitment in the alveoli and airway of mice. Environ Res 99(3):361–368
21. Kool M, Soullie T, van Nimwegen M, Willart MAM, Muskens F, Jung S et al (2008) Alum adjuvant boosts adaptive immunity by inducing uric acid and activating inflammatory dendritic cells. J Exp Med 205:869–882
22. Behrens MD, Wagner WM, Krco CJ, Erskine CL, Kalli KR, Krempski J et al (2008) The endogenous danger signal, crystalline uric acid, signals for enhanced antibody immunity. Blood 111:1472–1479
23. Willart MAM, Lambrecht BN (2009) The danger within: endogenous danger signals, atopy and asthma. Clin Exp Allergy 39:12–19
24. Kool M, Willart Monique AM, van Nimwegen M, Bergen I, Pouliot P, Virchow JC et al (2011) An unexpected role for uric acid as an inducer of T helper 2 cell immunity to inhaled antigens and inflammatory mediator of allergic asthma. Immunity 34:527–540
25. Kool M, Hammad H, Lambrecht B (2012) Cellular networks controlling Th2 polarization in allergy and immunity. F1000 Biol Rep 4:6
26. Coban C, Igari Y, Yagi M, Reimer T, Koyama S, Aoshi T et al (2010) Immunogenicity of whole-parasite vaccines against plasmodium falciparum involves malarial hemozoin and host TLR9. Cell Host Microbe 7:50–61
27. Reese TA, Liang H-E, Tager AM, Luster AD, Van Rooijen N, Voehringer D et al (2007) Chitin induces accumulation in tissue of innate immune cells associated with allergy. Nature 447:92–96
28. Hornung V, Bauernfeind F, Halle A, Samstad EO, Kono H, Rock KL et al (2008) Silica crystals and aluminum salts activate the NALP3 inflammasome through phagosomal destabilization. Nat Immunol 9:847–856
29. Coban C, Yagi M, Ohata K, Igari Y, Tsukui T, Horii T et al (2010) The malarial metabolite hemozoin and its potential use as a vaccine adjuvant. Allergol Int 59:115–124
30. Glenny AT, Pope CG, Waddington H, Wallace U (1926) Immunological notes XVLL.-XXIV. J Pathol Bacteriol 29(1):31–40
31. Hutchison S, Benson RA, Gibson VB, Pollock AH, Garside P, Brewer JM (2011) Antigen depot is not required for alum adjuvanticity. FASEB J 26:1272–1279
32. Eisenbarth SC, Colegio OR, O'Connor W, Sutterwala FS, Flavell RA (2008) Crucial role for the Nalp3 inflammasome in the immunostimulatory properties of aluminium adjuvants. Nature 453:1122–1126
33. Dostert C, Petrilli V, Van Bruggen R, Steele C, Mossman BT, Tschopp J (2008) Innate immune activation through Nalp3 inflammasome sensing of asbestos and silica. Science 320:674–677
34. Martinon F, Petrilli V, Mayor A, Tardivel A, Tschopp J (2006) Gout-associated uric acid crystals activate the NALP3 inflammasome. Nature 440:237–241
35. Tiemi Shio M, Eisenbarth SC, Savaria M, Vinet AF, Bellemare M-J, Harder KW et al (2009) Malarial hemozoin activates the NLRP3 inflammasome through Lyn and Syk kinases. PLoS Pathog 5:e1000559

36. Dostert C, Guarda G, Romero JF, Menu P, Gross O, Tardivel A et al (2009) Malarial hemozoin is a Nalp3 inflammasome activating danger signal. PLoS One 4:e6510
37. Griffith JW, Sun T, McIntosh MT, Bucala R (2009) Pure Hemozoin is inflammatory in vivo and activates the NALP3 inflammasome via release of uric acid. J Immunol 183:5208–5220
38. Li H, Willingham SB, Ting JP, Re F (2008) Cutting edge: inflammasome activation by alum and alum's adjuvant effect are mediated by NLRP3. J Immunol 181:17–21
39. McKee AS, Munks MW, MacLeod MKL, Fleenor CJ, Van Rooijen N, Kappler JW et al (2009) Alum induces innate immune responses through macrophage and mast cell sensors, but these sensors are not required for alum to act as an adjuvant for specific immunity. J Immunol 183:4403–4414
40. Kool M, Petrilli V, De Smedt T, Rolaz A, Hammad H, van Nimwegen M et al (2008) Cutting edge: alum adjuvant stimulates inflammatory dendritic cells through activation of the NALP3 inflammasome. J Immunol 181:3755–3759
41. Franchi L, Núñez G (2008) The Nlrp3 inflammasome is critical for aluminium hydroxide-mediated IL-1β secretion but dispensable for adjuvant activity. Eur J Immunol 38:2085–2089
42. Schnare M, Barton GM, Holt AC, Takeda K, Akira S, Medzhitov R (2001) Toll-like receptors control activation of adaptive immune responses. Nat Immunol 2:947–950
43. Gavin AL, Hoebe K, Duong B, Ota T, Martin C, Beutler B et al (2006) Adjuvant-enhanced antibody responses in the absence of toll-like receptor signaling. Science 314:1936–1938
44. Shi Y, Evans JE, Rock KL (2003) Molecular identification of a danger signal that alerts the immune system to dying cells. Nature 425:516–521
45. Shi Y, Mucsi AD, Ng G (2010) Monosodium urate crystals in inflammation and immunity. Immunol Rev 233:203–217
46. Ng G, Sharma K, Ward SM, Desrosiers MD, Stephens LA, Schoel WM et al (2008) Receptor-independent, direct membrane binding leads to cell-surface lipid sorting and Syk kinase activation in dendritic cells. Immunity 29:807–818
47. Flach TL, Ng G, Hari A, Desrosiers MD, Zhang P, Ward SM et al (2011) Alum interaction with dendritic cell membrane lipids is essential for its adjuvanticity. Nat Med 17:479–487
48. Narumiya S (2009) Prostanoids and inflammation: a new concept arising from receptor knockout mice. J Mol Med (Berl) 87:1015–1022
49. Uematsu S, Matsumoto M, Takeda K, Akira S (2002) Lipopolysaccharide-dependent prostaglandin E(2) production is regulated by the glutathione-dependent prostaglandin E(2) synthase gene induced by the toll-like receptor 4/MyD88/NF-IL6 pathway. J Immunol 168:5811–5816
50. Marichal T, Ohata K, Bedoret D, Mesnil C, Sabatel C, Kobiyama K et al (2011) DNA released from dying host cells mediates aluminum adjuvant activity. Nat Med 17:996–1002
51. Didierlaurent AM, Morel S, Lockman L, Giannini SL, Bisteau M, Carlsen H et al (2009) AS04, an aluminum salt- and TLR4 agonist-based adjuvant system, induces a transient localized innate immune response leading to enhanced adaptive immunity. J Immunol 183(10):6186–6197
52. Giannini SL, Hanon E, Moris P, Van Mechelen M, Morel S, Dessy F et al (2006) Enhanced humoral and memory B cellular immunity using HPV16/18 L1 VLP vaccine formulated with the MPL/aluminium salt combination (AS04) compared to aluminium salt only. Vaccine 24(33–34):5937–5949
53. Nagel J, Svec D, Waters T, Fireman P (1977) IgE synthesis in man. I. Development of specific IgE antibodies after immunization with tetanus-diphtheria (Td) toxoids. J Immunol 118:334–341
54. Kuroda E, Coban C, Ishii KJ (2013) Particulate adjuvant and innate immunity: past achievements, present findings, and future prospects. Int Rev Immunol 32(2):209–220

Chapter 12
Functional Nanoparticles for Vaccine Delivery Systems

Takami Akagi and Misturu Akashi

Abstract One of the most important current issues in vaccinology is the need for vaccine delivery systems and adjuvants as an immune stimulator (immunostimulant). Polymeric nanoparticles with entrapped vaccine antigens, such as proteins, peptides, and DNA, have recently been shown to possess significant potential as vaccine delivery systems and immunostimulants. Novel nanoparticle-based vaccines are being evaluated in a variety of vaccine therapy including infectious diseases, cancers, or autoimmune diseases. Biodegradable nanoparticles that can control physicochemical properties, such as particle size, surface charge, and polymer composition, are promising candidate adjuvant systems to enhance vaccine efficacy. In this review, polymeric nanoparticles as vaccine delivery systems and immunostimulants are addressed with focus on (1) targeting of antigens to antigen-presenting cells (APCs), (2) control of the intracellular trafficking and biodistribution of nanoparticles, and (3) activation of APCs by particles for the development of effective vaccines. Understanding the strategies and mechanisms of immune induction by nanoparticle-based vaccines will help in the design guide of nanoparticle for the development of novel adjuvants. The development of safe and efficacious novel adjuvants is strongly desired. Vaccine delivery systems mainly function to target antigens to APCs, and immunostimulants directly activate these cells through specific receptors. The targeting antigen specifically to dendritic cells (DCs) and their subsequent activation with nanoparticles has demonstrated exciting potential for developing new vaccine technology. Uptake of nanoparticles by DCs can be controlled by altering properties of the nanoparticles, including size and surface characteristics. Moreover, novel chemical strategies can be employed to modulate DC maturation and immune presentation of antigens. This approach will enable both preventative and therapeutic vaccination for immune diseases requiring cellular immunity.

Keywords Dendritic cells • Drug delivery system • Nanoparticles • Vaccine adjuvant

T. Akagi • M. Akashi (✉)
Department of Applied Chemistry, Graduate School of Engineering, Osaka University,
2-1 Yamadaoka, Suita 565-0871, Japan
e-mail: akashi@chem.eng.osaka-u.ac.jp

M. Akashi et al. (eds.), *Engineered Cell Manipulation for Biomedical Application*, Nanomedicine and Nanotoxicology,
DOI 10.1007/978-4-431-55139-3_12

12.1 Introduction

The purpose of vaccination is to generate a strong immune response, thus providing long-term protection against infection. When compared to traditional vaccines, which mainly consisted of attenuated pathogens, whole inactivated organisms, or inactivated bacterial toxins, the new generation of vaccines such as subunit antigenic proteins or peptides is less reactogenic and immunogenic and thus requires the use of adjuvants to induce optimal immune responses [1–5]. Adjuvants are compounds that enhance the immune response against co-inoculated antigens, with the word adjuvant coming from the Latin word *adjuvare*, which means to help or to enhance. In the past, many kinds of adjuvant have been developed, and they can be divided into two classes on the basis of their mechanism of action: vaccine delivery systems and immunostimulants [6]. Vaccine delivery systems generally have a particulate form (e.g., emulsions, liposomes, micelles, and polymeric nano-/microparticles) and function mainly to target associated antigens into antigen-presenting cells (APCs) such as dendritic cells (DCs) and macrophages. In contrast, immunostimulants mostly consist of pathogen-associated molecule (e.g., lipopolysaccharide, monophosphoryl lipid A, cholera toxin, CpG ODN), which activate cells of the innate immune system via specific receptors.

Until recently, hydroxide and phosphate salts of aluminum and calcium were the only adjuvants licensed for human use. Aluminum hydroxide or phosphate salts, commonly called alum, have dominated adjuvant use since the discovery of its adjuvant effect in the 1920s [7]. The mechanism of action of alum adjuvant is complex and not yet fully understood. It likely involves various mechanisms including the formation of depot, increasing targeting of antigens to APCs, and nonspecific activation of immune systems. Many adjuvants function in a manner similar to alum by providing an antigen depot. Antigen depots enhance immunogenicity of antigens by concentrating the peptides and extending the time antigen resides in the body, thus increasing the probability of interaction with immune cells. However, the use of alum-type adjuvant for vaccination has some disadvantages [8, 9]. They induce local reactions, induce IgE antibody responses, and generally fail to induce cell-mediated immunity, particularly cytotoxic T lymphocyte (CTL) responses. Therefore, the development of more efficient and safe adjuvants to obtain high and long-lasting immune responses is of primary importance.

Polymeric nanoparticles formulated from synthetic or biodegradable polymers are widely explored as carriers for controlled delivery of different agents including proteins, peptides, plasmid DNA (pDNA), and low-molecular-weight compounds [10–12]. Numerous investigators have shown that the biological distribution of drugs, proteins, and DNA can be modified, both at the cellular and organ levels, using nano-/microparticle delivery systems [13, 14]. For the development of vaccines, biodegradable nanoparticles show great promise as delivery systems. Controlled delivery systems consisting of nanoparticles can potentially delivery either the antigens or immunostimulants to the desired location at predetermined rates and durations to generate an optimal immune response. The carrier may also

protect the vaccine from degradation until it is released. Other potential advantages of the controlled delivery approach include reduced systemic side effects and the possibility of co-encapsulating multiple antigenic epitopes or both antigen and immunostimulant in a single carrier. Biodegradable polymers provide sustained release of the encapsulated antigen and degrade in the body to nontoxic, low-molecular-weight products that are easily eliminated.

This review focuses on biodegradable polymeric nanoparticles as vaccine delivery systems and immunostimulants by summarizing the preparation of antigen-conjugated particles and the mechanism of nanoparticle-based vaccines. Theoretically, nanoparticles are solid particles ranging in size from 1 to 1,000 nm, while microparticles are particles that have sizes that range from 1 to 1,000 μm [15]. In the design of optimal vaccine delivery systems, polymeric nanoparticles have the advantage that their physicochemical properties such as particle size, shape, surface charge, and polymer composition can be regulated. Using these systems, it is possible to target antigen delivery to APCs, activate these APCs, and control intracellular release and distribution of the antigen (Fig. 12.1). By understanding immune

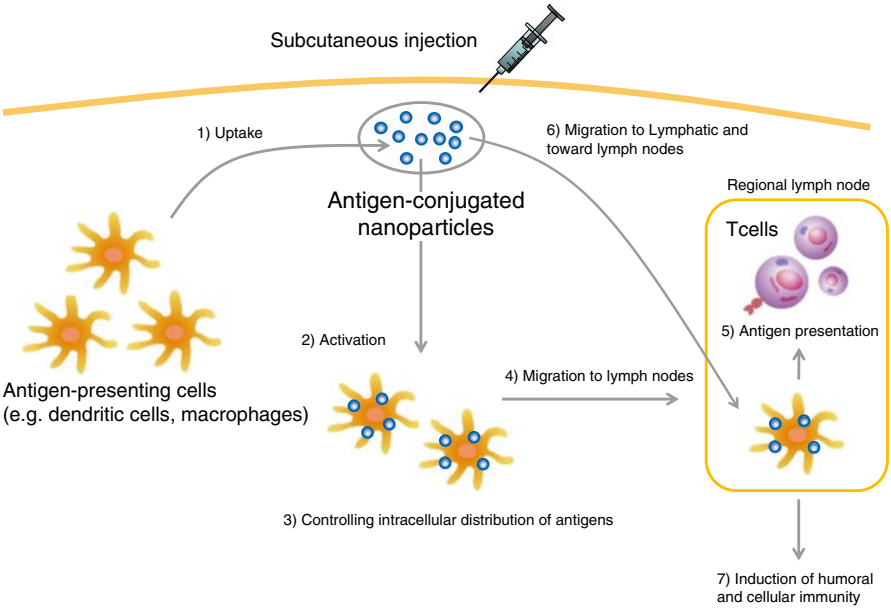

Fig. 12.1 Desired function of particulate antigens as vaccine delivery systems and immunostimulants for induction and regulation of antigen-specific immune responses. Antigen-conjugated nanoparticles administered by a systemic route may (*1*) be directly taken up by APCs, such as dendritic cells and macrophages; (*2*) activate APCs through specific receptors (may be related to Toll-like receptors). Particle size affects DC uptake and activation processes. Particles can be conjugated with DC-specific antibodies to increase targeting. (*3*) pH-sensitive particles can control intracellular distribution of antigen. The particles disrupt endosomes and release antigens to the cytoplasm. (*4*) Particles taken up by APCs migrate to lymph nodes, (*5*) where they mature and present antigen to T cells. (*6*) Small particles (>50 nm) can enter lymphatic vessels directly and migrate to lymph nodes with the lymphatic flow, where they are taken up by immature DCs resident in the nodes

activation, we can rationally design particulate adjuvant to not only deliver antigen but also directly activate innate immune cells providing the pro-inflammatory context for antigen recognition. The generation of more potent particulate adjuvants may allow the development of prophylactic and therapeutic vaccines against cancers and chronic infectious diseases.

12.2 Preparation of Biodegradable Polymeric Nanoparticles for Antigen Delivery

12.2.1 Aliphatic Polyester-Based Nanoparticles

Biodegradable polymeric nanoparticles have attracted much attention for their potential in biomedical applications. The biodegradation rate and the release kinetics of loaded drugs can be controlled by the composition ratio and the molecular weight of the polymer and block/graft copolymers [16–18]. Furthermore, by modulating the polymer characteristics, one can control the release of a therapeutic agent from the nanoparticles to achieve a desired therapeutic level in a target tissue for the required duration for optimal therapeutic efficacy. The commonly used biodegradable polymers are aliphatic polyesters, such as poly(lactic acid) (PLA), poly(glycolic acid) (PGA), poly(ε-caprolactone) (PCL), poly(hydroxybutyrate) (PHB), and their copolymers (Fig. 12.2) [19]. In particular, poly(lactide-*co*-glycolide) (PLGA) has been the most extensively investigated for developing nano-/microparticles

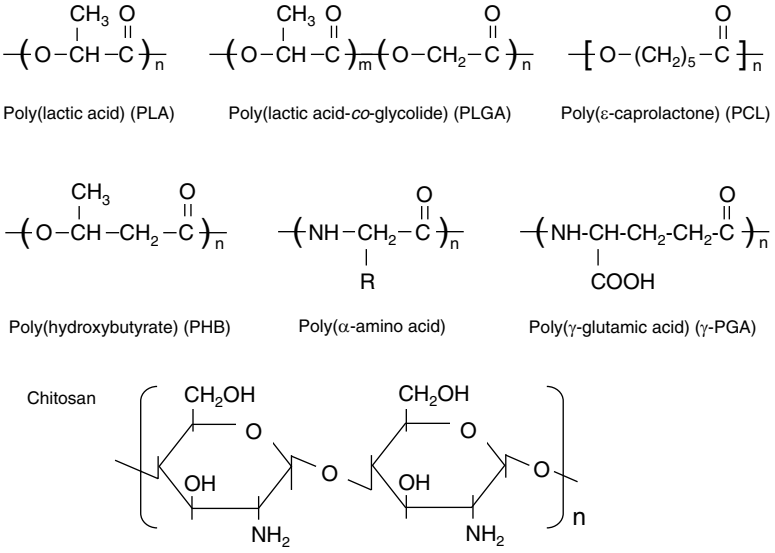

Fig. 12.2 Chemical structures of biodegradable polymers used for preparation of nanoparticles

encapsulating therapeutic drugs in controlled release applications [20–22] due to their inherent advantages. The copolymers have the advantage of sustaining the release of the encapsulated therapeutic agent over a period of days to several weeks. As polyesters in nature, these polymers undergo hydrolysis upon administration into the body, forming biologically compatible and metabolizable moieties (lactic acid and glycolic acid) that are eventually removed from the body by the citric acid cycle.

Antigen-conjugated nanoparticles are being investigated as vaccine delivery system alternatives to the currently used alum with an objective to develop better vaccine systems and minimize the frequency of immunization. The encapsulation of antigenic proteins or peptides into PLGA nanoparticle delivery system can be carried out through mainly three methods: the water-in-oil-in-water (w/o/w) emulsion technique, phase separation, and spray drying. The w/o/w double emulsion process is popularly used to load proteins into nanoparticles [23, 24]. In this process, an antigen is first dissolved in an aqueous solution, which is then emulsified in an organic solvent to make a primary water-in-oil emulsion. This initial emulsion is further mixed in an emulsifier-containing aqueous solution to make a w/o/w double emulsion. The ensuing removal of the solvent leaves nano-/microparticles in the aqueous continuous phase, making it possible to collect them by filtration or centrifugation. However, the possible denaturation of the proteins at the oil–water interface limits the usage of this method. It has been reported that this interface causes conformational changes in bovine serum albumin (BSA) [25, 26]. Moreover, it has a disadvantage in that the entrapment efficiency is very low. The prevention of protein denaturation and degradation, as well as high entrapment efficiency, would be of particular importance in the preparation of nanoparticles containing water-soluble drugs such as a protein. Improved protein integrity has been achieved by the addition of stabilizers such as carrier proteins (e.g., albumin), surfactants during the primary emulsion phase, or molecules such as trehalose and mannitol to the protein phase. The use for vaccines of these protein-loaded PLGA nanoparticles is described in the following sections.

12.2.2 Amphiphilic Poly(Amino Acid) Nanoparticles

Self-assembling polymer or block/graft copolymers that can form nanostructure have been extensively investigated in the field of biotechnology and pharmaceuticals. In general, hydrophobic interactions, electrostatic forces, hydrogen bonds, van der Waals forces, or combinations of these interactions are available as the driving forces for the formation of the polymer complexes [27–31]. Nanoparticles fabricated by the self-assembly of amphiphilic block copolymers or hydrophobically modified polymers have been explored as drug carrier systems. In general, these amphiphilic copolymers consisting of hydrophilic and hydrophobic segments are capable of forming polymeric structures in aqueous solutions via hydrophobic interactions. These self-assembled nanoparticles are composed of an inner core of hydrophobic moieties and an outer shell of hydrophilic groups [32, 33].

In particular, poly(amino acids) have received considerable attention for their medical applications as potential polymeric drug carriers. Several amphiphilic block and graft copolymers based on poly(amino acid) have been employed, such as poly(α-L-glutamic acid) [34], poly(γ-glutamic acid) [35], poly(ε-lysine) [36], poly(L-aspartic acid) [37], poly(L-lysine) [38], poly(L-arginine) [39], and poly(L-asparagine) [40] as hydrophilic segments and poly(β-benzyl-L-aspartate) [41], poly(γ-benzyl-L-glutamate) [42], and poly(L-histidine) [43] as hydrophobic segments. In general, amphiphilic copolymers based on poly(amino acid) form micelles through self-association in water.

Poly(γ-glutamic acid) (γ-PGA) is a naturally occurring poly(amino acid) that is synthesized by certain strains of *Bacillus* [44] (Fig. 12.2). The polymer is made of D- and L-glutamic acid units linked through the α-amino and the γ-carboxylic acid groups, and its α-carboxylate side chains can be chemically modified to introduce various bioactive ligands or to modulate the overall function of the polymer [45–49]. Unlike general poly(amino acids), γ-PGA has unique characteristics with regard to enzymatic degradation and immunogenicity, compared to poly(amino acid) consisting of L-amino acid. It has been reported that γ-PGA is resistant against many proteases because γ-linked glutamic acids are not easily recognized by common proteases [50, 51]. Moreover, several studies have shown that γ-PGA by itself is a poor immunogen and does not induce booster responses, probably because of its simple homopolymeric structure, similar to those of polysaccharides [52–56]. Therefore, the potential applications of γ-PGA and its derivatives have been of interest in a broad range of fields, including medicine, food, cosmetic, and water treatment [57].

Akashi et al. prepared nanoparticles composed of hydrophobically modified γ-PGA [36, 58, 59]. γ-PGA (400 kDa) as the hydrophilic backbone and L-phenylalanine (Phe) as the hydrophobic segment were synthesized by grafting Phe to γ-PGA using water-soluble carbodiimide. The γ-PGA-*graft*-Phe copolymers (γ-PGA-Phe) with more than 50 % grafting degree formed monodispersed nanoparticles in water due to their amphiphilic properties (Fig. 12.3). To prepare nanoparticles,

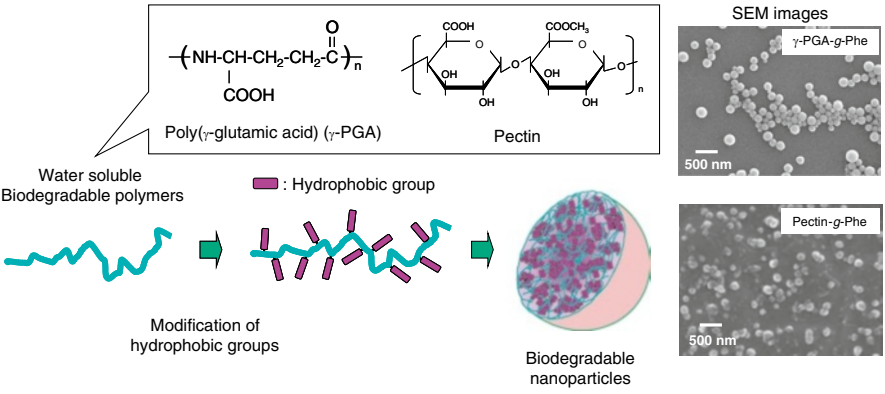

Fig. 12.3 Synthesis of biodegradable nanoparticles composed of amphiphilic copolymers for vaccine development

γ-PGA-Phe dissolved in dimethyl sulfoxide (DMSO) was added to various concentration of NaCl solution, and then the resulting solutions were dialyzed and freeze-dried. The γ-PGA-Phe formed monodispersed nanoparticles, and the particle size of the γ-PGA-Phe nanoparticles could be easily controlled (30–200 nm) by changing NaCl concentration [60]. In addition, the nanoparticles consisting of amphiphilic γ-PGA can efficiently and stably encapsulate various types of protein (11 different proteins with various molecular weights and isoelectric points, e.g., thyroglobulin, ovalbumin, lysozyme). Protein-loaded γ-PGA-Phe nanoparticles were prepared by encapsulation, covalent immobilization, or physical adsorption methods in order to study their potential applications as protein carriers [61]. To prepare the protein-encapsulated γ-PGA-Phe nanoparticles, proteins with various molecular weights and isoelectric points were dissolved in saline, and the γ-PGA-Phe dissolved in DMSO was added to the protein solutions. The resulting solutions were then centrifuged and repeatedly rinsed. The encapsulation of proteins into the nanoparticles was successfully achieved. The encapsulation efficiency was found to be in 50 % for most samples and was not markedly influenced by the physical properties of that protein [62]. Ovalbumin (OVA) encapsulated into the nanoparticles was not released (less than 10 %) over the pH range of 4–8, even after 10 days. Also, Portilla-Arias et al. reported the preparation of nanoparticles made of alkyl esters of γ-PGA and their potential application as drug and protein carrier [63]. Besides the particle formation of γ-PGA by using hydrophobic interaction, nanoparticles formed by complexation of γ-PGA with bivalent metal ion complex [64] or chemical cross-linking of carboxyl group of γ-PGA [65] have been reported.

12.2.3 Amphiphilic Polysaccharide Nanoparticles

Polysaccharidic hydrogel particles have been often used for designing protein-loaded systems for therapeutic applications. Polysaccharides are very hydrophilic polymers, and their hydrogels thus exhibit a good biocompatibility. Various types of hydrophobized polysaccharides, such as pullulan [66, 67], curdlan [68], dextran [69], alginic acid [70], and chitosan [71], have been used for preparation of nanoparticles. Akiyoshi et al. reported that self-aggregated hydrogel nanoparticles could be formed from cholesterol-bearing pullulan by an intra- and/or intermolecular association in diluted aqueous solutions [72]. Recently, much attention has been paid to chitosan as a drug or gene carrier because of its biocompatibility and biodegradability. Chitosan is a polysaccharide constituted by *N*-glucosamine and *N-acetyl-glucosamine* units, in which the number of *N*-glucosamine units exceeds 50 %. Chitosan can be degraded into nontoxic products in vivo, and thus, it has been widely used in various biomedical applications [73, 74]. Chitosan has cationic characters even in neutral condition to form complexes with negatively charged pDNA. Jeong et al. prepared nano-sized self-aggregates composed of hydrophobically modified chitosans with deoxycholic acids [75, 76]. The size of self-aggregates varied in the range of 130–300 nm in diameter, and their structures were found to depend strongly on the molecular weight of

chitosan. To explore the potential applications of self-aggregates as a gene delivery carrier, complexes between chitosan self-aggregates and pDNA were prepared. The complex formation had strong dependency on the size and structure of chitosan self-aggregates and significantly influenced the transfection efficiency of cells. It is expected that these approaches to control the size and structure of chitosan-derived self-aggregates have a wide range of applications in gene delivery. Also, Kida et al. reported that novel polysaccharide-based nanoparticles were successfully prepared by the self-assembly of amphiphilic pectins, which were easily synthesized by the reaction of pectins with L-PHENYLALANINE (Phe) as hydrophobic groups (Fig. 12.3) [77]. Pectin is a polymer of D-galacturonic acid. The galacturonic acid molecule has a carboxyl group on C5, some of which are esterified to form methyl esters. The pectin-*graft*-Phe could form about 200-nm-sized nanoparticles and were able to retain entrapped protein in the nanoparticles for 1 week without any significant leakage.

12.3 Uptake of Particulate Antigens by APCs

Biodegradable polymeric nanoparticles can be designed to fill various roles in antigen delivery, and they have been used to release antigens in a controlled manner. However, recent strategies for developing preventative and therapeutic vaccines have focused on the ability to deliver antigen to dendritic cells (DCs) in a targeted and prolonged manner. These strategies use nanoparticles because they can achieve longevity on intact antigen to increase the opportunity for DC uptake and processing. DCs are the most effective antigen-presenting cells (APCs) and have a crucial role in initiating T-cell-mediated immunity. DCs can control a substantial part of the adaptive immune response by internalizing and processing antigen through major histocompatibility complex (MHC) class I and class II pathways and then presenting antigenic peptides to $CD4^+$ and $CD8^+$ T lymphocytes [78]. Therefore, targeting DCs with an antigen delivery system provides tremendous potential in developing new vaccines [79]. Macrophages present endogenous antigens, such as those derived from viral expression, on MHC class I complexes. On the other hand, phagocytosed antigens are cleaved by lysosomal enzymes and expressed as MHC class II complexes. In contrast, dendritic cells can present soluble exogenous antigens as MHC class I complexes. This phenomenon has given rise to the theory of cross-priming, involving proteasomal degradation in the cytosol. Antigen uptake by DCs is enhanced by the association of the antigens with polymeric nanoparticles. It is mediated by several uptake mechanisms such as receptor-mediated endocytosis, macropinocytosis, and phagocytosis, depending on the nature of the particulate antigen [80]. Interactions between particulate formulations and cells in general depend on particle characteristics such as size, shape, and surface properties, including surface charge and hydrophobicity.

Akagi et al. demonstrated the use of nanoparticles composed of amphiphilic poly(amino acid) derivatives as adjuvants [81–84]. To evaluate the uptake of OVA-encapsulated γ-PGA-Phe nanoparticles (OVA-NPs) by DCs, murine bone

marrow-derived DCs were incubated with 250-nm-sized OVA-NPs for 30 min at 37 °C. The cells were then analyzed by flow cytometry (FCM) and confocal laser scanning microscopy (CLSM). OVA-NPs were efficiently taken up into DCs, whereas the uptake of OVA alone was barely detectable at the same concentration of OVA. OVA-NPs were more efficiently taken up than OVA alone by DCs, and the uptake of OVA-NPs was inhibited at 4 °C [81]. These results suggest that OVA-NPs were phagocytosed mainly via endocytosis by the DCs. In the case of OVA alone, an approximately 30-fold higher concentration was required to elicit a similar amount of intracellular OVA as compared to OVA-NPs. Likewise, it has been reported that PLGA nanoparticles or liposomes are efficiently phagocytosed by the DCs in culture, resulting in their intracellular localization [85–87]. Foged et al. investigated DC uptake of model fluorescent polystyrene particles with a broad size range (0.04–15 μm). The results showed that DC internalized particles in the tested size range with different efficiencies. The optimal particle size for DC uptake was 500 nm and below. In the smaller particle size, the higher percentage of the DCs interacted with the polystyrene spheres [88]. Kanchan et al. also reported that PLA nanoparticles (200–600 nm) were efficiently taken up by macrophages in comparison to microparticles (2–8 μm) [89]. In contrast, in hydrogel particles composed of polyacrylamide, there was no difference in uptake by APCs between 3.5-μm and 35-nm-sized particles [90]. This disparity in uptake may be related to fundamental differences in the material properties of those carriers.

Particle shape and surface charge are equally important particulate physicochemical factors and play a crucial role for the interaction between particles and APCs. In general, cationic particles induced high phagocytosis activity of APCs, because of anionic nature of cell membranes [88]. Recently, particle shape has been identified as having a significant effect on the ability of macrophages to internalize particles via actin-driven movement of the macrophage membrane. Champion et al. observed that the cellular uptake of particles strongly depends on the shape of particles. The wormlike particles with very high aspect ratios exhibited negligible phagocytosis when compared to traditional spherical particles [91, 92]. These results suggest that uptake of particles by APCs strongly depends on the local geometry at the interface of particle and the cells.

12.4 Control of Intracellular Distribution of Nanoparticles

In general, particulate materials can be easily internalized into the cells via endocytosis, depending on their sizes, shapes, and surface charges. However, the internalized materials are mostly trafficked from acidic endosomes to lysosomes, where the degradation may occur. Thus, degraded exogenous antigens are presented by the MHC class II presentation pathway, and a part of the pathway involves antibody-medicated immune responses. In contrast, antigens within the cytosol are processed into proteasomes and presented by the MHC class I pathway, a pathway involved in CTL response [93–95] (Fig. 12.4). Therefore, the induction of antigen-specific

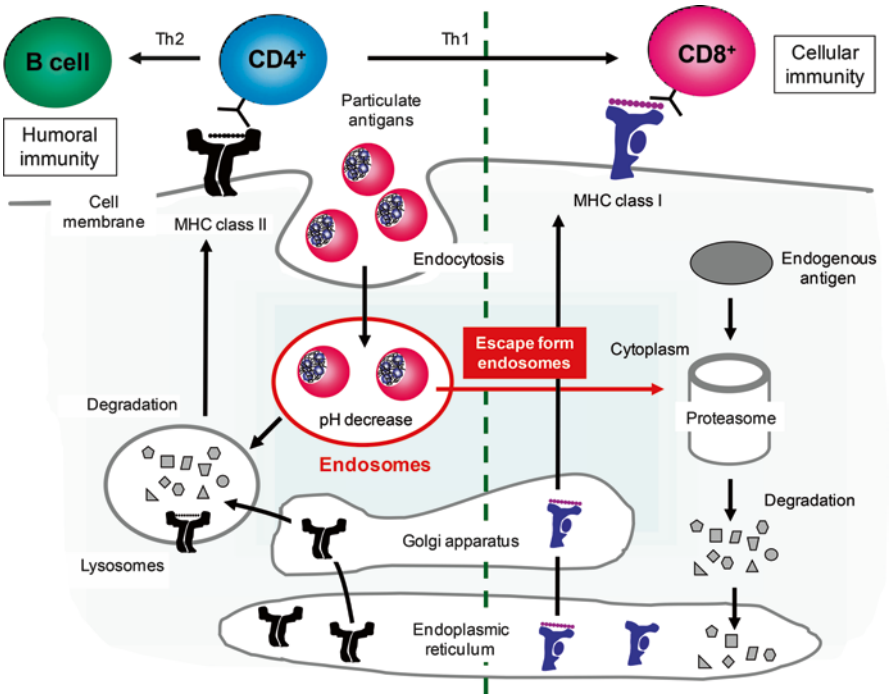

Fig. 12.4 Pathways of intracellular trafficking of particulate antigens in APCs. Antigens can be encapsulated within particles. Antigen-conjugated nanoparticles can be internalized into the cells via endocytosis, depending on their sizes, shapes, and surface charges. Polymers sensitive to pH can disrupt or destabilize the endosomal membrane and release antigen into the cytoplasm. Polymer hydrophobicity is also an important factor for endosome escape of antigens. Antigens taken up by APCs are processed into peptide epitopes and directed through two discrete pathways to MHC classes I and II, which present peptide for interaction with either $CD8^+$ or $CD4^+$ T cells, respectively

cellular immunity by exogenous antigens is needed in the regulation of intracellular distribution of antigens. The escape of internalized antigens from endosomes to the cytoplasm is an important subject to control the antigen processing/presentation pathways.

12.4.1 pH-Responsive Nanoparticles

The release of biomolecules from acidic endosomes requires a membrane-disruptive agent, which can release the internalized compounds into the cytoplasm. Approaches include the use of membrane-penetrating peptides, pathogen-derived pore-forming proteins, and “endosome-escaping” polymers or lipids that disrupt the endosomal membrane in response to the pH reduction, which occurs in these compartments. Thus, in recent years, there has been significant interest in developing pH-sensitive

nanoparticles that can enhance the cytoplasmic delivery of various biomolecules [96–99]. Standley et al. reported an acid-degradable particle composed of acrylamide and acid-degradable cross-linker for protein-based vaccines. These particles released encapsulated protein in a pH-dependent manner. They were stable at the physiological pH of 7.4 but degrade quickly in the pH 5.0 environment of endosomes. The degradation of particles led to the endosome escape of encapsulated proteins. The colloid osmotic mechanism is to generate a quick degradation of the particles into many molecules, thus increasing the osmotic pressure within the endosomes, leading to a rapid influx of water across the membrane resulting in its disruption. In fact, the MHC class I presentation levels achieved with these particles were vastly enhanced as a result of their ability to deliver more protein into the cytoplasm of APCs. In mouse immunization study, these acid-sensitive particles could induce antigen-specific CTL responses and showed antitumor activity [100, 101]. Hu et al. also reported the endosome escape of pH-responsive core–shell nanoparticles. pH-sensitive poly(diethylaminoethyl methacrylate) (PDEAEMA)-core/poly(ethylene glycol) dimethacrylate (PAEMA)-shell nanoparticles were capable of efficient cytosolic delivery of membrane-impermeable molecules such as calcein and OVA to DCs. These particles effectively disrupted endosomes and delivered molecules to the cytosol of cells without cytotoxicity and enhanced priming of $CD8^+$ T cells by DCs pulsed with OVA/PDEAEMA-core nanoparticles [102]. Polycations that absorb protons in response to the acidification of endosomes can disrupt these vesicles via the proton sponge effect. The proton sponge effect arises from a large number of weak conjugate bases with buffering capacities between 7.2 and 5.0, such as polyethylenimine (PEI), leading to proton absorption in acid organelles and an osmotic pressure buildup across the organelle membrane. This osmotic pressure causes swelling and/or rupture of the acidic endosomes and a release of the internalized molecules into the cytoplasm [103].

12.4.2 Amphiphilic Polymers for Cytosolic Delivery

Synthetic poly(alkylacrylic acid) [104, 105] and poly(alkylacrylic acid-*co*-alkyl acrylate) [106, 107] also have pH-dependent, membrane-disruptive properties. These polymers contain a combination of carboxyl groups and hydrophobic alkyl groups and are protonated at the endosomal pH range. Upon a decrease in pH, they increase their hydrophobicity and penetrate into the endosomal membranes and disrupt them. The hydrophobicity of the polymers is important for disrupting lipid membranes. Foster et al. have applied these amphiphilic polymers to nanoparticle delivery systems [108]. A pH-responsive nanoparticle (180 nm) incorporating OVA-conjugated poly(propylacrylic acid) (PPAA) (PPAA-OVA) was evaluated to test whether improved cytosolic delivery of a protein antigen could enhance $CD8^+$ CTL and prophylactic tumor vaccine responses. Nanoparticles containing PPAA-OVA were formed by ionic complexation of cationic poly(dimethylaminoethyl methacrylate) (PDMAEMA) with the anionic PPAA-OVA conjugate (PPAA-OVA/PDMAEMA).

The PPAA-OVA/PDMAEMA nanoparticles were stably internalized and could access the MHC class I pathway in the cytosol by triggering endosome escape. In an EG.7-OVA mouse tumor protection model, PPAA-OVA/PDMAEMA-immunized mice delayed tumor growth for nearly 5 weeks, while control mice injected with PBS and free OVA developed tumors in less than 10 days. This response was attributed to the eightfold increase in production of OVA-specific $CD8^+$ T lymphocytes and an 11-fold increase in production of anti-OVA IgG. However, these vinyl polymers are not biodegradable and, thus, their molecular weight presents a limitation for medical applications.

Recently, our group developed novel biodegradable nanoparticles composed of hydrophobically modified γ-PGA (γ-PGA-Phe). The nanoparticles showed a highly negative zeta potential (−25 mV) due to the ionization of the carboxyl groups of γ-PGA located near the surfaces. Protein-encapsulated γ-PGA-Phe nanoparticles efficiently delivered proteins from the endosomes to the cytoplasm in DCs [109]. To evaluate their potential applications as membrane-disruptive nanoparticles, the nanoparticles were characterized with respect to their hemolytic activity against erythrocytes as a function of pH. The nanoparticles showed hemolytic activity with decreasing pH from 7 to 5.5 and were membrane inactive at physiological pH. As the pH decreased, the hemolytic activity of the nanoparticles gradually increased, reaching a peak at pH 5.5. This activity was dependent on the hydrophobicity of γ-PGA. The mechanism responsible for the pH-dependent hemolysis by the nanoparticles involved a conformational change of γ-PGA-Phe and corresponding increase in the surface hydrophobicity. Increased polymer hydrophobicity resulted in increased membrane disruption. The γ-PGA-Phe has carboxyl side-chain groups, so the p*K*a of the proton of the carboxyl groups is also a very important factor for the pH sensitivity of the γ-PGA-Phe [84].

It has also been reported that antigen delivery to DCs via PLGA particles increased the amount of protein that escaped from endosomes into the cytoplasm. How PLGA particles encapsulated proteins or peptides become accessible to the cytoplasm is still not clear. It is suggested that the gradual acidification of endosomes would lead to the protonation of the PLGA polymer, resulting in enhanced hydrophobicity and attachment and rupture of the endosomal membrane [110].

12.5 Activation of APCs by Nanoparticles

Research on biomaterial adjuvant potential has been focused largely on determining the degree of DC maturation induced by exposure to polymeric nanoparticles or liposomes [111–113]. The maturation of DCs is associated with increased expression of several cell surface markers, including the co-stimulatory molecules CD40, CD80, CD83, CD86, and MHC class I and class II. It is well known that DC maturation can be induced by inflammatory factors such as lipopolysaccharide (LPS), bacterial DNA, or inflammatory cytokines such as TNF-α, and the process is highly important

for the innate immune responses [114, 115]. Therefore, in addition to the antigen delivery to DCs, DC maturation is crucial in the development of effective vaccines.

In vitro studies have shown that γ-PGA-Phe nanoparticle-pulsed DCs result in DC maturation by upregulation of co-stimulatory molecule expression and cytokine production. To determine whether the uptake of γ-PGA-Phe nanoparticles mediates the phenotypic maturation of DCs, DCs were incubated with γ-PGA-Phe nanoparticles for 24 or 48 h, and the expression of surface molecules was measured by flow cytometry. Upon exposure of these DCs to the nanoparticles, the expression of co-stimulatory molecules (maturation markers) was increased in a dose-dependent manner. The expression levels of co-stimulatory molecules in nanoparticle-pulsed DCs were similar to those of LPS-pulsed DCs. The effect of nanoparticles on DCs was not inhibited by treatment with polymyxin B (PmB), an inhibitor of LPS, suggesting that nanoparticle-induced DC maturation is not due to LPS contamination. These results suggest that γ-PGA-Phe nanoparticles have great potential as adjuvant for DC maturation [81–83]. Interestingly, the difference in DC activation was detected by changing the size of nanoparticles. The induction of maturation markers was increased with decreasing particle size. These results indicate that DC maturation was significantly affected by the size of nanoparticles. The mechanisms responsible for DC maturation by γ-PGA-Phe nanoparticles may be related to Toll-like receptors (TLRs) of DCs. TLRs are abundantly expressed on professional APCs. TLRs play a major role in pathogen recognition and in the initiation of the inflammatory and immune responses [116]. The stimulation of TLRs by TLR ligands induces the surface expression of co-stimulatory molecules, and this phenotypic modulation is a typical feature of DC maturation. Recently, soluble γ-PGA-induced innate immune responses have been reported in a TLR4-dependent manner in DCs [117, 118]. Treatment with high molecular mass γ-PGA (2,000 kDa), but not a low molecular one (10 kDa), induced a significant upregulation of CD40, CD80, and CD86 expression in wild-type DCs. The stimulatory capacity of γ-PGA was not significantly affected by pretreatment with PmB. In contrast, DCs from TLR4-defective mice did not show an enhanced expression of maturation markers in response to the 2,000 kDa γ-PGA treatment. These results suggest that not only the DC uptake process of γ-PGA-Phe nanoparticles but also the surface interactions between γ-PGA-Phe nanoparticles and DCs are important for induction of DC maturation. The DC uptake of 30-nm-sized nanoparticles was lower than for 200-nm-sized nanoparticles, but the effect of DC activation by the nanoparticles was high in the small sizes. Thus, it is considered that the surface interactions between the nanoparticles and DCs predominately affect the DC maturation. Tomayo et al. have also reported that poly(anhydride) nanoparticles act as agonists of various TLRs. The nanoparticles were useful as Th1 adjuvants in immunoprophylaxis and immunotherapy through TLR exploitation [119].

The efficacy of antigen-loaded γ-PGA-Phe nanoparticles on the induction of antigen-specific humoral and cellular immune responses was examined using OVA as a model antigen [82]. The immune responses were investigated in mice after subcutaneous immunization with OVA-encapsulated γ-PGA-Phe nanoparticles (OVA-NPs). The mice immunized with OVA-NPs showed a more potent CTL

response than those obtained from mice immunized with OVA plus complete Freund's adjuvant (CFA). It has been demonstrated that the γ-PGA-Phe nanoparticles are also effective for vaccines against human immunodeficiency virus (HIV) [81], influenza virus [120], or cancers [121].

Similar results on DC maturation by particulate materials have been obtained with PLGA nano-/microparticles [122, 123], liposomes [87], cationic polystyrene microparticles [124], polystyrene nanoparticles [125], and acid-degradable cationic nanoparticles [126]. Elamanchili et al. examined DC maturation by PLGA nanoparticles. The results showed that after PLGA nanoparticle pulsing, DCs exhibited a modest increase in the expression of MHC class II and CD86 compared to untreated controls. In addition, DCs pulsed with PLGA nanoparticles containing an immunomodulator, monophosphoryl lipid A (MPLA), further induced DC maturation [86]. The PLGA-based nanoparticulate system offers the flexibility for incorporation of broad range of TLR ligands. Copland et al. investigated whether formulation of antigen in mannosylated liposomes enhanced uptake and DC maturation. Exposure to liposomes containing OVA resulted in enhanced expression of maturation markers when compared to exposure to antigen in solution. Expression was highest following exposure to mannosylated liposomes [87]. These particulate systems hold promise as a vaccine delivery system and immunostimulant.

PLGA or PLA nano-/microparticles are suitable vehicles for the delivery of recombinant proteins, peptides, and pDNA to generate immune responses in vivo. Several studies have shown that PLGA nanoparticles can be used to modulate immune responses against encapsulated antigens due to their ability to efficiently target APCs and to facilitate appropriate processing and in presenting antigens to T cells [24, 127–135]. Gutierro et al. investigated the immune responses by BSA-loaded PLGA nanoparticles after subcutaneous, oral, and intranasal administration to evaluate parameters that can affect the immune response [136]. The vaccination of 1,000 nm particles generally elicited a higher serum IgG response than that obtained with the vaccination of 500- or 200-nm-sized particles, the immune response for 500 nm particles being similar than that obtained with 200 nm by the subcutaneous and the oral route and higher by the intranasal route.

Many different vaccine antigens encapsulated into PLGA nanoparticles were shown to induce broad and potent immune responses. For example, hepatitis B therapeutic vaccines were designed and formulated by loading the hepatitis B core antigen (HBcAg) into PLGA nanoparticles (300 nm) with or without monophospholipid A (MPLA) adjuvant [137]. A single immunization with HBcAg-encapsulated PLGA nanoparticles containing MPLA induced a stronger cellular immune response than those induced by HBcAg alone and HBcAg mixed with MPLA in a murine model. More importantly, the level of HBcAg-specific immune responses could be increased further significantly by a booster immunization with the PLGA nanoparticles. These results suggested that co-delivery of HBcAg and MPLA in PLGA nanoparticles promoted HBcAg-specific cellular immune responses. These findings suggest that appropriate design of the vaccine formulation and careful planning of the immunization schedule are important in the successful development of effective therapeutic vaccines for hepatitis B virus.

12.6 Targeting of APCs in Lymph Nodes with Nanoparticulate Systems

To improve the therapeutic potential of the nanoparticle-based nanoparticles for vaccine delivery, it is important to understand the physicochemical properties of nanoparticles affecting the biodistribution. To date, several reports have discussed the biodistribution of polymeric nanoparticles administered into the body [138–140]. The polymeric nanoparticles can be surface modified and functionalized to improve their biodistribution and also conjugated to targeting ligands which can direct nanoparticles to specific cells/tissues where drug delivery is desired. Polymer- and liposome-based delivery systems have focused primarily on vaccine delivery to peripheral DCs, where they first internalize the particles and then migrate to lymph nodes to activate T cells [141]. However, targeting DCs in vivo is very difficult because, in normal tissues, they exist in significantly lower numbers than other APCs such as macrophages. To overcome this problem, Kwon et al. prepared acid-degradable particles conjugated with anti-DEC-205 (anti-CD205) monoclonal Abs (mAbs). DEC-205 is an endocytosis receptor that is only expressed by lymphoid, interstitial, epidermal Langerhans DCs and thymic endothelial cells. Anti-DEC-205 mAb-conjugated particles increased receptor-mediated uptake of the particles by DCs as well as migration of particle-carrying DCs to lymph nodes and stimulation of naive T cells leading to enhanced cellular immune response [142]. Some subsets of DCs including plasmacytoid DCs (pDCs), which are known to play an important role in bridging the innate and adaptive immunities, do not express DEC-205. Therefore, the use of particles conjugated with anti-DEC-205 mAb is not suitable for targeting of pDCs. To further enhance targeting efficiency for DCs and reduce an unexpected toxicity, the use of a particle conjugated with a specific DC targeting molecule would be more beneficial.

A substantial fraction of resident DCs in lymph nodes are phenotypically immature and capable of internalizing antigens and particulate materials. Thus, resident APCs in lymph node may also be utilized as targets for vaccine antigens [143]. Therefore, antigen direct delivery to lymph nodes might provide an attractive alternative, because DCs are present in much higher concentration in these lymph nodes. It has been reported that delivery of particulate antigens to lymph nodes is affected by the size of nanoparticles [144]. Reddy et al. investigated the delivery of 20-, 45-, and 100-nm-sized poly(ethylene glycol) (PEG)-stabilized poly(propylene sulfide) (PPS) nanoparticles to DCs in the lymph nodes. The 20 nm particles were most readily taken up into the lymphatics following interstitial injection. The nanoparticles were internalized by up to 40–50 % of lymph node DCs, and the site of internalization was in the lymph nodes rather than at the injection site [145]. In mouse immunization study, OVA-conjugated 20 nm particles produced strong levels of immune response compared to 100 nm particles. The results indicate that by controlling size, PPS nanoparticles can be effectively taken up into the lymphatics as well as retained in lymph nodes without using any specific targeting ligand. In addition, these findings suggest that antigen delivery to lymph nodes is an important

strategy for vaccine developments. Vila et al. also demonstrated that the size of PLA–PEG particles affects the nasal transport of the encapsulated protein and lymph node uptake of nasal-administered particles. The tissue levels following nasal administration of tetanus toxoid (TT) encapsulated into PLA–PEG particles (200 nm, 1.5, 5, and 10 μm) were investigated. The efficacy of transport to lymph nodes was related to the particle size, reaching the most important transport for the smallest (200 nm) particle size [146]. The results suggest that the PLA–PEG nanoparticles could be transported through the nasal mucosa and reach the subepithelial layer which is highly irrigated by lymph and capillary vessels. From these observations, it was found that uptake of particles in regional lymph nodes after systemic or mucosal administration is affected by the size of particles.

12.7 Conclusion

Many of the vaccines currently in development are based on purified subunits, recombinant proteins, or synthetic peptides. This new generation of antigens is less immunogenic than traditional vaccines and has better delivery systems, and immunostimulants are required to induce acceptable immune responses. Polymeric nano-/microparticles have been shown to possess significant potential as antigen delivery systems. In particular, biodegradable polymeric nanoparticles with entrapped antigens, such as proteins, peptides, or DNA, represent an exciting approach to control the intracellular release of antigens and to optimize the desired immune response via selective targeting of the antigen to APCs. The efficient delivery of antigens to APCs, especially in DCs, is one of the most important issues in the development of effective vaccines. Using nanoparticle-based vaccine delivery systems, it is possible to target delivery to DCs. The nanoparticle surfaces can be conjugated with DC-specific antibodies or ligands to increase targeting specificity. Polymeric nanoparticles are suitable for conjugation with antigens and can protect the antigen from degradation in vivo. Following uptake of the nanoparticles by DCs, the antigens are released intracellularly in a manner that can activate MHC class I and II pathways and, therefore, induce both $CD4^+$ and $CD8^+$ T-cell immunity. To deliver exogenous antigen for inducing cellular immunity through the MHC class I pathway can be an important problem, as internalized antigen-conjugated nanoparticles are mostly trafficked from endosomes to lysosomes. To avoid lysosomal trafficking, pH-responsive nanoparticles have been studied to disrupt endosomes in a pH-dependent fashion. For successfully targeting lymph-node-resident DCs, it is crucial to engineer nanoparticles that can be readily taken up into lymphatic vessels after subcutaneous injection and can then be retained in draining lymph nodes. It has been well established that particle size is among the most crucial factors for DC and lymphatic uptake.

Polymeric nanoparticles can also be used as synthetic immunostimulants to induce DC maturation and initiate adaptive immune responses. The mechanisms of DC activation by nanoparticles, as an immunostimulant, are not fully understood.

DC maturation by nanoparticles may be related to Toll-like receptors (TLRs) of DCs. However, it has been reported that LPS contamination of gold nanoparticle preparations can stimulate DC maturation [147]. It is well known that LPS mainly interacts with TLR4 and induces DC maturation. In addition, LPS might act in synergy with these nanoparticles to activate/mature DCs. A trace of LPS in the nanoparticle might induce endotoxic effects. For clinical application of nanoparticle-based vaccine, this problem is a fundamental issue that cannot be avoided. To avoid misinterpretation of results, the production processes and handling of polymeric nanoparticles for vaccine use have to get plenty of attention.

There is a growing interest in identifying the relationship between the size of nanoparticles and their adjuvant activities, but the results from recent studies remain controversial. Many investigators are in agreement that the size of the particles is crucial to their adjuvant activities. Some factors may affect to the conflicting findings which include (1) polymeric materials used to form the particles, (2) nature of antigens used, (3) methods of antigen conjugation, and (4) immunization routes of antigens [148]. To clear the factor of particles that influence the adjuvant activity, there is a need to more comprehensively compare immune responses induced by precisely size-controlled nanoparticles prepared with the same materials and loaded with the same antigens by the proper method.

Acknowledgments The authors thank Dr. M. Baba and Dr. T. Uto (Kagoshima University, Japan) for their helpful discussion.

References

1. Singh M, O'Hagan DT (1999) Advances in vaccine adjuvants. Nat Biotechnol 17:1075–1081
2. Singh M, O'Hagan DT (2002) Recent advances in vaccine adjuvants. Pharm Res 19:715–728
3. Peek LJ, Middaugh CR, Berkland C (2008) Nanotechnology in vaccine delivery. Adv Drug Deliv Rev 60:915–928
4. Rice-Ficht AC, Arenas-Gamboa AM, Kahl-McDonagh MM, Ficht TA (2010) Polymeric particles in vaccine delivery. Curr Opin Microbiol 13:106–112
5. De Koker S, Lambrecht BN, Willart MA, van Kooyk Y, Grooten J, Vervaet C, Remon JP, De Geest BG (2011) Designing polymeric particles for antigen delivery. Chem Soc Rev 40:320–339
6. O'Hagan DT, Valiante NM (2003) Recent advances in the discovery and delivery of vaccine adjuvants. Nat Rev Drug Discov 2:727–735
7. Marrack P, McKee AS, Munks MW (2009) Towards an understanding of the adjuvant action of aluminium. Nat Rev Immunol 9:287–293
8. Gupta RK (1998) Aluminum compounds as vaccine adjuvants. Adv Drug Deliv Rev 32:155–172
9. Brewer JM (2006) How do aluminium adjuvants work? Immunol Lett 102:10–15
10. Hans ML, Lowman AM (2002) Biodegradable nanoparticles for drug delivery and targeting. Curr Opin Solid State Mater Sci 6:319–327
11. Greenland JR, Letvin NL (2007) Chemical adjuvants for plasmid DNA vaccines. Vaccine 25:3731–3741
12. Lu JM, Wang X, Marin-Muller C, Wang H, Lin PH, Yao Q, Chen C (2009) Current advances in research and clinical applications of PLGA-based nanotechnology. Expert Rev Mol Diagn 9:325–341

13. Panyam J, Labhasetwar V (2003) Biodegradable nanoparticles for drug and gene delivery to cells and tissue. Adv Drug Deliv Rev 55:329–347
14. Vasir JK, Labhasetwar V (2007) Biodegradable nanoparticles for cytosolic delivery of therapeutics. Adv Drug Deliv Rev 59:718–728
15. Kreuter J (1996) Nanoparticles and microparticles for drug and vaccine delivery. J Anat 189:503–505
16. O'Hagan DT, Jeffery H, Davis SS (1994) The preparation and characterization of poly(lactide-*co*-glycolide) microparticles: III. Microparticle/polymer degradation rates and the in vitro release of a model protein. Int J Pharm 103:37–45
17. Li X, Deng X, Yuan M, Xiong C, Huang Z, Zhang Y, Jia W (2000) In vitro degradation and release profiles of poly-DL-lactide-poly(ethylene glycol) microspheres with entrapped proteins. J Appl Polym Sci 78:140–148
18. Liggins RT, Burt HM (2001) Paclitaxel loaded poly(L-lactic acid) microspheres: properties of microspheres made with low molecular weight polymers. Int J Pharm 222:19–33
19. Lemoine D, Francois C, Kedzierewicz F, Preat V, Hoffman M, Maincent P (1996) Stability study of nanoparticles of poly(ε-caprolactone), poly(D,L-lactide) and poly(D,L-lactide-co-glycolide). Biomaterials 17:2191–2197
20. Jiang W, Gupta RK, Deshpande MC, Schwendeman SP (2005) Biodegradable poly(lactic-*co*-glycolic acid) microparticles for injectable delivery of vaccine antigens. Adv Drug Deliv Rev 57:391–410
21. Mohamed F, van der Walle CF (2008) Engineering biodegradable polyester particles with specific drug targeting and drug release properties. J Pharm Sci 97:71–87
22. Kumari A, Yadav SK, Yadav SC (2009) Biodegradable polymeric nanoparticles based drug delivery systems. Colloids Surf B 75:1–18
23. Tamber H, Johansen P, Merkle HP, Gander B (2005) Formulation aspects of biodegradable polymeric microspheres for antigen delivery. Adv Drug Deliv Rev 57:357–376
24. Mundargi RC, Babu VR, Rangaswamy V, Patel P, Aminabhavi TM (2008) Nano/micro technologies for delivering macromolecular therapeutics using poly(D,L-lactide-co-glycolide) and its derivatives. J Control Release 125:193–209
25. Sah H (1999) Stabilization of proteins against methylene chloride/water interface induced denaturation and aggregation. J Control Release 58:143–151
26. Panyam J, Dali MM, Sahoo SK, Ma W, Chakravarthi SS, Amidon GL, Levy RJ, Labhasetwar V (2003) Polymer degradation and in vitro release of a model protein from poly(D, L-lactide-co-glycolide) nano- and microparticles. J Control Release 92:173–187
27. Kakizawa Y, Kataoka K (2002) Block copolymer micelles for delivery of gene and related compounds. Adv Drug Deliv Rev 54:203–222
28. Zhang L, Eisenberg A (1995) Multiple morphologies of crew-cut aggregates of polystyrene-b-poly(acrylic acid) block copolymers. Science 1268:1728–1731
29. Dou H, Jiang M, Peng H, Chen D, Hong Y (2003) pH-dependent self-assembly: micellization and micelle-hollow-sphere transition of cellulose-based copolymers. Angew Chem Int Ed 42:1516–1519
30. Reihs T, Muller M, Lunkwitz K (2004) Preparation and adsorption of refined polyelectrolyte complex nanoparticles. J Colloid Interface Sci 271:69–79
31. Kang N, Perron ME, Prudhomme RE, Zhang Y, Gaucher G, Leroux JC (2005) Stereocomplex block copolymer micelles: core-shell nanostructures with enhanced stability. Nano Lett 5:315–319
32. Gaucher G, Dufresne MH, Sant VP, Kang N, Maysinger D, Leroux JC (2005) Block copolymer micelles: preparation, characterization and application in drug delivery. J Control Release 109:169–188
33. Letchford K, Burt H (2007) A review of the formation and classification of amphiphilic block copolymer nanoparticulate structures: micelles, nanospheres, nanocapsules and polymersomes. Eur J Pharm Biopharm 65:259–269
34. Holowka EP, Pochan DJ, Deming TJ (2005) Charged polypeptide vesicles with controllable diameter. J Am Chem Soc 127:12423–12428

35. Matsusaki M, Hiwatari K, Higashi M, Kaneko T, Akashi N (2004) Stably-dispersed and surface-functional bionanoparticles prepared by self-assembling amphipathic polymers of hydrophilic poly(γ-glutamic acid) bearing hydrophobic amino acids. Chem Lett 33:398–399
36. Matsusaki M, Fuchida T, Kaneko T, Akashi M (2005) Self-assembling bionanoparticles of poly(ε-lysine) bearing cholesterol as a biomesogen. Biomacromolecules 6:2374–2379
37. Arimura H, Ohya Y, Ouchi T (2005) Formation of core-shell type biodegradable polymeric micelles from amphiphilic poly(aspartic acid)-*block*-polylactide diblock copolymer. Biomacromolecules 6:720–725
38. Akiyoshi K, Ueminami A, Kurumada S, Nomura Y (2000) Self-association of cholesteryl-bearing poly(L-lysine) in water and control of its secondary structure by host-guest interaction with cyclodextrin. Macromolecules 33:6752–6756
39. Holowka EP, Sun VZ, Kamei DT, Deming TJ (2007) Polyarginine segments in block copolypeptides drive both vesicular assembly and intracellular delivery. Nat Mater 6:52–57
40. Jeong JH, Kang HS, Yang SR, Kim JD (2003) Polymer micelle-like aggregates of novel amphiphilic biodegradable poly(asparagine) grafted with poly(caprolactone). Polymer 44:583–591
41. Kataoka K, Matsumoto T, Yokoyama M, Okano T, Sakurai Y, Fukushima S, Okamoto K, Kwon GS (2000) Doxorubicin-loaded poly(ethylene glycol)-poly(β-benzyl-L-aspartate) copolymer micelles: their pharmaceutical characteristics and biological significance. J Control Release 64:143–153
42. Lin J, Zhang S, Chen T, Lin S, Jin H (2007) Micelle formation and drug release behavior of polypeptide graft copolymer and its mixture with polypeptide block copolymer. Int J Pharm 336:49–57
43. Lee ES, Shin HJ, Na K, Bae YH (2003) Poly(L-histidine)-PEG block copolymer micelles and pH-induced destabilization. J Control Release 90:363–374
44. Kubota H, Matsunobu T, Uotani K, Takebe H, Satoh A, Tanaka T, Taniguchi M (1993) Production of poly(γ-glutamic acid) by *Bacillus subtilis* F-2-01. Biosci Biotech Biochem 57:1212–1213
45. King EC, Watkins WJ, Blacker AJ, Bugg TDH (1998) Covalent modification in aqueous solution of poly-γ-D-glutamic acid from *Bacillus licheniformis*. J Polym Sci A Polym Chem 36:1995–1999
46. Morillo M, de Ilarduya AM, Munoz-Guerra S (2001) Comblike alkyl esters of biosynthetic poly(γ-glutamic acid) 1 Synthesis and characterization. Macromolecules 34:7868–7875
47. Prodhomme EJF, Tutt AL, Glennie MJ, Bugg TDH (2003) Multivalent conjugates of poly-γ-D-glutamic acid from *Bacillus licheniformis* with antibody F(ab′) and glycopeptide ligands. Bioconj Chem 14:1148–1155
48. Tachibana Y, Kurisawa M, Uyama H, Kobayashi S (2003) Thermo- and pH-responsive biodegradable poly(α-*N*-substituted γ-glutamine)s. Biomacromolecules 4:1132–1134
49. Shimokuri T, Kaneko T, Serizawa T, Akashi M (2004) Preparation and thermosensitivity of naturally occurring polypeptide poly(γ-glutamic acid) derivatives modified by alkyl groups. Macromol Biosci 4:407–411
50. Oppermann FB, Fickaitz S, Steinbiichel A (1998) Biodegradation of polyamides. Polym Degrad Stab 59:337–344
51. Obst M, Steinbuchel A (2004) Microbial degradation of poly(amino acid)s. Biomacromolecules 5:1166–1176
52. Schneerson R, Kubler-Kielb J, Liu TY, Dai ZD, Leppla SH, Yergey A, Backlund P, Shiloach J, Majadly F, Robbins JB (2003) Poly(γ-D-glutamic acid) protein conjugates induce IgG antibodies in mice to the capsule of *Bacillus anthracis*: a potential addition to the anthrax vaccine. Proc Natl Acad Sci U S A 100:8945–8950
53. Rhie GE, Roehrl MH, Mourez M, Collier RJ, Mekalanos JJ, Wang JY (2003) A dually active anthrax vaccine that confers protection against both bacilli and toxins. Proc Natl Acad Sci U S A 100:10925–10930
54. Wang TT, Fellows PF, Leighton TJ, Lucas AH (2004) Induction of opsonic antibodies to the gamma-D-glutamic acid capsule of *Bacillus anthracis* by immunization with a synthetic peptide-carrier protein conjugate. FEMS Immunol Med Microbiol 40:231–237

55. Joyce J, Cook J, Chabot D, Hepler R, Shoop W, Xu Q, Stambaugh T, Aste-Amezaga M, Wang S, Indrawati L, Bruner M, Friedlander A, Keller P, Caulfield M (2006) Immunogenicity and protective efficacy of *Bacillus anthracis* poly-γ-D-glutamic acid capsule covalently coupled to a protein carrier using a novel triazine-based conjugation strategy. J Biol Chem 281:4831–4843
56. Kubler-Kielb J, Liu TY, Mocca C, Majadly F, Robbins JB, Schneerson R (2006) Additional conjugation methods and immunogenicity of *Bacillus anthracis* poly-γ-D-glutamic acid-protein conjugates. Infect Immun 74:4744–4749
57. Shih IL, Van YT (2001) The production of poly(γ-glutamic acid) from microorganisms and its various application. Bioresour Technol 79:207–225
58. Kaneko T, Higashi M, Matsusaki M, Akagi T, Akashi M (2005) Self-assembled soft nanofibrils of amphipathic polypeptides and their morphological transformation. Chem Mater 17:2484–2486
59. Akagi T, Baba M, Akashi M (2007) Preparation of nanoparticles by the self-organization of polymers consisting of hydrophobic and hydrophilic segments: potential applications. Polymer 48:6729–6747
60. Kim H, Akagi T, Akashi M (2009) Preparation of size tunable amphiphilic poly(amino acid) nanoparticles. Macromol Biosci 9:842–848
61. Akagi T, Kaneko T, Kida T, Akashi M (2005) Preparation and characterization of biodegradable nanoparticles based on poly(γ-glutamic acid) with L-phenylalanine as a protein carrier. J Control Release 108:226–236
62. Akagi T, Kaneko T, Kida T, Akashi M (2006) Multifunctional conjugation of proteins on/into core-shell type nanoparticles prepared by amphiphilic poly(γ-glutamic acid). J Biomater Sci Polym Ed 17:875–892
63. Portilla-Arias JA, Camargo B, Garcia-Alvarez M, de Ilarduya AM, Munoz-Guerra S (2009) Nanoparticles made of microbial poly(γ-glutamate)s for encapsulation and delivery of drugs and proteins. J Biomater Sci Polym Ed 20:1065–1079
64. Bodnar M, Kjoniksen AL, Molnar RM, Hartmann JF, Daroczi L, Nystrom B, Borbely J (2008) Nanoparticles formed by complexation of poly-γ-glutamic acid with lead ions. J Hazard Mater 153:1185–1192
65. Radu JEF, Novak L, Hartmann JF, Beheshti N, Kjoniksen AL, Nystrom B, Borbely J (2008) Structural and dynamical characterization of poly-γ-glutamic acid-based cross-linked nanoparticles. Colloid Polym Sci 286:365–376
66. Akiyoshi K, Kobayashi S, Shichibe S, Mix D, Baudys M, Kim SW, Sunamoto J (1998) Self-assembled hydrogel nanoparticle of cholesterol-bearing pullulan as a carrier of protein drugs: complexation and stabilization of insulin. J Control Release 54:313–320
67. Jung SW, Jeong Y, Kim SH (2003) Characterization of hydrophobized pullulan with various hydrophobicities. Int J Pharm 254:109–121
68. Na K, Park KH, Kim SW, Bae YH (2000) Self-assembled hydrogel nanoparticles from curdlan derivatives: characterization, anti-cancer drug release and interaction with a hepatoma cell line (HepG2). J Control Release 69:225–236
69. Gref R, Rodrigues J, Couvreur P (2002) Polysaccharides grafted with polyesters: novel amphiphilic copolymers for biomedical applications. Macromolecules 35:9861–9867
70. Leonard M, Boisseson MRD, Hubert P, Dalenccon F, Dellacherie E (2004) Hydrophobically modified alginate hydrogels as protein carriers with specific controlled release properties. J Control Release 98:395–405
71. Park JH, Kwona S, Nam JO, Park RW, Chung H, Seo SB, Kim IS, Kwon IC, Jeong SY (2004) Self-assembled nanoparticles based on glycol chitosan bearing 5h-cholanic acid for RGD peptide delivery. J Control Release 95:579–588
72. Akiyoshi K, Deguchi S, Moriguchi N, Yamaguchi S, Sunamoto J (1993) Self-aggregates of hydrophobized polysaccharides in water. Formation and characteristics of nanoparticles. Macromolecules 26:3062–3068
73. Hsieh CY, Tsai SP, Wang DM, Chang YN, Hsieh HJ (2005) Preparation of γ-PGA/chitosan composite tissue engineering matrices. Biomaterials 26:5617–5623

74. Kang HS, Park SH, Lee YG, Son I (2007) Polyelectrolyte complex hydrogel composed of chitosan and poly(γ-glutamic acid) for biological application: preparation, physical properties, and cytocompatibility. J Appl Polym Sci 103:386–394
75. Kim YH, Gihm SH, Park CR, Lee KY, Kim TW, Kwon IC, Chung H, Jeong SY (2001) Structural characteristics of size-controlled self-aggregates of deoxycholic acid-modified chitosan and their application as a DNA delivery carrier. Bioconj Chem 12:932–938
76. Lee KY, Jo WH, Kwon IC, Kim YH, Jeong SY (1998) Structural determination and interior polarity of self-aggregates prepared from deoxycholic acid-modified chitosan in water. Macromolecules 31:378–383
77. Kida T, Inoue K, Akagi T, Akashi M (2007) Preparation of novel polysaccharide nanoparticles by the self-assembly of amphiphilic pectins and their protein-encapsulation ability. Chem Lett 36:940–941
78. Banchereau J, Steinman RM (1998) Dendritic cells and the control of immunity. Nature 392:245–252
79. Gamvrellis A, Leong D, Hanley JC, Xiang SD, Mottram P, Plebanski M (2004) Vaccines that facilitate antigen entry into dendritic cells. Immunol Cell Biol 82:506–516
80. Zhang S, Li J, Lykotrafitis G, Bao G, Suresh S (2009) Size-dependent endocytosis of nanoparticles. Adv Mater 21:419–424
81. Akagi T, Wang X, Uto T, Baba M, Akashi M (2007) Protein direct delivery to dendritic cells using nanoparticles based on amphiphilic poly(amino acid) derivatives. Biomaterials 28:3427–3436
82. Uto T, Wang X, Sato K, Haraguchi M, Akagi T, Akashi M, Baba M (2007) Targeting of antigen to dendritic cells with poly(γ-glutamic acid) nanoparticles induce antigen-specific humoral and cellular immunity. J Immunol 178:2979–2986
83. Uto T, Akagi T, Hamasaki T, Akashi M, Baba M (2009) Modulation of innate and adaptive immunity by biodegradable nanoparticles. Immunol Lett 125:46–52
84. Akagi T, Kim H, Akashi M (2010) pH-dependent disruption of erythrocyte membrane by amphiphilic poly(amino acid) nanoparticles. J Biomater Sci Polym Ed 21:315–328
85. Lutsiak ME, Robinson DR, Coester C, Kwon GS, Samuel J (2002) Analysis of poly(D, L-lactic-co-glycolic acid) nanosphere uptake by human dendritic cells and macrophages in vitro. Pharm Res 19:1480–1487
86. Elamanchili P, Diwan M, Cao M, Samuel J (2004) Characterization of poly(D,L-lactic-co-glycolic acid) based nanoparticulate system for enhanced delivery of antigens to dendritic cells. Vaccine 22:2406–2412
87. Copland MJ, Baird MA, Rades T, McKenzie JL, Becker B, Reck F, Tyler PC, Davies NM (2003) Liposomal delivery of antigen to human dendritic cells. Vaccine 21:883–890
88. Foged C, Brodin B, Frokjaer S, Sundblad A (2005) Particle size and surface charge affect particle uptake by human dendritic cells in an in vitro model. Int J Pharm 298:315–322
89. Kanchan V, Panda AK (2007) Interactions of antigen-loaded polylactide particles with macrophages and their correlation with the immune response. Biomaterials 28:5344–5357
90. Cohen JA, Beaudette TT, Tseng WW, Bachelder EM, Mende I, Engleman EG, Fréchet JM (2009) T-cell activation by antigen-loaded pH-sensitive hydrogel particles in vivo: the effect of particle size. Bioconj Chem 20:111–119
91. Champion JA, Mitragotri S (2006) Role of target geometry in phagocytosis. Proc Natl Acad Sci U S A 103:4930–4934
92. Champion JA, Mitragotri S (2009) Shape induced inhibition of phagocytosis of polymer particles. Pharm Res 26:244–249
93. O'Hagan DT (1998) Recent advances in immunological adjuvants: the development of particulate antigen delivery systems. Expert Opin Invest Drugs 7:349–359
94. Storni T, Kundig TM, Senti G, Johansen P (2005) Immunity in response to particulate antigen-delivery systems. Adv Drug Deliv Rev 57:333–355
95. Shen H, Ackerman AL, Cody V, Giodini A, Hinson ER, Cresswell P, Edelson RL, Saltzman WM, Hanlon DJ (2006) Enhanced and prolonged cross-presentation following endosomal escape of exogenous antigens encapsulated in biodegradable nanoparticles. Immunology 117:78–88

96. Plank C, Zauner W, Wagner E (1998) Application of membrane-active peptides for drug and gene delivery across cellular membranes. Adv Drug Deliv Rev 34:21–35
97. Shai Y (1999) Mechanism of the binding, insertion and destabilization of phospholipid bilayer membranes by α-helical antimicrobial and cell non-selective membrane-lytic peptides. Biochim Biophys Acta 1462:55–70
98. Yessine MA, Leroux JC (2004) Membrane-destabilizing polyanions: interaction with lipid bilayers and endosomal escape of biomacromolecules. Adv Drug Deliv Rev 56:999–1021
99. Chen R, Yue Z, Eccleston ME, Williams S, Slater NK (2005) Modulation of cell membrane disruption by pH-responsive pseudo-peptides through grafting with hydrophilic side chains. J Control Release 108:63–72
100. Murthy N, Xu M, Schuck S, Kunisawa J, Shastri N, Fréchet JM (2003) A macromolecular delivery vehicle for protein-based vaccines: acid-degradable protein-loaded microgels. Proc Natl Acad Sci U S A 29:4995–5000
101. Standley SM, Kwon TJ, Murthy N, Kunisawa J, Shastri N, Guillaudeu SJ, Lau L, Fréchet JM (2004) Acid-degradable particles for protein-based vaccines: enhanced survival rate for tumor-challenged mice using ovalbumin model. Bioconj Chem 15:1281–1288
102. Hu Y, Litwin T, Nagaraja AR, Kwong B, Katz J, Watson N, Irvine DJ (2007) Cytosolic delivery of membrane-impermeable molecules in dendritic cells using pH-responsive core-shell nanoparticles. Nano Lett 7:3056–3064
103. Boussif O, Lezoualc'h F, Zanta MA, Mergny MD, Scherman D, Demeneix B, Behr JP (1995) A versatile vector for gene and oligonucleotide transfer into cells in culture and in vivo. Proc Natl Acad Sci U S A 92:7297–7301
104. Murthy N, Robichaud JR, Tirrell DA, Stayton PS, Hoffman AS (1999) The design and synthesis of polymers for eukaryotic membrane disruption. J Control Release 61:137–143
105. Jones RA, Cheung CY, Black FE, Zia JK, Stayton PS, Hoffman AS, Wilson MR (2003) Poly(2-alkylacrylic acid) polymers deliver molecules to the cytosol by pH-sensitive disruption of endosomal vesicles. Biochem J 372:65–75
106. Kusonwiriyawong C, van de Wetering P, Hubbell JA, Merkle HP, Walter E (2003) Evaluation of pH-dependent membrane-disruptive properties of poly(acrylic acid) derived polymers. Eur J Pharm Biopharm 56:237–246
107. Yessine MA, Meier C, Petereit HU, Leroux JC (2006) On the role of methacrylic acid copolymers in the intracellular delivery of antisense oligonucleotides. Eur J Pharm Biopharm 63:1–10
108. Foster S, Duvall CL, Crownover EF, Hoffman AS, Stayton PS (2010) Intracellular delivery of a protein antigen with an endosomal-releasing polymer enhances CD8 T-cell production and prophylactic vaccine efficacy. Bioconj Chem 21:2205–2212
109. Yoshikawa T, Okada N, Oda A, Matsuo K, Matsuo K, Mukai Y, Yoshioka Y, Akagi T, Akashi M, Nakagawa S (2008) Development of amphiphilic γ-PGA-nanoparticle based tumor vaccine: potential of the nanoparticulate cytosolic protein delivery carrier. Biochem Biophys Res Commun 366:408–413
110. Panyam J, Zhou WZ, Prabha S, Sahoo SK, Labhasetwar V (2002) Rapid endo-lysosomal escape of poly(dl-lactide-*co*-glycolide) nanoparticles: implications for drug and gene delivery. FASEB J 16:1217–1226
111. Reddy ST, Swartz MA, Hubbell JA (2006) Targeting dendritic cells with biomaterials: developing the next generation of vaccines. Trends Immunol 27:573–579
112. Jones KS (2008) Biomaterials as vaccine adjuvants. Biotechnol Prog 24:807–814
113. Babensee JE (2007) Interaction of dendritic cells with biomaterials. Semin Immunol 20:101–108
114. Jilek S, Merkle HP, Walter E (2005) DNA-loaded biodegradable microparticles as vaccine delivery systems and their interaction with dendritic cells. Adv Drug Deliv Rev 57:377–390
115. Black M, Trent A, Tirrell M, Olive C (2010) Advances in the design and delivery of peptide subunit vaccines with a focus on toll-like receptor agonists. Expert Rev Vaccines 9:157–173
116. Kawai T, Akira S (2005) Pathogen recognition with Toll-like receptors. Curr Opin Immunol 17:338–344

117. Kim TW, Lee TY, Bae HC, Hahm JH, Kim YH, Park C, Kang TH, Kim CJ, Sung MH, Poo H (2007) Oral administration of high molecular mass poly-γ-glutamate induces NK cell-mediated antitumor immunity. J Immunol 179:775–780
118. Lee TY, Kim YH, Yoon SW, Choi JC, Yang JM, Kim CJ, Schiller JT, Sung MH, Poo HR (2009) Oral administration of poly-γ-glutamate induces TLR4- and dendritic cell-dependent antitumor effect. Cancer Immunol Immunother 58:1781–1794
119. Tamayo I, Irache JM, Mansilla C, Ochoa-Repáraz J, Lasarte JJ, Gamazo C (2010) Poly(anhydride) nanoparticles act as active Th1 adjuvants through Toll-like receptor exploitation. Clin Vaccine Immunol 17:1356–1362
120. Okamoto S, Matsuura M, Akagi T, Akashi M, Tanimoto T, Ishikawa T, Takahashi M, Yamanishi K, Mori Y (2009) Poly(γ-glutamic acid) nano-particles combined with mucosal influenza virus hemagglutinin vaccine protects against influenza virus infection in mice. Vaccine 27:5896–5905
121. Yamaguchi S, Tatsumi T, Takehara T, Sasakawa A, Yamamoto M, Kohga K, Miyagi T, Kanto T, Hiramatsu N, Akagi T, Akashi M, Hayashi N (2010) EphA2-derived peptide vaccine with amphiphilic poly(gamma-glutamic acid) nanoparticles elicits an anti-tumor effect against mouse liver tumor. Cancer Immunol Immunother 59:759–767
122. Yoshida M, Babensee JE (2004) Poly(lactic-*co*-glycolic acid) enhances maturation of human monocyte-derived dendritic cells. J Biomed Mater Res 71:45–54
123. Jilek S, Ulrich M, Merkle HP, Walter E (2004) Composition and surface charge of DNA-loaded microparticles determine maturation and cytokine secretion in human dendritic cells. Pharm Res 21:1240–1247
124. Thiele L, Rothen-Rutishauser B, Jilek S, Wunderli-Allenspach H, Merkle HP, Walter E (2001) Evaluation of particle uptake in human blood monocyte-derived cells in vitro. Does phagocytosis activity of dendritic cells measure up with macrophages? J Control Release 76:59–71
125. Matsusaki M, Larsson K, Akagi T, Lindstedt M, Akashi M, Borrebaeck CA (2005) Nanosphere induced gene expression in human dendritic cells. Nano Lett 5:2168–2173
126. Kwon YJ, Standley SM, Goh SL, Frechet JM (2005) Enhanced antigen presentation and immunostimulation of dendritic cells using acid-degradable cationic nanoparticles. J Control Release 105:199–212
127. Raghuvanshi RS, Katare YK, Lalwani K, Ali MM, Singh O, Panda AK (2002) Improved immune response from biodegradable polymer particles entrapping tetanus toxoid by use of different immunization protocol and adjuvants. Int J Pharm 245:109–121
128. Ataman-Onal Y, Munier S, Ganee A, Terrat C, Durand PY, Battail N, Martinon F, Le Grand R, Charles MH, Delair T, Verrier B (2006) Surfactant-free anionic PLA nanoparticles coated with HIV-1 p24 protein induced enhanced cellular and humoral immune responses in various animal models. J Control Release 112:175–185
129. Hamdy S, Elamanchili P, Alshamsan A, Molavi O, Satou T, Samuel J (2007) Enhanced antigen-specific primary CD4+ and CD8+ responses by codelivery of ovalbumin and toll-like receptor ligand monophosphoryl lipid A in poly(D,L-lactic-co-glycolic acid) nanoparticles. J Biomed Mater Res A 81:652–662
130. Solbrig CM, Saucier-Sawyer JK, Cody V, Saltzman WM, Hanlon DJ (2007) Polymer nanoparticles for immunotherapy from encapsulated tumor-associated antigens and whole tumor cells. Mol Pharm 4:47–57
131. Wendorf J, Chesko J, Kazzaz J, Ugozzoli M, Vajdy M, O'Hagan D, Singh M (2008) A comparison of anionic nanoparticles and microparticles as vaccine delivery systems. Hum Vaccin 4:44–49
132. Hamdy S, Molavi O, Ma Z, Haddadi A, Alshamsan A, Gobti Z, Elhasi S, Samuel J, Lavasanifar A (2008) Co-delivery of cancer-associated antigen and Toll-like receptor 4 ligand in PLGA nanoparticles induces potent CD8+ T cell-mediated anti-tumor immunity. Vaccine 26: 5046–5057
133. Caputo A, Sparnacci K, Ensoli B, Tondelli L (2008) Functional polymeric nano/microparticles for surface adsorption and delivery of protein and DNA vaccines. Curr Drug Deliv 5:230–242

134. Nayak B, Panda AK, Ray P, Ray AR (2009) Formulation, characterization and evaluation of rotavirus encapsulated PLA and PLGA particles for oral vaccination. J Microencapsul 26:154–165
135. Slutter B, Plapied L, Fievez V, Sande MA, Des Rieux A, Schneider YJ, Van Riet E, Jiskoot W, Préat V (2009) Mechanistic study of the adjuvant effect of biodegradable nanoparticles in mucosal vaccination. J Control Release 138:113–121
136. Gutierro I, Hernandez RM, Igartua M, Gascón AR, Pedraz JL (2002) Size dependent immune response after subcutaneous, oral and intranasal administration of BSA loaded nanospheres. Vaccine 21:67–77
137. Chong CS, Cao M, Wong WW, Fischer KP, Addison WR, Kwon GS, Tyrrell DL, Samuel J (2005) Enhancement of T helper type 1 immune responses against hepatitis B virus core antigen by PLGA nanoparticle vaccine delivery. J Control Release 102:85–99
138. Wilson KD, Raney SG, Sekirov L, Chikh G, de Jong SD, Cullis PR, Tam YK (2007) Effects of intravenous and subcutaneous administration on the pharmacokinetics, biodistribution, cellular uptake and immunostimulatory activity of CpG ODN encapsulated in liposomal nanoparticles. Int Immunopharmacol 7:1064–1075
139. He C, Hua Y, Yin L, Tang C, Yin C (2010) Effects of particle size and surface charge on cellular uptake and biodistribution of polymeric nanoparticles. Biomaterials 31:3657–3666
140. Decuzzi P, Godin B, Tanaka T, Lee SY, Chiappini C, Liu X, Ferrari M (2010) Size and shape effects in the biodistribution of intravascularly injected particles. J Control Release 141:320–327
141. Manolova V, Flace A, Bauer M, Schwarz K, Saudan P, Bachmann MF (2008) Nanoparticles target distinct dendritic cell populations according to their size. Eur J Immunol 38:1404–1413
142. Kwon YJ, James E, Shastri N, Fréchet JM (2005) In vivo targeting of dendritic cells for activation of cellular immunity using vaccine carriers based on pH-responsive microparticles. Proc Natl Acad Sci U S A 102:18264–18268
143. Reddy ST, van der Vlies AJ, Simeoni E, Angeli V, Randolph GJ, O'Neil CP, Lee LK, Swartz MA, Hubbell JA (2007) Exploiting lymphatic transport and complement activation in nanoparticle vaccines. Nat Biotechnol 25:1159–1164
144. Oussoren C, Storm G (2001) Liposomes to target the lymphatics by subcutaneous administration. Adv Drug Deliv Rev 50:143–156
145. Reddy ST, Rehor A, Schmoekel HG (2006) In vivo targeting of dendritic cells in lymph nodes with poly(propylene sulfide) nanoparticles. J Control Release 112:26–34
146. Vilaa A, Sancheza A, Evorab C, Soriano I, McCallion O, Alonso MJ (2005) PLA-PEG particles as nasal protein carriers: the influence of the particle size. Int J Pharm 292:43–52
147. Vallhov H, Qin J, Johansson SM, Ahlborg N, Muhammed MA, Scheynius A, Gabrielsson S (2006) The importance of an endotoxin-free environment during the production of nanoparticles used in medical applications. Nano Lett 6:1682–1686
148. Oyewumi MO, Kumar A, Cui Z (2010) Nano-microparticles as immune adjuvants: correlating particle sizes and the resultant immune responses. Expert Rev Vaccines 9:1095–1107

Chapter 13
Nanoparticle-Based Specific Targeting of Antigen-Presenting Cells for Immunotherapy

Malin Lindstedt and Sissela Broos

Abstract This chapter will address the use of polymeric nanoparticles as immunomodulators and drug delivery systems that specifically target human antigen-presenting cells (APCs). Providing APCs with either activating or inhibitory signals in parallel to antigenic stimulation enables modulation of immune responses and is an attractive approach in immunotherapy. Poly(γ-glutamic acid) nanoparticles have a potent intrinsic immune stimulatory capacity and trigger dendritic cell (DC) maturation accompanied by upregulation of costimulatory molecules and secretion of T cell-polarizing cytokines. This chapter discusses two different approaches that specifically target APCs, using either allergen- or antibody-loaded poly(γ-glutamic acid) nanoparticles for the purpose of developing novel immunotherapeutic regimens for allergy or cancer, respectively. For instance, loaded nanoparticles can protect the allergen from degradation and enhance internalization and subsequent presentation to specific T cells, while inducing polarizing cytokine responses. Nanoparticles can also be used as focused delivery devices of therapeutic antibodies, relevant for cancer immunotherapy, which enables hyper cross-linking of receptors and enhancement of antitumor responses. Thus, polymeric nanoparticles have several beneficial features that warrant further investigation of their suitability as components of novel immunotherapeutic strategies.

Keywords Adjuvant • Allergy • B cells • Cancer • Dendritic cells • Immunotherapy • Nanoparticles

M. Lindstedt (✉) • S. Broos
Department of Immunotechnology, Lund University, Medicon Village, 223 81 Lund, Sweden
e-mail: malin.lindstedt@immun.lth.se

M. Akashi et al. (eds.), *Engineered Cell Manipulation for Biomedical Application*, Nanomedicine and Nanotoxicology,
DOI 10.1007/978-4-431-55139-3_13

13.1 Introduction

Immunotherapy is the medical term for enhancing or suppressing immune responses for the purpose of treating disease. Stimulation of the immune response may be required if the body fails to respond adequately to dangerous events, such as rapid growth of malignant tumor cells. Furthermore, immune responses may be inaccurately directed against innocuous agents or self-antigens, which may lead to allergy or autoimmunity. For these diseases, suppression or redirection of the existing immune response is desired. For instance, in allergen immunotherapy, the objective is to introduce immunological tolerance by redirecting detrimental T helper (Th) 2 cell responses to a favorable activation of Th1 and regulatory T cells. In immunotherapy of cancer, it may be necessary to overcome immunosuppressive mechanisms caused by the tumor cells. Strategies that can be beneficial in this case include activation of cytotoxic T lymphocytes (CTL) and inhibition of suppressive mechanisms, such as stimulation of regulatory T cells.

Nanomedicine and the use of immune cell-targeting nanostructures have received considerable attention lately. Various particular biocompatible materials are being investigated for focused delivery of antigens for the purpose of initiating protective immune responses, and it has in several studies recently been demonstrated that nanoparticle-based vaccines can be much more potent than administration of vaccine alone. Benefits of using nanoparticles in immunotherapy include delivery to specific immune cells and slow release of therapeutic substances. Functional nanoparticle-based immunotherapy depends on several factors, including the intrinsic properties of the particles, such as their direct immunomodulatory effect through pathogen-recognition receptors, biodegradability, toxicity, size, charge, possibilities for protein conjugation, and hydrophobicity. Importantly, issues such as immune compatibility, stability, and reproducible production remain to be fully understood and solved before nanoparticles can be introduced into routine clinical practice.

In this chapter, different immunotherapeutic approaches that specifically target antigen-presenting cells (APCs), using poly(γ-glutamic acid)-*graft*-L-phenylalanine ethyl ester (γ-PGA-Phe) nanoparticles (NPs), are described. These biodegradable polymeric nanoparticles have an adjuvant effect on human dendritic cells (DCs) with regard to maturational changes and regulation of gene and protein expression. In addition, they are potent drug delivery systems through their ability to adsorb, encapsulate, and immobilize antigen. Thus, immunomodulatory polymeric nanoparticles as delivery devices that target antigen-presenting cells have several benefits that should be investigated for the purpose of developing novel immunotherapeutic regimens for allergy and cancer.

13.2 γ-PGA-Phe Nanoparticles as Protein Delivery Devices

Nanomedicine and the use of nanoparticles as immune stimulators and drug delivery systems for treatment of various diseases have received increased attention in recent years. Nanoparticles have several beneficial features relevant for immunotherapy,

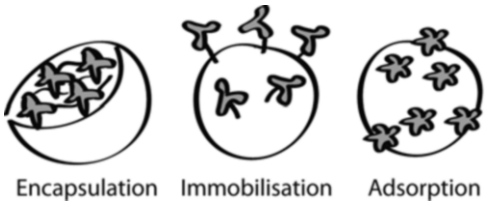

Fig. 13.1 Proteins can be physically attached to γ-PGA-Phe nanoparticles by encapsulation, immobilization, or adsorption

such as the possibility to control size and permeability, high drug loading capacity, as well as providing protection of the encapsulated substance from metabolism or degradation. Poly(γ-glutamic acid) (γ-PGA) is a naturally occurring polymer synthesized by certain strains of *Bacillus*, which is composed of D- and L-glutamic acid units linked through the α-amino and the γ-carboxylic acid groups [1]. The carboxylate side chains can easily be modified to introduce, e.g., hydrophobic groups to create self-assembling nanoparticles with a hydrophobic inner core and an outer shell of hydrophilic groups [2]. The size of the nanoparticles can simply be controlled during formation by adjusting the salt concentration. The most commonly used biodegradable γ-PGA nanoparticles are the hydrophobically modified version with L-phenylalanine ethyl ester (50 % grafting degree) of approximately 200 nm in size, termed poly(γ-glutamic acid)-*graft*-L-phenylalanine ethyl ester (γ-PGA-Phe) nanoparticles (NPs).

An important advantage of γ-PGA-Phe NPs is that a wide range of proteins can be physically attached to the nanoparticles without loss of protein function or stability [2, 3]. Protein loading can be achieved by adsorption, covalent immobilization, or encapsulation (Fig. 13.1). γ-PGA-Phe NPs have been demonstrated to induce both humoral and cellular antigen-specific immune responses as a result of their strong ability to activate human [4] and murine DCs [5, 6]. For instance, the potent role of γ-PGA-Phe NPs as vaccine carriers has been demonstrated in mice for various viral antigens such as HIV-1 p24 [7], influenza hemagglutinin (HA) [8], and HTLV-I [9], as well as tumor-associated antigens such as EphA2-derived peptides [10]. Thus, these nanoparticles have several beneficial properties for use in modern immunotherapies. However, as for other nanoparticles, several factors such as long-term toxicity, production of homogeneous nanoparticle preparation, and standardized protein conjugation or adsorption need to be addressed before NP-based immunotherapy can be transferred to the clinics.

13.3 Antigen-Presenting Cells as Central Players in the Immune Response

The immune system protects us from environmental exposure of pathogens, such as parasites, virus, and bacteria. It is also essential for removing cancerous cells and maintaining tolerance to self-antigens. APCs bridge innate and adaptive immunity by their ability to sample, process, and present antigens to T cells and activate specific effector cell responses. Activation of CTLs and different Th cell subsets depends on numerous factors, such as the stimulatory potential of the antigen, the

nature of the stimuli, the local tissue environment, and which DC subpopulation that are activated. Depending on the trigger, DCs can express soluble mediators and costimulatory molecules that influence the polarization of Th cells into different effector subsets, such as Th1, Th2, Th17, and regulatory T cells [11]. Consequently, DCs play a central decisive role in controlling the immune response to foreign antigens, as well as in maintaining tolerance to autologous or innocuous agents. Thus, modulating the function of APCs, and in particular DCs, is a potent strategy to stimulate or redirect specific immune responses, useful to treat diseases such as allergy and cancer.

13.3.1 Stimulatory Effect of γ-PGA-Phe Nanoparticles on Human Dendritic Cells

As DCs play such a central role in linking the innate and acquired immune responses, control of antigen delivery and maturation of DCs are important factors for the design of effective immunotherapies. Immature DCs are strategically positioned at body surfaces, ready to internalize antigens by phagocytosis, macropinocytosis, and endocytosis. In the presence of stimulatory antigens, such as those engaging pattern recognition receptors (PRRs), DCs mature while homing to secondary lymphoid organs. γ-PGA-Phe NPs have been demonstrated to have a potent stimulatory effect on DCs. They are rapidly internalized by DCs, which is followed by maturation with morphological changes, global transcriptional reprogramming, and upregulation of surface expression of CD80, CD86, and MHC class II molecules, which are prerequisites for DC's ability to induce T cell activation (Fig. 13.2) [4].

13.3.2 Transcriptional Activity Induced by γ-PGA-Phe Nanoparticles

Gene expression profiling of human monocyte-derived DCs (MoDCs) matured in the presence of γ-PGA-Phe NPs provides important information about the nature of the stimulatory effect of γ-PGA-Phe NPs. Recently, genome-wide transcriptional analysis has identified differential expression (more than 1.5-fold, $p < 0.05$) of 428 transcripts after 8 and/or 24 h of γ-PGA-Phe NP stimulation, compared to controls [4]. Among the upregulated transcripts, a number of costimulatory molecules, such as *CD40*, *CD80*, *CD137*, and *CD274* (*PD-L1*), were identified, which participate in the regulation of T cell activation. The transcriptional analysis also revealed induction of adhesion molecules, such as *CD48*, *ICAM1*, and *CD58*, as well as chemokine receptors, such as *CCR7* and *CXCR4*, molecules that are important for the ability of DCs to migrate from peripheral tissues to the T cell zone of secondary lymphoid organs. The transcriptional response of DCs stimulated with γ-PGA-Phe

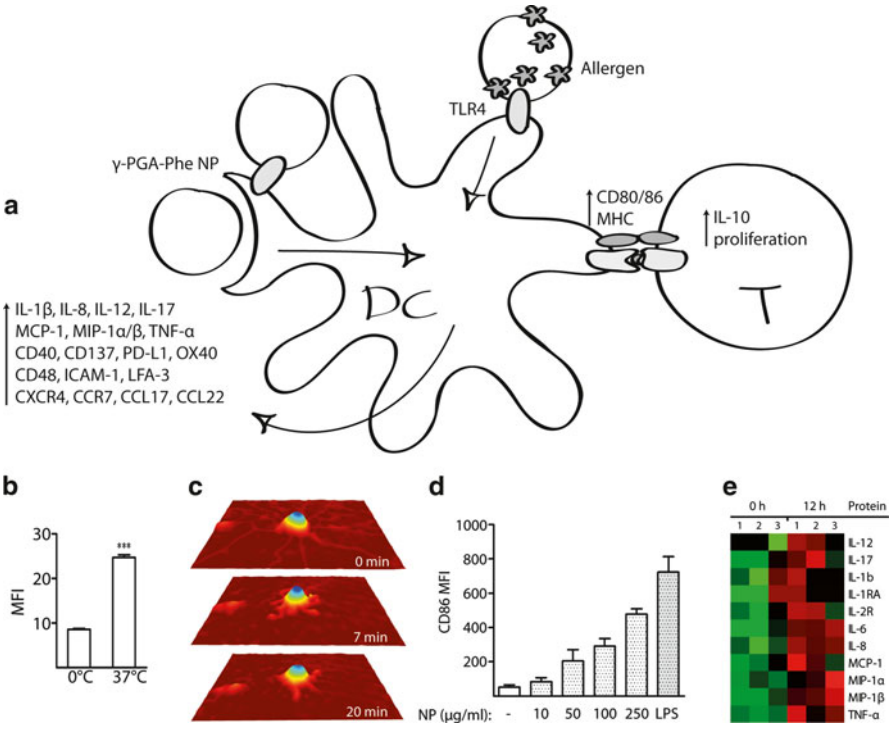

Fig. 13.2 γ-PGA-Phe NP-induced activation of human dendritic cells. (**a**) Schematic overview of DC maturation, accompanied by an increase in CD80, CD86, and MHC class II expression, as well as a global transcriptional reprogramming resulting in upregulation of polarizing proinflammatory cytokines, costimulatory receptors, adhesion, and homing molecules. Administration of grass pollen allergen with γ-PGA-Phe NPs leads to enhanced allergen uptake and presentation, as well as stimulating effect on allergen-specific T cells, resulting in proliferation and increased frequency of IL-10-producing T cells in vitro, while the production of IL-4, IL-5, IL-13, IFN-γ, and IL-17 was unaltered [4]. (**b**) γ-PGA-Phe NPs are rapidly internalized by human MoDCs, as demonstrated by flow cytometry. Alexa Fluor 488-conjugated γ-PGA-Phe NPs are internalized after 30 min incubation at 37 °C ($n = 9$). (**c**) Drastic morphological changes are induced in DCs during NP internalization, visualized by holographic microscopy images. (**d**) Concentration-dependent maturation of DCs. (**e**) Induction of soluble mediators by γ-PGA-Phe NP in DCs after 12 h stimulation, as determined by Luminex analysis. Adapted figures from [12] are used with permission from Elsevier

NPs was similar to the one observed after stimulation with pro-inflammatory mediators [13]. Many of the upregulated transcripts could be associated with an inflammatory response, such as *TNF-α*, *IL-1β*, and the major Th1-biasing cytokine *IL-12p40*. In addition, several chemokines were upregulated, such as *IL-8*, *MIP-1α*, *MIP-1β*, and *MCP-1*, that together attract e.g. neutrophils, monocytes, immature DCs, and T cell subsets [14]. These results suggest that γ-PGA-Phe NP-stimulated DCs can recruit other leukocytes to the site of inflammation, which play an important role in the augmentation of innate immune responses.

13.3.3 γ-PGA-Phe Nanoparticles Induced Phenotypic Alterations

γ-PGA-Phe NP also induces functional production of inflammatory cytokines by human DCs. Production of ten cytokines and cytokine receptor components (IL-1RA, IL-1β, IL-2R, IL-6, IL-8, IL-12, IL-17, MCP-1, MIP-1α, MIP-1β, and TNF-α) was confirmed using multiplex analysis, and cytokine transcripts induced by γ-PGA-Phe NPs after 8 h correlated well with the proteins found in DC supernatants after 12 h. Thus, γ-PGA-Phe NPs stimulate DCs to mature and produce inflammatory polarizing mediators, which may influence the immunological outcome in immunotherapy. The activation status of DCs is influenced by many different factors, such as the nature and the concentration of the antigen, which influence the immunological outcome. Furthermore, the physical properties of the antigen-nanoparticle complex, such as size, hydrophobicity, and charge, can vary depending on the antigen and how it is attached to the nanoparticles. It is also evident that the subtype and lineage of the stimulated DCs determine T cell polarization, and thus, it is important to understand the mechanisms of γ-PGA-Phe NP immune activation as this information would also give clues on suitable routes of administration.

13.3.4 Receptor Engagement by γ-PGA-Phe Nanoparticles

In order to develop safe and effective immunotherapies, it is imperative to understand how nanoparticles elicit their effect in vitro and in vivo, also at a molecular level. γ-PGA-Phe NPs affect ex vivo human DCs, isolated from peripheral blood, differently. Myeloid DCs mature and display transcriptional activity upon stimulation with γ-PGA-Phe NPs, while plasmacytoid DCs are poorly activated (unpublished observations). Thus, γ-PGA-Phe NPs seem to signal though specific receptors expressed by myeloid, but not plasmacytoid, DCs. Stimulation of human MoDCs with γ-PGA-Phe NPs results in regulation of a significant number of genes as described above, with activation of nuclear factor-kappa B (NF-κB) and mitogen-activated protein kinase (MAPK) signalling pathways, along with downregulation of TLR4 [4]. It has been found that surface expression of TLRs decreases dramatically upon TLR ligation [15]. Signalling through receptors of the TLR/IL-1R family is known to trigger activation of NF-κB, which plays a central role in the induction of innate and adaptive immune responses. TLR agonists are highly relevant adjuvants for vaccination, cancer immunotherapy, and allergen-specific immunotherapy. The TLR4 ligand MPL is an excellent example of a component of a recently approved adjuvant (AS04) that plays an important role in modulation of the innate response [16]. It was demonstrated that also γ-PGA-Phe NPs partially signal through TLR2 and/or TLR4, as neutralizing these receptors lead to reduced induction of costimulatory molecules in human DCs [4]. The mechanisms by which

γ-PGA-Phe NPs interact with TLRs are not yet understood; however, the hydrophobic regions on γ-PGA-Phe NPs may contribute, based on the observation that the stimulatory potential of γ-PGA-Phe NPs increases with hydrophobicity (unpublished observations) and both TLR2 and TLR4 are known to bind ligands that possess hydrophobic regions [17]. Also, additional mechanisms of activation are involved, as simultaneous neutralization of TLR2 and TLR4 cannot completely eliminate the capacity of γ-PGA-Phe NPs to induce DC maturation (unpublished observations). Uto et al. recently showed that phosphorylation of p38 was suppressed in TLR4- but not TLR2-deficient mice upon γ-PGA-Phe NP stimulation [18]. On the contrary, γ-PGA-Phe NP-induced antigen-specific cellular immune responses were not completely abolished in either MyD88 or TLR4 knockout mice, which also suggest involvement of other mechanisms. Thus, it is evident that γ-PGA-Phe NPs signal through TLR4 via the MyD88-dependent signalling pathway; however, the role of TLR2 is less clear. Various microparticulate adjuvants stimulate IL-1β secretion and caspase-1 activation, which has been shown to depend on activation of the NALP3 inflammasome [16]. Thus, this signalling pathway has also been suggested to contribute to the adjuvanticity of γ-PGA-Phe NPs [18]. Induction of IL-1β by γ-PGA-Phe NPs has been described in human DCs [4] and in rat middle ear mucosa (unpublished observations) and in murine bone marrow-derived DCs [6]. Thus far, there is however no clear evidence for the role of γ-PGA-Phe NP-induced inflammasome activation.

13.4 Nanoparticle-Based Allergy Immunotherapy

Promising results regarding the applicability of polymeric nanoparticles in the field of allergen immunotherapy are emerging, which can be used for development of new therapeutic strategies that improve clinical efficacy and safety. In addition to their intrinsic immune stimulatory function, nanoparticle encapsulation may for example be beneficial for protected delivery of allergen protein or peptides to DCs in allergy vaccination, thereby avoiding protein degradation as well as allergen-mediated side effects. The objective of allergen immunotherapy is to redirect the allergic response and induce tolerance. This treatment is presently the only long-term curative treatment for allergic diseases. However, treatment requires administration of repeated and increasing doses of allergen during an extended period of time and is often accompanied by local side effects, as well as the risk of anaphylaxis. The use of adjuvants, such as TLR ligands, is a promising strategy to improve the efficacy of allergy vaccines and reduce the required allergen dose, which may lead to improved treatment success rates as well as reduced treatment duration and side effects. This chapter will address the use of biodegradable nanoparticles as adjuvants in allergen immunotherapy and describe the functional effects of γ-PGA-Phe NPs on the T cell activating capacity of DCs in response to allergens.

13.4.1 Mechanisms of Allergen Immunotherapy

The objective of allergen immunotherapy is to obtain hyposensitization, associated with the induction of long-term allergen tolerance and a persistent switch in allergen-specific memory T and B cell responses. In this context, polarization of allergen-specific regulatory T cells by APCs plays a central role in counterbalancing Th2 responses. Regulatory T cells produce high levels of anti-inflammatory IL-10 and TGF-β, which induce class switch toward production of IgG4 and suppress IgE production [19]. IL-10 further downregulates the function of Th1 and Th2 cells by suppressing their proliferation and cytokine production [20]. Strategies that allow activation of the immune system while avoiding potential adverse reactions are highly desired. One such promising approach to bypass activation of effector cells via IgE is the use of recombinant hypoallergenic allergen derivatives [21], which may reduce the risk of provoking new sensitizations. Another strategy is to use Th1-stimulating adjuvants to improve the efficacy and decrease the allergen dose in immunotherapy, thereby limiting the side effects. Exploration of using immune modulatory allergen-carrying nanoparticles is relevant for both of these strategies.

13.4.2 γ-PGA-Phe Nanoparticles as Adjuvants and Allergen Carriers

Several strategies, employing various types of adjuvants, which modulate immune responses are currently being investigated for allergen immunotherapy. These include immunostimulating complexes (ISCOMs), liposomes, oligonucleotides, microorganism-derived adjuvants (i.e., MPL), as well as various particulate adjuvants, such as polymeric nanoparticles, polyesters, poly(anhydrides), and polysaccharides, as recently reviewed in [22]. Preferable, for a highly promising component of modern immunotherapy, novel adjuvants should function as both allergen carrier and stimulate desired immune responses. Traditional adjuvants, such as the most commonly clinically used aluminum salts, are considered safe and effective. However, they are far from ideal for all vaccine formulations as they are rather ineffective in inducing cellular immunity [23] and are associated with IgE-mediated allergic side effects [24]. Aluminum salts preferentially elicit humoral Th2 responses [10, 25], which is inappropriate when Th2 immunity is unfavorable, such as in immunotherapy of allergy or cancer. Alternatively, the γ-PGA-Phe NPs, triggering TLRs and a Th1 or a regulatory T cell-skewing cytokine profile, may serve to improve the efficacy of allergy vaccines as well as to reduce the dosing frequency and duration of the treatment. γ-PGA-Phe NPs stimulate DC maturation and production of inflammatory cytokines via TLR4, and possibly also TLR2, and, thus, worth evaluating for allergen immunotherapy. γ-PGA-Phe NPs were demonstrated to augment DC's ability to induce allergen-specific proliferation of autologous memory $CD4^+$ T cells in grass pollen-allergic subjects. Interestingly, this was accompanied

by an increased frequency of IL-10-producing T cells, while production of the Th2 cytokines IL-4, IL-5, and IL-13 or the Th1 and Th17 cytokines IFN-γ and IL-17 was unaffected, suggesting exclusive amplification of IL-10-producing $CD4^+$ memory T cells. Further studies are needed to evaluate the regulatory effects on T cell polarization and the exact nature of activated T cell subsets. Yet, the findings demonstrate that γ-PGA-Phe NPs have immunomodulatory effects on DCs that impact their function during allergen presentation in vitro, findings that are relevant for allergen immunotherapy in vivo. Their further ability to encapsulate and protect allergens from IgE interaction and degradation makes γ-PGA-Phe NPs interesting as a combined adjuvant and allergen-delivery system.

13.5 Nanoparticle-Based Cancer Immunotherapy

Cancer remains one of the leading causes of human mortality. It is a heterogeneous group of diseases, which can develop anywhere in the body and display a wide variety of molecular characteristics. Traditional treatment strategies, such as surgery, chemotherapy, and radiation therapy, have limited efficacy especially for treatment of disseminated cancers. Immunotherapy, which instead uses the host's own immune system to fight cancer, may provide long-term survival benefits and even a cure also for metastatic tumors. Immunotherapy strategies aim to counterbalance immunosuppressive tumor mechanisms by activating and enhancing antitumor immunity. This can be achieved either by directly activating cytotoxic T cell responses or indirectly by efficient activation of APCs, which is essential for priming of tumor-specific T cells.

13.5.1 Agonistic CD40 mAbs for Cancer Immunotherapy

CD40 is a member of the TNF receptor superfamily that is constitutively expressed on all APCs and plays a central role in regulation of both humoral and cellular immunity. CD40 ligation on APCs improves their antigen-presenting capacity, mainly through upregulation of MHC class II, costimulatory B7, and adhesion molecules, and induces secretion of inflammatory cytokines, such as IL-6, IL-12, TNF-α, and IL-1β, which contribute to further APC maturation as well as activation and survival of T cells [26]. CD40 is also expressed on many tumor cells, including non-Hodgkin's and Hodgkin's lymphomas, lymphocytic and acute myeloid leukemia, multiple myeloma, and some carcinomas, as reviewed in [26]. Treatment with agonistic CD40 monoclonal antibodies (anti-CD40 mAbs) has demonstrated promising antitumor effects preclinically in various tumor models [27, 28] as well as in Phase I clinical trials for patients with solid tumors, non-Hodgkin's lymphoma, and multiple myeloma [29–31]. Anti-CD40 mAbs have potential to generate anticancer immunity by various mechanisms. The primary consequence is activation of APC

and thus promotion of antitumor T cell responses by enhancing processing and presentation of tumor-associated antigens. Anti-CD40 mAbs may also generate tumoricidal myeloid cells and have a cytotoxic effect on tumors by initiating antibody-dependent cellular cytotoxicity (ADCC), complement-mediated cytotoxicity (CMC), or programmed cell death, as discussed in [32]. However, systemic exposure to anti-CD40 agonists is associated with severe side effects, such as cytokine release syndrome and liver damage, which severely limits the tolerated dose for human therapy. Thus, strategies to improve the safety of anti-CD40 treatment are highly attractive. This section will present different evaluated approaches to improve the efficacy and safety of agonistic anti-CD40 mAbs, both CD40-mediated effects on APCs in vitro and antitumor effects and systemic release of anti-CD40 mAbs and cytokines in vivo, following local drug administration.

13.5.2 Nanoparticle-Coupled Anti-CD40 mAbs for Local Cancer Therapy

The potent immunostimulatory effect and ability of γ-PGA-Phe NPs to deliver proteins to APCs can be beneficial for CD40-targeted cancer immunotherapy, as local treatment with anti-CD40 mAbs coupled to γ-PGA-Phe NPs would allow for improved immune activation and local drug retention in the tumor area. Adsorption to γ-PGA-Phe NPs, which could easily be attained by pure mixing, significantly improved CD40-mediated maturation of APC, as shown by enhanced expression of CD80 and CD86 on B cells and MoDCs [12]. Downregulation of costimulatory molecules is one key strategy used by tumors to evade immune surveillance, and thus, restoring their expression is critical for efficient priming of tumor-specific CTLs. Furthermore, adsorption of anti-CD40 mAbs (clone B44) to γ-PGA-Phe NPs also results in synergistically enhanced B cell proliferation, as well as increased secretion of IL-12 by MoDCs (Fig. 13.3). It has been demonstrated that IL-12 enhances antigen presentation, increases the activity of Th1 cells, CTLs, NK cells, and B cells [32], and has potent antitumor effects in preclinical models [26]. Therefore, induction of IL-12 production likely contributes to the immune-mediated efficacy of anti-CD40 mAbs. The synergistic effects observed for B cell proliferation when anti-CD40 mAb is administered adsorbed onto γ-PGA-Phe NPs suggest that physical adsorption is central for the enhanced anti-CD40 activity (Fig. 13.3b, c). The synergistic effects remained after several washing steps (Fig. 13.3b). Supposedly, a higher degree of CD40 receptor multimerization occurs after adsorption of anti-CD40 mAbs to γ-PGA-Phe NPs, which results in a stronger receptor-mediated signal and activation of downstream signalling pathways. Signalling through CD40 depends on transient multimerization of the receptor and recruitment of TNFR-associated factor (TRAF) adapter proteins, which bind to distinct domains of the cytoplasmic tail [27]. CD40-mediated responses reflect the signals from distinct TRAFs, and the strength of the signal is directly correlated to the valency of the CD40 ligand and the extent of receptor cross-linking [28]. While rescue from

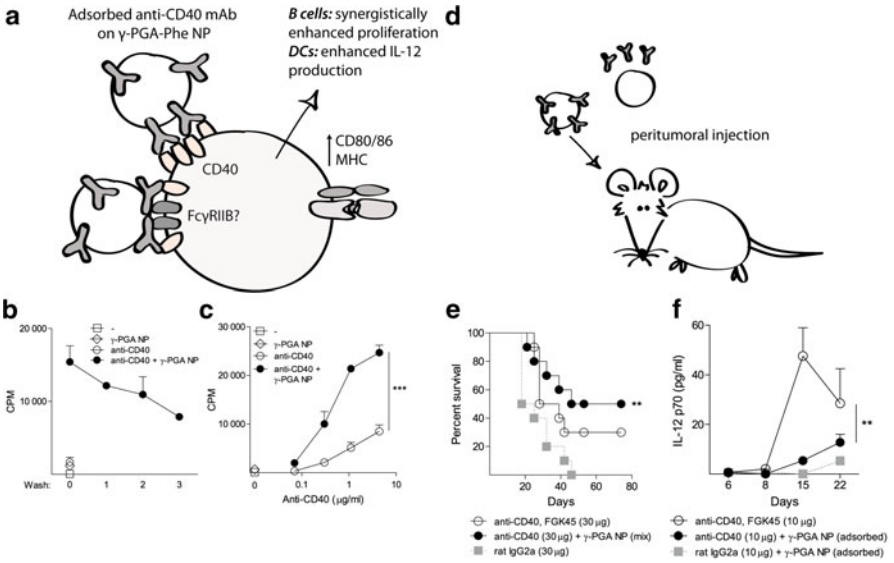

Fig. 13.3 Immune-stimulating effects of anti-CD40 mAbs in combination with γ-PGA-Phe NPs. (**a**) CD40 agonists adsorbed to γ-PGA-Phe NPs induce augmented expression of CD80 and CD86 on DCs and B cells, as well as increased IL-12 production by DCs and synergistically enhanced B cell proliferation, in vitro [12]. (**b**) Adsorption of anti-CD40 mAbs to NPs retains synergistic ability to induce B cell proliferation, even after three washes, as assessed by ^{3}H-thymidine incorporation. (**c**) Synergistic proliferative effects after addition of different concentrations of anti-CD40 mAbs and γ-PGA-Phe NPs, as compared to anti-CD40 mAbs or γ-PGA-Phe NPs alone. (**d**–**f**) Antitumor activity following treatment with anti-CD40 mAbs and γ-PGA-Phe NPs, as well as anti-CD40 mAb alone. (**e**) Percent survival of mice receiving treatment. Female C57BL/6 mice (10/treatment group) were injected subcutaneously with tumor cells and received peritumoral injections of anti-CD40 mAb, anti-CD40 mAb in combination with γ-PGA NPs, or rat IgG2a isotype control on days 8, 15, and 22. (**f**) Systemic release of inflammatory cytokines following treatment with anti-CD40 mAb adsorbed to γ-PGA NPs vs. soluble anti-CD40 mAb. Serum levels of IL-12, using Cytometric Bead Array, on day 6 before therapy started and 4 h post each treatment on days 8, 15, and 22. Adapted figures from [12] are used with permission from Elsevier

apoptosis requires minimal cross-linking, induction of, e.g., proliferation and upregulation of costimulatory molecules requires a high degree of CD40 multimerization and the recruitment of TRAF6 [29]. However, additional mechanisms are involved in mounting the synergistic effects, as cross-linking of anti-CD40 mAbs with secondary anti-IgG Abs could not replace the strong effects observed for adsorption to γ-PGA-Phe NPs (unpublished observations).

One such mechanism may be binding to FcγR. The importance of the Fc domain and coengagement of FcγRIIB has in several recent studies been demonstrated to be a requirement for the antitumor activities of agonistic anti-CD40, as well as for other anti-TNFR antibodies [30, 31, 33]. FcγRIIB coengagement has been suggested to provide a scaffold in vivo that is necessary for efficient cross-linking of CD40 on DCs [34]. Also, the in vitro activity of agonistic anti-CD40 mAbs is dependent on FcγR binding. By generating aglycosylated variants of anti-CD40

mAbs having impaired FcγR binding, it was shown that the stimulatory activity was dramatically compromised, suggesting that the Fc domain is highly important for immune activation [12]. These results suggest that FcγR binding contributes to the synergy between anti-CD40 mAbs and γ-PGA-Phe NPs, possibly though enhanced coengagement of FcγRIIB, facilitated by nanoparticle adsorption.

As mentioned previously, administration of CD40 mAbs with γ-PGA-Phe NPs may be an effective way to improve the efficacy and safety of locally administered anti-CD40 mAbs (Fig. 13.3d). Peritumoral treatment with a mixture of γ-PGA-Phe NPs and a murine anti-CD40 mAb (clone FGK45) significantly enhanced the survival of mice challenged with bladder cancer, compared to untreated mice [12]. However, no significant difference was observed between this treatment and soluble anti-CD40 mAb alone (Fig. 13.3e). On the other hand, when anti-CD40 mAb was administered adsorbed to γ-PGA-Phe NPs, the systemic release of TNF-α, IL-6, IL-10, and IL-12 (exemplified in Fig. 13.3f) was significantly reduced, compared to treatment with soluble anti-CD40 mAb. Thus, nanoparticle adsorption may lead to reduced systemic leakage of locally administered anti-CD40 mAbs and, consequently, minimized toxic side effects. Similarly, reduced systemic toxicity has also been demonstrated when anti-CD40 mAbs have been locally administered in other slow-release formulations [35, 36].

As a final point, particularly promising results have been presented when CD40-targeted therapies have been combined with other immunotherapeutic or conventional therapies [37–40]. For instance, CD40 activation has been demonstrated to facilitate CTL responses and sensitize tumor cells to chemotherapy-induced apoptosis in cervical carcinoma [41]. Furthermore, pre-activation of macrophages by CD40 ligation followed by CpG stimulation synergistically enhanced their antitumor activity [42]. Therefore, further benefits may be added if other types of antibodies are conjugated to the γ-PGA-Phe NPs, targeting, e.g., tumor-specific antigens or other immunomodulatory molecules.

13.6 Concluding Remarks

In this chapter, the applicability of nanoparticles as delivery systems and adjuvant to control cellular functions has been described, with focus on their beneficial role for development of novel immunotherapeutic regimens for cancer and allergy. Biodegradable polymeric γ-PGA-Phe NPs activate human DCs and stimulate a maturational process that favors polarization of Th1 cells, by inducing IL-1β, TNF-α, and IL-12 production in vitro. Even though the exact mechanisms of action remain to be clarified, it was demonstrated that γ-PGA-Phe NPs stimulate human DCs through TLR4 and possibly TLR2. γ-PGA-Phe NPs also modify the functional activity of allergen-stimulated DCs, resulting in increased IL-10 production by $CD4^+$ memory T cells, which suggests suppressive activity of Th2 cells, which may be beneficial in allergen immunotherapy. γ-PGA-Phe NPs may further protect the allergen from degradation if it is encapsulated within the NPs and prevent the

allergen from binding to IgE, thereby reducing the IgE-mediated side effects. In addition, a potent approach to improve treatment with agonistic anti-CD40 mAbs in cancer immunotherapy can be to administer the mAbs with γ-PGA-Phe NPs. Adsorption of anti-CD40 mAbs to γ-PGA-Phe NPs was demonstrated to synergistically enhance the stimulatory CD40-mediated effect on APCs in vitro, likely due to improved receptor cross-linking. Furthermore, administration of anti-CD40 mAbs adsorbed to γ-PGA-Phe NPs peritumorally resulted in reduced systemic release of cytokines in vivo after local drug delivery. Thus, allowing reduced dosing frequency and minimized side effects by nanoparticle adsorption may improve the efficacy and safety of CD40 therapy. In conclusion, γ-PGA-Phe NPs constitute an attractive delivery system for vaccines and immunotherapeutic substances for induction of desired immune responses required to combat cancer and control allergic reactions.

References

1. Sung MH, Park C, Kim CJ, Poo H, Soda K, Ashiuchi M (2005) Natural and edible biopolymer poly-gamma-glutamic acid: synthesis, production, and applications. Chem Rec 5:352–366
2. Akagi T, Kaneko T, Kida T, Akashi M (2005) Preparation and characterization of biodegradable nanoparticles based on poly(gamma-glutamic acid) with l-phenylalanine as a protein carrier. J Control Release 108:226–236
3. Akagi T, Kaneko T, Kida T, Akashi M (2006) Multifunctional conjugation of proteins on/into bio-nanoparticles prepared by amphiphilic poly(gamma-glutamic acid). J Biomater Sci 17:875–892
4. Broos S, Lundberg K, Akagi T, Kadowaki K, Akashi M, Greiff L, Borrebaeck CA, Lindstedt M (2010) Immunomodulatory nanoparticles as adjuvants and allergen-delivery system to human dendritic cells: Implications for specific immunotherapy. Vaccine 28:5075–5085
5. Uto T, Wang X, Sato K, Haraguchi M, Akagi T, Akashi M, Baba M (2007) Targeting of antigen to dendritic cells with poly(gamma-glutamic acid) nanoparticles induces antigen-specific humoral and cellular immunity. J Immunol 178:2979–2986
6. Akagi T, Wang X, Uto T, Baba M, Akashi M (2007) Protein direct delivery to dendritic cells using nanoparticles based on amphiphilic poly(amino acid) derivatives. Biomaterials 28:3427–3436
7. Wang X, Uto T, Akagi T, Akashi M, Baba M (2007) Induction of potent CD8+ T-cell responses by novel biodegradable nanoparticles carrying human immunodeficiency virus type 1 gp120. J Virol 81:10009–10016
8. Okamoto S, Yoshii H, Akagi T, Akashi M, Ishikawa T, Okuno Y, Takahashi M, Yamanishi K, Mori Y (2007) Influenza hemagglutinin vaccine with poly(gamma-glutamic acid) nanoparticles enhances the protection against influenza virus infection through both humoral and cell-mediated immunity. Vaccine 25:8270–8278
9. Matsuo K, Yoshikawa T, Oda A, Akagi T, Akashi M, Mukai Y, Yoshioka Y, Okada N, Nakagawa S (2007) Efficient generation of antigen-specific cellular immunity by vaccination with poly(gamma-glutamic acid) nanoparticles entrapping endoplasmic reticulum-targeted peptides. Biochem Biophys Res Commun 362:1069–1072
10. Yamaguchi S, Tatsumi T, Takehara T, Sasakawa A, Yamamoto M, Kohga K, Miyagi T, Kanto T, Hiramastu N, Akagi T, Akashi M, Hayashi N (2010) EphA2-derived peptide vaccine with amphiphilic poly(gamma-glutamic acid) nanoparticles elicits an anti-tumor effect against mouse liver tumor. Cancer Immunol Immunother 59:759–767

11. Mazzoni A, Segal DM (2004) Controlling the Toll road to dendritic cell polarization. J Leukoc Biol 75:721–730
12. Broos S, Sandin LC, Apel J, Totterman TH, Akagi T, Akashi M, Borrebaeck CA, Ellmark P, Lindstedt M (2012) Synergistic augmentation of CD40-mediated activation of antigen-presenting cells by amphiphilic poly(gamma-glutamic acid) nanoparticles. Biomaterials 33:6230–6239
13. Lindstedt M, Johansson-Lindbom B, Borrebaeck CA (2002) Global reprogramming of dendritic cells in response to a concerted action of inflammatory mediators. Int Immunol 14:1203–1213
14. Sallusto F, Lanzavecchia A, Mackay CR (1998) Chemokines and chemokine receptors in T-cell priming and Th1/Th2-mediated responses. Immunol Today 19:568–574
15. Visintin A, Mazzoni A, Spitzer JH, Wyllie DH, Dower SK, Segal DM (2001) Regulation of Toll-like receptors in human monocytes and dendritic cells. J Immunol 166:249–255
16. Sharp FA, Ruane D, Claass B, Creagh E, Harris J, Malyala P, Singh M, O'Hagan DT, Petrilli V, Tschopp J, O'Neill LA, Lavelle EC (2009) Uptake of particulate vaccine adjuvants by dendritic cells activates the NALP3 inflammasome. Proc Natl Acad Sci U S A 106:870–875
17. Seong SY, Matzinger P (2004) Hydrophobicity: an ancient damage-associated molecular pattern that initiates innate immune responses. Nat Rev Immunol 4:469–478
18. Uto T, Akagi T, Yoshinaga K, Toyama M, Akashi M, Baba M (2011) The induction of innate and adaptive immunity by biodegradable poly(gamma-glutamic acid) nanoparticles via a TLR4 and MyD88 signaling pathway. Biomaterials 32:5206–5212
19. Meiler F, Klunker S, Zimmermann M, Akdis CA, Akdis M (2008) Distinct regulation of IgE, IgG4 and IgA by T regulatory cells and toll-like receptors. Allergy 63:1455–1463
20. Del Prete G, De Carli M, Almerigogna F, Giudizi MG, Biagiotti R, Romagnani S (1993) Human IL-10 is produced by both type 1 helper (Th1) and type 2 helper (Th2) T cell clones and inhibits their antigen-specific proliferation and cytokine production. J Immunol 150:353–360
21. Levin M, Rydnert F, Kallstrom E, Tan LW, Wormald PJ, Lindstedt M, Greiff L, Ohlin M (2013) Phl p 1-specific human monoclonal IgE and design of a hypoallergenic group 1 grass pollen allergen fragment. J Immunol 191:551–560
22. De Souza Reboucas J, Esparza I, Ferrer M, Sanz ML, Irache JM, Gamazo C (2012) Nanoparticulate adjuvants and delivery systems for allergen immunotherapy. J Biomed Biotechnol 2012:474605
23. Brewer JM (2006) (How) do aluminium adjuvants work? Immunol Lett 102:10–15
24. Gupta RK (1998) Aluminum compounds as vaccine adjuvants. Adv Drug Deliv Rev 32:155–172
25. Grun JL, Maurer PH (1989) Different T helper cell subsets elicited in mice utilizing two different adjuvant vehicles: the role of endogenous interleukin 1 in proliferative responses. Cell Immunol 121:134–145
26. O'Donnell MA, Luo Y, Hunter SE, Chen X, Hayes LL, Clinton SK (2004) Interleukin-12 immunotherapy of murine transitional cell carcinoma of the bladder: dose dependent tumor eradication and generation of protective immunity. J Urol 171:1330–1335
27. Davies CC, Mak TW, Young LS, Eliopoulos AG (2005) TRAF6 is required for TRAF2-dependent CD40 signal transduction in nonhemopoietic cells. Mol Cell Biol 25:9806–9819
28. Haswell LE, Glennie MJ, Al-Shamkhani A (2001) Analysis of the oligomeric requirement for signaling by CD40 using soluble multimeric forms of its ligand, CD154. Eur J Immunol 31:3094–3100
29. Reyes-Moreno C, Girouard J, Lapointe R, Darveau A, Mourad W (2004) CD40/CD40 homodimers are required for CD40-induced phosphatidylinositol 3-kinase-dependent expression of B7.2 by human B lymphocytes. J Biol Chem 279:7799–7806
30. Li F, Ravetch JV (2011) Inhibitory Fcgamma receptor engagement drives adjuvant and anti-tumor activities of agonistic CD40 antibodies. Science 333:1030–1034
31. White AL, Chan HT, Roghanian A, French RR, Mockridge CI, Tutt AL, Dixon SV, Ajona D, Verbeek JS, Al-Shamkhani A, Cragg MS, Beers SA, Glennie MJ (2011) Interaction with FcgammaRIIB is critical for the agonistic activity of anti-CD40 monoclonal antibody. J Immunol 187:1754–1763

32. Trinchieri G (2003) Interleukin-12 and the regulation of innate resistance and adaptive immunity. Nat Rev Immunol 3:133–146
33. Li F, Ravetch JV (2012) Apoptotic and antitumor activity of death receptor antibodies require inhibitory Fcgamma receptor engagement. Proc Natl Acad Sci U S A 109:10966–10971
34. Nimmerjahn F, Ravetch JV (2012) Translating basic mechanisms of IgG effector activity into next generation cancer therapies. Cancer Immun 12:13
35. Fransen MF, Sluijter M, Morreau H, Arens R, Melief CJ (2011) Local activation of CD8 T cells and systemic tumor eradication without toxicity via slow release and local delivery of agonistic CD40 antibody. Clin Cancer Res 17:2270–2280
36. Kwong B, Liu H, Irvine DJ (2011) Induction of potent anti-tumor responses while eliminating systemic side effects via liposome-anchored combinatorial immunotherapy. Biomaterials 32:5134–5147
37. Jackaman C, Lew AM, Zhan Y, Allan JE, Koloska B, Graham PT, Robinson BW, Nelson DJ (2008) Deliberately provoking local inflammation drives tumors to become their own protective vaccine site. Int Immunol 20:1467–1479
38. Ahonen CL, Doxsee CL, McGurran SM, Riter TR, Wade WF, Barth RJ, Vasilakos JP, Noelle RJ, Kedl RM (2004) Combined TLR and CD40 triggering induces potent CD8+ T cell expansion with variable dependence on type I IFN. J Exp Med 199:775–784
39. Sorensen MR, Holst PJ, Steffensen MA, Christensen JP, Thomsen AR (2010) Adenoviral vaccination combined with CD40 stimulation and CTLA-4 blockage can lead to complete tumor regression in a murine melanoma model. Vaccine 28:6757–6764
40. Nowak AK, Robinson BW, Lake RA (2003) Synergy between chemotherapy and immunotherapy in the treatment of established murine solid tumors. Cancer Res 63:4490–4496
41. Hill SC, Youde SJ, Man S, Teale GR, Baxendale AJ, Hislop A, Davies CC, Luesley DM, Blom AM, Rickinson AB, Young LS, Eliopoulos AG (2005) Activation of CD40 in cervical carcinoma cells facilitates CTL responses and augments chemotherapy-induced apoptosis. J Immunol 174:41–50
42. Buhtoiarov IN, Lum HD, Berke G, Sondel PM, Rakhmilevich AL (2006) Synergistic activation of macrophages via CD40 and TLR9 results in T cell independent antitumor effects. J Immunol 176:309–318

Chapter 14
Barrier Signalling

Saif Salih and Charles Patrick Case

Abstract According to the Oxford dictionary a barrier is a fence or other obstacle that prevents movement or access. In this chapter we explore whether a cellular barrier, such as occurs in the placenta, brain or eye, has a similar function. We show that a process of signalling across model barriers is possible in tissue culture but only when the barrier is bilayered or multilayered. This may be triggered by nanoparticle exposure but also by other factors which generate oxygen free radicals. The signalling within the barrier is made possible by communication between cells in the barrier through connexin gap junctions/hemichannels and pannexin channels. It involves purinergic transmission and Ca^{2+} wave propagation. Cytokines and DNA-damaging molecules may be released from the barrier. We discuss whether this signalling across cell barriers may occur in vivo.

Keywords DNA damage • Gap junctions • Nanoparticles • Placenta • Trophoblast barriers

14.1 Introduction

The dictionary definition of barrier is an object that bars advance, progress or crossing. Biological barriers are more intricate than this and serve several functions in addition to the dictionary definition. This chapter will specifically discuss signalling within a barrier, potential mechanisms of signalling and its role within an organism.

Biologically, barriers are used by organisms for protection, separation and maintenance of shape. For example, the bacterial cell wall helps protect the bacteria from outside insult, the cell membrane in the neurone allows the separation of ions and maintenance of a cell membrane potential, and the plant cell wall maintains the plant cells' shape and prevents the cell from bursting with changes in osmotic pressure.

S. Salih • C.P. Case (✉)
Bristol Musculoskeletal Research Unit, Clinical Science at North Bristol,
University of Bristol, Learning and Research Centre, Southmead Hospital,
Avon BS10 5NB, UK
e-mail: c.p.case@bristol.ac.uk

M. Akashi et al. (eds.), *Engineered Cell Manipulation for Biomedical Application*, Nanomedicine and Nanotoxicology,
DOI 10.1007/978-4-431-55139-3_14

Signalling, or, as the dictionary defines it, "the transmission of a message or signal", is not a function typically associated with a barrier. The phospholipid bilayer is a barrier that contributes to signalling in a neurone. It controls and regulates the passage of ions across itself in a manner that permits an action potential to be propagated along its length. In this sense the phospholipid bilayer is a barrier that contributes to signalling but is not the generator of the signal itself. The barrier signalling discussed here is novel in that a signal is generated within the barrier and is transmitted across the barrier.

14.2 Signalling Across Cell Barriers

The concept of barrier signalling derives from work by Bhabra et al. [1]. But before discussing this, the concept of cobalt-chromium (CoCr) nanoparticles and their effect on human fibroblasts must be discussed. Papageorgiou et al. [2] showed that CoCr nanoparticles caused DNA damage in cells when applied to human fibroblasts. Bhabra et al. [1] investigated this further by asking whether the DNA damage that CoCr nanoparticles caused in human fibroblasts persisted in the presence of a cellular barrier. The authors used a co-culture experimental setup as a model (Fig. 14.1); the fibroblasts represented the target cells; the cells in the barrier, suspended above the fibroblasts on a transwell insert, represented a tissue culture model of a placental barrier.

Interestingly, the presence of the barrier did not prevent DNA damage in the fibroblasts. Furthermore the DNA damage in the cells was of a greater level than that seen when the cells were exposed to the same insult without the cellular barrier [1]. The DNA damage was not caused by nanoparticles crossing the barrier. In this sense the barrier behaved as the dictionary definition would suggest. Instead the nanoparticles appeared to be internalised by the barrier cells. Photomicrographs show nanoparticles within the superficial cell layer of the BeWo barrier, and rather than cross the barrier the particles undergo corrosion. This was suggested by the difference in the composition of the metal detected in the medium on the other side of the barrier compared to the composition of the metal in the particles.

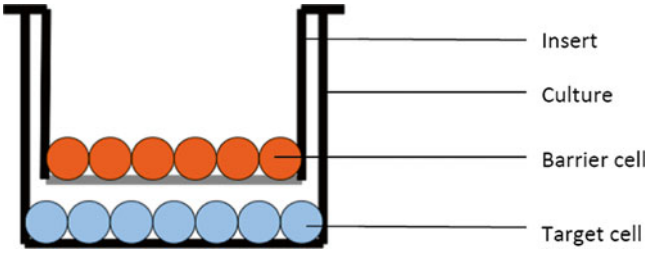

Fig. 14.1 Experimental setup. The barrier cells are suspended by the insert and represent the placental barrier in vivo. The target cell represents the foetus

However the DNA damage seen in cells across this barrier was not a direct result of the presence of any metal corrosion products but rather the result of a signalling process that occurred within the barrier.

To support this, the authors show a different type of DNA damage in cells exposed to the nanoparticles via the porous polyester membrane without cells grown upon it than those exposed to nanoparticles via a fully grown barrier. When applied directly to fibroblasts, nanoparticles induced aneuploidy as the predominant chromosomal aberration. When the particles were applied to the barrier, the cells underneath exhibited more tetraploidy. In both cases single-stranded and double-stranded breaks were detected using the comet assay.

Therefore there was a difference in the mechanism that caused DNA damage in the fibroblasts when nanoparticles were applied directly to the fibroblasts or indirectly via a barrier. The addition of gap junction blockers to the barrier cells was found to reduce the damage in the fibroblasts when nanoparticles were added to the barrier.

A gap junction is a protein-lined channel providing cytoplasmic continuity between adjacent cells [3]. A gap junction is comprised of two connexin hemichannels which are also known as connexons. A connexon is a hexameric *trans*-membranous protein that forms a pore in the phospholipid bilayer. The connexin protein family is highly conserved [4]. The protein consists of an intracellular N-terminus, four *trans*-membranous domains, two extracellular loops and an intracellular C-terminus. The greatest variability in the protein sequence occurs in the C-terminus which is subject to post-translational modification and interacts with different intracellular protein cascades. Connexin proteins are formed in the Golgi apparatus of the cell and transported to the cell's surface membrane where they aggregate in plaques. These plaques "dock" with plaques on other cells to form a gap junction, which affords the two cells' cytoplasmic continuity (Fig. 14.2).

The barrier cell used in by Bhabra et al. was the BeWo choriocarcinoma cell [1]. This cell line, which has been used as a model for the placenta extensively in the past, was an appropriate model. The authors also showed that the BeWo cell expressed connexin 43 as does the human placenta. Gap junctions have been implicated in intercellular signalling: they allow the transmission of action potentials between cardiac myocytes and between neurons. Abnormalities in connexin proteins and gap junction formation result in abnormal development and human diseases. For example, mutations in connexin 32 affect normal Schwann cell development and signalling resulting in neuropathy seen in Charcot–Marie–Tooth disease [5, 6].

Gap junctions allow the passage of small molecular messengers between cells, and the hemichannel on a cell membrane can allow the passage of these messenger molecules into the intercellular milieu [3]. ATP and calcium are examples of such molecular messengers, and they have been shown to pass through hemichannels and gap junctions [7]. Addition of apyrase, which hydrolyses ATP, reduced the DNA damage seen in fibroblasts underneath the BeWo cell barrier exposed to CoCr nanoparticles [1]. Blockade of ATP receptors using Compound 17 (C17) also reduced the DNA damage. This suggested a role for hemichannel-mediated release of ATP that binds to receptors in the mechanisms of the damage seen in the fibroblasts.

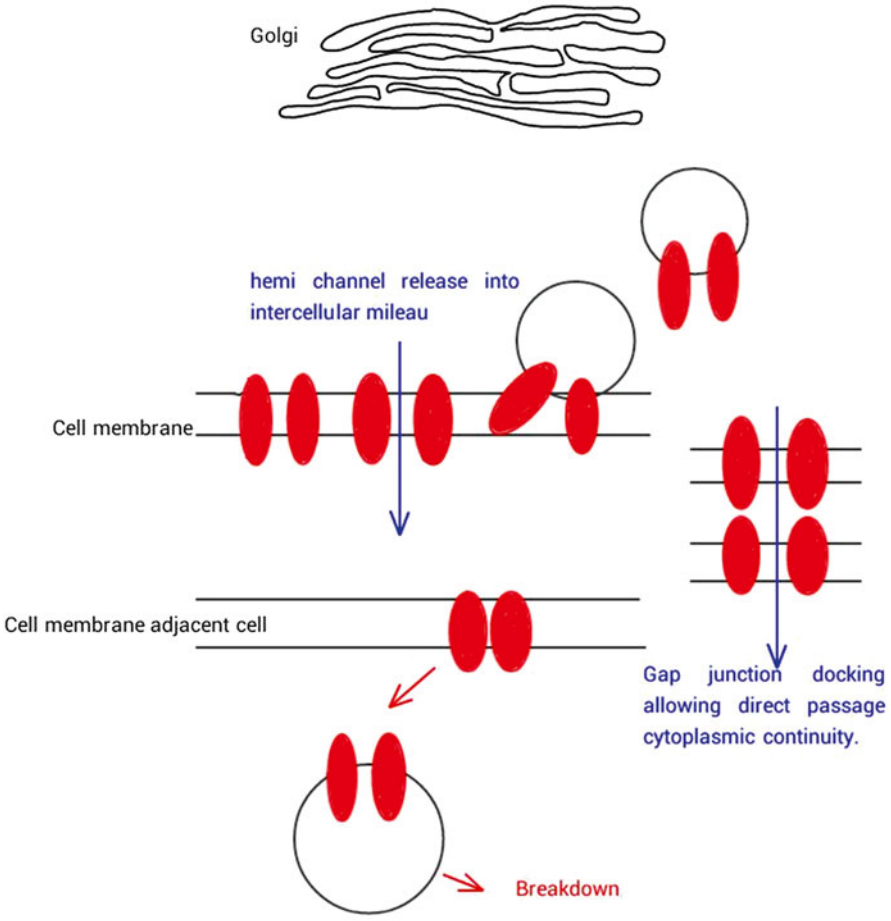

Fig. 14.2 Gap junction cycling

14.3 Radiation Induced Bystander Effect

The involvement of gap junctions in the barrier signalling mechanism echoed that seen in the bystander effect. The bystander effect describes a phenomenon in which a non-irradiated cell demonstrates the biological effects of a cell that has been irradiated [8]. It was first noted when cell colonies receiving a low- dose alpha-particle irradiation exhibited chromosomal abnormalities in a much larger proportion of cells than would have been expected from the dose of radiation [9, 10]. However these were statistical observations based on probability of cell nucleus being traversed by an alpha particle and whether the cell exhibited DNA damage. It was not

until medium transfer experiments were performed, whereby the medium bathing irradiated cells was applied to non-exposed cells, that the hypothesis of a secreted factor or factors from an irradiated cell could affect a non-irradiated cell [11]. The development of newer technology allowed the targeting of an individual cell in culture with an alpha-particle microbeam [8, 12]. Damage was demonstrated in cells and their progeny that had not been hit by an alpha particle. The DNA damage seen included double-stranded DNA breaks, micronuclei, chromosomal aberrations, chromatid breaks and apoptosis [12, 13]. The amount of DNA damage seen in non-irradiated cells was dependent also upon the density of the surrounding cells. When the density of the cells was high enough to allow cell–cell contact the amount of damage seen following the irradiation of a single cell was greater than the amount of damage seen when the cells were grown at a lower density [8]. This led to the suggestion that, as well as secretable paracrine factors, cell–cell interactions played a part in the bystander effect. Non-specific blockers of cell–cell communication such as lindane and octanol reduced the DNA damage seen in the bystander phenomenon. Irradiation of gap junction-deficient cell lines also reduced the level of damage [12]. The role of gap junctions in the bystander phenomenon is controversial however. Noncommunicating Jeg3 cells, a choriocarcinoma cell line like the BeWo cell but with inducible connexon protein intercellular connections, continued to exhibit bystander-like signalling after irradiation, even if the communicating channels are not induced [14]. Despite this, intercellular signalling remains an important factor in the bystander mechanism and the barrier mechanism.

14.4 Chemical-Induced Bystander Effect

The same group in Bristol has investigated the bystander effect with ionic Cr previously [15]. Fibroblasts were treated with Cr, washed to remove any traces of the Cr and then left in fresh medium. After 24 h this medium was transferred onto untreated fibroblasts. These medium transfer experiments suggested that a signalling mediator is released by the damaged cells that acts upon its neighbours and induces further damage. We will revisit the bystander effect later but for now return to the concept of the barrier and its ability to signal.

14.5 Monolayered Versus Bilayered/Multilayered Barriers

One comment arising from the work by Bhabra et al. was that the human placenta was not three to five cells thick like the BeWo barrier model used in their work [1]. The authors grew thick barriers like this to ensure that no nanoparticles could cross the barrier and cause direct DNA damage.

Sood and colleagues then grew the same cell line as barriers but produced barriers that were predominantly monolayered or predominantly bilayered [16]. This was an attempt to represent the human placenta; the human placenta has a layer of cytotrophoblast underneath a layer of syncytiotrophoblast as the placental "barrier" in the first trimester which becomes predominantly monolayered throughout the second and third trimester as the cytotrophoblast recedes leaving only the single layer of the syncytiotrophoblast [17].

Curiously when nanoparticles were placed above the monolayered barrier the level of DNA damage seen in the fibroblasts underneath was comparable to a control exposure and much less than that seen when the particles were placed above the bilayer [16]. Thus the thinner barrier appeared more "protective", or the bilayer is more damaging, or more than one cellular layer is required to signal. To further investigate this phenomenon a different cell line was used to grow barriers of single cell and multiple cell thickness. AS corneal cell barriers of one or two layers were grown and these behaved in the same way: the monolayers did not signal but the bilayers did. Also like the BeWo barrier, the signalling was inhibited by the use of gap junction blockers.

It is known that nanoparticles induce oxidative stress in cells [18–20]. Furthermore, cobalt, the major constituent of chromium-cobalt nanoparticles, induces a chemical hypoxia within cells with subsequent generation of reactive oxygen species and free radicals. Expression of hypoxia-inducible factor 1α (HIF1α) is induced by free radicals and hypoxic conditions and results in the upregulation of genes that increase glycolysis, angiogenesis and erythropoiesis [21, 22]. These cellular responses to cobalt exposure mimic the cellular responses to hypoxia. Chromium can also generate free radicals.

14.6 Role of Free Radicals

Hypoxia followed by return to normal oxygen tension (or "hypoxia-reperfusion") also generates free radicals [23]. Sood and colleagues [16] used this principle to induce free radicals in their barriers. They did this by growing BeWo barriers in a hypoxic incubator. When the barriers had grown they were transferred into normal oxygen tensions and placed above human fibroblasts. Just as was seen with nanoparticles only the bilayered barriers signalled damage following hypoxic culture. In this experimental setup free radicals could potentially be generated during the hypoxic culture period or on transfer to atmospheric oxygen. The transfer of the barriers from 1 % oxygen to atmospheric oxygen simulates a reperfusion of an ischaemic tissue. Ischaemia-reperfusion generates reactive oxygen species in cardiac myocytes and is important in the mechanism that further damages the myocardium after an ischaemic event. The reactive oxygen species are generated on reperfusion (or reintroduction of oxygen). This burst of reactive oxygen species is reduced in myocytes treated with antioxidants and also reduces resultant myocardial dysfunction [23].

It should also be emphasised that when a predominantly monolayered BeWo barrier was grown in hypoxic conditions and reintroduced to normal oxygen tensions, no significant DNA damage was seen in the fibroblasts. This implicates that there is an intercellular signalling mechanism. ROS may be involved by being released from one layer of cells in the barrier and acting on a second layer of cells. The "layer" concept is important as the free radicals could just as easily act on an adjacent cell in the same layer and cause signalling, but given that the monolayered barrier does not act in this way there must be a different characteristic afforded to the second layer of cells in the barrier that results in the signalling mechanism.

Although reactive oxygen species are capable of causing DNA damage in their own right, it is more likely that their role is in signalling. The signalling role of ROS is well documented and can trigger transcriptional changes [24]. When the free radical scavengers MitoQ and vitamin C are added to the bilayered barriers along with nanoparticles the DNA damage in the fibroblasts underneath the barrier is reduced to near control levels. Inducing free radicals in the BeWo cells using inhibitors of the electron transport chain also causes damage in the fibroblasts. However only blockade of complex III with antimycin A caused DNA damage; blockade of complex I with rotenone did not cause DNA damage in the fibroblasts [16]. Blockade of complex III with antimycin A causes release of $O_2\cdot$ both into the cellular cytosol and the mitochondrial matrix unlike rotenone which only causes $O_2\cdot$ release into the mitochondrial matrix. Therefore it seems that cytosolic ROS is required for the signalling mechanism that causes DNA damage in the barrier. The effect of vitamin C, reducing the DNA damage seen in the fibroblasts, supports this. MitoQ theoretically is concentrated into the mitochondria along the electropotential gradient generated by oxidative phosphorylation and thus selectively scavenges mitochondrial ROS. MitoQ is an analogue of CoQ10 which is found in the inner membrane of mitochondria [25] as part of the electron transport change and scavenges free radicals and therefore also reduces the cytosolic release of free radicals and thus also explains the effect MitoQ has on reducing DNA damage in the fibroblasts under the barrier following an indirect nanoparticle exposure.

Both the BeWo and AS corneal cell barriers express Cx43 on the cell surface and ROS have the potential to pass through these channels [1, 16]. Thus, one possible scenario would be the release of ROS through Cx43 hemichannels on the lower surface of the barrier into the medium bathing the fibroblasts. In the monolayered barrier this would allow direct exposure of the fibroblasts to the ROS (Fig. 14.3a). However it is unlikely that ROS themselves cause the DNA damage in the fibroblasts. If this was the case it would be expected that the predominantly monolayered BeWo barrier grown in 1 % oxygen would cause at least some DNA damage in the fibroblasts beneath the barrier. Therefore ROS and Cx43 must have some role in the bilayer or multilayer that then cause damage beneath the barrier and another possibility is that ROS generated in the top layer of the barrier acts on the second layer via gap junctions or hemichannels (Fig. 14.3b). There is then another event or signal that causes damage in the fibroblasts.

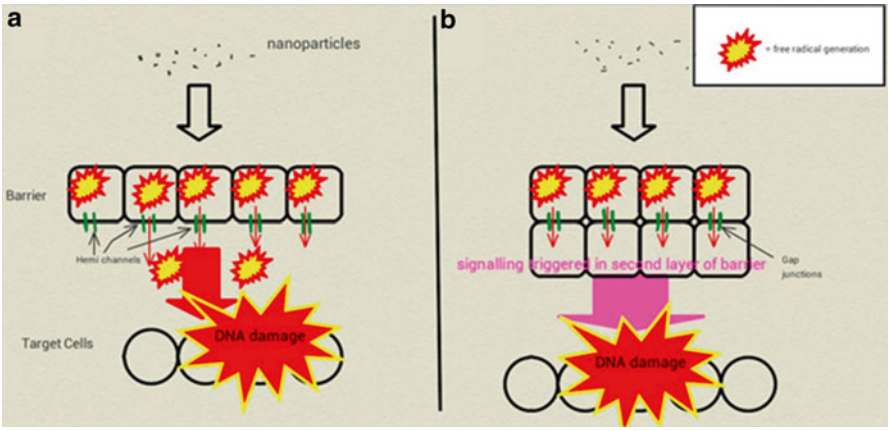

Fig. 14.3 Possible mechanisms of ROS action in barrier signalling. (**a**) Release of ROS through Cx43 hemichannels on the lower surface of the barrier into the medium bathing the cell underneath. However given that the predominantly monolayered barrier as depicted in (**a**) does not signal DNA damage, it is unlikely that this is the correct scenario. (**b**) Nanoparticle stimulation generates ROS in the top layer of the barrier, which enters the second layer in the barrier via gap junctions and triggers a signalling cascade in the second layer that causes DNA damage in the cells underneath. This scenario would explain why isolated BeWo cells generate ROS, yet a predominantly monolayered barrier does not signal damage in cells underneath, yet a predominantly bilayered barrier does signal DNA damage

14.7 Purinergic Transmission

Given the effect that addition of apyrase beneath the barrier and blockade of ATP channels in the barrier reduce DNA damage across the barrier [1] it is worth revisiting the potential role of purines in the barrier signal. ATP can pass through hemichannels and causes DNA damage in fibroblasts when applied directly. Apyrase, which breaks down ATP, added to the medium below the barrier reduces the DNA damage in the fibroblasts after indirect nanoparticle exposure. This suggests that ATP may be released from the barrier and contribute to the DNA damage seen in fibroblasts as a result of indirect nanoparticle exposure. BeWo barriers did express ATP receptors P2Y1 and P2Y2 [1, 16].

Detection of ATP in the medium below the barrier 24 h after an indirect nanoparticle exposure yielded no successful results. Detection of ATP breakdown products after an indirect exposure across a BeWo barrier also yielded no useful results [16]. However under the corneal cell barrier there was a significantly higher concentration of xanthine under the barrier after an indirect nanoparticle exposure. This change happens at 24 h after exposure, but this difference was not present at 1 h after the exposure.

Xanthine is formed by the action of xanthine oxidoreductase on hypoxanthine [26]. Xanthine is formed downstream of ATP metabolism, via IMP and adenosine.

Xanthine oxidoreductase is closely related to xanthine oxidase. Xanthine oxidase's action is modified to an oxidoreductase by a reversible sulphhydryl oxidation. Xanthine oxidase has been shown to be part of the HIF1α induction in some glioma cells exposed to cobalt chloride [21]. However other glioma cells did not have the xanthine oxidase-dependent mechanism of HIF1α induction. This may parallel the differences between the BeWo barrier and the corneal cell barrier. If there are other signalling pathways involved in the signalling pathway across a bilayered barrier, whatever the cells' type, then the differing importance of each pathway in each cell type may explain the differences seen with xanthine.

Xanthine oxidoreductase produces ROS when converting hypoxanthine to xanthine. There is a burst of ROS released from BeWo cells between 40 and 60 min after a nanoparticle exposure. Addition of allopurinol, a xanthine oxidase inhibitor, below the barrier during an indirect exposure prevents damage in fibroblasts underneath the barrier [1]. Although ROS were not looked for in the corneal cell barrier, the high level of xanthine suggests that oxidative stress is involved after a nanoparticle exposure. The effect of ROS scavenger, vitamin C and MitoQ on the indirect exposure across the corneal barrier supports this [16]. To this effect the BeWo barriers and the corneal cell barriers are similar. It seems that the ROS are required, but the generation of ROS may be by a different pathway. This parallels the findings in glioma cells in which some cell lines generate ROS in a xanthine oxidase-dependent manner to induce HIF1α, whereas a different glioma cell line generates ROS and induces HIF1α even when xanthine oxidase is pharmacologically inhibited [21].

To test whether ATP may be a signalling molecule within the barrier that contributes to the signalling mechanism that causes DNA damage to the fibroblasts, ATP was added to predominantly monolayered barriers in an attempt to replicate the release of ATP from the cell layer in the barrier exposed to nanoparticles. Addition of ATP on top of the barrier resulted in a small increase in the DNA damage under the monolayered barrier. Once released, ATP can act on purinergic receptors on the same cell or neighbouring cells.

ATP receptors can be sub-classified into P1 and P2 receptors [27]. P1 receptors bind adenosine, whilst P2 receptors bind ATP, ADP, UDP or UTP. P2 receptors are further sub-classified into P2X and P2Y. The latter are *trans*-membranous proteins that are G protein coupled and trigger intracellular calcium signalling. The former are ATP-gated non-selective cation channels that are modulated by Ca^{2+} and allow the passage of other ions such as sodium, magnesium, zinc and copper. Within the P2X group, there are further subtypes. It had been noted that the longer the P2X7 receptor was stimulated the larger the cation pore became. It was subsequently shown that prolonged stimulation of the receptor (for minutes rather than seconds) results in the recruitment of pannexin hemichannels in the cellular membrane, and therefore the increasing pore size was due to the P2X7 receptor's recruitment of the hemichannel rather than the channel itself [28]. Thus this is a potential link between the P2X7 receptor and Cx43, both of which have been found in the BeWo cells used in this work.

When the non-competitive P2X7 ATP receptor inhibitor, compound 17 (C17), is added to the monolayered barrier with ATP the DNA damage in the fibroblasts underneath the barrier is reduced. ATP receptors also rely on calcium signalling, be

it via G-protein-linked receptors (P2Y) or directly as a calcium ion channel. Bhabra et al. [1] reported a calcium surge following nanoparticle exposure on isolated BeWo cells and that pharmacological inhibition of calcium signalling prevented DNA damage in fibroblasts after an indirect nanoparticle exposure across the BeWo barrier.

Oxidative stress and ROS liberate calcium from the endoplasmic reticulum in a positive feedback-type loop [29]. ROS triggers calcium release from the endoplasmic reticulum which in turn adversely affects mitochondrial function increasing mitochondrial ROS generation. This can then lead to loss of the electrochemical gradient across the mitochondrial membrane, loss of ATP production and either cell necrosis if this ATP loss is catastrophic or apoptosis if enough ATP production can be maintained to control the "programmed cell death" or apoptosis pathways. Apoptosis itself has been shown to be propagated via gap junctions so that an apoptotic signal in one cell can induce apoptosis in a neighbouring cell [30]. This may be a potential contributor to the bystander effect discussed above, but it is unlikely to be the only pathway involved in barrier signalling, as it does not explain the differences between single and multilayered barriers.

14.8 Cytokines

As well as gap junctions, cytokines have been implicated in the mechanism underlying the bystander effect. The corneal cell bilayer but not the monolayered corneal barrier nor the mono- or bilayered BeWo barrier produced cytokines that could be detected in concentrations thought to contribute to the signalling mechanism. Cytokines are produced by any cell to help control and signal their milieu and adjacent cells. They therefore need only to be released in miniscule quantities to bind to a receptor if they are acting on an adjacent cell.

Those that were detected, IL-6, IL-8, GRO, GM-CSF and EGF, are all implicated in the senescence-associated secretory phenotype (SASP). The SASP is a pattern of gene expression that results in the production of messengers that maintain a cell's senescence [31, 32]. Cellular senescence is arrest of the cell cycle. Initially cellular senescence was noted in cells in culture. Unless cells had been immortalised, once they had been passaged a certain number of times (termed the Hayflick number), they entered a senescent state [33]. The shortening of telomeres has been attributed to this effect [34]. It is postulated that the older a cell is the shorter its telomeres and there is a critical point beyond which a cell cannot divide. This is termed replicative senescence. Therefore the SASP is linked to senescence and ageing.

These cytokines (IL-6, IL-8, GM-CSF, GRO, ERF and MCP-1) were all elevated following a nanoparticle exposure but not a control exposure. Given the BeWo barrier did not appear to release any cytokines, it was questioned whether the AS corneal cell barrier was merely older or was there a fundamental difference between the two barriers.

Both cell lines are immortal; the BeWo cells are immortal as a result of their malignant ancestry [35] and the corneal cells as a result of SV40 viral transfection

[36], but the corneal cells had shorter telomeres [16]. The length of these telomeres (approximately 3,000 base pairs) induces senescence in some cell lines. Given that oxidative stress can trigger senescence [32] and that oxidative stress appears to contribute to the signalling mechanism, it is suggested that the nanoparticle stimulation of the corneal cell barrier but not the BeWo barrier triggered a SASP-like state in the corneal cells. Given also that the concentrations in those detected cytokines did not reduce reliably when nanoparticles were added with Gap27 or MitoQ, unlike the DNA damage that was assessed using the alkaline comet assay under the same conditions, this suggests that these SASP-associated cytokines are unlikely to be the direct effectors of the signalling mechanism in the corneal cells. Therefore it may be that the cytokine release is upstream of a final pathway in the same way that TNFα has been shown to behave in the bystander effect. Alternatively the nanoparticles induced genotoxic senescence in the corneal cells but not the BeWo cells because the telomeres in the corneal cells are shorter, and as a result we detected an SASP cytokine profile in the corneal cells but not the BeWo cells. This may also explain the difference in xanthine concentrations measured after nanoparticle exposure to the corneal and BeWo barriers. Only the corneal cells showed a significant increase, and therefore whether this rise is a cause or an effect of the signalling mechanism is unclear. The increase in xanthine may be a sign of increased oxidative stress rather than being involved in the signalling mechanism, but given that the same exposures did not cause a significant increase in lactate production from the corneal barrier hypoxia as a cause of the oxidative stress is less likely [16].

There is limited evidence that the DNA damage seen in the cells underneath the barrier has further effects on the cells. If human embryonic stem cells are used instead of fibroblasts as the cells underneath the barrier and the differentiation of these cells followed, there is early evidence that the differentiation into neuroectoderm is altered.

14.9 Signalling In Vivo

Tail vein injection into a mouse allows the harvesting of the brain and any potential offspring. The brain is separated from the bloodstream by the blood–brain barrier which is predominantly monolayered. In the mouse, the placenta is a multilayered barrier. Nanoparticle exposure via tail vein injection and harvest of the mother's brain reveals no DNA damage. However when the offspring are examined their cells exhibit increased levels of DNA damage when compared to control mice offspring.

In humans the placenta develops in relative hypoxia in the first trimester before morphological changes in the uterine arteries and the establishment of the foetomaternal circulation results in the measured oxygen tension rising from 20 to 50 mmHg [29]. The early pregnancy hypoxia may be beneficial to the foetus as it may reduce oxygen-derived free radicals [37]. The concept that the early placenta grows in a relatively hypoxic environment is recent but may help explain early damage to the foetus or miscarriage. Any change in intrauterine conditions, for example,

an intrauterine bleed, may expose the placenta to increased oxygen tensions and the resultant oxidative stress which may be implicated in teratogenesis.

Therefore, in the first trimester, when there are syncytiotrophoblast and cytotrophoblast, there is a predominant bilayer of placental tissue in contact with the maternal tissues [17]. In the first trimester the lacunae have not yet fully formed and therefore direct blood contact is not made until the tenth week of gestation. Some argue that there are five layers (syncytiotrophoblast, cytotrophoblast, basal lamina, connective tissue and foetal endothelium) between the maternal blood and the foetal blood [38]. Therefore in vivo it may be that any nanoparticles that do reach the placenta could potentially signal DNA damage but this would be upon the underlying connective tissue. Therefore it can be argued that this potentially damaging situation where a bilayer can damage the unborn offspring is protected against by firstly avoiding direct maternal blood contact until the barrier becomes progressively more monolayered and by having other layers in between the maternal blood and the foetal blood. These connective tissue layers become decreasingly prominent as pregnancy continues and so the barrier in the final trimester can be considered to be predominantly a monolayer. Thus, as the maternal blood bathes the placenta later in pregnancy, any potentially DNA-damaging signals are not transmitted.

In vivo, there are many cellular barriers. Some cellular barriers are designed to contain some substances whilst allowing the passage of others, such as the capillary endothelium. “Leaky” capillary epithelium in the peripheral soft tissues allows the diffusion of nutrients and waste products from and into the bloodstream [39]. This type of capillary epithelium is the most commonly found in the body with a huge surface area and a distribution that ensures that most cells in the body are within a few microns distance of a capillary which can deliver it nutrients whilst also transporting away its waste products. Not all capillary epithelia are the same however and the capillary epithelium found in the majority of the brain has tight junctions between a predominantly monolayered cellular barrier [40]. This endothelium sits upon a basement membrane. Astrocyte foot processes are closely related to the basement membrane on the other side [41], but it is the endothelium that is the predominantly monolayered barrier as it controls the transport of nutrients and drugs from the bloodstream into the brain and cerebrospinal fluid.

The blood–retina barrier is another privileged site where the endothelial capillary membrane has tight junctions [42]. The vascular endothelium also has tight junctions in the testis, but the blood–testis barrier is also composed of specialised junctions of the extracellular matrix between Sertoli cells [43]. All of these privileged sites are very sensitive to toxins that may be circulating in the bloodstream. In the case of the testes there is another layer of security beyond the basement membrane to ensure that antibodies that may be sensitive to the new genetic material produced by meiosis do not cross the barrier. It should be noted however that this barrier could be considered as two predominantly monolayered barriers separated by a basement membrane rather than a bilayered barrier composed of two layers of the same cells. Therefore, it could be argued that like the fibroblasts on the other side of a monolayered BeWo or corneal cell barrier, the brain, retina or testes on the other side of their respective monolayered endothelial barriers should be immune from

the signalling that causes DNA damage following an indirect CoCr nanoparticle exposure that may result from circulating nanoparticles in the blood.

In vivo during the first trimester the foetus develops in a hypoxic environment [29, 37] and is susceptible to major teratologic insults as the major organs are formed [44, 45]. Organogenesis requires the embryo to change from a proliferative state to a state in which cellular differentiation occurs and it is thought that redox signalling plays a role in this [37]. The bilayered barrier signals in a redox-dependent manner and it may be that the placental barrier may also participate in this signalling actively rather than being merely a passive barrier between mother and foetus. As the foetus develops further, although still susceptible to teratogenic stimuli, the potential defects become less severe and the placental barrier becomes progressively more monolayered. The inference would be that the third trimester placenta does not signal. This may contribute to the decreased foetal vulnerability, but it may also represent the increased resilience of a larger more mature foetus.

References

1. Bhabra G et al (2009) Nanoparticles can cause DNA damage across a cellular barrier. Nat Nanotechnol 4:876–883
2. Papageorgiou I et al (2007) The effect of nano- and micron-sized particles of cobalt-chromium alloy on human fibroblasts in vitro. Biomaterials 28:2946–2958
3. Evans WH, De Vuyst E, Leybaert L (2006) The gap junction cellular internet: connexin hemichannels enter the signalling limelight. Biochem J 397:1–14
4. Kibschull M, Gellhaus A, Winterhager E (2008) Analogous and unique functions of connexins in mouse and human placental development. Placenta 29:848–854
5. Kleopa KA (2011) The role of gap junctions in Charcot-Marie-tooth disease. J Neurosci 31:17753–17760
6. Lin C et al (1999) Deletion and nonsense mutations of the connexin 32 gene associated with Charcot-Marie-tooth disease. Tohoku J Exp Med 188:239–244
7. Anselmi F et al (2008) ATP release through connexin hemichannels and gap junction transfer of second messengers propagate Ca2+ signals across the inner ear. Proc Natl Acad Sci U S A 105:18770–18775
8. Hall EJ (2003) The bystander effect. Health Phys 85:31–35
9. Kadhim MA et al (1992) Transmission of chromosomal instability after plutonium alpha-particle irradiation. Nature 355:738–740
10. Nagasawa H, Little JB (1992) Induction of sister chromatid exchanges by extremely low doses of alpha-particles. Cancer Res 52:6394–6396
11. Mothersill C, Seymour C (1997) Medium from irradiated human epithelial cells but not human fibroblasts reduces the clonogenic survival of unirradiated cells. Int J Radiat Biol 71:421–427
12. Hei TK et al (2008) Mechanism of radiation-induced bystander effects: a unifying model. J Pharm Pharmacol 60:943–950
13. Mitchell SA, Randers-Pehrson G, Brenner DJ, Hall EJ (2004) The bystander response in C3H 10 T1/2 cells: the influence of cell-to-cell contact. Radiat Res 161:397–401
14. Banaz-Yaşar F, Lennartz K, Winterhager E, Gellhaus A (2008) Radiation-induced bystander effects in malignant trophoblast cells are independent from gap junctional communication. J Cell Biochem 103:149–161
15. Cogan N et al (2010) DNA damaging bystander signalling from stem cells, cancer cells and fibroblasts after Cr(VI) exposure and its dependence on telomerase. Mutat Res 683:1–8

16. Sood A et al (2011) Signalling of DNA damage and cytokines across cell barriers exposed to nanoparticles depends on barrier thickness. Nat Nanotechnol 6:824–833
17. Huppertz B (2008) The anatomy of the normal placenta. J Clin Pathol 61:1296–1302
18. Møller P et al (2010) Role of oxidative damage in toxicity of particulates. Free Radic Res 44:1–46
19. Xiao GG, Wang M, Li N, Loo JA, Nel AE (2003) Use of proteomics to demonstrate a hierarchical oxidative stress response to diesel exhaust particle chemicals in a macrophage cell line. J Biol Chem 278:50781–50790
20. Nel A, Xia T, Mädler L, Li N (2006) Toxic potential of materials at the nanolevel. Science 311:622–627
21. Griguer CE et al (2006) Xanthine oxidase–dependent regulation of hypoxia-inducible factor in cancer cells. Cancer Res 66:2257–2263
22. Vengellur A, Woods BG, Ryan HE, Johnson RS, LaPres JJ (2003) Gene expression profiling of the hypoxia signaling pathway in hypoxia-inducible factor 1alpha null mouse embryonic fibroblasts. Gene Expr 11:181–197
23. Murphy E, Steenbergen C (2008) Mechanisms underlying acute protection from cardiac ischemia-reperfusion injury. Physiol Rev 88:581–609
24. Hamanaka RB, Chandel NS (2010) Mitochondrial reactive oxygen species regulate cellular signaling and dictate biological outcomes. Trends Biochem Sci 35:505–513
25. Smith RAJ, Kelso GF, James AM, Murphy MP (2004) Targeting coenzyme Q derivatives to mitochondria. Methods Enzymol 382:45–67
26. Harrison R (2002) Structure and function of xanthine oxidoreductase: where are we now? Free Radic Biol Med 33:774–797
27. Schwiebert EM, Zsembery A (2003) Extracellular ATP as a signaling molecule for epithelial cells. Biochim Biophys Acta 1615:7–32
28. Pelegrin P, Surprenant A (2006) Pannexin-1 mediates large pore formation and interleukin-1beta release by the ATP-gated P2X7 receptor. EMBO J 25:5071–5082
29. Halliwell B, Whiteman M (2004) Measuring reactive species and oxidative damage in vivo and in cell culture: how should you do it and what do the results mean? Br J Pharmacol 142:231–255
30. Li N et al (2003) Mitochondrial complex I inhibitor rotenone induces apoptosis through enhancing mitochondrial reactive oxygen species production. J Biol Chem 278:8516–8525
31. Coppé J-P, Desprez P-Y, Krtolica A, Campisi J (2010) The senescence-associated secretory phenotype: the dark side of tumor suppression. Annu Rev Pathol 5:99–118
32. Rodier F et al (2009) Persistent DNA damage signaling triggers senescence-associated inflammatory cytokine secretion. Nat Cell Biol 11:973–979
33. Campisi J, d'Adda di Fagagna F (2007) Cellular senescence: when bad things happen to good cells. Nat Rev Mol Cell Biol 8:729–740
34. Blackburn EH (1991) Structure and function of telomeres. Nature 350:569–573
35. Pattillo RA, Gey GO (1968) The establishment of a cell line of human hormone-synthesizing trophoblastic cells in vitro. Cancer Res 28:1231–1236
36. Reddel RR (1995) Immortalization techniques. Methods Cell Sci 17:65–66
37. Burton GJ, Jauniaux E (2011) Oxidative stress. Best Pract Res Clin Obstet Gynaecol 25:287–299
38. Myren M, Mose T, Mathiesen L, Knudsen LE (2007) The human placenta–an alternative for studying foetal exposure. Toxicol In Vitro 21:1332–1340
39. Hall JE (2010) Guyton and hall textbook of medical physiology: with STUDENT CONSULT Online Access. Saunders, Philadelphia
40. Brightman MW, Reese TS (1969) Junctions between intimately apposed cell membranes in the vertebrate brain. J Cell Biol 40:648–677
41. Pardridge WM (2012) Drug transport across the blood–brain barrier. J Cereb Blood Flow Metab 32:1959–1972
42. Cunha-Vaz J (1979) The blood-ocular barriers. Surv Ophthalmol 23:279–296
43. Cheng CY, Mruk DD (2012) The blood-testis barrier and its implications for male contraception. Pharmacol Rev 64:16–64
44. Teratology Society, Teratology Primer (2009) http://www.teratology.org/primer.asp
45. Wells PG et al (2009) Oxidative stress in developmental origins of disease: teratogenesis, neurodevelopmental deficits, and cancer. Toxicol Sci 108:4–18

Chapter 15
The Absorption, Distribution, Metabolism, and Excretion Profile of Nanoparticles

Yasuo Yoshioka, Kazuma Higashisaka, Shin-ichi Tsunoda, and Yasuo Tsutsumi

Abstract Advances in nanotechnology have led to the recent development of many nanoparticles. With the growing commercialization of nanoparticles, opportunities for human exposure to nanoparticles will increase substantially. For the development of nanoparticles with efficacy and safety, a systematic and thorough analysis of the absorption, distribution, metabolism, and excretion (ADME) of nanoparticles is essential. In this chapter, we present the current understanding regarding the ADME profile of nanoparticles.

Keywords ADME • Biologic barriers • Protein corona • Safety

Y. Yoshioka, Ph.D. (✉) • K. Higashisaka
Laboratory of Toxicology and Safety Science, Graduate School of Pharmaceutical Sciences, Osaka University, 1-6 Yamadaoka, Suita, Osaka 565-0871, Japan
e-mail: yasuo@phs.osaka-u.ac.jp

S.-i. Tsunoda
Laboratory of Biopharmaceutical Research, National Institute of Biomedical Innovation, 7-6-8 Saitoasagi, Ibaraki, Osaka 567-0085, Japan

The Center for Advanced Medical Engineering and Informatics, Osaka University, 1-6 Yamadaoka, Suita, Osaka 565-0871, Japan

Y. Tsutsumi, Ph.D. (✉)
Laboratory of Toxicology and Safety Science, Graduate School of Pharmaceutical Sciences, Osaka University, 1-6 Yamadaoka, Suita, Osaka 565-0871, Japan

Laboratory of Biopharmaceutical Research, National Institute of Biomedical Innovation, 7-6-8 Saitoasagi, Ibaraki, Osaka 567-0085, Japan

The Center for Advanced Medical Engineering and Informatics, Osaka University, 1-6 Yamadaoka, Suita, Osaka 565-0871, Japan
e-mail: ytsutsumi@phs.osaka-u.ac.jp

M. Akashi et al. (eds.), *Engineered Cell Manipulation for Biomedical Application*, Nanomedicine and Nanotoxicology,
DOI 10.1007/978-4-431-55139-3_15

15.1 Introduction

Nanotechnology makes it possible to design, characterize, and produce nanostructured materials by controlling their shape and size at the nanoscale. In general, nanoparticles are defined as materials whose structures have at least one dimension on the order of 100 nm or less, although there is no reason to assume that 100 nm would be an absolute threshold for changes in the physicochemical properties of these particles. Nanoparticles have various desirable properties, including enhanced electrical conductivity, tensile strength, and chemical reactivity, which are due to their increased surface area per unit weight compared with that of bulk-scale counterparts. Diverse nanoparticles such as silica nanoparticles and carbon nanotubes (CNTs) have become widespread in use through their applications in electronics, sunscreens, cosmetics, diagnostic medicines, and drug-delivery systems, among other products. In particular, the clinical applications of nanoparticles have been investigated for more than 30 years. For biomedical applications, nanoparticles including mesoporous silica nanoparticles, CNTs, quantum dots, and superparamagnetic nanoparticles have been evaluated as drug-delivery and diagnostic vehicles. For example, because of their unique mesostructural features, high drug-loading capacity, and sustained-release profiles, mesoporous silica nanoparticles are potential candidates for controllable drug-delivery agents, gene delivery vehicles, vaccine carriers, and many other biologic applications.

The increasing use of nanoparticles has prompted public concern regarding their potential toxicity. In particular, recent reports have indicated that CNTs cause mesothelioma-like lesions in mice, in a manner similar to that of asbestos-induced mesothelioma [1, 2]. Because nanoparticles have great potential to improve the quality of human life, it is essential to ensure the safety of nanoparticles for the development of safety-assessed products. The toxicity of nanoparticles is related to the dose, concentration, and duration of the exposure and their abundance and persistence in tissue. Accordingly, a systematic and thorough analysis of the absorption, distribution, metabolism, and excretion (ADME) of nanoparticles is essential as the basis for determining the potential for risk to human health. In addition, understanding of the ADME of nanoparticles is necessary not only in regard to their tissue toxicity but also their potential biomedical applications. In this chapter, we present the current understanding regarding the ADME profile of nanoparticles (particularly inorganic nanoparticles).

15.2 ADME via Several Exposure Routes

Various barriers prevent the entry of foreign substances, including viruses and bacteria, into the body. These same barriers modulate the access of nanoparticles and include the skin, gastrointestinal tract, and pulmonary system. Previously, only

small lipophilic molecules (<600 Da) and metallic ions (e.g., nickel and cobalt) have been able to penetrate the skin barrier. However, because of their small size, nanoparticles might be readily absorbed through the dermis of the skin and the pulmonary and gastrointestinal mucosa, thus positioning these compounds for distribution through the vascular circulation to all tissues in the body. With an average pore size of ~5 nm in mammals, the vascular endothelium presents another potential barrier to the absorption and delivery of nanoparticles, but nanoparticles smaller than this limit penetrate rapidly from blood across the endothelium and into tissue. In addition, nanoparticles potentially can translocate efficiently from blood into the liver, spleen, and bone marrow, because the discontinuous endothelium characteristic of these organs has pores of 50–100 nm in diameter. Therefore, methods for estimating the amount of the total external exposure, efficacy of absorption, and tissue biodistribution of nanoparticles are needed.

Many studies have reported that nanoparticles penetrate the biologic barriers after inhalation or oral or dermal exposure and have used qualitative and quantitative methods to assess the effect of the size and surface properties of nanoparticles on biologic behaviors. In the following sections, we discuss the absorption of nanoparticles via several exposure routes.

15.2.1 Dermal Exposure

Because clothing, drugs, cosmetics, and various skin care products contain nanoparticles, their contact with the skin occurs intentionally as well as accidentally. In particular, nanoparticles have been included in cosmetics and sunscreen to provide protection against ultraviolet radiation. Therefore, understanding the absorption rate of nanoparticles after exposure via the skin has garnered increasing attention during the past several years. However, whether nanoparticles actually penetrate the skin barrier in vivo is unclear, although many studies have assessed the skin penetration of nanoparticles after topical application of compounds. Several reports have stated that titanium dioxide, ZnO nanoparticles, and silver nanoparticles penetrate into the upper layers of the stratum corneum but not deeper into the viable epidermis and dermis [3–5]. In contrast, other studies showed that 40-nm, but not 750- or 1,500-nm, polystyrene nanoparticles and 40-nm silica nanoparticles can translocate to the viable epidermis in human skin explants with partially disrupted stratum corneum [6, 7]. In addition, Mortensen and colleagues showed that quantum dot nanoparticles penetrate deep into the epidermis and dermis of mice exposed to ultraviolet irradiation [8], which induces skin-barrier defects such as disruption of stratum corneum lipids and loosening of cell–cell junctions. Because consumers often apply sunscreen to sun-damaged skin, it is more important to examine the effect of ultraviolet radiation on the ability of nanoparticles to penetrate the skin.

15.2.2 Gastrointestinal Exposure

People in developed countries ingest an estimated 10^{12} to 10^{14} manufactured fine (diameter, 0.1–1 mm) to ultrafine (diameter, <100 nm) particles in food every day [9]. In particular, amorphous silica particles (including nanosize particles) are widely applied in food products and registered within the European Union as a food additive (E551). These particles are used mainly as thickening medium for pastes, as an anticaking agent to maintain flow properties in powdered products, and as a carrier for fragrances and flavors in food and nonfood products [10]. However, little information about the absorption of nanosilica particles after oral exposure is available, mainly because there is no high-sensitivity method for detecting silicon in biologic tissues. One study showed the effect of size on the absorption of nanoparticles after oral administration in rats by using gold nanoparticles of different sizes (1.4–200 nm) [11]. The smallest particles had the highest absorption across intestinal membranes: after 24 h, 0.37 % of the applied 1.4-nm particles had reached the circulation. Surface charge was important in the absorption across intestinal membranes also, and more negatively charged gold nanoparticles were absorbed than were positively charged particles. Furthermore, the greatest accumulation of particles in the heart and brain after oral administration was associated with the 18-nm particles, which accumulated to even greater amounts than did the 1.4-nm particles; the precise mechanism underlying this effect is unknown. In summary, although small nanoparticles tend to be absorbed more readily than are large particles, no general assumption regarding tissue accumulation after particle absorption can yet be made.

15.2.3 Pulmonary Exposure

Nanoparticle-facilitated drug delivery through the lung is attractive because of the organ's large surface area. In addition, knowing the ADME profile of nanoparticles after lung exposure is particularly important, because the inhalation of nanoparticles increasingly is recognized as a major cause of adverse health effects. Gold nanoparticles 1.4 nm in diameter efficiently cross the air–blood barrier of the respiratory tract, whereas almost all 18-nm particles remain trapped in the lungs after intratracheal instillation in rats [12]. In addition, the biodistribution patterns (e.g., organ ratios) of 1.4-nm gold nanoparticles differed markedly after intravenous injection compared with intratracheal instillation. For example, the liver–blood ratio is 1.1 to 1 after instillation compared with 12.5 to 1 after intravenous injection, suggesting that 1.4-nm nanoparticles undergo some unknown chemical or biochemical transformation process during translocation through the lung. Another possibility is that the interaction of nanoparticles with alveolar fluid in the lungs during inhalation exposure or with blood proteins during intravenous injection has different effects on the surface properties of nanoparticles, leading to differences in tissue uptake. Therefore, data after intravenous injection might be unreliable for

predicting the biodistribution of nanoparticles after their passage through various barriers and may give misleading information about potential harmful effects.

Most of the biodistribution studies that have assessed nanoparticles to date occur over a relatively long time, from several hours to weeks. In contrast, Choi and colleagues used near-infrared fluorescent nanoparticles to examine biodistribution during the first hour after their administration [13]. In that study, nanoparticles with a hydrodynamic size less than 34 nm rapidly moved from the lung to mediastinal lymph nodes, and nanoparticles smaller than 6 nm rapidly moved from the lung to lymph nodes and the bloodstream, leading ultimately to renal clearance. This and other new experimental methodologies may provide new insights into the ADME profile of nanoparticles. In addition, future studies should minimize doses and examine biodistribution in more organs for prolonged periods to fully characterize the potential health effects of exposure to nanoparticles.

15.3 Translocation of Nanoparticles Across Internal Biologic Barriers

The blood–brain, blood–testis, and placental barriers protect particularly sensitive tissues from foreign chemicals. In this section, we discuss the translocation of nanoparticles across various internal barriers, especially the placenta.

Considerable evidence shows that, because of their physiologic immaturity, fetuses are more sensitive than are adults to numerous environmental toxins. Recurrent pregnancy loss affects 1–3 % of couples; many of these miscarriages undergo extensive—but ultimately uninformative—diagnostic testing. In addition, intrauterine growth restriction occurs in as many as 10 % of pregnancies and predisposes the child to a lifelong increased risk for hypertension, cardiovascular disorders, and renal disease, among others. Although many factors for miscarriage and intrauterine growth restriction have been suggested, the precise mechanism and mediators remain unknown. It is essential to assess the potential risk of nanoparticles to cause these pregnancy complications.

Normal placental development is required for successful embryonic growth, and placental dysfunction has been associated with miscarriage and fetal growth restriction. Some reports have warned about the potential adverse effects of nanoparticles on fetuses [14–17]. In one study, silica nanoparticles (diameter, 70 nm) and titanium dioxide nanoparticles induced miscarriage and fetal growth restriction in pregnant mice, whereas microscale silica particles did not induce these complications [15]. The observed pregnancy complications resulted from placental dysfunction, such as destruction of the placental vasculature. Notably, surface-modified silica nanoparticles (diameter, 70 nm) did not induce any pregnancy complications in mice. Furthermore, whereas maternal pulmonary exposure to carbon black during pregnancy had adverse effects on the offspring [18, 19], repeated oral administration of multi-walled CNTs during pregnancy did not cause fetal toxicities [20].

Several studies have addressed the biodistribution of nanoparticles to the fetus and placenta. For example, after intravenous injection of pregnant mice, silica nanoparticles (diameter, 70 nm) were detected in the maternal liver and placenta and the fetal liver and brain, although microscale silica particles were not noted in any of these tissues [15]. In addition, when administered by intravenous injection early during pregnancy, PEGylated single-walled CNTs reached the conceptus, whereas these nanotubes reached only the placenta and yolk sac—not the embryo—when injection occurred during later pregnancy stages [17]. Furthermore, gold nanoparticles (diameter, 13 nm) accumulated in fetuses more efficiently when pregnant mice were injected before embryonic day E11.5 than after E11.5, indicating that the stage of placental maturity influences the translocation of nanoparticles to murine fetuses [21]. This same study showed that modification of the surface of nanoparticles altered their translocation to fetuses. Therefore, the translocation of nanoparticles to fetuses during murine pregnancy is influenced both by the stage of placental maturity and by nanoparticle surface composition.

Mouse and human placentas differ in their modes of implantation, the relative importance of yolk sac placentation, and the structure (labyrinthine compared with villous) of the exchange area. For example, by using an ex vivo human placental perfusion model, Wick and colleagues showed that polystyrene nanoparticles smaller than 240 nm can cross human placental tissues to reach fetuses [22].

15.4 Translocation of Nanoparticles Across Cellular Barriers

Various pathways, including passive and active diffusion, enable nanoparticles to travel across external and internal barriers. For example, small nanoparticles might access the paracellular pathway by evading the tight junctions between epithelial and endothelial cells, which are considered to exclude molecules larger than 0.6–5 nm [23].

In the gastrointestinal tract, enterocytes (especially M cells) may facilitate the transport of nanoparticles through transcytosis. Chitosan nanoparticles enhance intestinal paracellular uptake by modulating tight junctions between cells [24]. Another potential mechanism for the translocation of nanoparticles in the gastrointestinal tract involves degrading enterocytes, which are shed in high numbers daily (mice, 2×10^8 cells; humans, 10^{11} cells) in the small intestine [25].

In human endothelial cells in vitro, iron particles induced the production of reactive oxygen species [3] and oxidative stress, consequently increasing microtubule remodeling and permeability in these cells [26]. In a particularly novel mechanism of nanoparticle transport, titanium dioxide nanoparticles have been shown to interact directly with the protein VE-cadherin at the inter-endothelial adherens junction niche to promote actin remodeling as well as internalization and degradation of VE-cadherin, thus increasing the leakiness of endothelial cells [27]. Therefore, the pathway that nanoparticles use to traverse cellular barriers likely varies depending on their material, size, and charge; these relationships need to be explored more thoroughly to fully understand the ADME profile of nanoparticles.

15.5 Metabolism, Degradation, Excretion, Clearance, and Biopersistence of Nanoparticles

The clearance or excretion of nanoparticles is important for assessing their long-term toxicity, because nanoparticles may be inherently stable. For example, quantum dots with the appropriate coating were retained in mice and remained fluorescent for at least 2 years [28]. In this way, the biopersistence of nanoparticles is a key factor in understanding their toxicity. The ability of cells to metabolize or degrade nanoparticles and to excrete or otherwise clear them from the body minimizes their potential toxicity. To this end, we need to learn the pathways that are responsible for breaking down nanoparticles and for removing them from the body. In addition, monitoring the concentration of nanoparticles in cells and tissues over long time periods (e.g., months) will inform us regarding the lifespan of these particles as well as their long-term biologic effects. In this section, we discuss the metabolism, degradation, excretion, clearance, and biopersistence of nanoparticles.

15.5.1 Excretion and Clearance of Nanoparticles

There are two major routes for the excretion and clearance of nanoparticles: renal filtration, with excretion into the urine, and hepatobiliary processing, with excretion into the bile. In general, proteins with a hydrodynamic diameter of <5–6 nm are cleared rapidly from the body by renal filtration and urinary excretion. Choi and colleagues used quantum dots to show that the renal clearance of nanoparticles similarly is related to their hydrodynamic diameter: quantum dots smaller than 5.5 nm were excreted into urine rapidly and efficiently and eliminated from the body, but the renal clearance of quantum dots larger than 15 nm was relatively low [29]. In another study, the accumulation of 1.4-nm gold nanoparticles in the liver and spleen was significantly lower than that of 18-nm nanoparticles, and 1.4-nm gold nanoparticles were excreted by both the renal and hepatobiliary systems after intravenous injection [12]. In comparison, single-walled CNTs (average diameter, 1 nm; average length, 300–1,000 nm) and multi-walled CNTs (average diameter, 20–30 nm; average length, 500–2,000 nm) undergo rapid and effective renal clearance and urinary excretion after intravenous injection, although the precise mechanism is unknown [30].

In the reticuloendothelial system, hepatic Kupffer cells are the representative cells that have the ability to uptake particles. In general, the liver is the predominant target organ of nanoparticle accumulation as well as an important excretion route. Various studies have shown that about 4 % of the administered dose of polystyrene nanoparticles (diameter, 50 nm) was excreted as intact particles in bile within 24 h after intravenous injection, and about 30 % of the total dose accumulated in hepatocytes [31, 32].

Recent investigations have revealed a novel clearance mechanism in the immune system. Macrophages play an important role in the uptake of nanoparticles, and the biodistribution of nanoparticles (e.g., blood clearance) differed between strains of

mice with differences in global immune status [33]. In the cited study, Jones and colleagues used intravital microscopy to show that PEGylated particles (diameter, 300 nm) are cleared more slowly in Th1-prone mice than in Th2-prone mice. M2 macrophages, which are induced by Th2 cytokines and have high levels of endocytosis, were important in the enhanced clearance observed in Th2-prone mice. In addition, these results were observed in macrophages from humans, suggesting that global immune regulation might significantly affect nanoparticle clearance in humans. Furthermore, the study suggested that granulocytes, especially neutrophils, are also important in the clearance of nanoparticles, although this cell type is seldom addressed in this context [33]. In addition to their phagocytic capacity, neutrophils can release complexes of DNA and protein into the extracellular space, thus trapping pathogens at infection sites (neutrophil extracellular traps); neutrophils may trap nanoparticles in extracellular structures by a similar mechanism [34]. Clearly future studies need to address the excretion or clearance of nanoparticles targeted not only to the kidney and liver but also immune cells.

15.5.2 Metabolism and Degradation of Nanoparticles

Nanoparticles had been thought to be resistant to metabolism and degradation under in vivo conditions, but several recent reports suggest that CNTs are degraded through natural enzymatic catalysis. In that regard, Kagan showed that myeloperoxidase (MPO), an abundant enzyme of inflammatory cells (neutrophils), played an important role in the oxidative biodegradation of single-walled CNTs [34]. In addition, single-walled CNTs that had been degraded by MPO in vitro failed to induce inflammatory and oxidative-stress responses after pharyngeal aspiration in mice, whereas intact nanotubes induced these responses. Consistent with these results, the clearance of single-walled CNTs from the lungs was much less effective in MPO-deficient than in wild-type mice after pharyngeal aspiration, whereas the inflammatory responses were much robust compared to wild-type mice [35]. In addition, single-walled CNTs are degraded by eosinophil peroxidase, a key oxidant-producing enzyme during inflammatory states [36]. Collectively, these findings suggest new ways to control the biopersistence of CNTs through genetic or pharmacologic manipulations. However, few studies have investigated the metabolism and degradation of nanoparticles in cells, because methods for monitoring a single particle in cells over time are currently unavailable. Given the numerous factors that might influence the metabolism and degradation of nanoparticles, methods for investigating these processes at the nanoscale are urgently needed.

15.5.3 Biopersistence of Nanoparticles

The precise mechanism underlying the biopersistence of nanoparticles is not yet fully understood. To this end, Balasubramanian and coworkers found that gold nanoparticles were rapidly and consistently accumulated in the liver and spleen of

rats within 1 day after a single intravenous injection and remained at high levels at 2 months thereafter [37]. These findings are consistent with several studies showing that, regardless of their size, shape, dose, and material, intravenously injected nanoparticles accumulate in the liver and spleen and are retained in those organs for long periods of time. For example, regardless of the size of the silver nanoparticles (10 or 25 nm) to which rats were exposed orally for 28 days, the silver content in most tissues gradually decreased to control levels over the 4-month observation period [38]. However, the silver concentrations in the testes and brain did not decrease to control levels, suggesting reduced clearance of silver nanoparticles across biologic barriers such as the blood–brain and blood–testis barriers.

15.6 Protein Corona

When nanoparticles enter the body, they typically become coated with various proteins, thereby developing a "protein corona." The binding of proteins to nanoparticles depends on their various physical characteristics, such that the size and surface properties of nanoparticles play important roles in determining the protein corona. Some studies have suggested that these interactions with proteins actually define the biologic effects and biodistribution of nanoparticles. For example, a recent in vitro study suggested that the formation of coronas of blood proteins reduced undesirable cellular responses to and the cytotoxicity of CNTs [39]. In addition, protein coronas have proven to be a key factor in the recognition and phagocytosis of nanoparticles by macrophages. Deng and coworkers showed in vitro that negatively charged gold nanoparticles bind to and induce the unfolding of fibrinogen, consequently promoting its interaction with the integrin receptor Mac-1 [40].

Nanomaterials can be covered with biologic molecules other than proteins as well. For example, creating a "corona" of lipids has been suggested as a means to influence the cellular uptake and toxicity of nanoparticles [41, 42]. In this regard, Konduru and colleagues showed that the adsorption of phosphatidylserine onto the surface of single-walled CNTs enhanced their uptake by macrophages and dendritic cells in vitro [43]. In addition, single-walled CNTs were found to be coated with surfactant proteins and phospholipids after pharyngeal aspiration of the nanotubes in mice, and the presence of this surfactant coating enhanced the uptake of the nanotubes into macrophages in vitro [44].

The ADME of many nanoparticles in vivo likely is largely defined by the protein corona rather than the nanoparticle itself. However, little information is available that addresses relationships between differences in the ADME profiles of nanoparticles in vivo and the formation of protein coronas. In this context, one study revealed that attaching plasma proteins onto dextran-coated superparamagnetic iron oxide nanoparticles is unlikely to alter their clearance by the liver and spleen, because the plasma proteins do not mask the entire surface of the nanoparticle [45]. One key question is whether the corona present at the point of entry (e.g., blood, lung, or other) or that resulting from modification during subsequent translocation determines the biodistribution and effects of nanoparticles.

The detailed mechanism underlying the fate of the original corona as the coated nanoparticle passes through membranes and barriers and interacts with the extracellular matrix is unknown currently: the original corona may remain intact or be replaced by new biomolecules. Another important question is whether the exposure route influences the protein corona. For instance, the physicochemical changes in the protein corona that occur while nanoparticles reside in the lung or gastrointestinal tract may dramatically change their ability to cross various internal barriers. Whether the exposure route directs the formation of different coronas needs to be determined.

15.7 Manipulation of the ADME Profile for the Development of Nanomedicine

Foreign particles—including nanoparticles—are removed from the body by phagocytes, such as macrophages, which also recognize and avoid live, nonforeign cells. In medical applications, systemically administered nanoparticles should evade rapid clearance so that they achieve sufficient accumulation in targeted tissues and cells to yield effective local drug concentrations. One way to delay the clearance of nanoparticles is to conjugate them with polyethylene glycol (PEG) or another water-soluble polymeric modifier. The surface modification of nanoparticles with PEG decreases their uptake by macrophages and retards renal clearance, thereby prolonging the half-life of nanoparticles in vivo. The prolonged circulation of nanoparticles in the blood induces the enhanced permeability and retention effect, which is based on the leaky nature of tumor blood vessels and results in increased delivery of conjugates to tumor tissue [46, 47]. However, PEG modification of nanoparticles might hinder their uptake by and drug-delivery to diseased target cells. In this regard, Rodriguez and colleagues suggested another approach to prolonging the circulation time of nanoparticles. The membrane protein CD47, which is expressed on all cell membranes, is a marker of self that impedes the phagocytosis of nonforeign cells in mice. Nanoparticles carrying peptides designed from CD47 avoided macrophage-mediated clearance and were retained in the circulation, resulting in both enhanced tumor imaging and increased drug delivery [48]. Other homeostatic self factors might similarly be used to prevent the phagocytosis of nanoparticles and target them to specific tissues, thereby enhancing the delivery of therapeutics and imaging agents to these sites.

15.8 Conclusion

Engineered nanoparticles have remarkable structural diversity and adopt characteristic forms including tubes, dots, wires, fibers, and capsules. Several reports have shown that the shape of nanoparticles plays an important role in their biologic

effects in vitro. However, the in vivo behavior of nanoparticles can be influenced significantly by their physicochemical characteristics, such as particle size, surface charge, surface hydrophobicity, and particle shape. In addition, although aggregation appears to be a ubiquitous phenomenon among all nanoparticles, its influence on their ADME profiles is unclear. Furthermore, many reports have examined the effect of surface charge on the biodistribution of nanoparticles, but the results are conflicting, and a consistent rule has not yet emerged. The discrepancy among these studies likely results from the differences in the types of nanoparticles used, their charged groups, and other factors. In this regard, the complexity of the various experimental scenarios used to date complicates and perhaps even prevents the comparison of data between studies. Consequently, to collect information useful for developing general rules about the ADME profiles of nanoparticles, methodologies must be developed that facilitate the overarching interpretation of resulting experimental data. The data collected from such studies would contribute toward an improved understanding of the potential risk of nanoparticles in human health.

References

1. Donaldson K, Murphy FA, Duffin R, Poland CA (2010) Asbestos, carbon nanotubes and the pleural mesothelium: a review of the hypothesis regarding the role of long fibre retention in the parietal pleura, inflammation and mesothelioma. Part Fibre Toxicol 7:5
2. Poland CA, Duffin R, Kinloch I, Maynard A, Wallace WA, Seaton A et al (2008) Carbon nanotubes introduced into the abdominal cavity of mice show asbestos-like pathogenicity in a pilot study. Nat Nanotechnol 3:423–428
3. Cross SE, Innes B, Roberts MS, Tsuzuki T, Robertson TA, McCormick P (2007) Human skin penetration of sunscreen nanoparticles: in-vitro assessment of a novel micronized zinc oxide formulation. Skin Pharmacol Physiol 20:148–154
4. Lademann J, Weigmann H, Rickmeyer C, Barthelmes H, Schaefer H, Mueller G et al (1999) Penetration of titanium dioxide microparticles in a sunscreen formulation into the horny layer and the follicular orifice. Skin Pharmacol Appl Skin Physiol 12:247–256
5. Spiegel R (1991) Cholinergic drugs, affective disorders and dementia: problems of clinical research. Acta Psychiatr Scand Suppl 366:66–69
6. Rancan F, Gao Q, Graf C, Troppens S, Hadam S, Hackbarth S et al (2012) Skin penetration and cellular uptake of amorphous silica nanoparticles with variable size, surface functionalization, and colloidal stability. ACS Nano 6:6829–6842
7. Vogt A, Combadiere B, Hadam S, Stieler KM, Lademann J, Schaefer H et al (2006) 40 nm, but not 750 or 1,500 nm, nanoparticles enter epidermal CD1a+cells after transcutaneous application on human skin. J Invest Dermatol 126:1316–1322
8. Mortensen LJ, Oberdorster G, Pentland AP, Delouise LA (2008) In vivo skin penetration of quantum dot nanoparticles in the murine model: the effect of UVR. Nano Lett 8:2779–2787
9. Mahler GJ, Esch MB, Tako E, Southard TL, Archer SD, Glahn RP et al (2012) Oral exposure to polystyrene nanoparticles affects iron absorption. Nat Nanotechnol 7:264–271
10. Peters R, Kramer E, Oomen AG, Rivera ZE, Oegema G, Tromp PC et al (2012) Presence of nano-sized silica during in vitro digestion of foods containing silica as a food additive. ACS Nano 6:2441–2451
11. Schleh C, Semmler-Behnke M, Lipka J, Wenk A, Hirn S, Schaffler M et al (2012) Size and surface charge of gold nanoparticles determine absorption across intestinal barriers and accumulation in secondary target organs after oral administration. Nanotoxicology 6:36–46

12. Semmler-Behnke M, Kreyling WG, Lipka J, Fertsch S, Wenk A, Takenaka S et al (2008) Biodistribution of 1.4- and 18-nm gold particles in rats. Small 4:2108–2111
13. Choi HS, Ashitate Y, Lee JH, Kim SH, Matsui A, Insin N et al (2010) Rapid translocation of nanoparticles from the lung airspaces to the body. Nat Biotechnol 28:1300–1303
14. Keelan JA (2011) Nanotoxicology: nanoparticles versus the placenta. Nat Nanotechnol 6:263–264
15. Yamashita K, Yoshioka Y, Higashisaka K, Mimura K, Morishita Y, Nozaki M et al (2011) Silica and titanium dioxide nanoparticles cause pregnancy complications in mice. Nat Nanotechnol 6:321–328
16. Pietroiusti A, Massimiani M, Fenoglio I, Colonna M, Valentini F, Palleschi G et al (2011) Low doses of pristine and oxidized single-wall carbon nanotubes affect mammalian embryonic development. ACS Nano 5:4624–4633
17. Campagnolo L, Massimiani M, Palmieri G, Bernardini R, Sacchetti C, Bergamaschi A et al (2013) Biodistribution and toxicity of pegylated single wall carbon nanotubes in pregnant mice. Part Fibre Toxicol 10:21
18. Jackson P, Vogel U, Wallin H, Hougaard KS (2011) Prenatal exposure to carbon black (printex 90): effects on sexual development and neurofunction. Basic Clin Pharmacol Toxicol 109:434–437
19. Jackson P, Hougaard KS, Boisen AM, Jacobsen NR, Jensen KA, Moller P et al (2012) Pulmonary exposure to carbon black by inhalation or instillation in pregnant mice: effects on liver DNA strand breaks in dams and offspring. Nanotoxicology 6:486–500
20. Lim JH, Kim SH, Shin IS, Park NH, Moon C, Kang SS et al (2011) Maternal exposure to multi-wall carbon nanotubes does not induce embryo-fetal developmental toxicity in rats. Birth Defects Res B Dev Reprod Toxicol 92:69–76
21. Yang H, Sun C, Fan Z, Tian X, Yan L, Du L et al (2012) Effects of gestational age and surface modification on materno-fetal transfer of nanoparticles in murine pregnancy. Sci Rep 2:847
22. Wick P, Malek A, Manser P, Meili D, Maeder-Althaus X, Diener L et al (2010) Barrier capacity of human placenta for nanosized materials. Environ Health Perspect 118:432–436
23. Ruenraroengsak P, Cook JM, Florence AT (2010) Nanosystem drug targeting: facing up to complex realities. J Control Release 141:265–276
24. Sonaje K, Chuang EY, Lin KJ, Yen TC, Su FY, Tseng MT et al (2012) Opening of epithelial tight junctions and enhancement of paracellular permeation by chitosan: microscopic, ultrastructural, and computed-tomographic observations. Mol Pharm 9:1271–1279
25. Hillyer JF, Albrecht RM (2001) Gastrointestinal persorption and tissue distribution of differently sized colloidal gold nanoparticles. J Pharm Sci 90:1927–1936
26. Apopa PL, Qian Y, Shao R, Guo NL, Schwegler-Berry D, Pacurari M et al (2009) Iron oxide nanoparticles induce human microvascular endothelial cell permeability through reactive oxygen species production and microtubule remodeling. Part Fibre Toxicol 6:1
27. Setyawati MI, Tay CY, Chia SL, Goh SL, Fang W, Neo MJ et al (2013) Titanium dioxide nanomaterials cause endothelial cell leakiness by disrupting the homophilic interaction of VE-cadherin. Nat Commun 4:1673
28. Ballou B, Ernst LA, Andreko S, Harper T, Fitzpatrick JA, Waggoner AS et al (2007) Sentinel lymph node imaging using quantum dots in mouse tumor models. Bioconjug Chem 18:389–396
29. Choi HS, Liu W, Misra P, Tanaka E, Zimmer JP, Itty Ipe B et al (2007) Renal clearance of quantum dots. Nat Biotechnol 25:1165–1170
30. Singh R, Pantarotto D, Lacerda L, Pastorin G, Klumpp C, Prato M et al (2006) Tissue biodistribution and blood clearance rates of intravenously administered carbon nanotube radiotracers. Proc Natl Acad Sci U S A 103:3357–3362
31. Ogawara K, Yoshida M, Furumoto K, Takakura Y, Hashida M, Higaki K et al (1999) Uptake by hepatocytes and biliary excretion of intravenously administered polystyrene microspheres in rats. J Drug Target 7:213–221
32. Furumoto K, Ogawara K, Yoshida M, Takakura Y, Hashida M, Higaki K et al (2001) Biliary excretion of polystyrene microspheres depends on the type of receptor-mediated uptake in rat liver. Biochim Biophys Acta 1526:221–226

33. Jones SW, Roberts RA, Robbins GR, Perry JL, Kai MP, Chen K et al (2013) Nanoparticle clearance is governed by Th1/Th2 immunity and strain background. J Clin Invest 123:3061–3073
34. Bartneck M, Keul HA, Zwadlo-Klarwasser G, Groll J (2010) Phagocytosis independent extracellular nanoparticle clearance by human immune cells. Nano Lett 10:59–63
35. Shvedova AA, Kapralov AA, Feng WH, Kisin ER, Murray AR, Mercer RR et al (2012) Impaired clearance and enhanced pulmonary inflammatory/fibrotic response to carbon nanotubes in myeloperoxidase-deficient mice. PLoS One 7:e30923
36. Andon FT, Kapralov AA, Yanamala N, Feng W, Baygan A, Chambers BJ et al (2013) Biodegradation of single-walled carbon nanotubes by eosinophil peroxidase. Small 9:2721–2729
37. Balasubramanian SK, Jittiwat J, Manikandan J, Ong CN, Yu LE, Ong WY (2010) Biodistribution of gold nanoparticles and gene expression changes in the liver and spleen after intravenous administration in rats. Biomaterials 31:2034–2042
38. Lee JH, Kim YS, Song KS, Ryu HR, Sung JH, Park JD et al (2013) Biopersistence of silver nanoparticles in tissues from Sprague-Dawley rats. Part Fibre Toxicol 10:36
39. Ge C, Du J, Zhao L, Wang L, Liu Y, Li D et al (2011) Binding of blood proteins to carbon nanotubes reduces cytotoxicity. Proc Natl Acad Sci U S A 108:16968–16973
40. Deng ZJ, Liang M, Monteiro M, Toth I, Minchin RF (2011) Nanoparticle-induced unfolding of fibrinogen promotes Mac-1 receptor activation and inflammation. Nat Nanotechnol 6:39–44
41. Gasser M, Rothen-Rutishauser B, Krug HF, Gehr P, Nelle M, Yan B et al (2010) The adsorption of biomolecules to multi-walled carbon nanotubes is influenced by both pulmonary surfactant lipids and surface chemistry. J Nanobiotechnology 8:31
42. Schleh C, Rothen-Rutishauser B, Kreyling WG (2011) The influence of pulmonary surfactant on nanoparticulate drug delivery systems. Eur J Pharm Biopharm 77:350–352
43. Konduru NV, Tyurina YY, Feng W, Basova LV, Belikova NA, Bayir H et al (2009) Phosphatidylserine targets single-walled carbon nanotubes to professional phagocytes in vitro and in vivo. PLoS One 4:e4398
44. Kapralov AA, Feng WH, Amoscato AA, Yanamala N, Balasubramanian K, Winnica DE et al (2012) Adsorption of surfactant lipids by single-walled carbon nanotubes in mouse lung upon pharyngeal aspiration. ACS Nano 6:4147–4156
45. Simberg D, Park JH, Karmali PP, Zhang WM, Merkulov S, McCrae K et al (2009) Differential proteomics analysis of the surface heterogeneity of dextran iron oxide nanoparticles and the implications for their in vivo clearance. Biomaterials 30:3926–3933
46. von Maltzahn G, Park JH, Agrawal A, Bandaru NK, Das SK, Sailor MJ et al (2009) Computationally guided photothermal tumor therapy using long-circulating gold nanorod antennas. Cancer Res 69:3892–3900
47. Lipka J, Semmler-Behnke M, Sperling RA, Wenk A, Takenaka S, Schleh C et al (2010) Biodistribution of PEG-modified gold nanoparticles following intratracheal instillation and intravenous injection. Biomaterials 31:6574–6581
48. Rodriguez PL, Harada T, Christian DA, Pantano DA, Tsai RK, Discher DE (2013) Minimal "Self" peptides that inhibit phagocytic clearance and enhance delivery of nanoparticles. Science 339:971–975

ERRATUM

Chapter 11
Particulate and Immunity

Etsushi Kuroda, Cevayir Coban, and Ken J. Ishii

M. Akashi et al. (eds.), *Engineered Cell Manipulation for Biomedical Application*, Nanomedicine and Nanotoxicology,
DOI 10.1007/978-4-431-55139-3_11

DOI 10.1007/978-4-431-55139-3_16

The earlier version of print book has 53 references in this chapter. Now, a new reference (54) mentioned below was added in the chapter of both print and online version.

54. Kuroda E, Coban C, Ishii KJ (2013) Particulate adjuvant and innate immunity: past achievements, present findings, and future prospects. Int Rev Immunol 32(2):209–220.

On p. 201, line 14 from top: following text included in print and online

'(**This is a modified review based on ref. 54*)'

The updated original online version for this chapter can be found at
DOI 10.1007/978-4-431-55139-3_11

M. Akashi et al. (eds.), *Engineered Cell Manipulation for Biomedical Application*, Nanomedicine and Nanotoxicology,
DOI 10.1007/978-4-431-55139-3_16